**U.S. DEPARTMENT OF COMMERCE**
**National Technical Information Service**

PB-293 119

# The Development of Mathematical Models for the Prediction of Anthropogenic Visibility Impairment. Volume I

**Systems Applications, Inc, San Rafael, CA**

**Prepared for**

**Environmental Protection Agency, Research Triangle Park, NC Office of Air Quality Planning and Standards**

Sep 78

PB 293119

United States
Environmental Protection
Agency

Office of Air Quality
Planning and Standards
Research Triangle Park NC 27711

EPA-450/3-78-110a
September 1978

Air

EPA

# The Development of Mathematical Models for the Prediction of Anthropogenic Visibility Impairment

## Volume I

REPRODUCED BY
NATIONAL TECHNICAL
INFORMATION SERVICE
U. S. DEPARTMENT OF COMMERCE
SPRINGFIELD, VA. 22161

210

## TECHNICAL REPORT DATA

*(Please read Instructions on the reverse before completing)*

**1. REPORT NO.**
EPA-450/3-78-110a

**2.**

**3. RECIPIENT'S ACCESSION NO.**
PB293119

**4. TITLE AND SUBTITLE**
THE DEVELOPMENT OF MATHEMATICAL MODELS FOR THE PREDICTION OF ANTHROPOGENIC VISIBILITY IMPAIRMENT
VOLUME 1

**5. REPORT DATE**
November 1978

**6. PERFORMING ORGANIZATION CODE**

**7. AUTHOR(S)**
D. A. Latimer, R. W. Bergstrom, S. R. Hayes, M. K. Liu, J. H. Seinfeld, G. Z. Whitten, M. A. Wojcik, M.J. Hillyer

**8. PERFORMING ORGANIZATION REPORT NO.**
EF78-68A

**9. PERFORMING ORGANIZATION NAME AND ADDRESS**
Systems Applications, Incorporated
950 Northgate Drive
San Rafael, California 94903

**10. PROGRAM ELEMENT NO.**

**11. CONTRACT/GRANT NO.**
EPA 68-01-3947 and 68-02-2593

**12. SPONSORING AGENCY NAME AND ADDRESS**
U. S. Environmental Protection Agency
Waterside Mall
401 M Street, S.W.
Washington, D.C. 20460

**13. TYPE OF REPORT AND PERIOD COVERED**
Final Report: 10/77 to 9/78

**14. SPONSORING AGENCY CODE**
EPA-OPE/OAQPS

**15. SUPPLEMENTARY NOTES**

**16. ABSTRACT**

This report describes a nine-month study to recommend and develop models that predict the contribution of man-made air pollution to visibility impairment in federal Class I areas. Two models were developed. A near-source plume model based on a Gaussian formulation was designed to compute the impact of a plume on visual range and atmospheric coloration. A regional model was designed to calculate pollutant concentrations and visibility impairment resulting from emissions from multiple sources within a region with a spatial scale of 1000 km and a temporal scale of several days. The objective of this effort was to develop models that are useful predictive tools for making policy and regulatory decisions, for evaluating the impacts of proposed new sources, and for determining the amount of emissions reduction required from existing sources, as mandated by the Clean Air Act Amendments of 1977. Volume I of this report contains the main text; Volume II contains the appendices; Volume III presents case studies of power plant plume visual impact for a variety of emission, meteorological, and ambient background scenarios.

**17. KEY WORDS AND DOCUMENT ANALYSIS**

| a. DESCRIPTORS | b. IDENTIFIERS/OPEN ENDED TERMS | c. COSATI Field/Group |
|---|---|---|
| Air quality modeling<br>Visual range<br>Atmospheric discoloration<br>Power plants | | |

**18. DISTRIBUTION STATEMENT**
RELEASE TO PUBLIC

**19. SECURITY CLASS** *(This Report)*
UNCLASSIFIED

**20. SECURITY CLASS** *(This page)*
UNCLASSIFIED

**21. NO. OF PAGES**
210

**22. PRICE**
PCA10/MFA01

EPA Form 2220-1 (9-73)

EPA-450/3/78-110a

Volume I

# THE DEVELOPMENT OF MATHEMATICAL MODELS FOR THE PREDICTION OF ANTHROPOGENIC VISIBILITY IMPAIRMENT

by

Douglas A. Latimer, Robert W. Bergstrom, Stanley R. Hayes
Mei-Kao Liu, John H. Seinfeld, Gary Z. Whitten
Michael A. Wojcik, Martin J. Hillyer

Systems Application, Incorporated
San Rafael, California 94903

Contract 68-01-3947

EPA Project Officers: John Butler, David Shaver, James Dicke

Prepared for

U. S. ENVIRONMENTAL PROTECTION AGENCY

Office of Planning and Evaluation
401 M Street, SW
Washington, DC 20460

Office of Air Noise and Radiation
Office of Air Quality Planning and
Standards
Research Triangle Park, NC 27711

September 1978

1a

# DISCLAIMER

This report has been reviewed by the Office of Air Quality Planning and Standards and the Office of Planning and Evaluation, U.S. Environmental Protection Agency and approved for publication. Approval does not signify that the contents necessarily reflect the views and policies of the U.S. Environmental Protection Agency, nor does mention of trade names or commercial products constitute endorsement or recommendation for use.

# EXECUTIVE SUMMARY

This three-volume report describes a nine-month study performed by Systems Applications, Incorporated for the Environmental Protection Agency to recommend and develop models that predict the contribution of manmade air pollution to visibility impairment in Class I areas. Two models were developed: One is a near-source plume model, based on a Gaussian formulation, that is designed to compute the impact of a plume on visual range and atmospheric coloration. The other is a regional model designed to calculate pollutant concentrations and visibility impairment resulting from emissions from multiple sources within a region with a spatial scale of 1000 km on a temporal scale of several days.

The objective of this effort was to develop models that are useful predictive tools for making policy and regulatory decisions, for evaluating the impacts of proposed new sources, and for determining the amount of emissions reduction required from existing sources, as mandated by the Clean Air Act Amendments of 1977.

Both visibility models (plume and regional) are based on atmospheric dispersion models that account for the transport, diffusion, and surface deposition of emissions from point sources. Concentrations of nitrogen dioxide ($NO_2$) are computed using a modified steady-state relationship; sulfate and nitrate concentrations are calculated from $SO_2$ and $NO_x$ emissions using user-inputed pseudo-first-order rate constants. The aerosol size distribution is assumed to consist of four log-normally distributed modes: background submicron (accumulation), background coarse, plume coarse (primary particulate), and plume submicron (secondary particulate). The effect of relative humidity on the mass of liquid water associated with submicron aerosol is included in the calculation of aerosol volume. The

spectral light intensities at 39 wavelengths of light in the visible spectrum are calculated for given lines of sight through the plume and the background atmosphere by treating the plume as a homogeneous layer and the background atmosphere as two homogeneous layers. The plume optical thickness is calculated taking into account the geometry of the plume and the observer's line of sight.

For a given line of sight, the spectral light intensities are used to compute parameters that characterize visibility impairment, including visual range, luminance, chromaticity coordinates, contrast between plume and background at various wavelengths, the blue-red luminance ratio, and a parameter that characterizes plume perceptibility due to changes in both light intensity and color. These quantitative specifications of discoloration can be translated to Munsell color notation so that a representative color paint chip can be selected, thereby providing a subjective understanding of the computed color. Finally, with these color chips and a computer graphics capability that displays perspective views of plumes and background terrain, color illustrations of calculated atmospheric discoloration and plume impact can be prepared.

The plume model was applied to the hypothetical case of a 2250 Mwe coal-fired power plant emitting primary particulate, $SO_2$, and $NO_x$ at the maximum rates permitted by EPA's New Source Performance Standards. Ambient conditions typical of the Southwest were used in these calculations, including a background visual range of 130 km (80 miles). For an assumed sulfate formation rate of 0.5 percent per hour, the plume's impact on visual range was small near the source, but it increased with distance from the source as sulfate aerosol was formed. For neutral stability and for sight paths perpendicular to the plume centerline, the calculated visual range was reduced approximately 5 percent from the background value at distances 200 to 300 km downwind of the power plant. Except at short downwind distances, where scattering is dominated by primary particulate (fly ash), sulfate formed in the atmosphere was the principal cause of reductions in visual range. The calculations, however, indicate that plume discoloration was caused principally by $NO_2$. Yellow-brown plume discoloration was most prominent during stable conditions at downwind distances of 40 to 100 km. Light scattered by primary particulate and sulfate aerosol tended to mask the discoloration due to $NO_2$; thus, control of particulate and $SO_2$ emissions would increase discoloration. Sulfate aerosol, by itself, tended to cause a white plume (in forward scatter) or a grey plume (in back scatter) when viewed against the horizon sky.

The regional model was applied to point source emissions of $SO_x$ in the Northern Great Plains for two cases: estimated 1975 emissions of 430 tons/day and projected 1986 emissions of 1990 tons/day. For a stagnation episode characterized by light, variable winds, the maximum reduction in visual range was calculated to be 10 percent for the 1975 emissions and 25 percent for the 1986 emissions. The most significant reductions in visual range occurred hundreds of kilometers from the emissions sources. For comparison, the impact of a hypothetical complex of copper smelters with a total $SO_x$ emissions rate of 6000 tons/day (equivalent to the 1972 emissions from copper smelters in Arizona) was evaluated with the Northern Great Plains regional visibility model. The maximum reduction in visual range (for stagnation conditions) was calculated to be 50 percent and to occur hundreds of kilometers from the sources. Calculated maximum sulfate concentrations were in rough agreement with maximum sulfate concentrations measured in nonurban locations in Arizona in 1972-1973.

National Weather Service visual range and meteorological data for the period 1948-1976 at 18 locations in the western United States were analyzed. Trends in visibility in Phoenix and Tucson were found to be correlated with trends in $SO_x$ emissions from copper smelters. During periods of copper strikes when smelter $SO_x$ emissions were eliminated, and during the period 1973-1976 when $SO_x$ emissions from copper smelters were reduced from 6000 to 3000 tons/day, visibility improved. The effect of smelter $SO_x$ emissions on visual range at distant nonurban locations was evaluated by comparing visual range frequency distributions at Prescott, Winslow, and Farmington during the 1967-1968 copper strike with other periods. Significant improvements in visibility during the copper strike were particularly associated with winds that would transport smelter emissions directly to the given locations.

# CONTENTS

DISCLAIMER . . . . . . . . . . . . . . . . . . . . . . . . . . . . ii

EXECUTIVE SUMMARY . . . . . . . . . . . . . . . . . . . . . . . . . iii

LIST OF ILLUSTRATIONS . . . . . . . . . . . . . . . . . . . . . . . ix

LIST OF TABLES . . . . . . . . . . . . . . . . . . . . . . . . . . xiii

LIST OF EXHIBITS . . . . . . . . . . . . . . . . . . . . . . . . . xiii

ACKNOWLEDGMENTS . . . . . . . . . . . . . . . . . . . . . . . . . . xiv

DEDICATION . . . . . . . . . . . . . . . . . . . . . . . . . . . . xv

I INTRODUCTION . . . . . . . . . . . . . . . . . . . . . . . . . . 1

II THE NATURE OF VISIBILITY IMPAIRMENT . . . . . . . . . . . . . . . 8

- A. Definition of Visibility Impairment . . . . . . . . . . . . . 8
- B. Fundamental Causes of Visibility Impairment . . . . . . . . . . 17
- C. Visibility Impairment in the Western United States . . . . . 24

III THE ELEMENTS OF VISIBILITY MODELS . . . . . . . . . . . . . . . 35

- A. Pollutant Transport, Diffusion, and Removal . . . . . . . . . . 35
  - 1. Initial Dilution in a Buoyant Plume . . . . . . . . . . . . 37
  - 2. Gaussian Plume Diffusion . . . . . . . . . . . . . . . . . . 39
  - 3. Observer-Plume Orientation . . . . . . . . . . . . . . . . 40
  - 4. Limited Mixing . . . . . . . . . . . . . . . . . . . . . . 42
  - 5. Plume Trajectory Box Model . . . . . . . . . . . . . . . . 42
  - 6. Regional Transport and Diffusion . . . . . . . . . . . . . 46
- B. Atmospheric Chemistry . . . . . . . . . . . . . . . . . . . . 48
  - 1. Conversion of NO to $NO_2$ . . . . . . . . . . . . . . . . . 48
  - 2. Conversion of Gases to Particles . . . . . . . . . . . . . 53
- C. Aerosol Size Distribution . . . . . . . . . . . . . . . . . . 57
- D. Atmospheric Optics . . . . . . . . . . . . . . . . . . . . . 65
  - 1. Calculation of the Scattering and Absorption Properties . . . . . . . . . . . . . . . . . . . 65
  - 2. Calculation of Light Intensity . . . . . . . . . . . . . . 71

III THE ELEMENTS OF VISIBILITY MODELS (continued)

E. Quantifying Visibility Impairment . . . . . . . . . . . . 75
  1. Visual Range . . . . . . . . . . . . . . . . . . . . 76
  2. Contrast of Haze Layers and Plumes . . . . . . . . . 78
  3. Color . . . . . . . . . . . . . . . . . . . . . . . 81
  4. Color Changes . . . . . . . . . . . . . . . . . . . 86

IV THE OUTPUT OF VISIBILITY MODELS . . . . . . . . . . . . . 89

A. The Plume Visibility Model . . . . . . . . . . . . . . . 90

B. Plume/Terrain Perspective Model . . . . . . . . . . . . . 110

C. Color Display Techniques . . . . . . . . . . . . . . . . 113
  1. Color Illustration . . . . . . . . . . . . . . . . . 130
  2. Color Video Display . . . . . . . . . . . . . . . . 136

D. The Regional Visibility Model . . . . . . . . . . . . . . 138

V RECOMMENDATIONS FOR FUTURE WORK. . . . . . . . . . . . . . 155

A. Impact Analysis in Support of Regulation Development . . 156

B. Model Refinement and Testing. . . . . . . . . . . . . . . 157
  1. Model Testing . . . . . . . . . . . . . . . . . . . 158
  2. Gas-to-Particle Conversion and Aerosol Growth . . . . 160
  3. Assessment of Color Impact Thresholds . . . . . . . . 161
  4. Refinement of Color Display . . . . . . . . . . . . 161

C. Model Validation . . . . . . . . . . . . . . . . . . . . 163
  1. The Type of Measurement Program . . . . . . . . . . . 163
  2. Specific Measurements . . . . . . . . . . . . . . . 165
  3. Data Analysis, Assessment of Model Performance, and Model Refinement . . . . . . . . . . . . . . . . . 170

D. Further Data Analysis . . . . . . . . . . . . . . . . . 172

E. Development of a Southwest Regional Visibility Model . . 174

REFERENCES . . . . . . . . . . . . . . . . . . . . . . . . . 176

GLOSSARY . . . . . . . . . . . . . . . . . . . . . . . . . . 187

FORM 2220-1 . . . . . . . . . . . . . . . . . . . . . . . . 193

NOTE . . . . . . . . . . . . . . . . . . . . . . . . . . . . 194

# ILLUSTRATIONS

1 Outline of SAI's Study To Develop Models for Predicting Visibility Impairment . . . . . . . . . . . . . . . . . . . . . . . . 4

2 Elements and Potential Uses of Visibility Models . . . . . . . . . . 6

3 An Example of Reduced Visual Range: Marble Canyon, Arizona . . . . 10

4 An Example of Near-Source Visibility Impairment: Plume Discoloration Downwind of the Navajo Generating Station in Northern Arizona . . . . . . . . . . . . . . . . . . . . . . . . 13

5 An Example of Visibility Impairment: A Uniform Haze Layer Visible from Bryce Canyon National Park . . . . . . . . . . . 14

6 Natural Causes of Visibility Impairment . . . . . . . . . . . . . . 16

7 Effect of an Atmosphere on the Perceived Light Intensity of Objects . . . . . . . . . . . . . . . . . . . . . . . . 21

8 Map of the Western United States Showing the Locations of Large Point Sources, Mandatory Federal Class I Areas, and NWS Stations Where Visibility Observations Are Made . . . . . . . . 26

9 Frequency Distributions of Extinction Coefficients Based on Visual Range Observations at 13 Western U.S. Locations on Days Without Precipitation or Fog in 1976 . . . . . . . . . . . 27

10 Dependence of Visual Range on Relative Humidity at Four Locations in the Southwest . . . . . . . . . . . . . . . . . . . . 28

11 Historical Trends in Visibility in Phoenix, Arizona . . . . . . . . . 30

12 Percentage of Daylight Observations with RH < 60 Percent for Which Visual Range Exceeded 121 km, as a Function of Wind Direction, at Farmington, New Mexico, 1949-1976 . . . . . . . . 31

13 Schematic Logic Flow Diagram of the Visibility Models . . . . . . . 36

14 Gaussian Plume Visual Impact Model: Observer-Plume Geometry . . . 41

15 Plume Trajectory Box Model . . . . . . . . . . . . . . . . . . . . 43

16 Sensitivity of NO to $NO_2$ Conversion in Power Plant Plumes to the Rate of Plume Dilution, Background Ozone Concentration, and Solar Radiation . . . . . . . . . . . . . . . . . . . 52

17 Comparison of Measured $NO_2/NO_x$ Mole Ratios (Circled Points) in the Plume Centerline Downwind of a Coal-Fired Power Plant with Computer-Calculated Values (Solid Lines) Using Standard Pasquill and Fitted $\sigma_y \sigma_z$ . . . . . . . . . . . . . . . . . 54

18 Schematic of an Atmospheric Aerosol Surface Area Distribution Showing the Principal Modes, Sources of Mass for Each Mode, Process Involved in Inserting Mass in Each Mode, and Removal Mechanisms . . . . . . . . . . . . . . . . . 58

19 Average Urban Model Aerosol Distribution Plotted in Five Different Ways . . . . . . . . . . . . . . . . . . . . . . . . 59

20 Scattering-to-Volume Ratios for Various Size Distributions . . . 63

21 Ratio of Light Scattering to Mass as a Function of Relative Humidity . . . . . . . . . . . . . . . . . . . . . . . . . 70

22 Light Scattering and Absorption in the Atmosphere . . . . . . . . 72

23 An Example of Plume Visual Impact . . . . . . . . . . . . . . . . 79

24 Chromaticity Diagram . . . . . . . . . . . . . . . . . . . . . . 82

25 Spectral Tristimulus Values $\bar{x}(\lambda)$, $\bar{y}(\lambda)$, $\bar{z}(\lambda)$ . . . . . . . . . . 84

26 Representation of a Color Solid . . . . . . . . . . . . . . . . . 85

27 Calculated Plume Visibility Impairment for a Hypothetical 2250 Mwe Coal-Fired Power Plant with a Light Scattering Angle of 45° and Stability Class C . . . . . . . . . . . . . . . . 100

28 Calculated Plume Visibility Impairment for a Hypothetical 2250 Mwe Coal-Fired Power Plant with a Light Scattering Angle of 45° and Stability Class D . . . . . . . . . . . . . . . . 101

29 Calculated Plume Visibility Impairment for a Hypothetical 2250 Mwe Coal-Fired Power Plant with a Light Scattering Angle of 45° and Stability Class E . . . . . . . . . . . . . . . . 102

30 Calculated Plume Visibility Impairment for a Hypothetical 2250 Mwe Coal-Fired Power Plant with a Light Scattering Angle of 90° and Stability Class C . . . . . . . . . . . . . . . . 103

31 Calculated Plume Visibility Impairment for a Hypothetical 2250 Mwe Coal-Fired Power Plant with a Light Scattering Angle of 90° and Stability Class D . . . . . . . . . . . . . . . . 104

32 Calculated Plume Visibility Impairment for a Hypothetical 2250 Mwe Coal-Fired Power Plant with a Light Scattering Angle of 90° and Stability Class E . . . . . . . . . . . . . . . . 105

33 Calculated Plume Visibility Impairment for a Hypothetical 2250 Mwe Coal-Fired Power Plant with a Light Scattering Angle of 180° and Stability Class C . . . . . . . . . . . . . . . 106

34 Calculated Plume Visibility Impairment for a Hypothetical 2250 Mwe Coal-Fired Power Plant with a Light Scattering Angle of 180° and Stability Class D . . . . . . . . . . . . . . . . . 107

35 Calculated Plume Visibility Impairment for a Hypothetical 2250 Mwe Coal-Fired Power Plant with a Light Scattering Angle of 180° and Stability Class E . . . . . . . . . . . . . . . . 108

36 Observer Locations for Plume-Terrain Perspective Views . . . . . 112

37 View from Location 1 . . . . . . . . . . . . . . . . . . . . 114

38 View from Location 2 . . . . . . . . . . . . . . . . . . . . 115

39 View from Location 3 . . . . . . . . . . . . . . . . . . . . 116

40 View from Location 4 . . . . . . . . . . . . . . . . . . . . 117

41 View from Location 5 . . . . . . . . . . . . . . . . . . . . 118

42 View from Location 6 . . . . . . . . . . . . . . . . . . . . 119

43 View from Location 7 . . . . . . . . . . . . . . . . . . . . 120

44 View from Location 8 . . . . . . . . . . . . . . . . . . . . 121

45 View from Location 9 . . . . . . . . . . . . . . . . . . . . 122

46 View from Location 10 . . . . . . . . . . . . . . . . . . . 123

47 View from Location 11 . . . . . . . . . . . . . . . . . . . 124

48 View from Location 12 . . . . . . . . . . . . . . . . . . . 125

49 View from Location 13 . . . . . . . . . . . . . . . . . . . 126

50 View from Location 14 . . . . . . . . . . . . . . . . . . . 127

51 View from Location 15 . . . . . . . . . . . . . . . . . . . 128

52 Schematic Showing Color Display Techniques . . . . . . . . . . . 129

53 Photocopy of the Power Plant Plume in Northern Arizona Selected for Simulation . . . . . . . . . . . . . . . . . . . . 132

54 Photocopy of the Perspective Terrain View with Calculated Munsell Color Notation and Corresponding Color Chips . . . . . . 134

55 Photocopy of Color Illustration Created by an Artist from Indicated Munsell Color Chips . . . . . . . . . . . . 135

56 Photocopy of a Color Video Display of Plume Visual Impact . . . . 137

57 Predicted Regional Three-Hour-Average $SO_2$ Concentrations ($\mu g/m^3$) Based on 1986 Emissions in the Northern Great Plains for the Meteorological Conditions of 1400-1700 MST on 6 April 1976. . . . 140

58 Predicted Regional Three-Hour-Average $NO_2$ Concentrations (ppb) Based on 1986 Emissions in the Northern Great Plains for the Meteorological Conditions of 1400-1700 MST on 6 April 1976 . . . 141

59 Predicted Regional Three-Hour-Average Sulfate Concentrations ($\mu g/m^3$), Assuming a 0.5 Percent per Hour Sulfate Formation Rate, Based on 1986 Emissions in the Northern Great Plains for the Meteorological Conditions of 1400-1700 MST on 6 April 1976 . . . 142

60 Predicted Regional Visual Range (km), Assuming a Background Visual Range of 130 km and a 0.5 Percent per Hour Sulfate Formation Rate, Based on 1986 Emissions in the Northern Great Plains for the Meteorological Conditions of 1400-1700 MST on 6 April 1976 . . . . . . . . . . . . . . . . . . . . . . . 143

61 Predicted Regional Three-Hour-Average $SO_2$ Concentrations ($\mu g/m^3$) Based on Hypothetical Copper Smelter Emissions for the Meteorological Conditions of 1400-1700 MST on 6 April 1976 in the Northern Great Plains . . . . . . . . . . . . 145

62 Predicted Regional Three-Hour-Average Sulfate Concentrations ($\mu g/m^3$), Assuming a 0.5 Percent per Hour Sulfate Formation Rate, Based on Hypothetical Copper Smelter Emissions for Meteorological Conditions of 1400-1700 MST on 6 April 1976 in the Northern Great Plains . . . . . . . . . . . . . . . . . . 146

63 Predicted Regional Visual Range (km), Assuming a Background Visual Range of 130 km and a 0.5 Percent per Hour Sulfate Formation Rate, Based on Hypothetical Copper Smelter Emissions for Meteorological Conditions of 1400-1700 MST on 6 April 1976 in the Northern Great Plains . . . . . . . . . . . . . . . . . . 147

64 Predicted Regional Visual Range (km), Assuming a Background Visual Range of 130 km and a 0.3 Percent per Hour Sulfate Formation Rate, Based on Hypothetical Copper Smelter Emissions for Meteorological Conditions of 1400-1700 MST on 6 April 1976 in the Northern Great Plains . . . . . . . . . . . . . . . . . . 149

65 Predicted Regional Visual Range (km), Assuming a Background Visual Range of 130 km and a 1 Percent per Hour Sulfate Formation Formation Rate, Based on Hypothetical Copper Smelter Emissions for Meteorological Conditions of 1400-1700 MST on 6 April 1976 in the Northern Great Plains . . . . . . . . . . . . . . . . . . 150

# TABLES

1 Main Milestones in Visibility Protection Regulation . . . . . . . 2

2 Percent Reduction in Visual Range by Three Levels of $SO_2$ Emissions . . . . . . . . . . . . . . . . . . . . . . . . . 45

3 Measured Size Distributions of Atmospheric Aerosol . . . . . . . 62

4 Estimates of Extinction Coefficients per Unit Mass . . . . . . . 67

5 Mean and Maximum 24-Hour-Average Sulfate Concentrations Measured in Arizona in 1972-1973 . . . . . . . . . . . . . . . . . 151

# EXHIBITS

1 Sample Plume Model Output: Input Emissions and Ambient Conditions . . . . . . . . . . . . . . . . . . . . 91

2 Sample Plume Model Output: Pollutant Concentrations . . . . . . 93

3 Sample Plume Model Output: Visual Effects for Horizontal Sight Paths . . . . . . . . . . . . . . . . . . . . 95

4 Sample Plume Model Output: Visual Effects for Nonhorizontal Sight Paths . . . . . . . . . . . . . . . . . . . . 97

5 Sample Plume Model Output: Visual Effects for White, Grey, and Black Backgrounds . . . . . . . . . . . . . . . . 98

6 Example of Visual Effects at a Given Location in a Region with 2 $\mu g/m^3$ $SO_4^=$ and 30 $\mu g/m^3$ Coarse Particulate . . . . . 153

# ACKNOWLEDGMENTS

Many people inside and outside of SAI have assisted us in this work. At SAI we particularly want to thank Gary Lundberg for his excellent computer work and Shep Burton for his guidance. The support of John Butler, David Shaver, James Dicke, John Bachmann, Steve Eigsti, Joseph Tikvart, Terry Thoem, and Donald Henderson of the EPA is greatly appreciated. We thank Donald LaBash for his color illustrations and Ellen Leonard and Michael Williams of Los Alamos Scientific Laboratory for their help with the color video display techniques. Also, we gratefully acknowledge the conversations and helpful suggestions of George Hidy, Robert Charlson, John Trijonis, Thomas Peterson, William Wagner, and Edwin Roberts.

# DEDICATION

We dedicate this report to the memory of Terry N. Jerskey.

# I INTRODUCTION

The Clean Air Act was amended in August 1977 to contain a section requiring the restoration and protection of visibility in national parks, wilderness areas, and forests that have been classified as mandatory Class I federal areas.* In that section Congress boldly declared "as a national goal the prevention of any future, and the remedying of any existing [our emphasis], impairment of visibility in mandatory Class I Federal areas which impairment results from man-made air pollution." Furthermore, Congress defined "impairment of visibility" as a reduction in visual range, an atmospheric discoloration, or both.

Although many sources of air pollution cause or contribute to visibility impairment, including vehicular emissions from urban areas and sulfur dioxide emissions from copper smelters, Congress was particularly concerned with the alleged impact of power plant emissions on the magnificent vistas in national parks such as the Grand Canyon and Bryce Canyon. The 1977 Clean Air Act Amendments require that the following action be taken (see Table 1):

> The Department of the Interior, in conjunction with the Environmental Protection Agency (EPA), must identify all mandatory Class I areas where visibility is deemed to be aesthetically important.

> The EPA must report to Congress on the emissions sources and the air pollutants that cause or contribute to visibility impairment, on recommended methods of measuring

---

* Section 128 of Public Law 95-95 amends Part C of Title I of the Clean Air Act by adding Section 169A concerning "visibility protection for Federal Class I areas."

TABLE 1. MAIN MILESTONES IN VISIBILITY PROTECTION REGULATION

| Date | Milestone |
|---|---|
| August 1977 | Congress passed the 1977 Clean Air Act Amendments containing Section 169A on visibility protection: "Congress hereby declares as a national goal the prevention of any future, and the remedying of any existing, impairment of visibility [defined as a 'reduction in visual range' or an 'atmospheric discoloration'] in mandatory Class I Federal areas which impairment results from manmade air pollution" |
| February 1978 | Department of Interior is required to identify all mandatory Class I areas where visibility is an important aesthetic value |
| August 1978 | EPA is required to promulgate a list of mandatory Class I federal areas where visibility is an important aesthetic value |
| February 1979 | EPA is required to report to Congress recommending methods to characterize visibility in Class I areas, modeling techniques (or other methods) for determining the impact of man-made air pollution on visibility, and methods to prevent and remedy air pollution |
| August 1979 | EPA is required to promulgate regulations requiring states to "make reasonable progress" toward preventing and remedying visibility impairment, including use of the best available retrofit technology for point sources less than 15 years old and development of a 10 to 15 year long-term strategy |

visibility impairment in Class I areas, on recommended modeling techniques for determining the contribution of man-made air pollution to visibility impairment in Class I areas, and on methods for preventing and remedying such air pollution.

> The EPA must promulgate regulations that ensure reasonable progress toward meeting the national visibility goal.

It is clear that Congress intended that existing sources be controlled so that visibility would not be significantly impaired in Class I areas. Each existing major stationary source less than 15 years old that emits an air pollutant that causes or contributes to any Class I area visibility impairment is required to procure, install, and operate the "best available retrofit technology" for controlling air pollutant emissions "as expeditiously as possible." However, the Environmental Protection Agency may exempt a source from this retrofit requirement on the grounds that the source does not emit pollutants that cause or contribute to significant visibility impairment in Class I areas. Although the main focus of the visibility protection section (No. 169A) is on existing sources, other sections of the 1977 Clean Air Act Amendments require that new-source reviews demonstrate that the emissions from a proposed major facility do not cause "an adverse impact on the air quality related values (including visibility)" of Class I areas.

This report describes a nine-month study performed by Systems Applications, Incorporated (SAI) for the Environmental Protection Agency to recommend and develop models that predict the contribution of man-made air pollution to visibility impairment in Class I areas. As shown in Figure 1, this study was divided into three main phases, consisting of seven tasks:

> Model formulation
  - Recommendations for modeling approaches.
  - Collection and analysis of data to characterize existing visibility impairment.

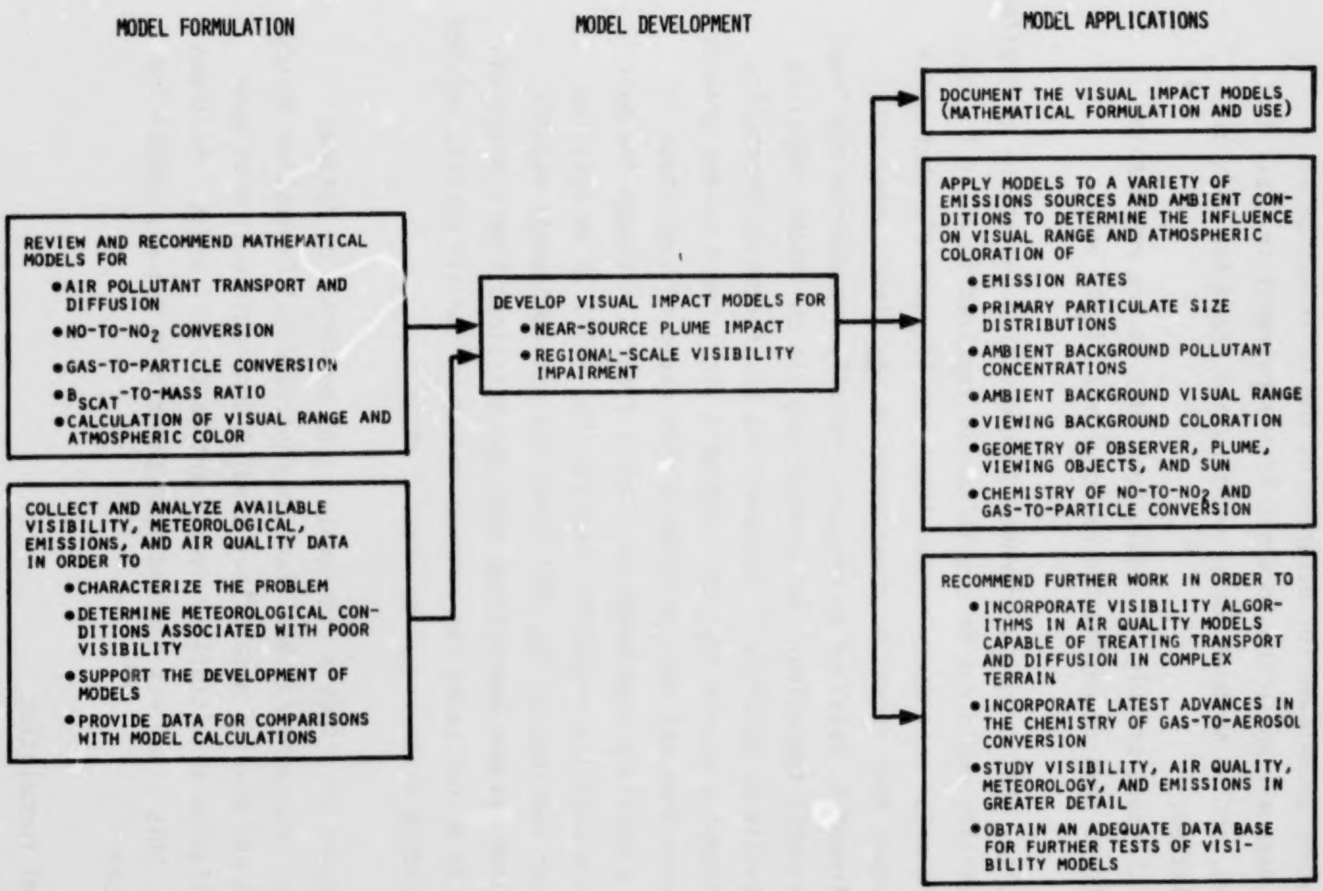
MODEL FORMULATION
MODEL DEVELOPMENT
MODEL APPLICATIONS
REVIEW AND RECOMMEND MATHEMATICAL MODELS FOR
•AIR POLLUTANT TRANSPORT AND DIFFUSION
•NO-TO-$NO_2$ CONVERSION
•GAS-TO-PARTICLE CONVERSION
•$B_{SCAT}$-TO-MASS RATIO
•CALCULATION OF VISUAL RANGE AND ATMOSPHERIC COLOR
COLLECT AND ANALYZE AVAILABLE VISIBILITY, METEOROLOGICAL, EMISSIONS, AND AIR QUALITY DATA IN ORDER TO
•CHARACTERIZE THE PROBLEM
•DETERMINE METEOROLOGICAL CONDITIONS ASSOCIATED WITH POOR VISIBILITY
•SUPPORT THE DEVELOPMENT OF MODELS
•PROVIDE DATA FOR COMPARISONS WITH MODEL CALCULATIONS
DEVELOP VISUAL IMPACT MODELS FOR
•NEAR-SOURCE PLUME IMPACT
•REGIONAL-SCALE VISIBILITY IMPAIRMENT
DOCUMENT THE VISUAL IMPACT MODELS (MATHEMATICAL FORMULATION AND USE)
APPLY MODELS TO A VARIETY OF EMISSIONS SOURCES AND AMBIENT CONDITIONS TO DETERMINE THE INFLUENCE ON VISUAL RANGE AND ATMOSPHERIC COLORATION OF
•EMISSION RATES
•PRIMARY PARTICULATE SIZE DISTRIBUTIONS
•AMBIENT BACKGROUND POLLUTANT CONCENTRATIONS
•AMBIENT BACKGROUND VISUAL RANGE
•VIEWING BACKGROUND COLORATION
•GEOMETRY OF OBSERVER, PLUME, VIEWING OBJECTS, AND SUN
•CHEMISTRY OF NO-TO-$NO_2$ AND GAS-TO-PARTICLE CONVERSION
RECOMMEND FURTHER WORK IN ORDER TO
•INCORPORATE VISIBILITY ALGORITHMS IN AIR QUALITY MODELS CAPABLE OF TREATING TRANSPORT AND DIFFUSION IN COMPLEX TERRAIN
•INCORPORATE LATEST ADVANCES IN THE CHEMISTRY OF GAS-TO-AEROSOL CONVERSION
•STUDY VISIBILITY, AIR QUALITY, METEOROLOGY, AND EMISSIONS IN GREATER DETAIL
•OBTAIN AN ADEQUATE DATA BASE FOR FURTHER TESTS OF VISIBILITY MODELS

FIGURE 1. OUTLINE OF SAI'S STUDY TO DEVELOP MODELS FOR PREDICTING VISIBILITY IMPAIRMENT

- > Model development
  - Near-source plume visibility model.
  - Regional, multiple source visibility model.
- > Model applications
  - Documentation of models.
  - Application of models to typical emission, meteorological, and ambient conditions.
  - Recommendations for further work.
  - Information for the Report to Congress.

Two basic types of models were developed for the prediction of visibility impairment caused by anthropogenic pollutant emissions. One is a near-source plume model, applicable to a wide range of emission, meteorological, and ambient conditions, that is based on a Gaussian formulation. This model is designed to estimate plume concentrations and visual effects on a spatial scale of up to 350 km. The other is a regional-scale model designed to estimate pollutant concentrations and visual effects in the Northern Great Plains over a spatial scale of 1000 km. Both models calculate the reduction in visual range and the atmospheric discoloration resulting from directly emitted primary particulate matter and from nitrogen dioxide, sulfates, and nitrates formed in the atmosphere from pollutant precursors.

The goal of this development is models that are useful predictive tools for making policy and regulatory decisions, for evaluating the impact of proposed new sources, and for determining the amount of emissions reduction required from existing sources. Figure 2 shows the elements and potential uses of visibility models. The critical decisions that must be made in the future regarding the definition of "significant visibility impairment" cannot be made without a basic understanding of the implications for enforcement in new and existing source reviews, and, in particular, the impact on energy development in the western United States. We believe that visibility issues will have a significant influence on the siting and design of new coal-fired power plants in

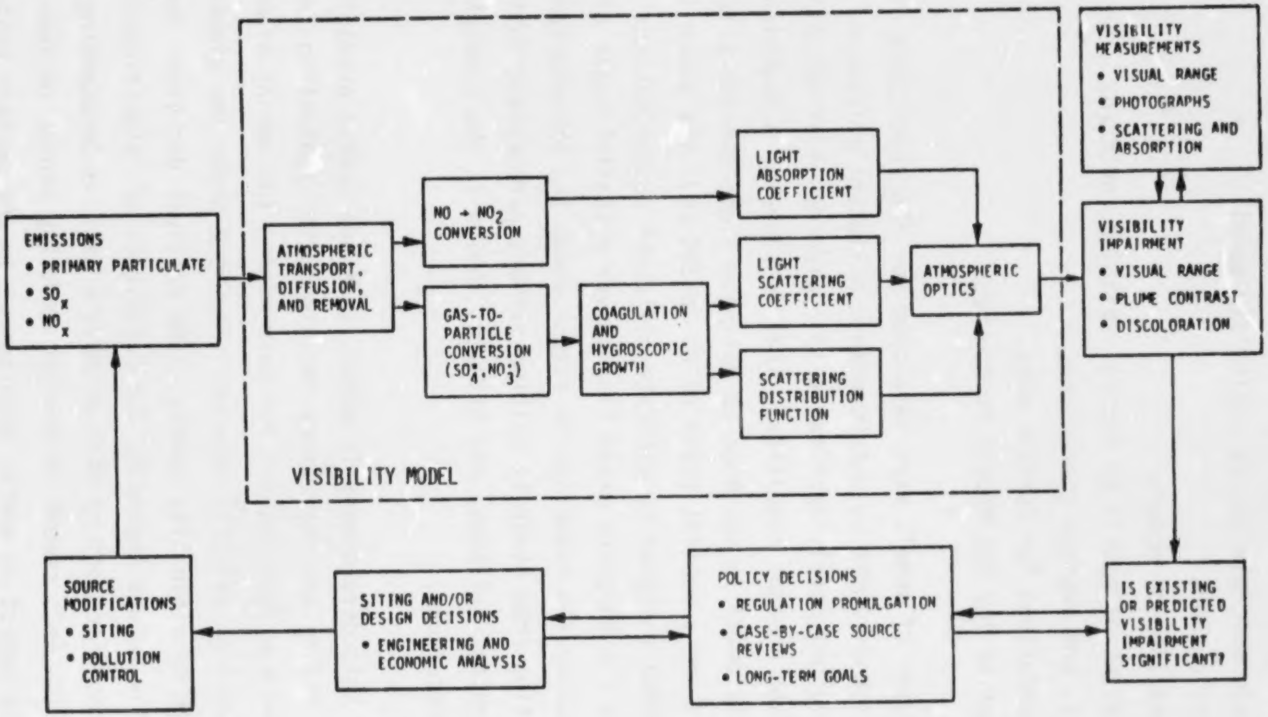
EMISSIONS
• PRIMARY PARTICULATE
• $SO_x$
• $NO_x$
ATMOSPHERIC TRANSPORT, DIFFUSION, AND REMOVAL
$NO \rightarrow NO_2$ CONVERSION
GAS-TO-PARTICLE CONVERSION ($SO_4^=$, $NO_3^-$)
COAGULATION AND HYGROSCOPIC GROWTH
LIGHT ABSORPTION COEFFICIENT
LIGHT SCATTERING COEFFICIENT
SCATTERING DISTRIBUTION FUNCTION
ATMOSPHERIC OPTICS
VISIBILITY MODEL
VISIBILITY MEASUREMENTS
• VISUAL RANGE
• PHOTOGRAPHS
• SCATTERING AND ABSORPTION
VISIBILITY IMPAIRMENT
• VISUAL RANGE
• PLUME CONTRAST
• DISCOLORATION
IS EXISTING OR PREDICTED VISIBILITY IMPAIRMENT SIGNIFICANT?
POLICY DECISIONS
• REGULATION PROMULGATION
• CASE-BY-CASE SOURCE REVIEWS
• LONG-TERM GOALS
SITING AND/OR DESIGN DECISIONS
• ENGINEERING AND ECONOMIC ANALYSIS
SOURCE MODIFICATIONS
• SITING
• POLLUTION CONTROL

FIGURE 2. ELEMENTS AND POTENTIAL USES OF VISIBILITY MODELS

the West and on the evaluation of retrofit requirements for existing plants. Thus, modeling of visibility impairment is likely to become an integral part of the environmental assessment of new and existing sources, providing a basis for major siting and pollution control decisions in the future.

This report contains five chapters and seven appendices. Chapter II discusses the nature of existing visibility impairment in Class I areas, with particular emphasis on the western United States. The elements of the visibility models are discussed in Chapter III, and a summary of the plume and regional models and their output is given in Chapter IV. Chapter V discusses our recommendations for future work. Appendix A presents the details of our analysis of visibility data in the western United States, and Appendix B, the details of the atmospheric optics calculations. Appendix C discusses sulfate formation in the atmosphere, Appendix D describes the plume model, and Appendix E shows plume model calculations and the results of a sensitivity analysis. Appendices F and G describe the Northern Great Plains regional model and calculations for seven scenarios. The appendices are bound separately in Volume II. Volume III presents a series of case studies of power plant plume visual impact for a number of emission, meteorological, and ambient background scenarios.

# II THE NATURE OF VISIBILITY IMPAIRMENT

"Visibility impairment" must be defined before discussing the components of the mathematical models used to predict anthropogenic visibility impairment and the specific plume and regional visibility models developed as a part of this study. This chapter defines and classifies "visibility impairment" by type, magnitude, spatial and temporal extent, and cause, and it provides examples of visibility impairment. The fundamental physical concepts of visibility impairment are also briefly discussed, and the analysis of visual range data from the Southwest and the Northern Great Plains is summarized; this material is presented in more detail in Appendix A.

## A. DEFINITION OF VISIBILITY IMPAIRMENT

"Visibility impairment" has been defined generally by Congress in the Clean Air Act Amendments of 1977 as a "reduction in visual range" or an "atmospheric discoloration," but the term must be defined more precisely and illustrated by examples before we discuss the models and quantitative specifications of visibility impairment.

Visibility impairment can be defined and classified according to:

- Type (e.g., the appearance of distant objects, general haziness, yellow-brown or grey discoloration).
- Magnitude (e.g., visual range, degree of coloration, contrast, "any" or "significant" impairment of visibility in the terminology of the Clean Air Act Amendments).
- Spatial extent (e.g., localized plume appearance, uniform haze, distance downwind of source).
- Temporal extent (frequency of occurrence of reduced visual range or of discoloration).

> Location relative to Class I areas (impact on a vista from a Class I area or on a vista looking into a Class I area).
> Cause (natural or man-made aerosols of coarse particulate matter, sulfate, nitrate, organics, soot, or nitrogen dioxide gas).

The term "visibility" is generally used synonymously with "visual range," meaning the farthest distance at which one can see a large, black object against the sky at the horizon. One can make subjective evaluations of "visibility" every time he views objects outdoors. Although large black objects are not generally available for observing and evaluating visual range, dark objects such as buildings, TV towers, hills, or mountains can be viewed against the horizon sky.

Even if no distant objects are within view, subjective judgments about visual range can be made by noting the coloration and light intensity of the sky and nearby objects. For example, one perceives reduced visual range if a distant mountain that is usually visible cannot be seen, if nearby objects look "hazy" or have diminished contrast, or if the sky is white, grey, yellow, or brown rather than blue.

Figure 3 shows an example of reduced visual range in Marble Canyon in northern Arizona. As shown by this photograph, reduced visual range is detectable because the distant walls of the canyon are difficult to distinguish. The contrast between the given object (part of the canyon) and the background (the horizon or a more distant terrain feature) is reduced by light scattered from particles in the intervening atmosphere. Also, even if terrain features were not visible, the intensity and the yellowish coloration of the scattered light would degrade the aesthetic quality of the atmosphere. Many of the Class I areas (e.g., national parks, national forests, wilderness areas) were so designated because of their scenic views of such distant terrain features as mountains, canyon walls, plateaus, and buttes. Indeed, in the western United States, where most of the Class I areas are located, spectacular scenery is enhanced by generally excellent visibility, which makes the colorful terrain features stand out with great

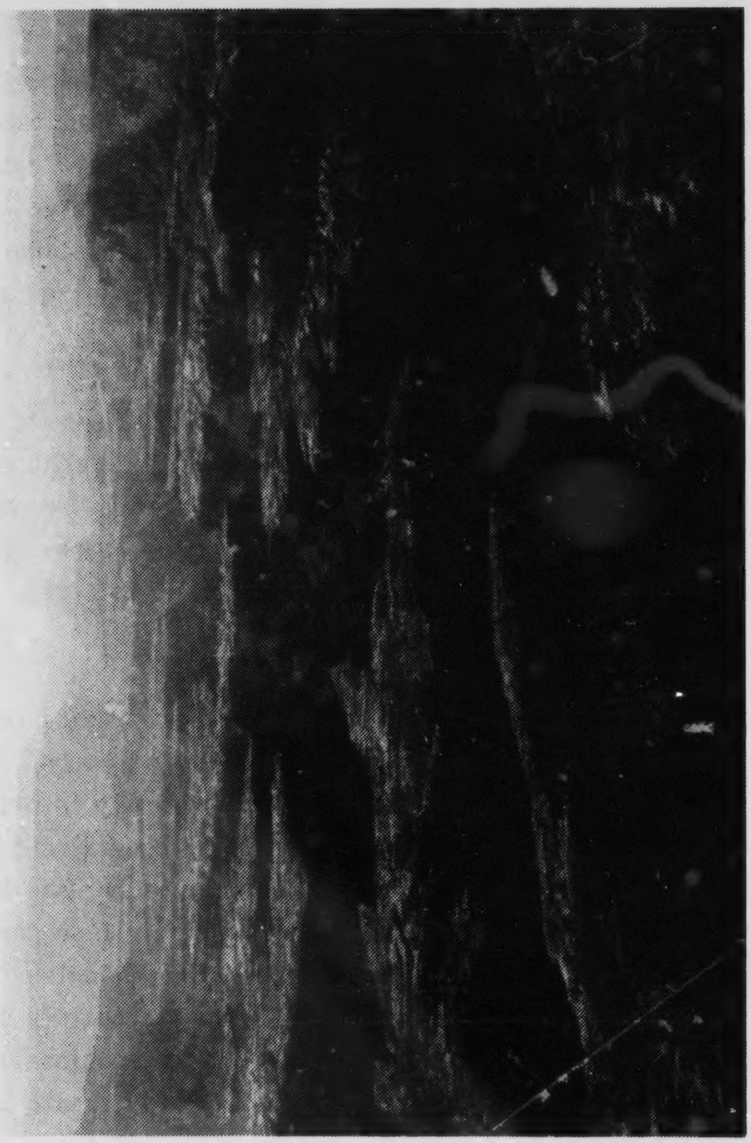

FIGURE 3. AN EXAMPLE OF REDUCED VISUAL RANGE: MARBLE CANYON, ARIZONA

clarity. However, even in flat areas (e.g., the Big Sky Country of the Northern Great Plains), a slight reduction in visual range or a slight atmospheric discoloration can change what originally appeared to be an "infinite" horizon to a less desirable white, yellow, grey, or brown horizon.

The magnitude of impairment can be characterized by the reduction in visual range from some reference value, by a reduction in contrast between an object and the horizon sky at a known distance from the observer, or by a shift in coloration or light intensity of the sky or distant objects, such as clouds or terrain features, compared with what is perceived on a "clear" day. In all cases, the magnitude of visibility impairment can be characterized by the change in light intensity or coloration of an object (or part of the sky) compared with that of some reference object. For example, a distant mountain is visible because the intensity and coloration of light from the mountain is different from that of the horizon sky. Another example is a plume or haze layer seen against the background sky or terrain features. The pollution is visible only if the light intensity or coloration of the plume contrasts with that of the surrounding sky or terrain.

The most subjective impairment observation occurs when an observer compares the appearance of the sky or distant terrain features on a hazy day with recollections of what it was on a clear day in the past. Examples of such subjective comparisons are those of old-timers who recall that visibility used to be much better. Although these observations cannot be discounted entirely, it is possible that such judgments may be the result of nostalgia or poor memory.

The spatial extent of visibility impairment is important to both the perception and the significance of impairment to observers in Class I areas. The sensitivity of an observer to brightness and color differences between two objects depends on the geometric relationship between the objects. If each of the objects is uniformly colored and there is a sharp line of demarcation between the objects, such as when a mountain is viewed against a horizon sky, a smaller change in light intensity or color can be perceived than if the boundary between the two objects is vague, as in the case of a plume viewed against the horizon sky. If the observer is located in a uniformly colored atmosphere, atmospheric discoloration is perceived, not by comparison of two colored fields, but by comparison with his recollection of a clear atmosphere.

Figure 4 provides an example of near-source visibility impairment. The spatial extent of visibility impairment is defined by the dimensions of the plume. The plume is visible because the light intensity and color of the plume are different from those of the clouds in the background. Because of the resultant relatively sharp boundary between the plume and the background, the visual impact on the observer is dramatic. Figure 5 shows another example of the importance of the spatial extent of impairment on its perceptibility. In that photograph, the haze layer is clearly visible because of the sharp demarcation line between it and the layer of clean air above it.

The temporal extent (or the frequency of occurrence) of visibility impairment) is of great importance in determining the acceptability of air pollution levels. The frequency of occurrence of impairment could be characterized by stating the number of days or hours in a year that the magnitude of visibility impairment is greater than some standard. Using these data, one might state that at a given location it is acceptable for visual range to be less than y km for x percent of the daylight hours.

The location of visibility impairment is extremely important in terms of visibility protection legislation because the law states that only the visibility in Class I areas is to be protected and restored. We assume that this definition can include impairment caused by pollution outside of a Class I area that is visible within a Class I area. In areas with excellent background visibility, visual degradation perceived by an observer in a Class I area could be caused by pollution many kilometers away. It is not

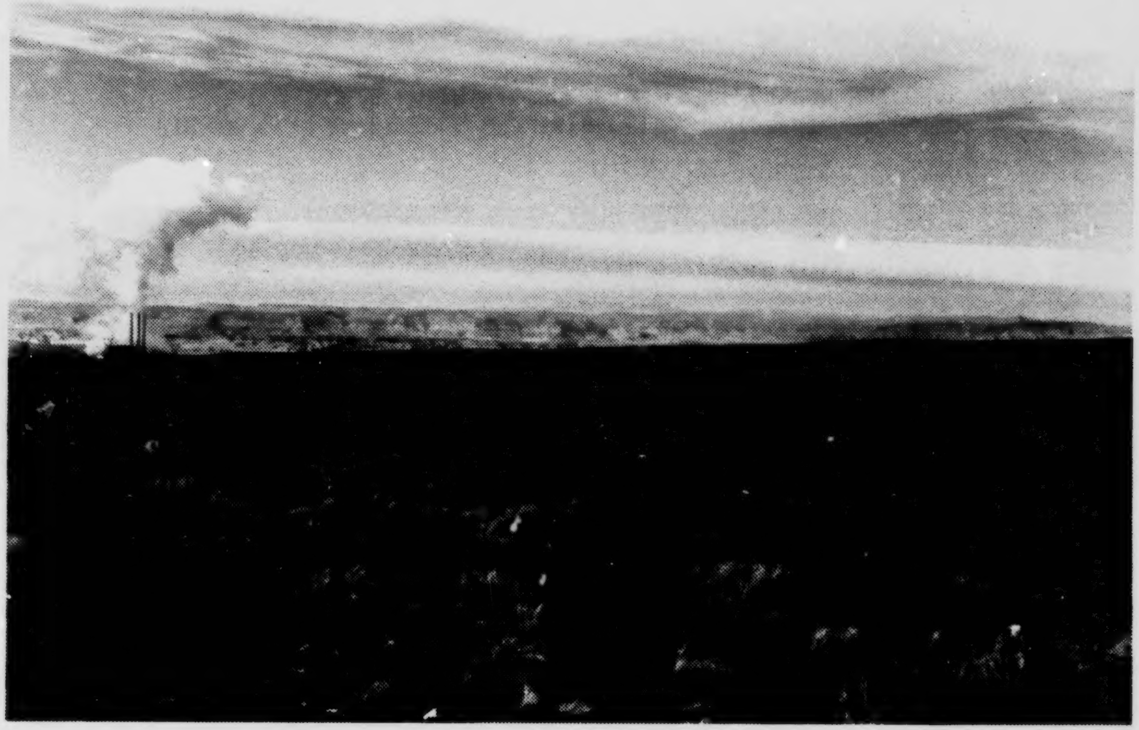

FIGURE 4. AN EXAMPLE OF NEAR-SOURCE VISIBILITY IMPAIRMENT: PLUME DISCOLORATION DOWNWIND OF THE NAVAJO GENERATING STATION IN NORTHERN ARIZONA

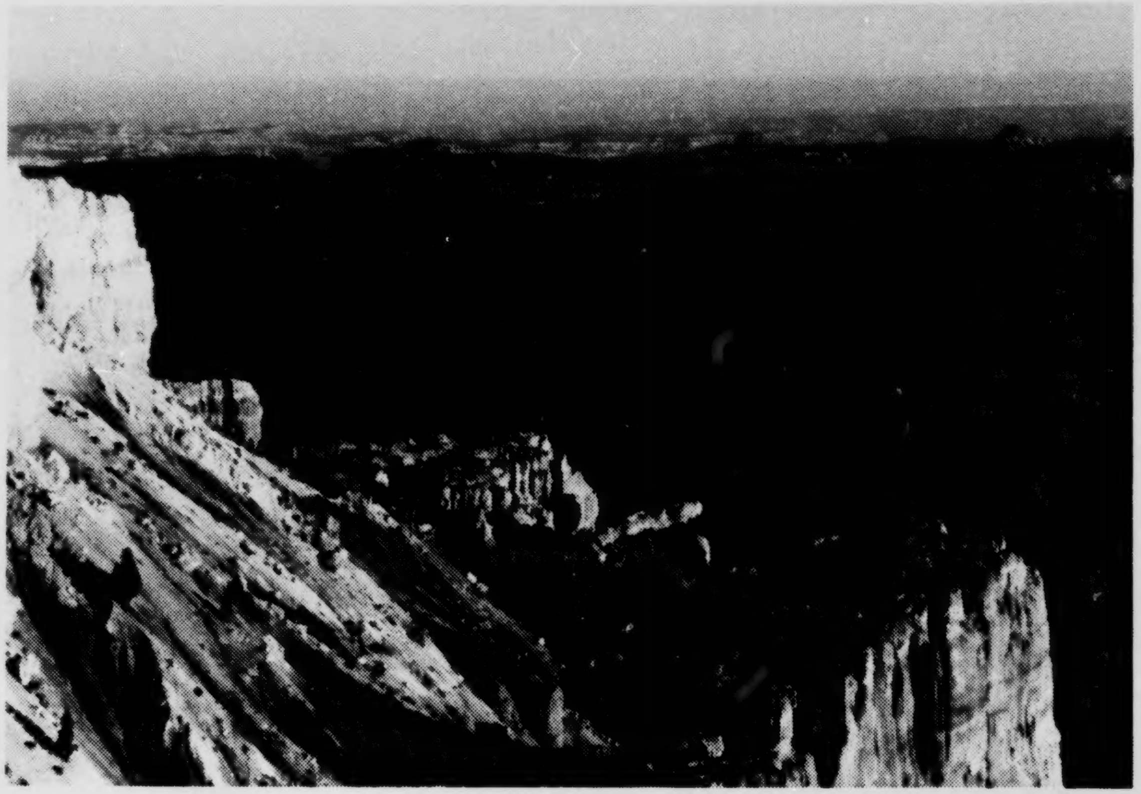

FIGURE 5. AN EXAMPLE OF VISIBILITY IMPAIRMENT: A UNIFORM HAZE LAYER VISIBLE FROM BRYCE CANYON NATIONAL PARK

5

clear whether Congress meant to protect the visibility in Class I areas from such distant pollutants.

Finally, perhaps the most important classification of visibility impairment is by cause, in particular, whether the cause is natural or anthropogenic sources. Clearly, Congress has been concerned only with anthropogenic visibility impairment. Reductions in visual range caused by precipitation, fog, clouds, windblown dust, sand, snow, or "natural" aerosol are natural occurrences and cannot be controlled by man. Indeed, some natural visibility impairment may contribute to the enjoyment of Class I areas. Examples of such phenomena are the blue haze of the Great Smoky Mountains and the fog and hazes along the California and Oregon coast.

Assessment of anthropogenic contributions to visibility impairment can be difficult when background visibility varies spatially and temporally and when natural atmospheric constituents interact with anthropogenic emissions to create a combined effect, such as that of the haze formed when anthropogenically emitted hygroscopic particles absorb liquid water in the atmosphere. For the purpose of discussion only, the Venn diagram in Figure 6 shows the frequency of occurrence of visibility impairment, which is defined here as visual range less than 80 km (50 miles). Some natural causes of visibility impairment, such as windblown dust, precipitation, fog, and cloud cover, are represented by circles whose total areas and areas of overlap represent the frequency of occurrence of the given phenomenon and the associations among phenomena. Note in Figure 6 that fog always causes visibility impairment and precipitation usually does. In this highly schematic representation, the diagonally lined area represents the fraction of time that man-made emissions cause or contribute to visibility impairment. In actual situations, it is difficult to separate the relative magnitudes of natural and man-made contributions to

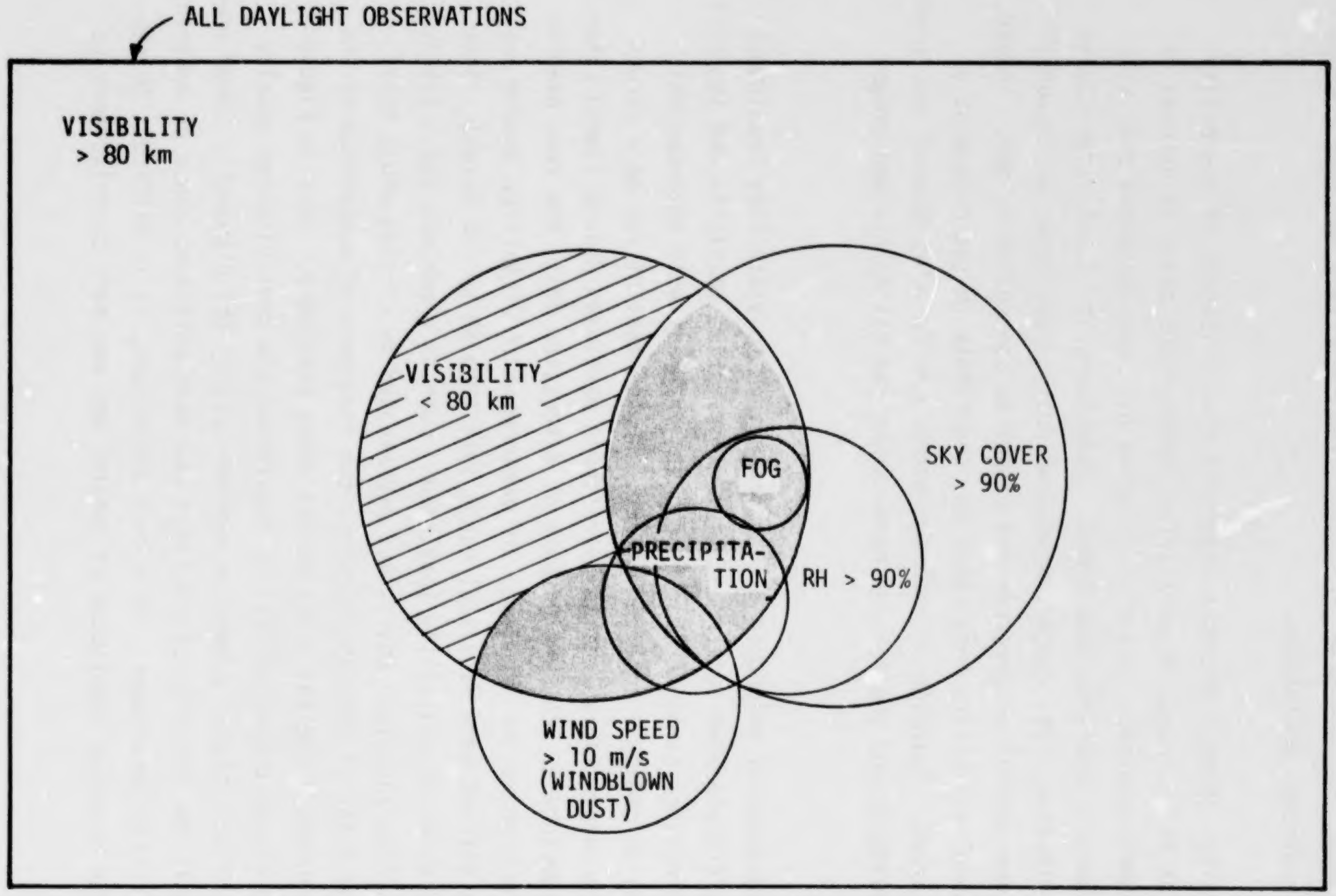
ALL DAYLIGHT OBSERVATIONS
VISIBILITY > 80 km
VISIBILITY < 80 km
FOG
SKY COVER > 90%
PRECIPITATION
RH > 90%
WIND SPEED > 10 m/s (WINDBLOWN DUST)

FIGURE 6. NATURAL CAUSES OF VISIBILITY IMPAIRMENT

visibility impairment. For example, as noted above, during humid conditions, natural and anthropogenic hygroscopic particles may absorb water, thereby causing visibility impairment. Because the atmosphere is a complex system consisting of both natural and anthropogenic aerosol, the contribution of man-made pollution to visibility impairment may be difficult to characterize by measurements. The causes of visibility impairment are discussed in further detail in the sections below from both fundamental and phenomenological viewpoints.

## B. FUNDAMENTAL CAUSES OF VISIBILITY IMPAIRMENT

Visibility impairment is caused by the following interactions in the atmosphere:

- Light scattering
  - By molecules of air
  - By particles
- Light absorption
  - By gases
  - By particles.

Light scattering by gaseous molecules of air (Rayleigh scattering), which causes the blue color of the atmosphere, is dominant when the air is relatively free of aerosols and light-absorbing gases. Light scattering by particles is the most important mechanism causing reductions in visual range. Fine solid or liquid particulates whose diameters range from 0.1 to 1.0 μm (the most effective size per unit mass in scattering light) account for most of atmospheric light scattering. Light absorption by gases is particularly important in the discussion of anthropogenic visibility impairment because nitrogen dioxide, a major constituent of power plant plumes, absorbs light. Nitrogen dioxide is reddish-brown because it absorbs strongly at the blue end of the visible spectrum while allowing light at the red end to pass through. Light absorption by particles is important when black soot (finely divided carbon) is present. However, most atmospheric particles are not generally considered to be light absorbers.

Anthropogenic contributions to visibility impairment result from the emission of primary particulate matter (such as fly ash, acid, or water droplets, soot, and fugitive dust) and of pollutant precursors that are converted in the atmosphere to the following secondary species:

- > Nitrogen dioxide ($NO_2$) gas, from emissions of nitric oxide (NO).
- > Sulfate ($SO_4^=$) particles, from $SO_x$ emissions.
- > Nitrate ($NO_3^-$) particles, from $NO_x$ emissions.
- > Organic particles, from hydrocarbon and $NO_x$ emissions.

Before particulate control technology was commonly employed, primary particulate matter, such as smoke, windblown dust, and soot, was a major contributor to visibility impairment. Coal-fired power plants emit primary particles of fly ash and combustion-generated particulates to the atmosphere. If such plants are equipped with efficient precipitators or other abatement equipment, the emission rate of primary particles may be small. However, some emissions escape the control equipment and do contribute to the ambient particulate concentration and hence to general visibility impairment. If the emission rate of primary particulates is sufficiently large, the plume itself may be visible.

In the past, many of the older coal-fired power plants generated conspicuous, visible plumes resulting from the large emission rates of primary particulate matter. Old plants still in operation and newer plants have benefited from more efficient particulate abatement equipment and a state-of-the-art that has reached the point where particulate removal efficiencies in excess of 99 percent are commonly specified and achieved. In addition, with the installation of flue gas desulfurization systems (scrubbers) and with boiler combustion modifications, sulfur dioxide and nitrogen oxide emissions have also been reduced. As a result, the visual impact of power plant plumes has been sharply reduced, as evidenced by the nearly invisible plumes of modern coal-fired power plants. Unfortunately, however, the contribution to visibility impairment of the secondary pollutants--nitrogen dioxide gas and sulfate, nitrate, and organic aerosol--is now becoming increasingly evident and is of growing concern.

Since nitrogen dioxide absorbs light selectively, it can discolor the atmosphere, causing a yellow or brown plume when present in sufficient concentrations. Almost all of the nitrogen oxide emitted from power plant stacks is nitric oxide, a colorless gas. But chemical reactions in the atmosphere can oxidize a substantial portion of the colorless NO to the reddish-brown $NO_2$.

Secondary sulfate, nitrate, and organic particles have a dominating effect on visual range in many situations because these particles range in size between 0.1 and 1.0 µm in diameter, which is the most efficient size per unit mass for light scattering. As is noted later, submicron aerosol (with diameters in the range from 0.1 to 1.0 µm) is 10 times more effective in light scattering than the same mass of coarse (> 1 µm) aerosol. Also, because secondary aerosol forms slowly in the clean atmospheres typical of Class I areas in the western United States, maximum aerosol concentrations and associated visibility impairment may occur at large distances from emissions sources. We discuss this problem further in Section C, which concerns visual range observations in the West, and in the chapters that describe the models.

The effect of the intervening atmosphere on the visibility and coloration of a viewed object (e.g., the horizon sky, a mountain, a cloud) can be calculated by solving the radiation transfer equation along the line of sight. As we noted in Section A, visibility impairment can be quantified by comparing the intensity or the coloration of two objects (e.g., a distant mountain against the horizon sky). The effect of the intervening atmosphere on the light intensity, as a function of wavelength, of the viewed object can be determined if the concentration and characteristics of air molecules, aerosol, and nitrogen dioxide are known along the line of sight.

The change in spectral light intensity $I(\lambda)$ as a function of distance along the sight path at any point in the atmosphere, neglecting multiple scattering (see Figure 7), can be calculated as:

$$\frac{dI(\lambda)}{dr} = -b_{ext}(\lambda)I(\lambda) + \frac{p(\lambda,\Theta)}{4\pi} b_{scat}(\lambda)\, F_s(\lambda) \quad , \qquad (1)$$

where

$r$ = the distance along the sight path from the object to the observer,

$p(\Theta)$ = the scattering distribution function for scattering angle $\Theta$ [see glossary and Figure 7(a) for definitions],

$F_s$ = the solar flux (watts/$m^2$) incident on the atmosphere,

$b_{scat}$ = the sum of the Rayleigh scattering (due to air molecules) and the scattering due to particles:

$$b_{scat}(\lambda) = b_R(\lambda) \text{ and } b_{sp}(\lambda) \quad , \qquad (2)$$

$b_{ext}$ = the sum of the scattering and absorption coefficients:

$$b_{ext}(\lambda) = b_{scat}(\lambda) + b_{abs}(\lambda) \quad . \qquad (3)$$

On the right-hand side of Eq. (1), the first term represents light absorbed or scattered out of the line of sight; the second term represents light scattered into the line of sight. The values of $b_{scat}$ and $b_{ext}$ can be evaluated if the aerosol and $NO_2$ concentrations and such characteristics as the refractive index and the size distribution of the aerosol are known. Except in the cleanest atmospheres, $b_{scat}$ is dominated by $b_{sp}$: also, unless soot is present, $b_{abs}$ is dominated by the absorption coefficient due to

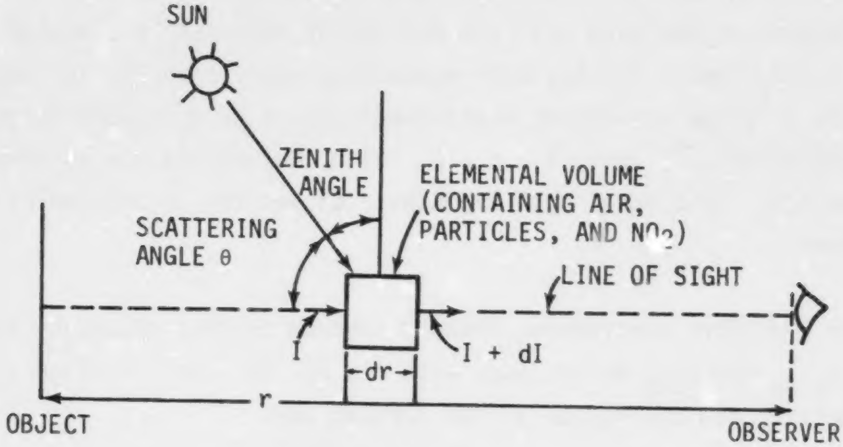
SUN
ZENITH ANGLE
ELEMENTAL VOLUME (CONTAINING AIR, PARTICLES, AND $NO_2$)
SCATTERING ANGLE θ
LINE OF SIGHT
I
I + dI
dr
r
OBJECT
OBSERVER

(a) Geometry

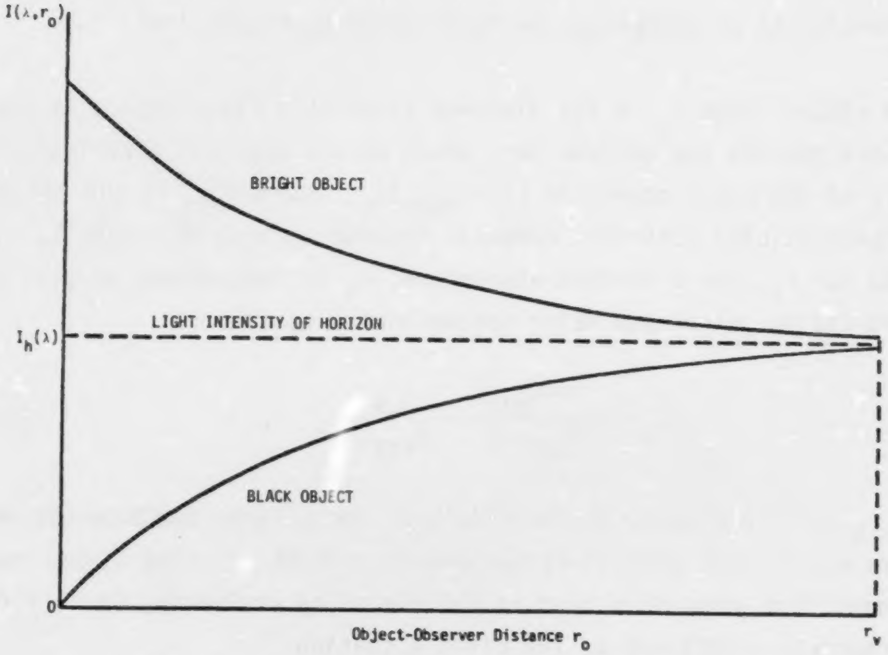

(b) Visual Range $r_v$ (Homogeneous Atmosphere)

FIGURE 7. EFFECT OF AN ATMOSPHERE ON THE PERCEIVED LIGHT INTENSITY OF OBJECTS

$NO_2$. Scattering and absorption are wavelength-dependent, with effects being largest at the blue end ($\lambda = 0.4$ μm) of the visible spectrum ($0.4 < \lambda < 0.7$ μm). The Rayleigh scattering coefficient $b_R$ is proportional to $\lambda^{-4}$; the scattering coefficient caused by particles is generally proportional to $\lambda^{-n}$, where $1 < n < 2$. Also, $NO_2$ absorption is greatest at the blue end. This wavelength dependence causes the coloration of the atmosphere.

For a uniform atmosphere, without inhomogeneities caused by plumes (where $b_{scat}$ and $b_{ext}$ do not vary with r), Eq. (1) can be solved to find the intensity and coloration of the horizon sky:

$$I_h(\lambda) = \frac{p(\lambda,\Theta)}{4\pi} \frac{b_{scat}(\lambda)}{b_{ext}(\lambda)} F_s(\lambda) \quad . \tag{4}$$

The perceived intensity of distant bright and dark objects will approach this intensity as an asymptote, as illustrated by Figure 7(b).

The visual range $r_v$ is the distance at which a black object is barely perceptible against the horizon sky, which occurs when the perceived light intensity of the black object is $(1 - C_{min})I_h$, where $C_{min}$ is the liminal (barely perceptible) contrast, commonly assumed to be 0.02. When Eq. (1) is solved for $r_v$, for a uniform atmosphere, $r_v$ is independent of $p(\Theta)$ and $F_s(\lambda)$ and can be calculated using Koschmieder's equation:

$$r_v = \frac{\ell n(C_{min})}{b_{ext}(\lambda)} = \frac{3.912}{b_{ext}(\lambda)} \quad , \tag{5}$$

where $b_{ext}(\lambda)$ is evaluated at the middle of the visible spectrum (to which the human eye is most sensitive) and where $\lambda = 0.55$ μm. The visual range for a nonuniform atmosphere must be calculated by evaluating Eq. (1) for the appropriate conditions of the given situation.

Atmospheric coloration is determined by the wavelength-dependent scattering and absorption in the atmosphere. The spectral distribution of $I(\lambda)$ for $\lambda$ over the visible spectrum determines the perceived color and light intensity of the viewed object. The relative contributions of scattering (aerosols plus Rayleigh) and absorption ($NO_2$) to coloration can be illustrated by rearranging Eq. (1):

$$\frac{1}{I(\lambda)}\,\frac{dI(\lambda)}{dr} = b_{scat}(\lambda)\left[\frac{\frac{p(\lambda,\Theta)}{4\pi}\,F_s(\lambda)}{I(\lambda)} - 1\right] - b_{abs}(\lambda) \quad . \tag{6}$$

Note from Eq. (4) that when light absorption is negligible compared with light scattering the clear horizon intensity is simply:

$$I_{h0}(\lambda) = \frac{p(\lambda,\Theta)\,F_s(\lambda)}{4\pi} \quad . \tag{7}$$

We now can rewrite Eq. (6):

$$\frac{1}{I(\lambda)}\,\frac{dI(\lambda)}{dr} = b_{scat}(\lambda)\left[\frac{I_{h0}(\lambda)}{I(\lambda)} - 1\right] - b_{abs}(\lambda) \quad . \tag{8}$$

Equation (8) is thus an expression relating the effects of light scattering and light absorption to the change in spectral light intensity with distance along a sight path. On the right-hand side of Eq. (8) the first term is the effect of light scattering (aerosol plus Rayleigh), and the second term is the effect of light absorption ($NO_2$). As noted previously, since $b_{scat}$ and $b_{abs}$ (due to $NO_2$) are strong functions of wavelength and are larger at the blue end ($\lambda = 0.4\ \mu m$) of the spectrum than the red end ($\lambda = 0.7\ \mu m$), coloration can result.

Equation (8) makes clear that $NO_2$ always tends to cause a decrease in light intensity and a yellow-brown coloration by preferentially absorbing blue light, whereas particles may cause a blue-white or a yellow-brown coloration, depending on the value of the quantity in the brackets. If, at a given point along the sight path, $I(\lambda)$ is greater than the "clean" horizon sky intensity $I_{h0}(\lambda)$, then the quantity in brackets in the first term on the right-hand side of Eq. (8) will be negative, which means that the net effect of scattering will be to remove predominantly blue light from the line of sight. This effect would occur when a bright, white cloud or distant snowbank was observed through an aerosol not containing $NO_2$; scattering would cause a yellow-brown coloration. If, however, $I(\lambda)$ is less than $I_{h0}(\lambda)$, then the quantity in brackets in Eq. (8) will be positive, which means that the net effect of scattering will be to add predominantly blue light into the line of sight. This effect would occur when a distant, dark mountain was observed through an aerosol not containing $NO_2$; scattering would cause the mountain to appear lighter and bluish. Only light absorption can cause $I_h(\lambda)$ to be less than $I_{h0}(\lambda)$, and whenever $I(\lambda) \leq I_{h0}(\lambda)$, scattering will add light to the sight path, thereby masking the coloration caused by $NO_2$ light absorption.

Our visibility models are simply mathematical expressions for the solution to Eq. (1) for different boundary conditions and for different values of $b_{scat}$, $b_{ext}$, $p(\theta)$, and $F_s$, as they are affected by natural and man-made light scatterers and absorbers. We turn now from this fundamental viewpoint to a phenomenological viewpoint, with a summary of the results of an analysis of visual range in the western United States, before describing the elements and outputs of the plume and regional visibility models in Chapters III and IV.

## C. VISIBILITY IMPAIRMENT IN THE WESTERN UNITED STATES

In support of the development and validation of visibility models, we analyzed visibility data, including National Weather Service and National Park Service visibility observations, available nephelometer and telephotometer measurements, and photographs of power plant plumes. The overall objectives of the data analysis were:

- > To determine the magnitude, temporal and spatial variations, and natural and source-related causes of visibility impairment in the western United States.
- > To identify the meteorological and geographical conditions associated with visibility impairment.

Figure 8 shows the locations in the western United States of large point sources, mandatory federal Class I areas, and National Weather Service (NWS) stations from which meteorological data (including visual range) were analyzed. Three-hourly, daytime visual range observations for each of the 18 stations over the period from 1948 to 1976 were analyzed and were stratified by associated meteorological conditions--precipitation, surface wind speed and direction, atmospheric pressure, relative humidity, total sky cover, ceiling height, season, time of day, mixing depth, mixed layer wind speed, and ventilation--and by year--season, month, and time of day. The details and results of this analysis are presented in Appendix A.

Figure 9 displays the frequency distributions of extinction coefficients calculated from visual range observations at 13 NWS stations in 1976. Only observations made on days without precipitation or fog were used to compile these frequency distributions. Extinction coefficients were calculated from observed visual ranges using the Koschmieder relationship [see Eq. (5)].

Several interesting observations can be made on the basis of Figure 9. Median visual ranges for nonurban locations are on the order of 120 km or greater, corresponding to extinction coefficients less than $0.32 \times 10^{-4}$ $m^{-1}$. At nonurban locations the visual range is greater than 100 km nearly three-fourths of the time, and extinction coefficients appear to be asymptotically approaching a lower bound on the order of $0.2 \times 10^{-4}$ $m^{-1}$, which corresponds to a visual range of 196 km, or 122 miles. The dominant cause of the shape of the extinction coefficient frequency distribution in nonurban areas is the strong dependence of the scattering coefficient on relative humidity. This effect is due to the hygroscopic growth of submicron aerosol particles, thereby adding to aerosol mass, an effect discussed in greater detail in Appendices A and B.

Figure 10 summarizes the strong dependence of visual range on relative humidity at four locations in the Southwest. The frequency of occurrence of visual range greater than the indicated values decreases dramatically with relative humidity at all locations except Phoenix. In addition,

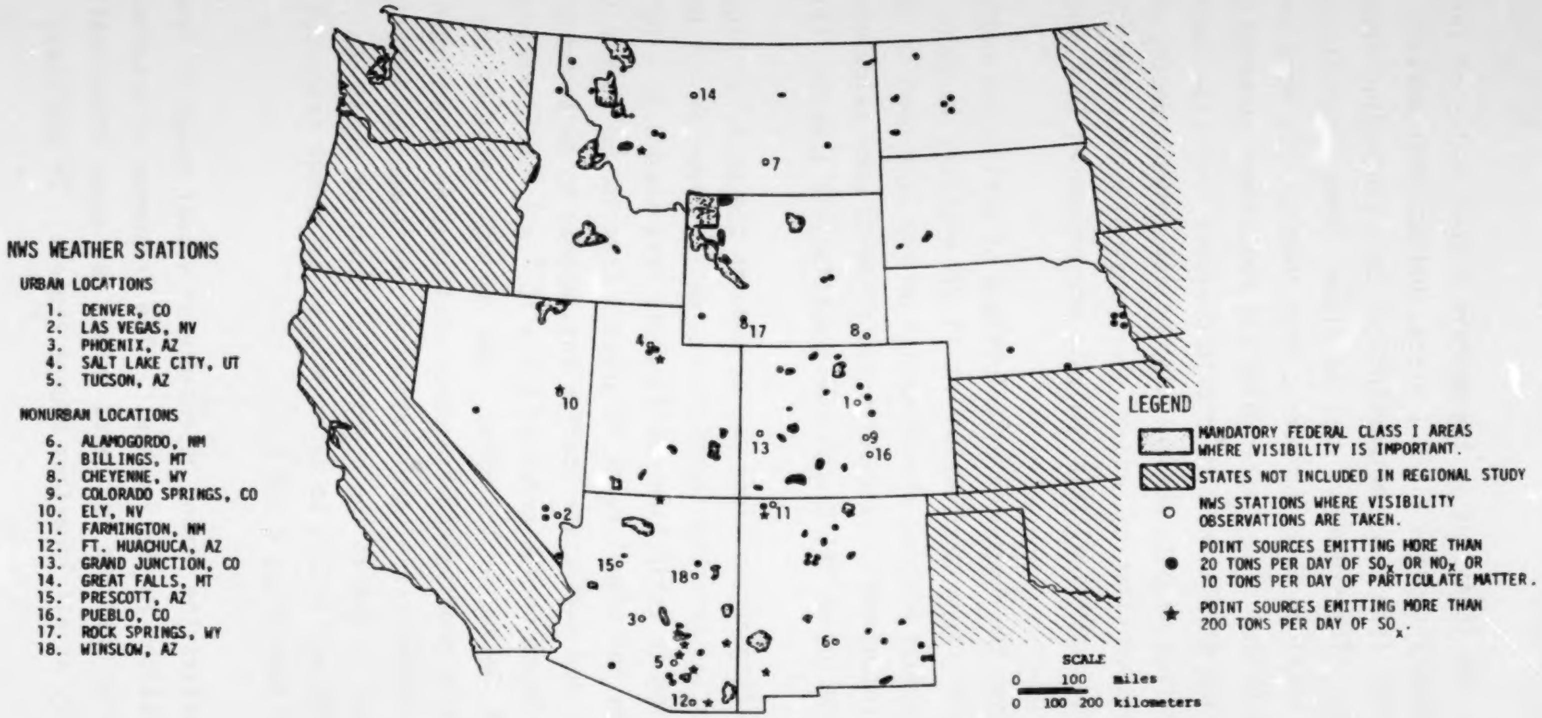
NWS WEATHER STATIONS
URBAN LOCATIONS
1. DENVER, CO
2. LAS VEGAS, NV
3. PHOENIX, AZ
4. SALT LAKE CITY, UT
5. TUCSON, AZ
NONURBAN LOCATIONS
6. ALAMOGORDO, NM
7. BILLINGS, MT
8. CHEYENNE, WY
9. COLORADO SPRINGS, CO
10. ELY, NV
11. FARMINGTON, NM
12. FT. HUACHUCA, AZ
13. GRAND JUNCTION, CO
14. GREAT FALLS, MT
15. PRESCOTT, AZ
16. PUEBLO, CO
17. ROCK SPRINGS, WY
18. WINSLOW, AZ
LEGEND
MANDATORY FEDERAL CLASS I AREAS WHERE VISIBILITY IS IMPORTANT.
STATES NOT INCLUDED IN REGIONAL STUDY
NWS STATIONS WHERE VISIBILITY OBSERVATIONS ARE TAKEN.
POINT SOURCES EMITTING MORE THAN 20 TONS PER DAY OF $SO_x$ OR $NO_x$ OR 10 TONS PER DAY OF PARTICULATE MATTER.
POINT SOURCES EMITTING MORE THAN 200 TONS PER DAY OF $SO_x$.
SCALE
0 100 miles
0 100 200 kilometers
1
2
3
4
5
6
7
8
9
10
11
12
13
14
15
16
17
18

FIGURE 8. MAP OF THE WESTERN UNITED STATES SHOWING THE LOCATIONS OF LARGE POINT SOURCES, MANDATORY FEDERAL CLASS I AREAS, AND NWS STATIONS WHERE VISIBILITY OBSERVATIONS ARE MADE

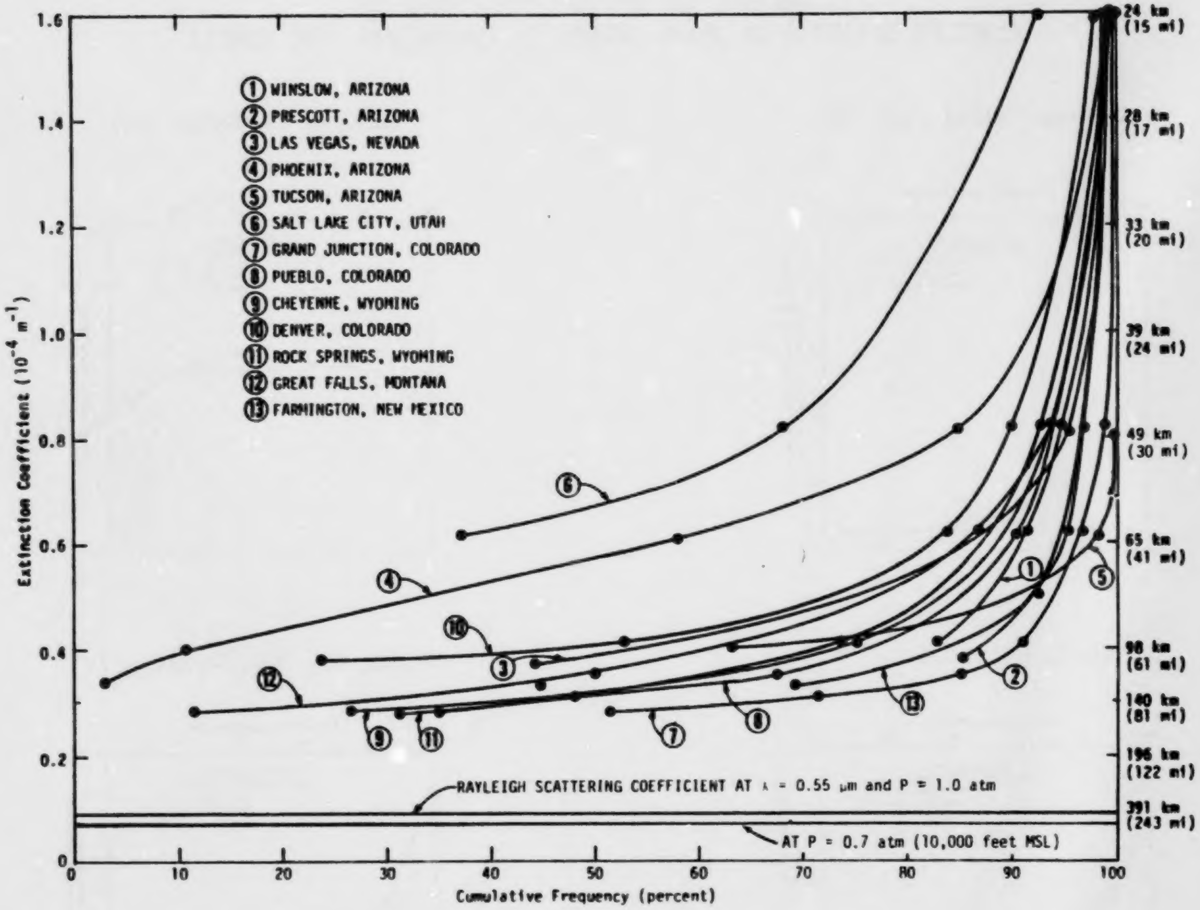

FIGURE 9. FREQUENCY DISTRIBUTIONS OF EXTINCTION COEFFICIENTS BASED ON VISUAL RANGE OBSERVATIONS AT 13 WESTERN U.S. LOCATIONS ON DAYS WITHOUT PRECIPITATION OR FOG IN 1976

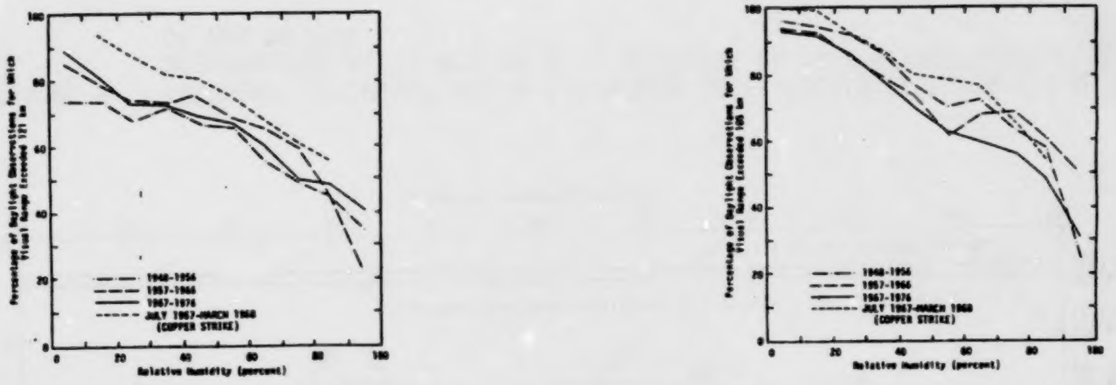

(a) Farmington, New Mexico

(b) Prescott, Arizona

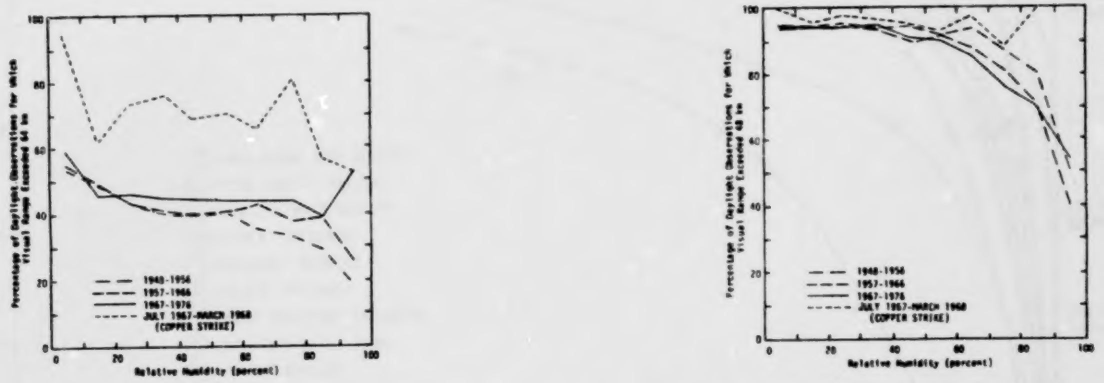

(c) Phoenix, Arizona

(d) Las Vegas, Nevada

FIGURE 10. DEPENDENCE OF VISUAL RANGE ON RELATIVE HUMIDITY AT FOUR LOCATIONS IN THE SOUTHWEST

the trends in visual range over three decades--1948 to 1956, 1957 to 1966, and 1967 to 1976--can be determined from Figure 10. During the period from 1948 to 1976, the frequency of good visibility decreased slightly in both Las Vegas and Prescott, it remained relatively constant in Farmington, and it improved in Phoenix. The significant quantities of $SO_x$ emitted by the copper smelters in Arizona (about 6000 tons per day in 1973) appear to be the most significant anthropogenic contributions to visibility impairment in the Southwest.

The improvement in visibility in Phoenix during the decade from 1967 to 1976 can be explained by the reduction in emissions (by a factor of two) that occurred during the period from 1973 to 1976. As a result of this pollution control effort, visibility in Phoenix increased significantly from 1973 to 1976, as evidenced by Figure 11. The effect of sulfate formed in the atmosphere from $SO_x$ emissions from the copper smelters on visual range in Phoenix is even more clearly indicated by the increases in visibility (as shown in Figure 11) that occurred during the years when smelter emissions were diminished because of strikes (1949, 1959, and 1967 to 1968). The effect of total elimination of copper smelter $SO_x$ emissions on visual range is also illustrated in Figure 10, which shows the frequency distribution of visual range as a function of relative humidity for the copper strike period, which was July 1967 to March 1968. Improvements in visual range during this period were observed not only in Phoenix, but also in remote nonurban areas, such as Farmington and Prescott.

The effect of smelter emissions on visual range in remote nonurban locations is even more convincingly illustrated by Figure 12, which shows the frequency of occurrence with which the distant visibility marker (121 km) was visible in Farmington, New Mexico, stratified by surface wind direction. Only observations for which relative humidity was less than 60 percent were used in this figure so as to minimize the effect that any dependence of relative humidity would have on wind direction. When the frequencies for the copper strike period are compared with those for the three decades, a

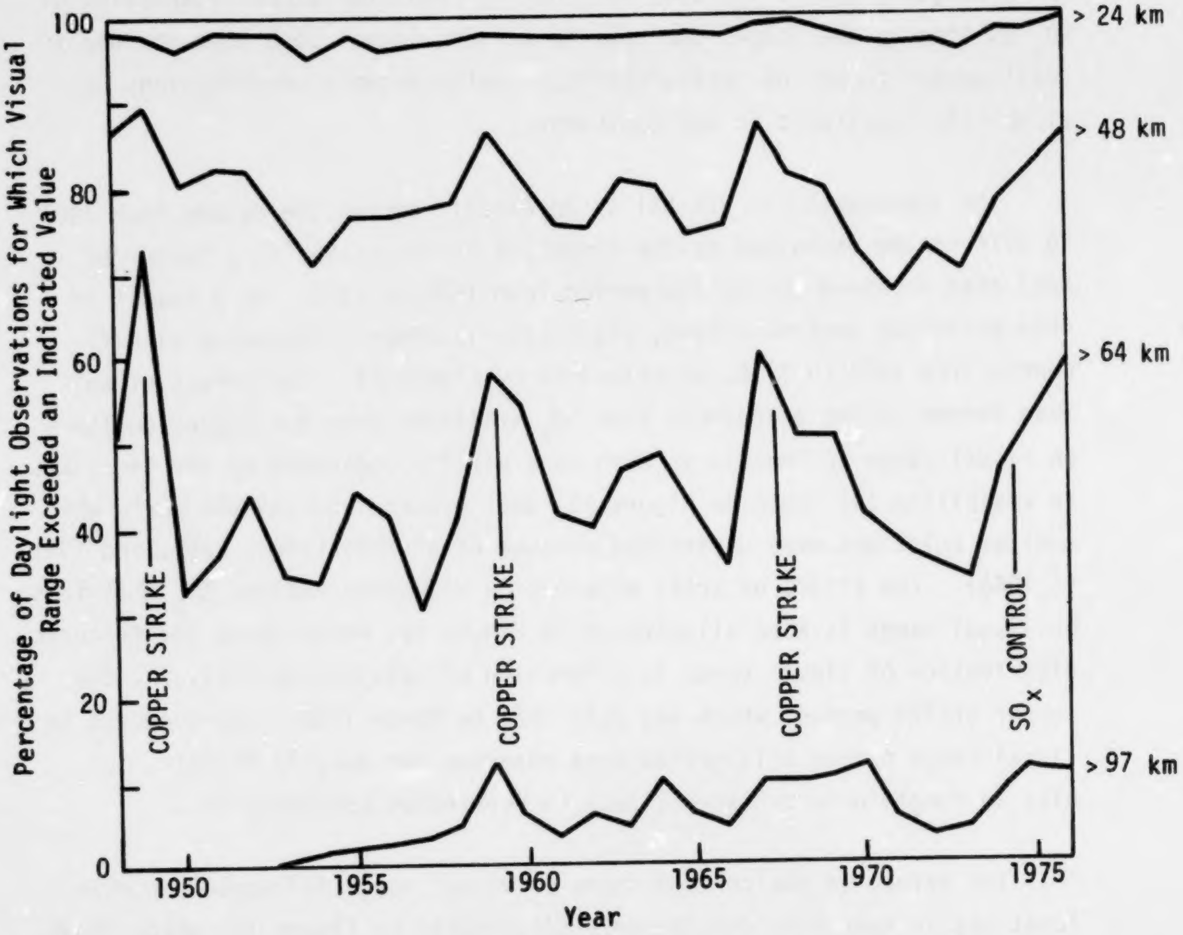

FIGURE 11. HISTORICAL TRENDS IN VISIBILITY IN PHOENIX, ARIZONA

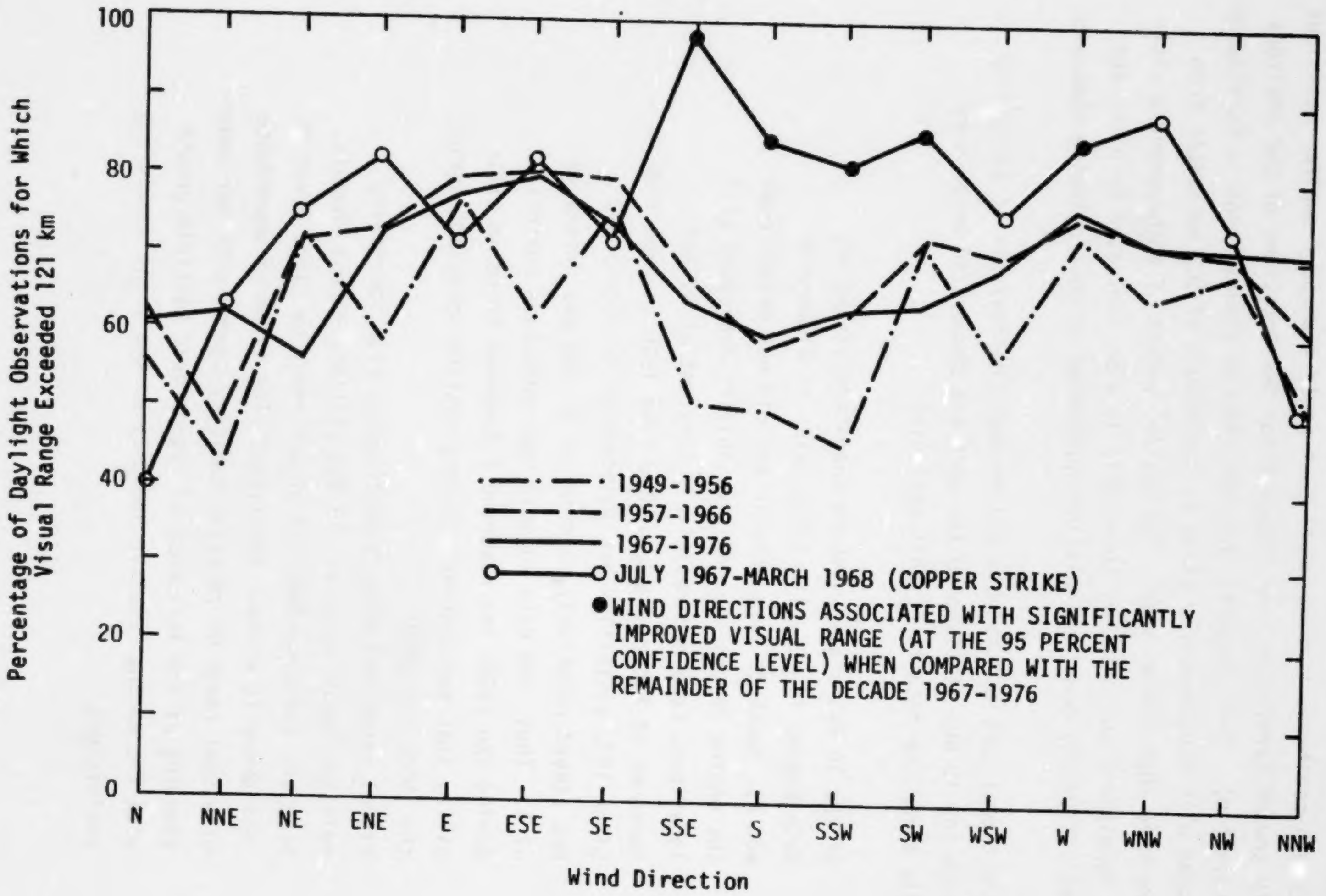

FIGURE 12. PERCENTAGE OF DAYLIGHT OBSERVATIONS WITH RH < 60 PERCENT FOR WHICH VISUAL RANGE EXCEEDED 121 km, AS A FUNCTION OF WIND DIRECTION, AT FARMINGTON, NEW MEXICO, 1949-1976

striking improvement in visual range is apparent, particularly for the winds (south-southeast through west) that would transport smelter emissions directly toward Farmington (see Figure 8 for the locations of the smelters and Farmington). This suggests that the reduced visual range in Farmington associated with southwesterly winds is the result of $SO_x$ emissions from smelters more than 400 km away. The spatial extent of anthropogenic visibility impairment suggested by these data is also indicated by plume and regional visibility model calculations presented in the following chapters.

Additional conclusions obtained through the analysis of visibility data from the 18 NWS stations in the West are summarized below (see Appendix A for the details of this analysis):

- Of the 16 NWS stations where long-term visibility data appear to be valid (data taken at Alamogordo and Ft. Huachuca were erratic and did not extend over the entire 29-year period), visibility decreased at 7 locations, remained relatively constant at 8, and improved at 1 during the period from 1948 through 1970. Since 1970 visibility has improved at 12 locations, has stayed relatively constant at 3, and has decreased at 1. Thus, the data suggest that pollution control during the 1970s has reversed a downward trend in visibility that was observed in many western locations during the 1950s and 1960s.
- Visual range decreases significantly with increasing relative humidity at all 18 NWS stations except Phoenix; however, the dependence of visual range on cloud cover is less dramatic at most locations. The trend of dependence of visual range on relative humidity agrees with our understanding of the influence of hygroscopic particle growth with increasing relative humidity on the light scattering coefficient.

- At most locations reductions in visual range are correlated with low barometric pressure, which probably results from the occurrence of high relative humidity during lows. However, at Salt Lake City, Ely, Grand Junction, and Pueblo, reduced visual range was correlated with high pressure conditions. Since high pressure systems sometimes cause air stagnation, the reduced visual range during highs at Ely and Salt Lake City (which are near copper smelters emitting $SO_x$) may be the result of air stagnation.
- The stratification of visual range data by ventilation (the product of mixing depth and average wind speed in the mixed layer) indicates that reduced visual range is correlated with reduced ventilation (stagnation conditions) in Phoenix, Salt Lake City, Tucson, Billings, Cheyenne, Ely, Ft. Huachuca, Grand Junction, Great Falls, and Rock Springs. Reductions in visual range were found to be correlated with high ventilation in Denver and Las Vegas, possibly because urban pollutants were transported into the sight path between the city and nearby mountains used as visibility markers.
- At 11 of the 18 locations, visual range decreased significantly with increasing surface wind speed, suggesting that windblown dust, particularly at wind speeds greater than 10 m/s, contributes to visibility impairment. This effect might explain the decrease in visual range with increasing ventilation observed in several locations, particularly Denver, Las Vegas, Alamogordo, and Winslow.
- At most locations there are no significant seasonal variations in visual range. Denver, Las Vegas, and Colorado Springs have minimum seasonal average visibilities in the summer. At Phoenix, Salt Lake City, Ely, Grand Junction, and Rock Springs, minimum visibilities occur during the winter.

> Variation in visual range with time of day is negligible at most locations. However, at some locations, such as Billings, Cheyenne, Farmington, Great Falls, and Rock Springs, visibilities at midday (1000 to 1400 hrs) were slightly greater than at other times.

> Visual range varies significantly with wind direction at Denver, Las Vegas, Phoenix, Colorado Springs, Farmington, Prescott, and Winslow. This relationship can be explained by the geographical locations of emissions sources relative to the sight paths of the NWS observers. Reductions in visual range in both Billings and Great Falls, Montana, are associated with generally easterly flow; the cause of this effect is unknown. The significant reductions in visual range in Prescott, Winslow, and Farmington that are associated with winds that transport smelter $SO_2$ emissions directly to the given location were not observed during the copper strike period of 1967 to 1968. During that period, visual range increased significantly throughout the Southwest.

To summarize, reduced visual range has been found to be associated with:

> $SO_x$ emissions from copper smelters
> High relative humidity
> Strong winds (windblown dust)
> Precipitation
> Stagnation conditions (low ventilation).

# III THE ELEMENTS OF VISIBILITY MODELS

This chapter discusses the elements of visibility modeling that are common to both the plume and the regional visibility models. The specific models and their outputs are discussed in Chapter IV. Appendices B and C discuss the modeling of atmospheric optics and sulfate formation in greater detail. Appendices D and E describe the plume visibility model and output; the regional visibility model and output are discussed in Appendices F and G.

As shown schematically in Figure 13, modeling of visibility impairment requires mathematical descriptions for the following physical and chemical atmospheric processes in succession:

> Emissions.
> Atmospheric transport, diffusion, and removal.
> Chemical and physical reactions and transformations of precursors in the atmosphere.
> Light scattering and absorption characteristics of the resultant aerosol.
> Radiative transfer through the aerosol along different lines of sight.

Because visibility models are based on atmospheric dispersion and chemistry models, the accuracy of the former depends on that of the latter. We recognize that future improvements in modeling dispersion--particularly on the regional scale and in complex terrain--as well as improvements in secondary aerosol formation will increase the accuracy of visibility models.

## A. POLLUTANT TRANSPORT, DIFFUSION, AND REMOVAL

We have developed two visibility models based on two basic types of dispersion models:

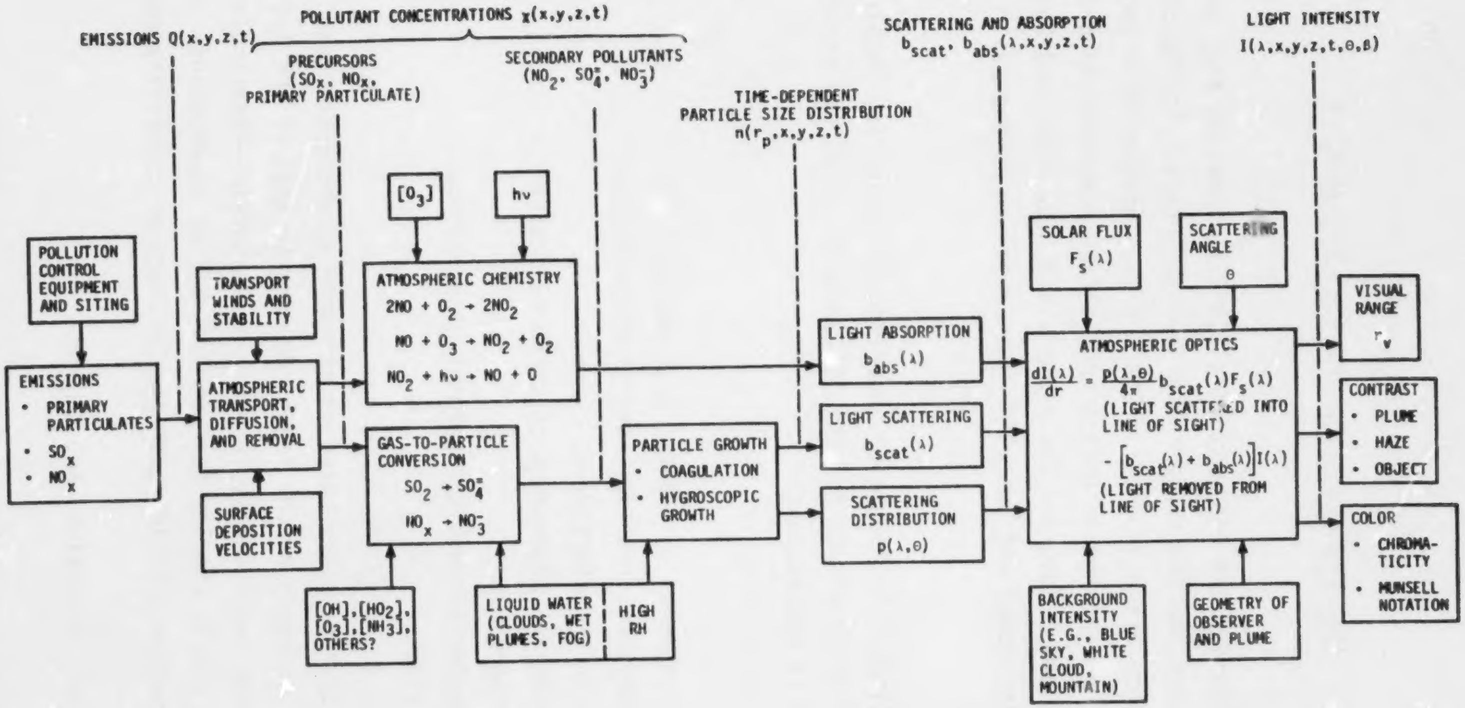
EMISSIONS Q(x,y,z,t)
POLLUTANT CONCENTRATIONS χ(x,y,z,t)
PRECURSORS (SOx, NOx, PRIMARY PARTICULATE)
SECONDARY POLLUTANTS (NO2, SO4=, NO3-)
TIME-DEPENDENT PARTICLE SIZE DISTRIBUTION n(rp,x,y,z,t)
SCATTERING AND ABSORPTION bscat, babs(λ,x,y,z,t)
LIGHT INTENSITY I(λ,x,y,z,t,θ,β)
POLLUTION CONTROL EQUIPMENT AND SITING
EMISSIONS
• PRIMARY PARTICULATES
• SOx
• NOx
TRANSPORT WINDS AND STABILITY
ATMOSPHERIC TRANSPORT, DIFFUSION, AND REMOVAL
SURFACE DEPOSITION VELOCITIES
[O3]
hν
ATMOSPHERIC CHEMISTRY
2NO + O2 → 2NO2
NO + O3 → NO2 + O2
NO2 + hν → NO + O
GAS-TO-PARTICLE CONVERSION
SO2 → SO4=
NOx → NO3-
[OH],[HO2], [O3],[NH3], OTHERS?
LIQUID WATER (CLOUDS, WET PLUMES, FOG)
HIGH RH
PARTICLE GROWTH
• COAGULATION
• HYGROSCOPIC GROWTH
LIGHT ABSORPTION babs(λ)
LIGHT SCATTERING bscat(λ)
SCATTERING DISTRIBUTION p(λ,θ)
SOLAR FLUX Fs(λ)
SCATTERING ANGLE θ
ATMOSPHERIC OPTICS
dI(λ)/dr = p(λ,θ)/4π bscat(λ)Fs(λ)
(LIGHT SCATTERED INTO LINE OF SIGHT)
- [bscat(λ) + babs(λ)]I(λ)
(LIGHT REMOVED FROM LINE OF SIGHT)
BACKGROUND INTENSITY (E.G., BLUE SKY, WHITE CLOUD, MOUNTAIN)
GEOMETRY OF OBSERVER AND PLUME
VISUAL RANGE rv
CONTRAST
• PLUME
• HAZE
• OBJECT
COLOR
• CHROMA-TICITY
• MUNSELL NOTATION

FIGURE 13. SCHEMATIC LOGIC FLOW DIAGRAM OF THE VISIBILITY MODELS

- A near-source plume model designed to predict the incremental impact of one emissions source (such as a power plant or smelter) at distances from 1 to 350 km downwind.
- A regional model designed to predict, over time periods of several days, the impact of several emissions sources within a region with a spatial scale of 1000 km.

Calculation of near-source visual impacts requires a basic plume model that accurately predicts the spatial distribution of pollutants and the chemical conversion of NO to $NO_2$ and $SO_x$ and $NO_x$ to sulfates and nitrates. The plume model must be capable of handling the spatial scale from emissions at the source to at least 100 km downwind. Because the regional-scale problem may be caused by long-range transport of pollutants over a spatial scale of 1000 km, an air quality model is needed that can account for multiple sources and for temporal variations in mixing heights, dispersion parameters, emission rates, reaction rates, and wind speed and direction.

In the following subsections, we discuss atmospheric dispersion modeling as it relates to visibility modeling. In addition, we classify the spatial scale of the models in further detail:

- Initial dilution in a buoyant plume
- Gaussian plume diffusion
- Limitations on mixing
- Plume trajectory box model
- Regional transport and diffusion.

## 1. Initial Dilution in a Buoyant Plume

Modeling of the initial dilution of a plume from the top of the stack to the point at which final plume rise is achieved is important when modeling the conversion of nitric oxide to nitrogen dioxide in a power plant plume because of the quick quenching of the thermal oxidation of NO. Because the rate of this reaction is second order with respect to NO concentrations, the rate is fastest in the initial stages of plume dilution. It is also important to account for the initial dilution of buoyant releases because the rate of dilution caused by the turbulent entrainment of ambient air by the rising plume parcel can be considerably greater than that indicated by diffusion coefficients based on measurements for nonbuoyant releases (e.g., Pasquill-Gifford $\sigma_y$, $\sigma_z$).

Briggs (1969) suggested that the characteristic plume radius increases linearly with height of the plume above the stack and can be represented as follows:

$$R_p = 0.5\ (\Delta h) \quad . \tag{9}$$

Briggs described the plume rise as a function of downwind distance (the "2/3 power law") as follows:

$$\Delta h = 1.6\ F^{1/3} x^{2/3} u^{-1} \quad . \tag{10}$$

For initial dilution, we can assume that the plume is circular in cross section:

$$R_p = y_p = z_p = 2.15\ \sigma_y = 2.15\ \sigma_z \quad . \tag{11}$$

The concentration of a given species at the centerline of the plume can be calculated by a modified Gaussian model that can be represented as:

$$\chi = \frac{Q}{2\pi\sigma_y\sigma_z V} \tag{12}$$

where V is the velocity of the parcel, which has a horizontal component (the wind speed u) and a vertical component w, which can be calculated by differentiating Eq. (10) as follows:

$$w = \frac{dz}{dt} = \frac{2}{3} 1.6 F^{1/3} u^{-1/3} t^{-1/3} \quad . \tag{13}$$

With this formulation, time-dependent plume temperature and NO concentrations can be calculated for accurate prediction of the thermal oxidation of NO during plume rise.

## 2. Gaussian Plume Diffusion

After the plume has achieved its final height (about 1 km downwind), plume concentrations for uniform wind fields can be adequately predicted using a Gaussian model if the wind speed u at plume elevation H ($h_s + \Delta h$) and the rate of diffusion are known for the particular situation so that dispersion coefficients ($\sigma_y, \sigma_z$) can be selected:

$$\chi = \frac{Q}{2\pi\sigma_y\sigma_z u} \exp\left[-\frac{1}{2}\left(\frac{y}{\sigma_y}\right)^2\right]\left\{\exp\left[-\frac{1}{2}\left(\frac{H+z}{\sigma_z}\right)^2\right] + \exp\left[-\frac{1}{2}\left(\frac{H-z}{\sigma_z}\right)^2\right]\right\} \quad . \tag{14}$$

Equation (14) is appropriate for a conservative species and can be modified to be appropriate for a nonconservative species by changing the source term Q.

It is necessary for calculating plume visual impact to integrate, along the line of sight, the primary and secondary particulate and nitrogen dioxide concentrations. Equation (14) can be integrated (Ensor, Sparks, and Pilat, 1973) in the cross-wind direction $y$ from $y = -\infty$ to $y = +\infty$ to obtain the optical thickness of the plume:

$$\tau_{py} = \int_{-\infty}^{+\infty} \chi_{ext}\, dy = \frac{Q'(x)}{(2\pi)^{1/2}\, \sigma_z u} \left\{ \exp\left[ -\frac{1}{2}\left(\frac{H+z}{\sigma_z}\right)^2 \right] + \exp\left[ -\frac{1}{2}\left(\frac{H-z}{\sigma_z}\right)^2 \right] \right\} \quad , \qquad (15)$$

where Q' is the integral of the flux of plume extinction coefficient over the entire plume cross section at downwind distance x. In the vertical direction z, from z = 0 to z = +∞, the optical thickness is:

$$\tau_{pz} = \int_0^{\infty} \chi_{ext}\, dz = \frac{Q'(x)}{(2\pi)^{1/2}\, \sigma_y u} \exp\left[ -\frac{1}{2}\left(\frac{y}{\sigma_y}\right)^2 \right] \quad . \qquad (16)$$

### 3. Observer-Plume Orientation

The magnitude of the visual impact of a plume depends on the orientation of the observer with respect to the plume because the plume optical thickness will vary depending on this orientation. Figure 14 shows plan and elevation views of an observer and a plume and indicates that the sight path distance through the constituents of the plume is a function of angles $\alpha$ and $\beta$. The optical thickness at any angle $\alpha$ and any angle $\beta$ can be determined as follows:

$$\tau_p(\alpha,\beta) = \frac{1}{\sin \alpha} \left[ (\tau_{py} \cos \beta)^2 + (\tau_{pz} \sin \beta)^2 \right]^{1/2} \quad . \qquad (17)$$

Figure 14 suggests that plume optical thickness is greater for horizontal sight paths than vertical ones, particularly during stable conditions when the plume cross section is flattened.

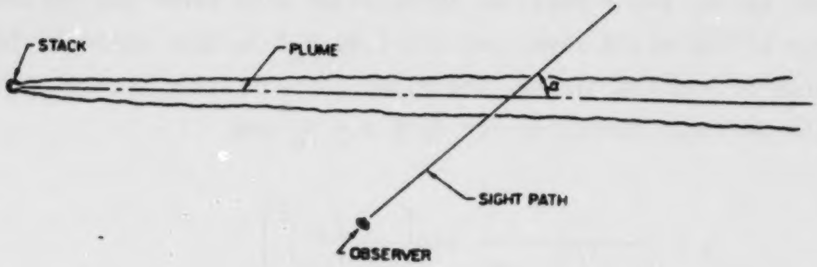
STACK
PLUME
α
SIGHT PATH
OBSERVER

(a) Plan View

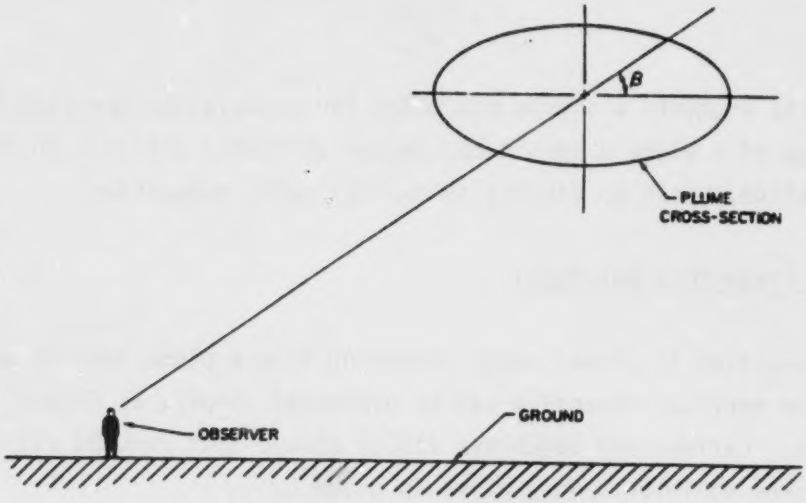
β
PLUME CROSS-SECTION
OBSERVER
GROUND

(b) Elevation View

Source: Latimer and Samuelsen (1978).

FIGURE 14. GAUSSIAN PLUME VISUAL IMPACT MODEL: OBSERVER-PLUME GEOMETRY

## 4. Limited Mixing

When vertical diffusion is limited by a stable capping layer, Eq. (14) is no longer valid, and a Gaussian formulation with terms for reflection from the top of the mixed layer (at altitude $H_m$) is more appropriate. In this instance of limited mixing, the plume concentration becomes uniformly mixed in the vertical direction for $0 \leq z \leq H_m$ and:

$$\chi = \frac{Q}{(2\pi)^{1/2}\,\sigma_y u H_m} \exp\left[-\frac{1}{2}\left(\frac{y}{\sigma_y}\right)^2\right] \quad . \tag{18}$$

The calculation of plume optical thickness in the y-direction becomes simply:

$$\tau_{py} = \frac{Q'(x)}{uH_m} \quad . \tag{19}$$

Equation (19) suggests a simple box model for calculating the reduction in visual range of a plume after it has become uniformly diffused in the vertical direction, which we discuss in the following subsection.

## 5. Plume Trajectory Box Model

The reduction in visual range resulting from a plume that is uniformly mixed in the vertical direction can be evaluated simply, as Figure 15 illustrates. Latimer and Samuelsen (1978) showed that reduced visual range resulting from pollutants in a plume is given by:

$$r_v = \frac{1}{b_{ext-0}}\left[3.912 - \ell n\left(\frac{I_{hp}}{I_h}\right) - \tau_p\right] \quad . \tag{20}$$

When plume material does not significantly affect the intensity of the horizon sky, the second term in the brackets drops out. After noting that the background visual range (without the plume) is:

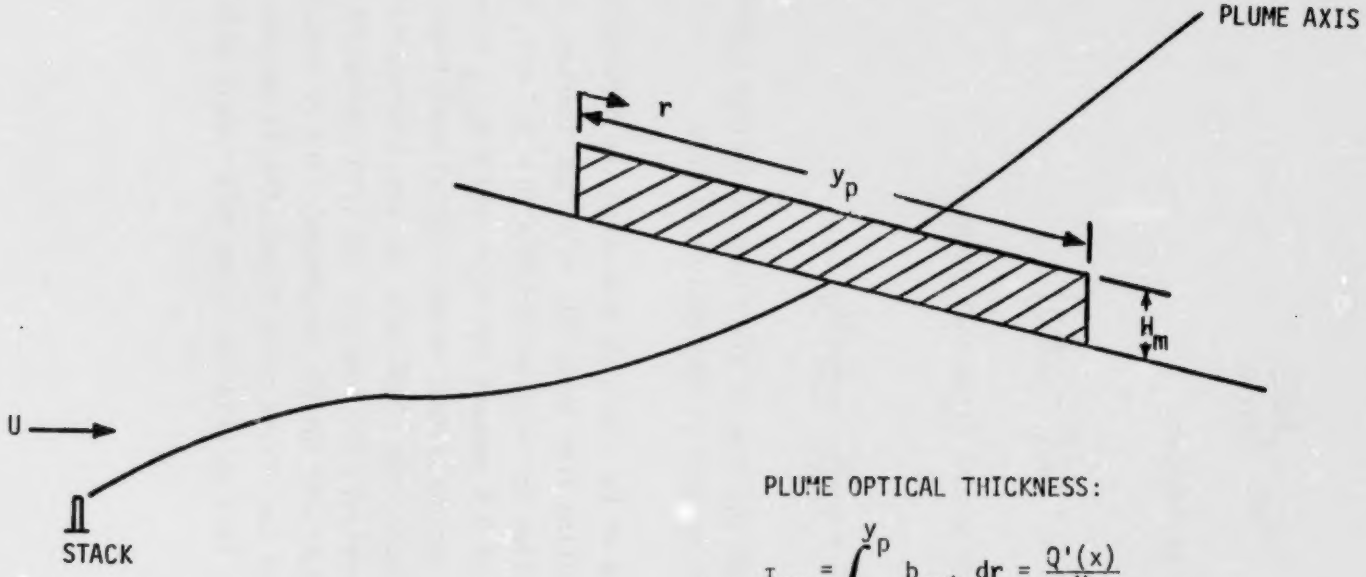
PLUME AXIS
r
$y_p$
$H_m$
U
STACK

PLUME OPTICAL THICKNESS:

$$\tau_{py} = \int_0^{y_p} b_{ext}\, dr = \frac{Q'(x)}{uH_m}$$

FIGURE 15. PLUME TRAJECTORY BOX MODEL

$$r_{v0} = \frac{3.912}{b_{ext-0}} \quad , \tag{21}$$

we can rearrange Eq. (20) as follows:

$$r_v = r_{v0}\left(1 - \frac{\tau_p}{3.912}\right) \quad . \tag{22}$$

The fractional reduction in visual range then becomes:

$$\frac{r_{v0} - r_v}{r_{v0}} = \frac{\tau_p}{3.912} = \frac{Q'(x)}{3.912\ uH} \quad , \tag{23}$$

where Q' is the integral of the flux of the plume extinction coefficient over the total plume cross section at downwind distance x.

To illustrate the use of Eq. (23), we evaluated the percentage reduction in visual range resulting from three $SO_2$ emissions sources, assuming average afternoon ventilation for Winslow, Arizona ($u = 6.7$ m/s, $H_m = 2613$ m), a sulfate formation rate of 0.5 percent per hour, and a $b_{scat}$-to-mass ratio of 0.04 $m^{-1}/\mu g/m^3$ of $SO_4^=$ and persistent meteorological conditions. Three $SO_2$ emissions rates were selected: 2000 tons per day (representative of a large copper smelter complex), 200 tons per day (representative of a large coal-fired power plant without $SO_2$ scrubbers), and 20 tons per day (representative of a large coal-fired power plant with 90 percent $SO_2$ control). The results of this calculation using this simple model are shown in Table 2.

TABLE 2. PERCENT REDUCTION IN VISUAL RANGE BY THREE LEVELS OF $SO_2$ EMISSIONS

| Downwind Distance (km) | 2000 Tons/Day | 200 Tons/Day | 20 Tons/Day |
|---|---|---|---|
| 50 | 1.9% | 0.2% | 0.0% |
| 100 | 3.8 | 0.4 | 0.0 |
| 200 | 7.5 | 0.8 | 0.1 |
| 500 | 18.1 | 1.8 | 0.2 |
| 1000 | 34.5 | 3.5 | 0.3 |

As the sample calculations summarized in Table 2 illustrate, the most significant reduction in visual range from anthropogenic emissions may not occur close to the source, but rather, at locations hundreds of kilometers downwind from the source. However, the values in Table 2 are examples for average conditions and an assumed sulfate formation rate. Equation (23) makes clear that visibility impairment is a function of the ventilation and the total quantity of light scatterers and absorbers in the plume. It should be noted that these calculations ignore the effect of $SO_2$ and sulfate removal processes that decrease the sulfate concentrations and thereby reduce visibility impairment. (Such processes are considered in the plume and regional visibility models.) As demonstrated by these simple calculations, secondary aerosol formation has a significant effect on the magnitude of impairment for given emission and meteorological conditions. Equation (23) is a simple calculation through which a first-order estimate of an emission source's impact on visual range can be made.

## 6. Regional Transport and Diffusion

The modeling of visibility impairment on a regional scale requires the use of a model that accounts for time-dependent meteorological conditions, multisource emissions, and pollutant removal through surface deposition, washout, rainout, and the like. We selected the SAI Northern Great Plains grid model (Liu and Durran, 1977) as the basis for our regional visibility model. Appendix F describes the model in detail.

The model is composed of two interconnected submodels: a mixed layer model and a surface layer model. The mixed layer model treats transport and diffusion above the surface. A grid approach is adopted to facilitate the handling of multiple sources and complex chemistry. The major feature of this model is the assumption that pollutant distribution is nearly uniform in the vertical direction. With this assumption, a simplified form of the general atmospheric diffusion equation can be invoked.

The surface layer model calculates the pollutant fluxes lost to the ground. The surface layer, a shallow layer immediately above the terrain, is embedded within the mixing layer. If pollutants originate from either elevated sources or distant ground-level sources, most of the pollutant mass is contained in a layer aloft, i.e., in the mixed layer. The removal processes consist of the diffusion of the pollutants through the surface layer to the ground, followed by absorption or adsorption at the atmosphere-ground interface. A unique feature of the surface layer is its diurnal variation in surface temperature, which is a result of daytime heating and nighttime cooling. This variation affects the vertical pollutant distribution through atmospheric stabilities, and, consequently, the rate of surface uptake of pollutants.

The regional model assumes vertical homogeneity in the concentration distribution. One of the reasons for this assumption is that the vertical diffusion term, based on dimensional analysis, is about 100 times greater than the transport term, and the horizontal diffusion term is only a fraction of the transport term.

Assuming that the concentration distribution in the vertical is nearly uniform below the base of the temperature inversion, a vertically averaged concentration of species i may be computed from the following equation:

$$\frac{\partial \bar{c}_i}{\partial t} + \bar{u}\frac{\partial \bar{c}_i}{\partial x} + v\frac{\partial \bar{c}_i}{\partial y} = \frac{\partial}{\partial x}\left(K_x\frac{\partial \bar{c}_i}{\partial y}\right) + \frac{\partial}{\partial y}\left(K_y\frac{\partial \bar{c}_i}{\partial y}\right) + R_i(\bar{c}_1,\bar{c}_2,\ldots,c_N) + S_i(c_i)$$

$$- (\bar{c}_i - \bar{c}_{0_i})\cdot D\cdot \zeta(D) \quad , \quad i = 1, 2, \ldots, N \quad , \qquad (24)$$

where

$c_{0_i}$ = the background concentration of species i,

$\bar{u}$, $\bar{v}$ = the vertically averaged horizontal wind components ($\bar{u} = \int_0^H u\, dz/H$, $\bar{v} = \int_0 v\, dz/H$),

D = the two-dimensional divergence [$D = (\partial\bar{u}/\partial x) + (\partial\bar{v}/\partial y)$],

$\zeta(D)$ = a step function defined by

$$\zeta(D) = \begin{cases} 1 & \text{for} \quad D > 0 \quad , \\ 0 & \text{for} \quad D \leq 0 \quad , \end{cases} \qquad (25)$$

$S_i$ $R_i$ = rate of change of concentration of species i due to emission sources and chemical reaction.

In the derivation of Eq. (24), the following assumptions were made:

> Deviations from the average concentration, $\bar{c}_i$, in the vertical direction are small.

> The vertical velocity at the top boundary is approximately given by:

$$w = -\int_0^H \cdot \left(\frac{\partial u}{\partial x} + \frac{\partial v}{\partial y}\right) dz \simeq -H\left(\frac{\partial \overline{u}}{\partial x} + \frac{\partial \overline{v}}{\partial y}\right) \quad . \qquad (26)$$

> The diffusive flux of pollutants at the top boundary is negligible.

> The following relationships hold for the reaction and source/sink terms:

$$\overline{R}_i(\overline{c}_1, \overline{c}_2, \ldots, c_N) = R_i(\overline{c}_1, \overline{c}_2, \ldots, \overline{c}_N) \qquad (27)$$

$$\overline{S}_i(c_i) = S_i(\overline{c}_i) \quad . \qquad (28)$$

## B. ATMOSPHERIC CHEMISTRY

The visibility models require calculations of the conversion of precursors to species that cause visual effects, namely, nitrogen dioxide and secondary aerosol (sulfate, nitrate, organics).

### 1. Conversion of NO to $NO_2$

As previously noted, nitrogen dioxide gas causes a yellow-brown discoloration of the atmosphere. Although some discoloration can be caused by wavelength-dependent light scattering by submicron aerosol, we demonstrate in Chapter IV that the dominant colorant of power plant plumes is $NO_2$ and that yellow-brown discoloration may be apparent at significant distances downwind of large coal-fired power plants, particularly in areas where the background visual range is excellent.

Very little $NO_2$ is emitted directly from power plants. However, colorless nitric oxide is formed by the thermal oxidation of atmospheric nitrogen at the high temperatures experienced in the combustion zone (the boiler in a power plant) and the oxidation of nitrogen that may be present in the fuel. Chemical reactions in the atmosphere can form sufficient $NO_2$ from NO to cause atmospheric discoloration. Available measurements of NO and $NO_2$ concentrations in power plant plumes in nonurban areas suggest that the conversion of NO to $NO_2$ can be calculated from a simple set of three reactions.

The first of these is the thermal oxidation of NO to $NO_2$:

$$2NO + O_2 \rightarrow 2NO_2 \quad . \tag{29}$$

The reaction is termolecular but bimolecular with respect to NO; it is therefore very fast at high concentrations of NO but slow at the lower concentrations that exist in the atmosphere or in a plume. The reaction rate for Eq. (29) [based on Baulch, Drysdale, and Horne (1973)] is:

$$\frac{d[NO_2]}{dt} = \left[4.015 \times 10^{-12} \exp\left(\frac{1046}{RT}\right)\right][NO]^2[O_2] \text{ ppm/s} \quad . \tag{30}$$

The reaction with ozone also affects the conversion of NO to $NO_2$:

$$NO + O_3 \rightarrow NO_2 + O_2 \quad . \tag{31}$$

The reaction is fast, with a rate (Leighton, 1961; Davis, Smith, and Klauber, 1974; Niki, 1974) at 25°C of:

$$\frac{d[NO_2]}{dt} = 0.44\ [NO][O_3] \text{ ppm/s} \quad . \tag{32}$$

This reaction accounts for the ozone depletion measured within power plant plumes and is important because ozone concentrations can be high even in nonurban regions. Measured ozone concentrations in nonurban areas of the western United States range from 0.02 to 0.04 ppm.

Whereas the thermal oxidation rate [Reaction (30)] decreases as the plume mixes (because the NO concentration decreases), the formation of nitrogen dioxide via Reaction (31) is enhanced as the plume mixes, because additional ozone from the atmosphere is mixed into the plume, allowing Reaction (31) to proceed. When there are no reactions converting $NO_2$ to NO (e.g., at night), Reaction (31) proceeds until all of the NO in the plume is converted to $NO_2$ or until the ozone concentration in the plume drops to zero. Therefore, the rate of conversion of NO to $NO_2$ via Reaction (31) is limited by the rate of plume mixing that provides the necessary atmospheric ozone.

To complete the set of chemical reaction mechanisms, we must consider the photodissociation of $NO_2$. When sunlight illuminates a plume containing nitrogen dioxide, short wavelength light and ultraviolet radiation are absorbed by the $NO_2$. As noted above, absorption of the shorter wavelength light produces the characteristic yellow-brown color associated with $NO_2$. Absorption of the more energetic ultraviolet light ($\lambda < 0.4\ \mu m$) results in dissociation of the $NO_2$ molecule:

$$NO_2 + h\nu \rightarrow NO + O \quad . \tag{33}$$

$$O + O_2 \rightarrow O_3 \quad . \tag{34}$$

Leighton (1961) gave the rate of Reaction (34) as:

$$\frac{d[NO_2]}{dt} = -K_d\ [NO_2]\ \text{ppm/s} \quad , \tag{35}$$

where $K_d$ depends on the amount of light incident on the nitrogen dioxide. Davis, Smith, and Klauber (1974) gave the following expression for $K_d$ as a function of the solar zenith angle X:

$$K_d = 1 \times 10^{-2} \exp\left(- \frac{0.38}{\cos X}\right) s^{-1} \quad . \tag{36}$$

With this set of chemical reactions, the chemical conversion of NO to $NO_2$ in the atmosphere can be calculated from background pollutant concentrations and from plume $NO_x$ increments using the technique suggested by

Latimer and Samuelsen (1975) and White (1977). Making the steady-state approximation, we have:

$$[NO_2] = \frac{K_r}{K_d}[NO][O_3] \quad , \tag{37}$$

where

$$[NO] = [NO_x] - [NO_2] \tag{38}$$

and

$$[O_3] = [O_3]_b - \left([NO_2] - [NO_2]_t - [NO_2]_b\right) \quad . \tag{39}$$

Substituting Eqs. (38) and (39) into Eq. (37) we can solve for the concentration of $NO_2$:

$$\begin{aligned}[NO_2] = 0.5\Bigg[ & [NO_x] + [O_3]_b + [NO_2]_t + [NO_2]_b + \frac{K_d}{K_r} \\ & - \left\{\left([NO_x] + [O_3]_b + [NO_2]_t + [NO_2]_b + \frac{K_d}{K_r}\right)^2 \right. \\ & \left. - 4[NO_x]\left([O_3]_b + [NO_2]_t + [NO_2]_b\right)\right\}^{1/2}\Bigg] \quad .\end{aligned} \tag{40}$$

Using this formulation to compute NO to $NO_2$ conversion in a hypothetical power plant plume, Latimer and Samuelsen (1978) studied the sensitivity of $NO_2$ formation to the rate of plume dilution, background ozone concentration, and solar radiation. The results of this analysis are presented in Figure 16. This figure shows that thermal oxidation (e.g., $[O_3] = 0$) converts up to 10 percent of the plume NO to $NO_2$, and additional conversion results when ambient ozone is mixed into the plume. A recent comparison of observations with calculations using Eq. (40) indicates good agreement, particularly if the

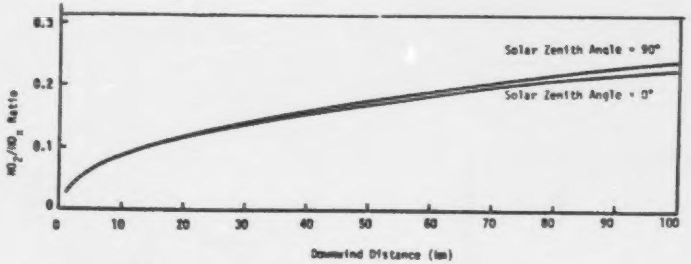

(a) Solar Radiation

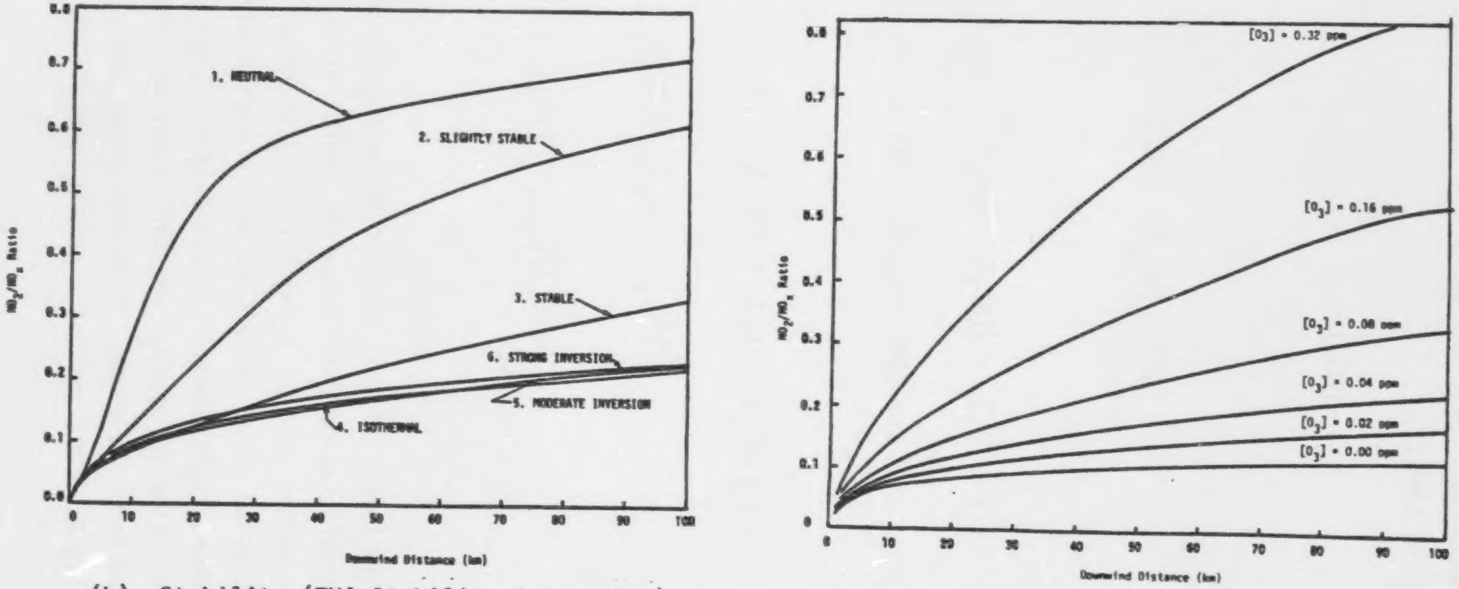

(b) Stability (TVA Stability Categories)

(c) Background Ozone

Source: Latimer and Samuelsen (1978).

FIGURE 16. SENSITIVITY OF NO TO $NO_2$ CONVERSION IN POWER PLANT PLUMES TO THE RATE OF PLUME DILUTION, BACKGROUND OZONE CONCENTRATION, AND SOLAR RADIATION

diffusion of the plume is correctly calculated by using fitted dispersion coefficients based on plume diffusion measurements (see Figure 17).

## 2. Conversion of Gases to Particles

Although $SO_2$, NO, and $NO_2$ gas do not scatter light appreciably, they react in the atmosphere to form secondary sulfate and nitrate particles in the size range that is most effective at light scattering (0.1 to 1.0 μm). In many situations, sulfate and nitrate are the dominant contributors to the scattering coefficient of the atmospheric aerosol. It is essential, therefore, that the effect of these secondary aerosols and the rate at which they are formed from precursors be included in visibility models.

During this first year of development work, we have concentrated on developing the atmospheric optics and visibility impairment components of the plume and regional visibility models. The development of a model to predict the rate of formation of sulfate and nitrate aerosol based on the fundamental chemical reactions and physical processes would be a tremendous undertaking. Furthermore, even if such a model were available, we do not know the background atmospheric concentrations of the species responsible for the conversion of gases to particles.

We have therefore adopted the approach of calculating gas-to-particle conversion using measured rates of reaction appropriate for the clean (Class I) areas of the country. We recommend, however, that consideration be given in future visibility model development work to the incorporation of fundamental gas-to-particle reaction mechanisms in the visibility models.

The measured rates of conversion of the gaseous species to particles vary over several orders of magnitude, depending on the amount of sunlight, the concentrations of hydrocarbons, ammonia, manganese, iron, and other chemical species, and the relative humidity. Available data suggest that

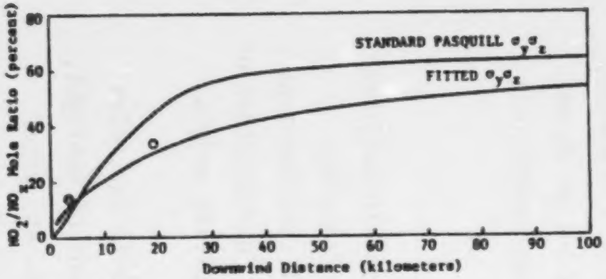

(a) Case 1

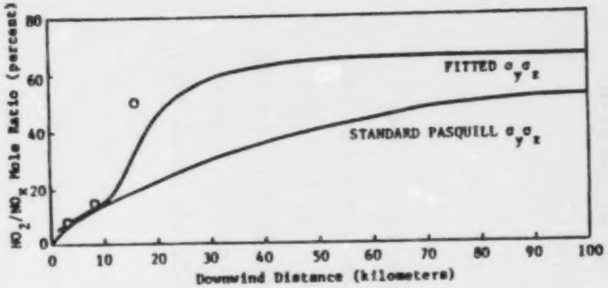

(b) Case 2

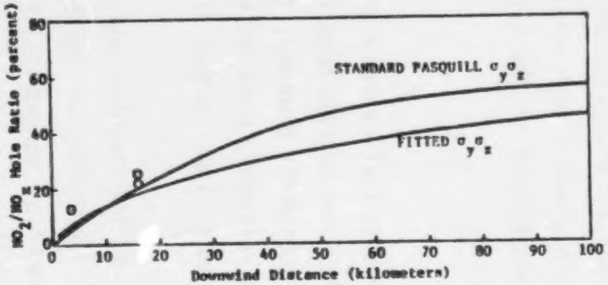

(c) Case 3

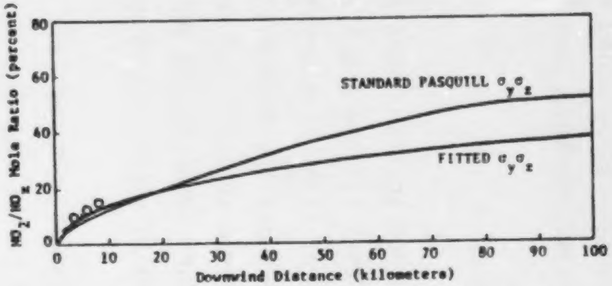

(d) Case 4

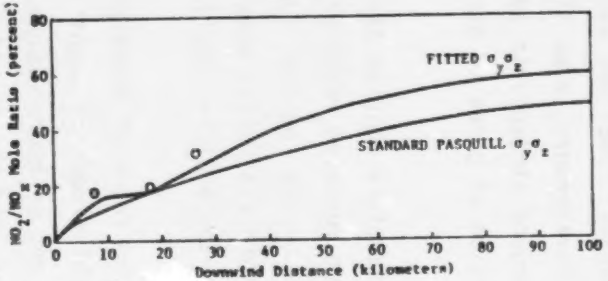

(e) Case 5

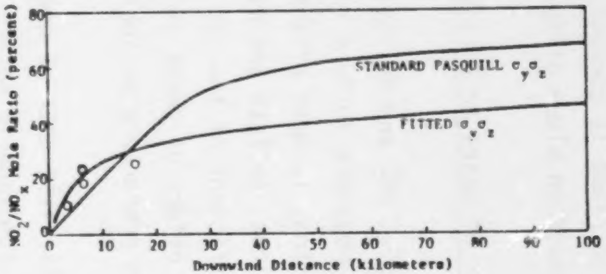

(f) Case 6

FIGURE 17. COMPARISON OF MEASURED $NO_2/NO_x$ MOLE RATIOS (CIRCLED POINTS) IN THE PLUME CENTERLINE DOWNWIND OF A COAL-FIRED POWER PLANT WITH COMPUTER-CALCULATED VALUES (SOLID LINES) USING STANDARD PASQUILL AND FITTED $\sigma_y\sigma_z$

the rate of conversion of $SO_2$ to sulfate particles is much greater in polluted urban atmospheres and in locations where relative humidity is high. Appendix C summarizes the fundamental reaction mechanisms and the available measurements of the rate of sulfate formation in the atmosphere. Other recent reviews of sulfate formation include those of Calvert et al. (1977), ER&T (1977), and Levy, Drewes, and Hales (1976). Orel and Seinfeld (1977) have reviewed nitrate as well as sulfate information, particularly in polluted urban atmospheres. For our initial visibility model development work, we have modeled gas-to-particle conversion using pseudo-first-order rate constants typical of clean areas. Levy, Drewes, and Hales (1976), in their review of $SO_2$ oxidation in plumes, supported such an approach.

We calculate the conversion of $SO_2$ and $NO_x$ to sulfate and nitrate as follows:

$$\frac{\partial [SO_2]}{\partial t} = -k_1 [SO_2] \quad , \qquad (41)$$

$$\frac{\partial [NO_x]}{\partial t} = -k_2 [NO_x] \quad . \qquad (42)$$

The integral of the flux sulfate and nitrate mass contributed by a given emissions source ($Q_{SO_2}$, $Q_{NO_x}$) over the entire plume cross section at a given downwind distance or transit time ($t = x/u$) can be calculated as follows:

$$Q'_{SO_4^=} = r_1 \; Q_{SO_2} \left(1 - e^{-k_1 t}\right) \quad , \qquad (43)$$

$$Q'_{NO_3^-} = r_2 \; Q_{NO_x} \left(1 - e^{-k_2 t}\right) \quad , \qquad (44)$$

where $r_1$ and $r_2$ are simply the ratios of molecular weights of sulfate to $SO_2$ ($r_1 = 1.5$) and nitrate to $NO_2$ ($r_2 = 1.35$). The mass of the ammonium ion (or other cation) and water associated with the sulfate and nitrate also contributes to the total aerosol mass concentration.

The effect of plume dilution on gas-to-particle conversion can vary depending on the relative contribution of reactions with plume constituents (e.g., catalytic oxidation of $SO_2$ on particle surfaces or in the liquid phase by metal ions) and reactions with trace species in the background atmosphere (e.g., the reaction of $SO_2$ and $NO_x$ with $OH\cdot$, $HO_2\cdot$, $H_2O$, $NH_3$, and $RO_2\cdot$). For heterogeneous catalytic reactions on emitted primary particles, the rate of aerosol formation decreases with plume dilution. For example, the fractional rate of $SO_2$ conversion to sulfate becomes:

$$- \frac{1}{[SO_2]} \frac{\partial [SO_2]}{\partial t} \propto [\text{Catalyst}] \quad . \tag{45}$$

The concentration C of conservative plume species (e.g., precursor $SO_x$ and $NO_x$ or primary particulate) decreases with time after emission and can be described mathematically (Schwartz and Newman, 1978) as:

$$C \propto t^{-n} \quad . \tag{46}$$

Thus, if heterogeneous reactions with primary particles are the sole contributors to secondary aerosol, one would expect a secondary aerosol formation rate that rapidly decreases with time after emission from the stack; for example,

$$- \frac{1}{[SO_2]} \frac{\partial [SO_2]}{\partial t} \propto t^{-n} \quad . \tag{47}$$

Furthermore, if a catalyst were used up, this reaction would decrease even more rapidly and would eventually be quenched. However, the formation rate of secondary aerosol by reactions with trace constituents of the background atmosphere (such as $OH\cdot$, $HO_2\cdot$, $NH_3$) or background aerosol increase with increasing plume dilution and will dominate at long reaction times. This occurs because, with increased mixing associated with plume dilution, fresh ambient air (containing the reactive species) is mixed into the plume. Without plume dilution, the reactive species are used up and no further conversion takes place. The process becomes diffusion-limited in the same way $NO_2$ production in a plume is limited by the rate at which ambient ozone is mixed into the plume.

At this stage in visibility modeling, we are using pseudo-first-order rate constants to model the conversion of $SO_2$ and $NO_x$ to sulfates and nitrates. In our sensitivity analyses, described in Chapter IV, we selected sulfate formation rates ranging between 0.3 and 1 percent per hour and, due to the lack of quantitative data due, in part, to the uncertainty in measured nitrate concentrations (Spicer and Schumacher, 1977), a nitrate formation rate of zero.

## C. AEROSOL SIZE DISTRIBUTION

To determine the visual effects of aerosols, one must specify or calculate aerosol physical size and composition. This section reviews the available data on atmospheric aerosol size distributions, particularly the recent work of Whitby and his coworkers. We then discuss the types of aerosols that are important for visibility considerations--background, primary, and secondary aerosols--and how they are currently treated in the visibility models.

Atmospheric aerosols can be grouped into a trimodal size distribution. Figure 18 shows the three modes (nuclei, accumulation, and coarse particles) and the processes that form them. According to Whitby and Sverdrup (1978):

> The physical separation of the fine and coarse modes originates because condensation produces fine particles while mechanical processes produce mostly coarse particles. The dynamics of fine particle growth ordinarily operate to prevent the fine particles from growing larger than about 1 μm. Thus as a first approximation, the fine and coarse modes originate separately, are transformed separately, are removed separately, and are usually chemically different.

Figure 19 shows the various ways of plotting size distribution information. Figure 19(a), a number size distribution, is the plot that Junge (1963) originally used for his data. This plot led to the aerosol power law formulation:

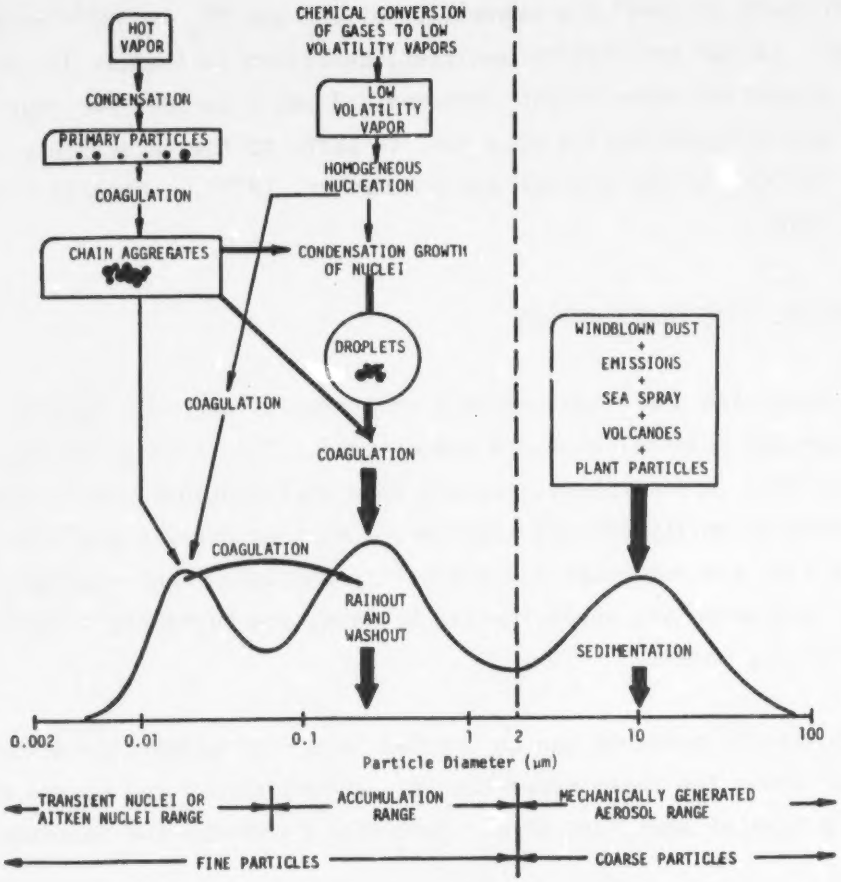
HOT VAPOR
CONDENSATION
PRIMARY PARTICLES
COAGULATION
CHAIN AGGREGATES
CHEMICAL CONVERSION OF GASES TO LOW VOLATILITY VAPORS
LOW VOLATILITY VAPOR
HOMOGENEOUS NUCLEATION
CONDENSATION GROWTH OF NUCLEI
DROPLETS
COAGULATION
COAGULATION
WINDBLOWN DUST + EMISSIONS + SEA SPRAY + VOLCANOES + PLANT PARTICLES
COAGULATION
RAINOUT AND WASHOUT
SEDIMENTATION
0.002
0.01
0.1
1
2
10
100
Particle Diameter (µm)
TRANSIENT NUCLEI OR AITKEN NUCLEI RANGE
ACCUMULATION RANGE
MECHANICALLY GENERATED AEROSOL RANGE
FINE PARTICLES
COARSE PARTICLES

Source: Whitby and Sverdrup (1978).

FIGURE 18. SCHEMATIC OF AN ATMOSPHERIC AEROSOL SURFACE AREA DISTRIBUTION SHOWING THE PRINCIPAL MODES, SOURCES OF MASS FOR EACH MODE, PROCESSES INVOLVED IN INSERTING MASS IN EACH MODE, AND REMOVAL MECHANISMS

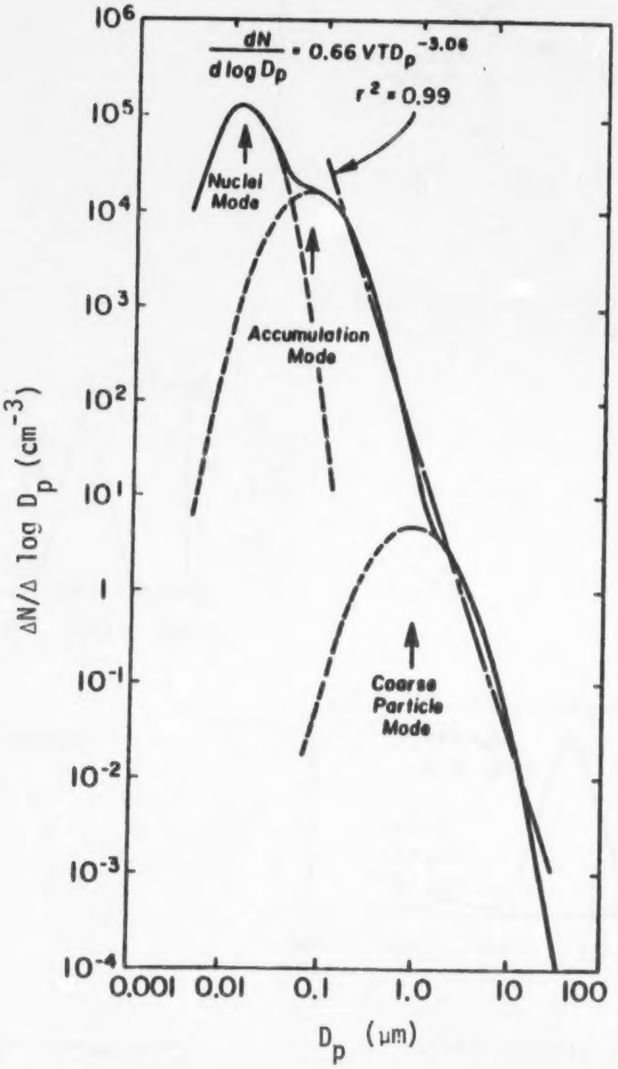

(a) Power Function Fitted to the Number Distribution over the Size Range 0 to 32 μm

FIGURE 19. AVERAGE URBAN MODEL AEROSOL DISTRIBUTION PLOTTED IN FIVE DIFFERENT WAYS

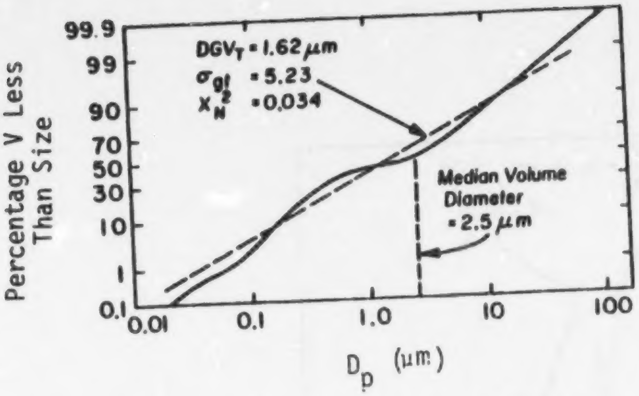

(b) Lognormal Distribution Fitted to the Size Range 0.1 to 32 µm

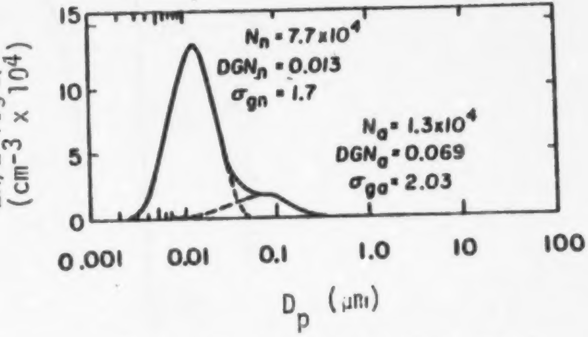

(c) Number Size Distribution

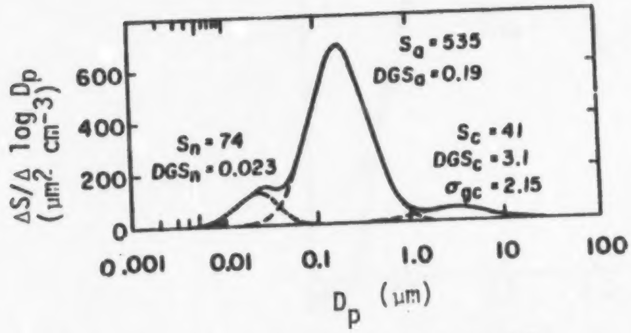

(d) Surface Area Size Distribution

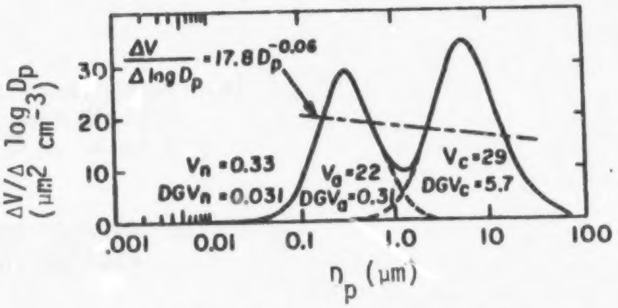

(e) Volume Size Distribution

Source: Whitby and Sverdrup (1978).

FIGURE 19 (Concluded)

$$\frac{dN}{d \log D_p} = cD_p^{-n} \quad , \tag{48}$$

where N is the number of particles of diameter $D_p$. Figure 19(b) shows the standard lognormal plot. Figures 19(c), 19(d), and 19(e) show the number, surface area, and volume distributions of an urban aerosol. These last three plots show the three distinct aerosol modes: nuclei (0.001 to 0.1 μm), accumulation (0.1 to 1.0 μm), and coarse (>1 μm).

Whitby and Sverdrup (1978) recently computed a table showing typical aerosol size distributions and concentrations based on measurements in many locations. Table 3 summarizes the mass median diameters (DG), the geometric standard deviations ($\sigma_g$), and the volume concentration (V in $\mu m^3/cm^3$, which is equal to the mass concentration in $\mu g/m^3$, divided by density in $g/cm^3$) of each of the modes for eight classifications of aerosol. Table 3 shows only a small variability in the accumulation and coarse mode size distributions for the variety of aerosol types measured (excluding the marine aerosol). The average specifications for the accumulation mode and the coarse distributions are summarized below:

| Mode | DG | $\sigma_g$ |
|---|---|---|
| Accumulation | 0.29 ± 0.06 μm | 2.0 ± 0.1 |
| Coarse | 6.3 ± 2.3 μm | 2.3 ± 0.2 |

The data suggest that the average specifications (mass median diameter and standard deviation) of the accumulation and coarse modes fit a wide range of atmospheric conditions, a finding that greatly simplifies the calculation of the scattering properties of the atmosphere.

Figure 20 shows the results of our calculations of the scattering coefficient-to-volume ratio for a variety of different aerosol size distributions. The calculations are based on Mie theory. The average specifications and corresponding scattering properties of the accumulation and coarse modes are also given in Figure 20. As this figure shows, the accumulation mode aerosol is roughly an order of magnitude more effective per unit volume than the coarse mode aerosol.

TABLE 3. MEASURED SIZE DISTRIBUTIONS OF ATMOSPHERIC AEROSOL

| | Nuclei Mode | | | Accumulation Mode | | | Coarse Particle Mode | | |
|---|---|---|---|---|---|---|---|---|---|
| Type of Aerosol | DG ($\mu$m) | $\sigma_g$ | V ($\mu m^3/cm^3$) | DG ($\mu$m) | $\sigma_g$ | V ($\mu m^3/cm^3$) | DG ($\mu$m) | $\sigma_g$ | V ($\mu m^3/cm^3$) |
| Marine, surface background | 0.019 | 1.6* | 0.0005 | 0.3 | 2.0* | 0.10 | 12.0 | 2.7 | 12.0 |
| Clean continental background | 0.03 | 1.6 | 0.006 | 0.35 | 2.1 | 1.5 | 6.0 | 2.2 | 5.0 |
| Average background | 0.034 | 1.7 | 0.037 | 0.32 | 2.0 | 4.45 | 6.04 | 2.16 | 25.9 |
| Background and aged urban plume | 0.028 | 1.6 | 0.029 | 0.36 | 1.84 | 44.0 | 4.51 | 2.12 | 27.4 |
| Background and local sources | 0.021 | 1.7 | 0.62 | 0.25 | 2.11 | 3.02 | 5.6 | 2.09 | 39.1 |
| Urban average | 0.038 | 1.8 | 0.63 | 0.32 | 2.16 | 38.4 | 5.7 | 2.21 | 30.8 |
| Urban and freeway | 0.032 | 1.74 | 9.2 | 0.25 | 1.98 | 37.5 | 6.0 | 2.13 | 42.7 |
| Labadie plume (1976)† | 0.015 | 1.5 | 0.1 | 0.18 | 1.96 | 12.0 | 5.5 | 2.5 | 24.0 |

---

* Assumed.

† Typical distribution observed in the plume from the Labadie coal-fired power plant near St. Louis, Missouri.

Source: Whitby and Sverdrup (1978).

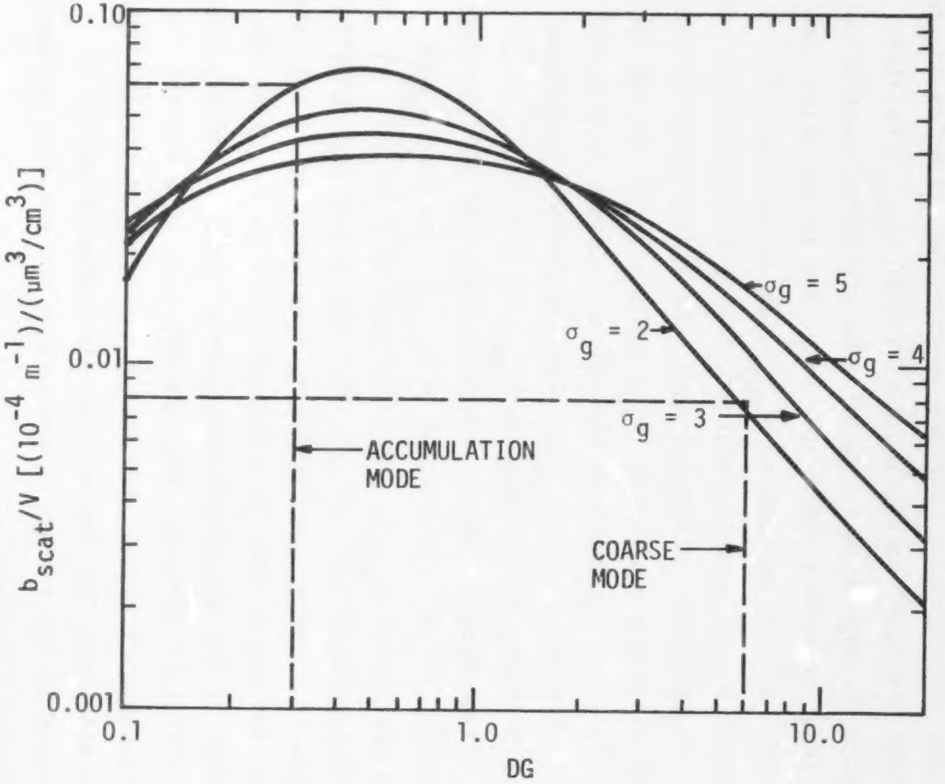

FIGURE 20. SCATTERING-TO-VOLUME RATIOS FOR VARIOUS SIZE DISTRIBUTIONS

If the scattering coefficient corresponding to each of the modes for the different aerosols sampled by Whitby and Sverdrup (see Table 3) is calculated, the accumulation mode is the dominant scattering mode, with the coarse mode contributing a small amount and the nuclei mode a negligible amount. For the clean continental background aerosol (second entry in Table 3), we calculated that the total scattering coefficient ($b_{scat}$) equaled $0.23 \times 10^{-4}$ $m^{-1}$, which is very close to the minimum scattering coefficient suggested by the data shown in Figure 9 (Chapter II). The accumulation mode contributes $0.09 \times 10^{-4}$ $m^{-1}$ (39 percent of $b_{scat}$), the coarse mode $0.04 \times 10^{-4}$ $m^{-1}$ (17 percent of $b_{scat}$), and Rayleigh scattering $0.10 \times 10^{-4}$ $m^{-1}$ (43 percent of $b_{scat}$). In the clean background case, the contribution of the accumulation mode to the extra extinction ($b_{sp}$) above Rayleigh was 69 percent of the total. This clean background aerosol corresponds to a visual range of 170 km, or 105 miles ($3.912/b_{scat}$). For the average background aerosol (third entry in Table 3) the computed $b_{scat}$ is $0.57 \times 10^{-4}$ $m^{-1}$, corresponding to a visual range of 69 km. In this case, the accumulation mode contributed $0.27 \times 10^{-4}$ $m^{-1}$ (46 percent of $b_{scat}$), the coarse mode $0.21 \times 10^{-4}$ $m^{-1}$ (36 percent of $b_{scat}$), and Rayleigh $0.10 \times 10^{-4}$ $m^{-1}$ (17 percent of $b_{scat}$). These calculations indicate that for background conditions the accumulation mode is a larger contributor to light scattering than the coarse mode but that the coarse mode is a nonnegligible component of the scattering coefficient of the background atmosphere. This situation strikingly contrasts with that of polluted urban atmospheres, in which the accumulation mode causes more than 90 percent of the total scattering coefficient. We should also note that the average background presented in Table 3 is not as clean as the average background in the nonurban western United States, as Figure 9 suggests.

In our visibility models, we have used the size distributions given in Table 3 for specifying ambient background (second and third items in Table 3) and plume aerosol (eighth item). We then calculated optical properties of the aerosol (using Mie theory) from the computed concentrations of coarse and accumulation mode (sulfate, nitrate, and associated cations and water) aerosol.

## D. ATMOSPHERIC OPTICS

In the atmospheric optics component of the visibility models, the light scattering and absorption properties of the aerosol and the resultant light intensity for various illumination and viewing situations are computed. The details of these calculations are given in Appendix B; the major points are summarized in this section to give the reader an overall view of the process.

### 1. Calculation of the Scattering and Absorption Properties

After the concentrations of the pollutants are specified by the transport and chemistry subroutines, their radiative properties must be determined. For $NO_2$, the absorption at a particular wavelength is a tabulated function (Nixon, 1940) multiplied by the concentration. For aerosols, the procedure is more complicated, however.

In general, a particle's ability to scatter and absorb radiation at a particular frequency is a function of size, composition, shape, and relative humidity. Because we wanted to be able to alter the size distribution of both primary and secondary particles, we needed to be able to compute the effect of particle size on the wavelength dependence of the extinction coefficient and the scattering distribution function. The only rational method of making this computation is to use the solution of Maxwell's equations for scattering by a sphere, the so-called Mie equations. To verify that these calculations were appropriate for atmospheric aerosols, we compared them with the empirical correlations of scattering to mass and found substantial agreement, as discussed below.

The calculations were performed using an IBM subroutine written by J. V. Dave (Dave, 1970). The required inputs are the particle size parameter (ratio of the circumference to the wavelength of radiation), the index of refraction (real and imaginary part), and the number and location of the scattering angles (between 0° and 180°). The output is the scattering and absorption cross sections and the Stokes transformation matrix (Van De Hulst, 1957), which can be simply converted to the scattering distribution assuming randomly polarized light. The scattering and absorption properties per particle are then summed over the particular size distribution in such a way that as the size distribution changes so do the radiative properties.

Different types of empirical correlations have been made in recent years relating particle scattering properties to particle mass. The property measured has been either the volumetric scattering coefficient, as measured by an integrating nephelometer, or the extinction coefficient, calculated from the observed visual range. Among recent discoveries is the conclusion that the scattering properties of urban atmospheres correlate much better with the submicron accumulation mode concentration than with total mass. A second important development is that for most of the United States and Europe, sulfates are generally a significant fraction of submicron accumulation mode mass.

Many studies of the empirical correlations of scattering coefficients to sulfate mass have been performed. Table 4 summarizes some of these measurements. Similar tables have appeared in other reports, such as that by Trijonis and Yuan (1977). The correlation coefficients for these relationships have been very high (0.7 to 0.9), supporting the dominant role of sulfate in scattering. Of particular importance is the use, by many researchers, of visual range data (e.g., airport visibility) derived from actual, though somewhat imprecise, visual perception of objects in the atmosphere. Thus, it appears that sulfates play an important role in visibility impairment.

Calculations of scattering-to-volume ratios (see Figure 20) reveal that the maximum theoretically possible value is about 0.06, as expressed in the

## TABLE 4. ESTIMATES OF EXTINCTION COEFFICIENTS PER UNIT MASS

| Source | Location | Extinction Coefficients $[(10^4\ m^{-1}/(\mu g/m^3))]$ | | |
|---|---|---|---|---|
| | | Sulfates | Nitrates | Remainder of TSP |
| Regression models (Trijonis and Yuan, 1978) | Chicago | 0.04 | (0.00) | (0.000) |
| | | 0.03* | (0.00*) | (0.000*) |
| | Newark | (0.02) | (0.00) | 0.026 |
| | | 0.06* | (0.00*) | 0.014* |
| | Cleveland | 0.08 | (0.00) | (0.000) |
| | | 0.07* | (0.00*) | (0.000*) |
| | Lexington | 0.06 | (0.00) | (0.000) |
| | | 0.06* | (0.04*) | 0.019* |
| | Charlotte | 0.11 | (0.00) | (0.001) |
| | | 0.11* | (0.00*) | (0.000*) |
| | Columbus | 0.12 | 0.09 | (0.000) |
| | | 0.13* | (0.06*) | (0.001*) |
| Regression models (Trijonis and Yuan, 1977) | Salt Lake City | 0.04 | 0.13 | 0.004 |
| | | 0.04* | 0.10* | 0.004* |
| | Phoenix (county data) | 0.04 | 0.05 | (0.000) |
| | Phoenix (NASN data) | 0.03 | 0.03 | (0.000) |
| Dust storms (Hagen and Woodruff, 1973) | Great Plains | NC | NC | 0.001 |
| Regression model (White and Roberts, 1975) | Los Angeles | 0.07 | 0.05 | 0.015 |
| Regression model (Cass, 1976) | Los Angeles | 0.16 | (0.00) | 0.008 |
| | | 0.09* | 0.05* | (0.004*) |
| Calculations for a model aerosol of $(NH_4)_2SO_4^{=}$ at 70% RH (Waggoner et al., 1976) | | 0.05-0.10 | NC | NC |
| Regression model (Waggoner et al., 1976) | Southern Sweden | 0.05 | NC | NC |

---

( ) = not significant at the 95 percent confidence level.
NC = not calculated.
*Based on nonlinear RH regression model, with insertion of average RH.

Source: Trijonis and Yuan (1978).

units used in Table 4.[*] However, the reported empirically determined values range from about 0.03 to 0.1. This discrepancy was resolved by including the mass of liquid water associated with the sulfate. Investigators have found better correlations with scattering-to-mass ratios that depend on relative humidity. These fits are of the form:

$$\frac{b_{scat}}{M} = \frac{c}{1 - RH} \quad , \tag{49}$$

where c represents the scattering-to-mass ratio at 0 percent relative humidity. The range of these values is between 0.02 and 0.04, which is in agreement with theoretical values shown in Figure 20.[†]

To account for the effects of relative humidity, we simply added the amount of water absorbed by the sulfate particles:

$$b_{scat} = \left(\frac{b_{scat}}{M}\right)_{Sulfate} \left(Mass_{Sulfate} + Mass_{Cation} + Mass_{Water}\right) \quad .$$

Then we used a formula from Winkler (1973) to account for the mass of water as a function of relative humidity. Finally, we compared the dependence of the scattering-to-mass ratio on relative humidity determined by Cass and Trijonis with calculations using the following assumptions:

---

[*] This was computed from the maximum value of $0.08 \times 10^{-4}\ m^{-1}/\mu m^3/cm^3$ in Figure 20 assuming the sulfate was associated with ammonium ion as $(NH_4)_2SO_4$:

$$\left(\frac{0.08 \times 10^{-4}\ m^{-1}}{\mu m^3/cm^3}\right)\left(\frac{m^3}{10^6\ cm^3}\right)\left(\frac{10^{12}\ \mu m}{cm^3}\right)\left(\frac{cm^3}{1.8\ g(NH_4)_2SO_4}\right)\left(\frac{g}{10^6\ \mu g}\right)\left(\frac{132\ g(NH_4)_2SO_4}{96\ gSO_4^=}\right)$$

$$= 0.06 \times 10^{-4}\ m^{-1}/(\mu g/m^3\ SO_4^=) \quad .$$

[†] If we use an accumulation mode $b_{scat}/V = 0.06 \times 10^{-4}\ m^{-1}/\mu m^3/cm^3$, we obtain $b_{scat}/(\mu g/m^3\ SO_4^=)$ ranging from 0.034 to 0.046 x $10^{-4}\ m^{-1}/\mu g/m^3$ depending on whether the sulfate is $H_2SO_4$ or $(NH_4)_2SO_4$.

> Aerosol with a lognormal size distribution and a mass median diameter of 0.2 μm and a geometric standard deviation equal to 2.0 at RH = 0 percent.
> Index of refraction equal to 1.5 - 0i (typical, non-absorbing aerosol).
> Density equal to 1.8 g/cm$^3$.
> Light of 0.55 μm wavelength.
> Sulfate as $NH_4HSO_4$ (molecular weight of 115).

Figure 21 shows the striking agreement between our calculations and the dependence of scattering-to-mass ratio on relative humidity observed by Trijonis in the Southwest. This agreement gives support to our calculation method for the scattering properties of the secondary aerosol.

The computational procedure used in the visibility models then takes the input size distribution, assuming that the particles are spherical with an index of refraction of 1.5 - 0i, and computes the scattering properties of the aerosol as a function of wavelength from the Mie equations. The background size distribution properties are taken from the Whitby and Sverdrup model of clean continental aerosols (see Table 3). The accumulation mode in the plume is assumed to be the size of those measured in the plume downwind of the Labadie power plant near St. Louis. The properties of the sulfates and other accumulation mode particles are assumed to change with relative humidity, as discussed above. A more complete inclusion of relative humidity would require a modification of the refractive indices and a recomputation from the Mie equations. This modification could easily be done later if desired.

The limitations of the process of specifying the radiative properties of aerosols are the usual ones: uncertainties in the size distribution, nonspherical particles, and ambiguities in mean refractive indices. However, the close agreement shown for the sulfate scattering-to-mass values suggests that the errors are not large.

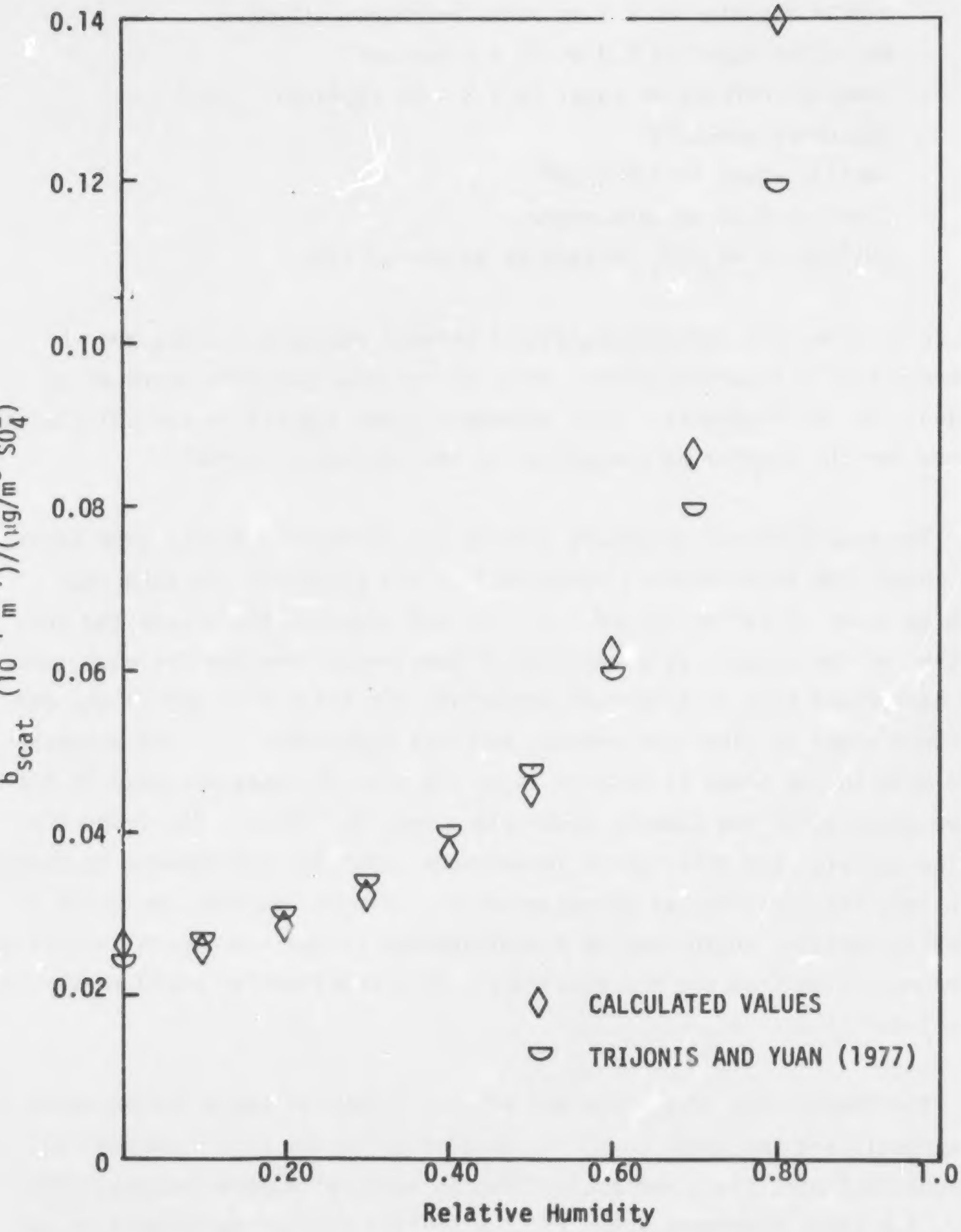

FIGURE 21. RATIO OF LIGHT SCATTERING TO MASS AS A FUNCTION OF RELATIVE HUMIDITY

## 2. Calculation of Light Intensity

The light intensity (watts/$m^2$/steradian) at a particular location in the atmosphere is a function of the direction of observation $\Omega$ and the wavelength $\lambda$. Calculation of the light intensity in a medium follows from the radiative transfer equation. This equation is a conservation of energy statement that accounts for the light added to the line of sight by scattering and the light lost because of absorption and scattering. Approximations and solution techniques applicable to planetary atmospheres have been discussed by Hansen and Travis (1974) and Irvine (1975).

The physical situation that we are concerned with is shown schematically in Figure 22. To compute the spectral light intensity at the observer, we sum (integrate) the scattered and absorbed light over the path, r, associated with the line of sight $\Omega$. The resultant general expression for the background sky intensity at a particular wavelength is

$$I_b(\Omega) = \int_0^{\tau_\infty} \frac{\omega(\tau)}{4\pi} \int_{\Omega'=4\pi} I(\Omega',\tau')p(\Omega'\rightarrow\Omega,\tau')\, d\Omega'\, e^{-\tau'}\, d\tau' \quad , \qquad (51)$$

where

$\tau$ = the optical depth ($\tau \equiv \int_0^r b_{ext}\, dr$, where $b_{ext}$ is the extinction coefficient),

$\omega$ = the albedo for single scattering ($\omega \equiv b_{scat}/b_{ext}$ where $b_{scat}$ is the scattering coefficient),

$p(\Omega' \rightarrow \Omega)$ = the scattering distribution function for the angle $\Omega' \rightarrow \Omega$,

$I$ = the spectral intensity at $\tau'$ from direct and diffuse solar radiation.

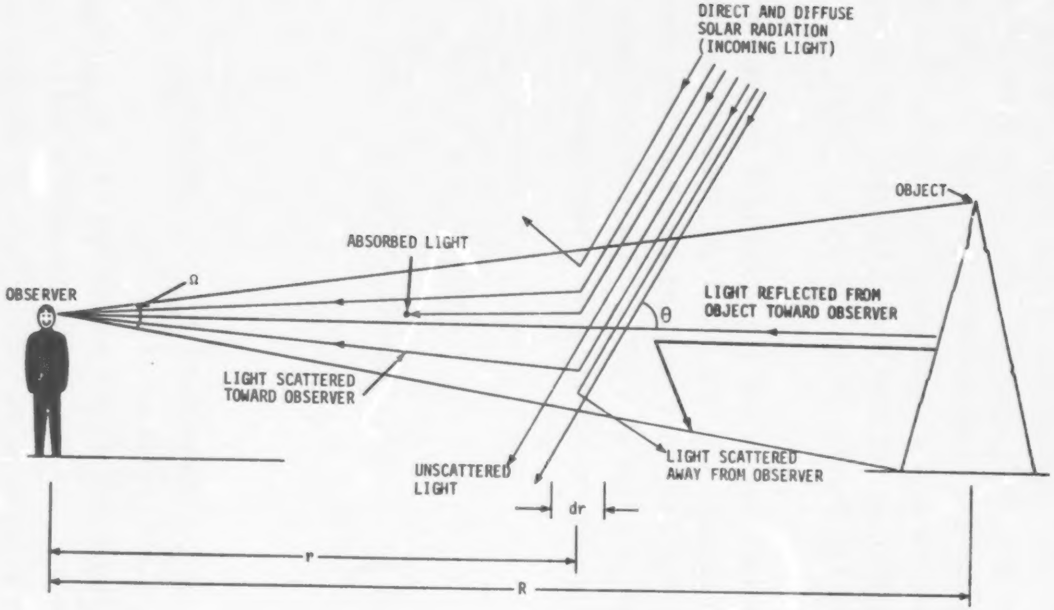
DIRECT AND DIFFUSE
SOLAR RADIATION
(INCOMING LIGHT)
OBJECT
ABSORBED LIGHT
OBSERVER
Ω
LIGHT REFLECTED FROM
OBJECT TOWARD OBSERVER
θ
LIGHT SCATTERED
TOWARD OBSERVER
UNSCATTERED
LIGHT
LIGHT SCATTERED
AWAY FROM OBSERVER
dr
r
R

FIGURE 22. LIGHT SCATTERING AND ABSORPTION IN THE ATMOSPHERE

Equation (51) is valid for the usual continuum, no refraction, random polarization assumptions.

The intensity seen by an observer in direction $\Omega$ of an object at distance R is:

$$I_{obj}(\Omega) = I_o(\Omega)e^{-\tau_R}$$

$$+\int_0^{\tau_R} \frac{\omega(\tau')}{4\pi} \int_{\Omega'=4\pi} I(\Omega',\tau')\ p(\Omega'\to\Omega,\tau')\ d\Omega'\ e^{-\tau'}\ d\tau' \quad . \quad (52)$$

Equations (51) and (52) then completely describe the spectral intensity of the background and an object. Once these two quantities are known, the visual effects of the intervening atmosphere can be quantified. In evaluating Eqs. (51) and (52), we encounter two main difficulties: First, the quantity in the integral is a fairly complicated function, and accurate specification is tedious. Second, the atmosphere is inherently inhomogeneous, and thus, the radiative properties $\omega$, p are somewhat complicated functions of r and $\Omega$. Approximations are therefore necessary. Appendix B outlines in some detail the approximations we have used; we present only a summary here. The approximations we used are the following:

> Plane parallel atmosphere.
> Two homogeneous layers.
> Average solar flux approximation.
> Average diffuse intensity approximation.

The equation for the background intensity at the surface becomes, for a direction $\mu$, $\phi$,

$$I_b(\mu,\phi) = I_{sky}(\mu,\phi)e^{-\tau_{OD}} + \frac{\bar{\omega}_{OD}}{4\pi}\,\bar{P}_{OD}(\Theta)\,F_{s,av}\left(1 - e^{-\tau_{OD}}\right)$$

$$+ \bar{\omega}_{OD}\, I_{av}^{dif}\left(1 - e^{-\tau_{0\infty}}\right) \quad , \qquad (53)$$

and for the intensity in the direction of an object in the planetary boundary layer,

$$I_{obj}(\mu,\phi) = I_o(\mu,\phi)e^{-\tau_R} + \frac{\bar{\omega}_{OD}}{4\pi}\,\bar{P}_{OD}(\Theta)\,F_{s,av}\left(1 - e^{-\tau_R}\right)$$

$$+ \bar{\omega}_{OD}\, I_{av}^{dif}\left(1 - e^{-\tau_R}\right) \quad , \qquad (54)$$

where

$\bar{\omega}_{OD}$, $\bar{P}_{OD}(\Theta)$ = the average albedo and phase function, respectively,
$\tau_{OD}$ = the optical depth of the path in the boundary layer,
$F_{s,av}$, $I_{av}^{dif}$ = the average solar direct intensity and diffuse intensity, respectively,
$I_{sky}$, $I_o$ = the intensities from the upper atmosphere and object, respectively.

The exact definitions of the terms are given in Appendix B.

Thus, the background intensity and the intensity in the direction of an object at distance R from the observer can be computed given the following inputs:

> Background radiative properties (e.g., size distribution, visual range).
> Solar zenith angle.
> Scattering angle.
> Direction of observation, $\mu$, $\phi$.
> Planetary boundary layer height.

The intensities, including the effects of air pollution, are computed from essentially the same formulae with the radiative effects of the pollutants included in the background atmosphere. In the regional model, the intensity for a given optical path is calculated from an integration of the concentration through the cells of the grid model. For an initial approximation, we used the expressions for a homogeneous atmosphere.

In the plume model, it was necessary to treat the plume as a homogeneous layer with an optical depth and mean properties $\overline{\omega}_{plume}$ and $\overline{p}_{plume}(\Theta)$. We also assumed that the plume did not affect the solar radiation illumination (optically thin plume). This approximation was based on the belief that the model would not be applied to near-stack optically thick situations; provisions for optically thick plumes can be added later if desired.

The major weakness of the calculations for the intensities appears to be the calculation of the diffuse intensity. The magnitude of the error is difficult to assess without appropriate testing, but it is likely to be largest near sunrise and sunset (see Appendix B).

## E. QUANTIFYING VISIBILITY IMPAIRMENT

We can quantify visibility impairment once the spectral light intensity $I(\lambda)$ has been calculated for the specific lines of sight $(\mu, \phi)$ of an observer located at a given location in an atmosphere with known aerosol and pollutant concentrations. As we noted in Chapter II, visibility impairment--including reduction in visual range, the visibility of plumes and haze layers, and atmospheric discoloration--is caused by changes in light intensity as a result of light scattering and absorption in the atmosphere.

We can classify visibility impairment in terms of visual effects as follows:

> Coloration of objects.
  - Brightness
  - Hue and saturation.

> Contrast and color difference between two objects.
  - Black object and horizon sky (to calculate visual range).
  - Haze layers.
  - Plume and background.

The perception of an object such as a distant mountain results from changes in light intensity, coloration, or both. Visual range is defined in terms of differences in light intensity (contrast) between a distant black object and the horizon sky. Contrast is also a useful concept for characterizing the appearance of plumes and haze layers. However, a plume may be perceived against a background as the result of a color change unaccompanied by a change in light intensity (i.e., with no contrast). We therefore need a means of characterizing the perception of changes in both the intensity and the coloration of light. We discuss the different means of characterizing visibility impairment in the following subsections.

### 1. Visual Range

Visual range is defined as the farthest distance at which a black object can be perceived against the horizon sky. As we have noted in Chapter II, the threshold of perception of differences between the light intensity of two objects has been characterized by a liminal contrast. The value of the liminal contrast is commonly taken to be 0.02, as first suggested by Koschmieder in 1924 (Middleton, 1952). However, the liminal contrast is a function of the observer and his state of mind (e.g., fatigue, attentiveness) as well as the intensity of the background lighting. Under the best conditions, the liminal contrast may be as low as 0.005 (Committee on Colorimetry, Optical Society of America, 1963). The Federal Aviation Administration assumes a value of 0.055. Based on an experiment using 10 observers and a total of 1000 observation hours, Middleton (1952) reported a median of 0.03 and a mode of 0.02 for the liminal contrast. For the purposes of standardization, it is reasonable to describe the perception of a "standard observer" and to select and use a single value for the liminal contrast. We used the Koschmieder value (0.02) for our calculations.

It is clear then that the observation of distant targets such as mountains is not an accurate measurement of strictly defined visual range, i.e., the farthest distance at which a black object is distinguishable from the horizon sky by a standard observer where liminal contrast is 0.02. This is true not only because of the variability in the contrast threshold, but also because distant markers such as mountains are usually not perfectly black.

The contrast between two objects is defined as:

$$C(\lambda) = \frac{I_1(\lambda) - I_2(\lambda)}{I_2(\lambda)} \quad . \tag{55}$$

If the two objects are the same color [i.e., $I_1(\lambda)/I_2(\lambda)$ is constant over $0.4 < \lambda < 0.7$ μm], then the contrast at all wavelengths will be the same. However, if the objects have different colors, then C is a function of wavelength. For the calculation of visual range, we evaluate the contrast at a wavelength of 0.55 μm, which is at the middle of the visible spectrum and is the wavelength to which the human eye is most sensitive. The intrinsic contrast of a black object ($I_1 = 0$) against the horizon sky ($I_2 = I_h$) is -1; the visual range is the distance at which this contrast is reduced by the light scatter and absorption of the intervening atmosphere to -0.02. Thus, visual range can be evaluated by computing contrast iteratively as a function of distance from the observer until it drops to -0.02. This approach is necessary if one is dealing with a nonhomogeneous atmosphere.

For a homogeneous atmosphere, however, the calculation of visual range is analytic, using the Koschmieder relationship:

$$r_v = \frac{3.912}{b_{ext}} \quad . \tag{56}$$

For the computation of visual range through a homogeneous atmosphere containing an optically thin plume, Latimer and Samuelsen (1978) suggested the following simplified approach:

$$r_v = \frac{1}{b_{ext-0}} \left[ 3.912 - \ell n\left(\frac{I_{hp}}{I_h}\right) - \tau_p \right] \quad . \tag{57}$$

The second term in the brackets is necessary to account for the effect of light absorption caused by plume $NO_2$ on the contrast between the horizon sky ($I_{hp}$) and the black object seen through the plume. It can easily be shown that the effect of the plume on visual range is significantly less when the plume is discolored by $NO_2$ ($I_{hp}/I_h < 1$), and greater when the plume is bright ($I_{hp}/I_h > 1$). As a corollary, it is also true that with increasing distance between the observer and the plume, the impact of plume $NO_2$ on visual range increases as plume coloration decreases. This somewhat surprising result was confirmed in the sensitivity analysis of the plume visibility code.

## 2. Contrast of Haze Layers and Plumes

Contrast can be used to characterize the perceptibility of a haze layer or a plume against a background--the sky, a cloud, or a distant mountain. A plume would be visible if the absolute value of the contrast between it and the background were greater than a threshold or liminal contrast. Figure 23 is a photograph of a plume illustrating plume contrast. The plume is clearly visible against the mountain because the plume light intensity is greater than that of the mountain. Thus, the contrast of the plume against the mountain can be calculated using Eq. (45):

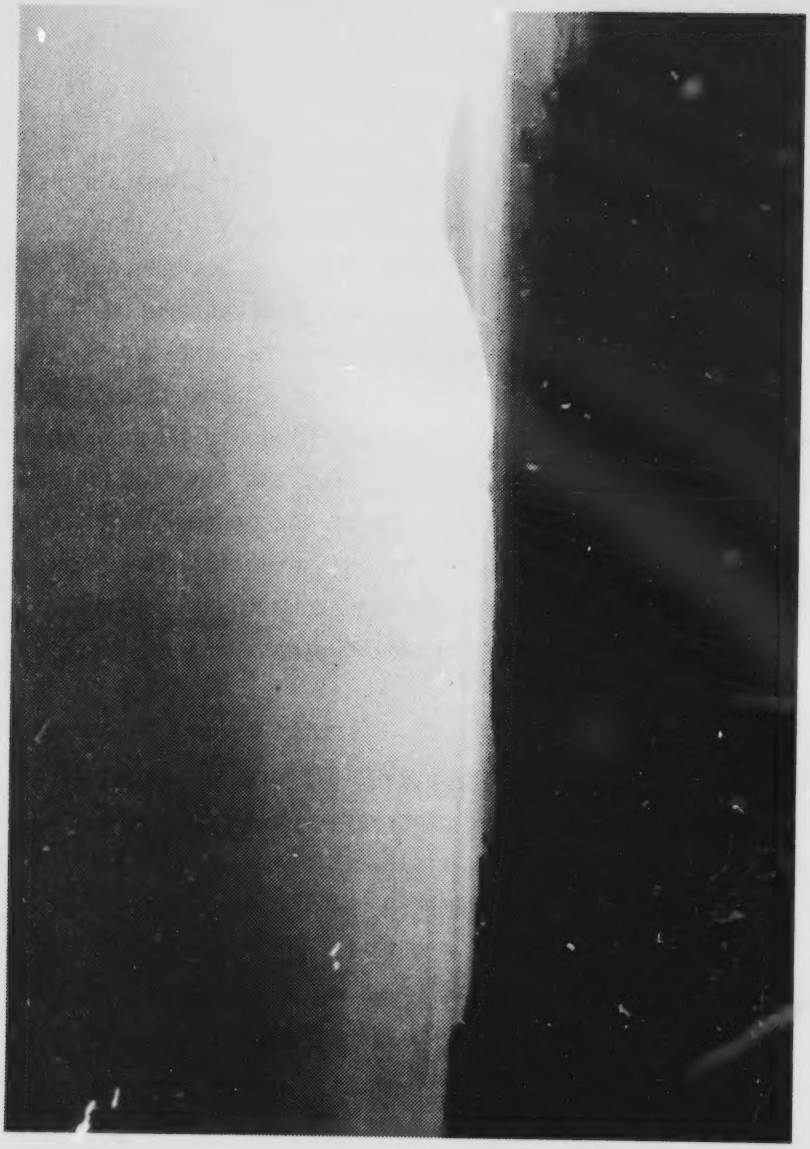

FIGURE 23. AN EXAMPLE OF PLUME VISUAL IMPACT

$$C_p = \frac{I_p - I_m}{I_m} > 0 \quad . \tag{58}$$

The plume is also visible against the horizon sky, perhaps mainly because of the color change, but also because of contrast:

$$C_p = \frac{I_p - I_h}{I_h} < 0 \quad . \tag{59}$$

The magnitude and the sign of the contrast of a haze layer or plume against a background is therefore a useful way to characterize visibility impairment. Positive contrasts refer to plumes brighter than the background, whereas negative contrasts refer to plumes darker than the background. We do not have any experimental data for liminal contrast (the barely perceptible threshold contrast) in the case of a plume against a background. The same liminal contrast used to define visual range (0.02) could be used to define plume visibility. However, it seems likely that the liminal contrast for plumes is greater than 0.02 because in many cases the boundary between a plume and the background is not distinct owing to the nature of plume dilution. It would be useful to carry out some experiments with several observers and plume views to determine the liminal contrast for an average observer.

Contrast of plumes can be evaluated at several different wavelengths; we used 0.55 μm for the evaluation of plume contrast. However, plume contrast may be greater at the blue end of the visible spectrum. Latimer and Samuelsen (1975, 1978) used the ratio of plume to background intensities at the blue end ($\lambda = 0.4$ μm) and at the red end ($\lambda = 0.7$ μm) as a means of characterizing the wavelength-dependent plume contrast and plume coloration with respect to the background. This blue-red luminance ratio is defined as:

$$R = \frac{I_p(0.4\ \mu m)/I_h(0.4\ \mu m)}{I_p(0.7\ \mu m)/I_h(0.7\ \mu m)} = \frac{C_p(0.4\ \mu m) + 1}{C_p(0.7\ \mu m) + 1} \quad . \tag{60}$$

The use of the luminance ratio in conjunction with the plume contrast at 0.55 μm is a simple way of characterizing plume color. When $R > 1$, the plume is more blue than the background; when $R < 1$, the plume is redder (or more yellow-brown); when $R = 1$, with $C_p(0.55\ \mu m) > 0$, the plume is a brighter white than the horizon, and with $C_p(0.55\ \mu m) < 0$, the plume is a darker grey. We discuss more sophisticated methods of quantifying color in the next subsection.

### 3. Color

The color associated with a given spectral light intensity distribution is due to processes occurring in the human eye. The retina has three different frequency sensors that convert signals into color sensations by means of the brain. The system operates so that an object that reflects half blue light and half yellow light is identified not as yellow-blue, but rather as a new color, green. This attribute of the eye-brain system gives rise to another mode of detecting an object, that of color change or discoloration. Thus, an object can be perceived because it has a different brightness from that of the background (contrast) or because it has a different color (so-called color contrast). Gases and particles in the atmosphere can give rise to coloration by their scattered light (blue sky or white clouds) or by altering the color of objects seen through them (brown coloration due to $NO_2$).

The chromaticity diagram was developed to quantify the concept of color. In such a diagram, the spectral distribution of light is weighted with three functions corresponding to the detectors in the eye. For any distribution of light, there are three numbers, which define a point in space. Next, the projection of the point onto a unit plane ($x + y + z = 1$) is computed. The result is a two-dimensional surface called a chromaticity diagram (see Figure 24). Monochromatic light forms the outside of the surface, and white light is located in the center. Any color can thus be represented by its chromaticity coordinates $(x,y)$, which are defined by:

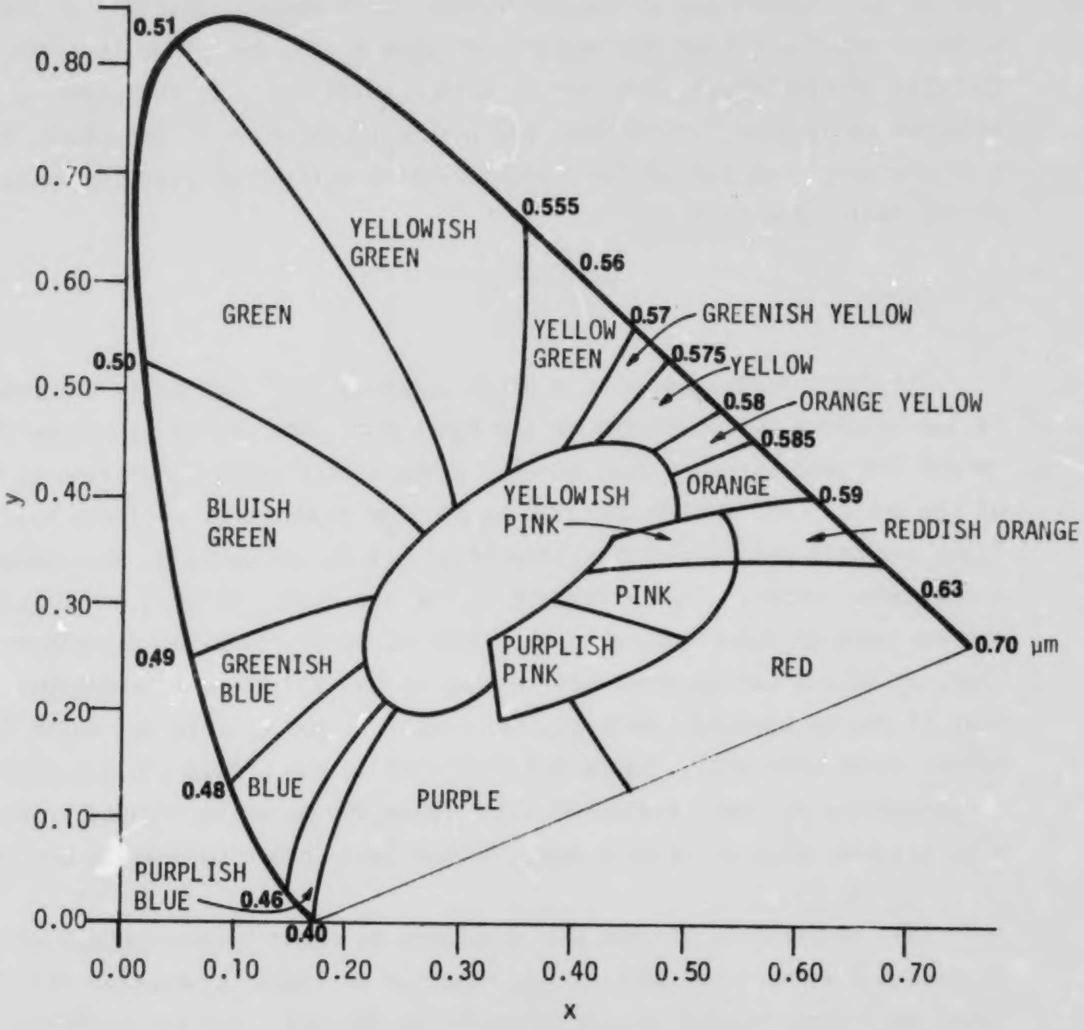

FIGURE 24. CHROMATICITY DIAGRAM

$$x = \frac{X}{X + Y + Z} \quad ; \quad y = \frac{Y}{X + Y + Z} \quad , \qquad (61)$$

where

$$X = \int_{\lambda} I(\lambda)\ \bar{x}\ d\lambda \quad ,$$

$$Y = \int_{\lambda} I(\lambda)\ \bar{y}\ d\lambda \quad ,$$

$$Z = \int_{\lambda} I(\lambda)\ \bar{z}\ d\lambda \quad ,$$

and $I(\lambda)$ is the wavelength distribution of light and $x$, $y$, $z$ are the three weighting functions. The weighting functions (called tristimulus values) are shown in Figure 25.

Horvath (1971) and Husar and White (1976) computed chromaticity coordinates of atmospheric scattered or transmitted light and showed that the light would be distinguishable from white light for various sun angles, aerosol properties, and $NO_2$ concentrations. Since the chromaticity diagram does not differentiate between differences in intensity (e.g., between yellow and brown or between white, grey, and black), chromaticity coordinates must be used in conjunction with a descriptor of light intensity for a complete specification of color. Thus, if we establish a color solid by taking the two-dimensional chromaticity diagram and adding a third dimension perpendicular to this plane to represent brightness, we have a means of completely specifying by three coordinates the color and intensity of a color.

Figure 26 is a drawing of such a color solid. The brightness in such a coordinate system is usually specified by the value of Y [see Eq. (61)] or by a parameter ($L^*$), which is directly proportional to the subjective perception of brightness and is related to Y as follows:

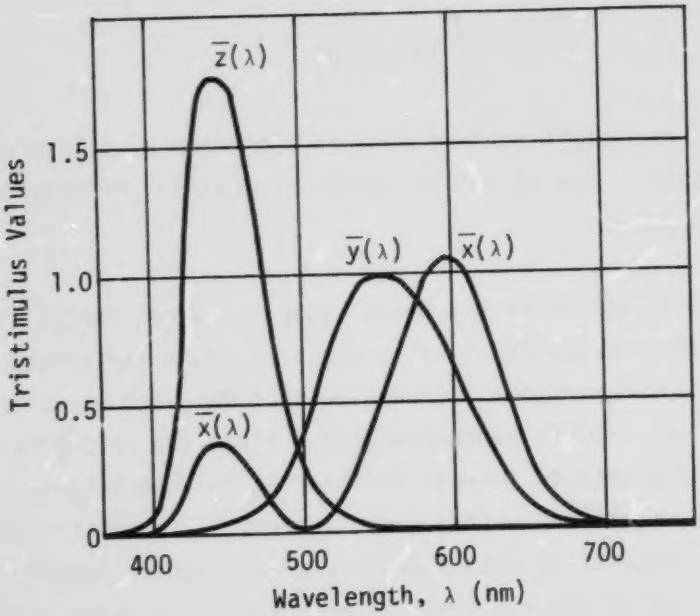

Source: Judd and Wyszecki (1975).

FIGURE 25. SPECTRAL TRISTIMULUS VALUES $\bar{x}(\lambda)$, $\bar{y}(\lambda)$, $\bar{z}(\lambda)$

$$L^* = 25\ Y^{1/3} - 17 \quad . \tag{62}$$

L* is used in quantifying color differences and is simply the parameter called "value" in the Munsell color system multiplied by 10.

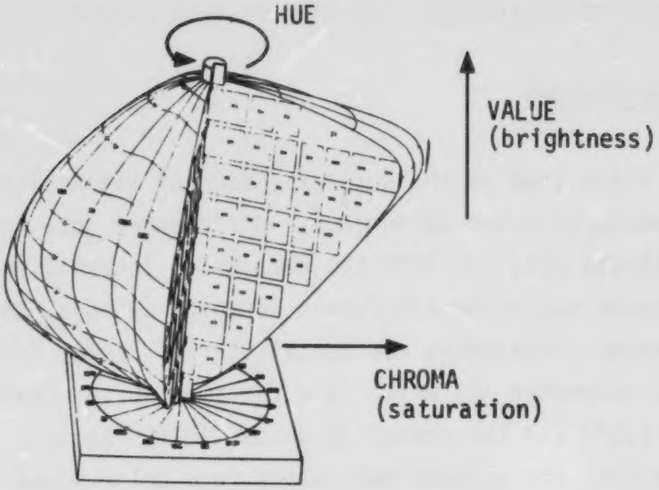

Source: Munsell Color Company (1976).

FIGURE 26. REPRESENTATION OF A COLOR SOLID

The Munsell color system is the most widely used means of specifying colors. In this system, colors are arranged in order by value (brightness), hue (the shade of color, for example, yellow, red, green, blue), and chroma or saturation (the degree of departure of a given hue from a neutral grey of the same value). By specifying a given hue, value, and chroma, one can obtain a sample color chip from the Munsell Book of Color that corresponds to the specification. By this means, the objective specification of color

(L*,x,y) can be related to the subjective perception of color by visually examining the color paint chip. ASTM Standard D 1535-68 (American Society for Testing and Materials, 1974) is the reference method for converting objective color specifications (L*,x,y) to the Munsell hue, value, and chroma notations by which a colored paint sample can be selected. We used this method to convert light intensity (Y or L*) and chromaticity coordinates (x,y) calculated by the plume and regional visibility models to Munsell notation to be used by a commercial artist in illustrating atmospheric discoloration. We discuss this process in Chapter IV.

### 4. Color Changes

The final step in the quantification of visibility impairment is the specification of color differences--differences both in chromaticity (x,y) and brightness (Y). In 1976 the Commission Internationale de l'Eclairage (CIE) adopted two color difference formulae by which the perceived magnitude of color differences can be calculated. Color differences are specified by a parameter $\Delta E$, which is a function of the change in light intensity or value ($\Delta L^*$) and the change in chromaticity ($\Delta x, \Delta y$). $\Delta E$ can be considered as a distance between two colors in a color space that is transformed in such a way that equal distances ($\Delta E$) between any two colors correspond to equally perceived color changes. This suggests that a threshold ($\Delta E_0$) can be found to determine whether a given color change is perceptible.

Since the CIE could not decide between two different proposed formulae for $\Delta E$, both were adopted in 1976 as standard means by which color differences can be specified. These color differences, which are labeled $\Delta E(L^*U^*V^*)$ and $\Delta E(L^*a^*b^*)$, are calculated as follows:

$$\Delta E(L^*U^*V^*) = [(\Delta L^*)^2 + (\Delta U^*)^2 + (\Delta V^*)^2]^{1/2} \quad ,$$

where

$$L^* = 116\,(Y/Y_0)^{1/3} - 16,$$
$$U^* = 13W^*(u - u_0),$$
$$V^* = 13W^*(v - v_0),$$

and u and v are defined as

$$u = \frac{4X}{(X + 15Y + 3Z)} \quad , \quad v = \frac{6Y}{(X + 15Y + 3Z)}$$

and $u_0$, $v_0$ as

$$u_0 = \frac{4X_0}{(X_0 + 15Y_0 + 3Z_0)} \quad , \quad v_0 = \frac{6Y_0}{(X_0 + 15Y_0 + 3Z_0)} \quad .$$

Similarly,

$$\Delta E(L^*a^*b^*) = [(\Delta L^*)^2 + (\Delta a^*)^2 + (\Delta b^*)^2]^{1/2} \quad ,$$

where L* is defined as above and

$$a^* = 500\left[\left(\frac{X}{X_0}\right)^{1/3} - \left(\frac{Y}{Y_0}\right)^{1/3}\right] \quad ,$$

$$b^* = 200\left[\left(\frac{Y}{Y_0}\right)^{1/3} - \left(\frac{Z}{Z_0}\right)^{1/3}\right] \quad .$$

In these equations, the tristimulus values $X_0$, $Y_0$, $Z_0$ define the color of the nominally white object-color stimulus. In our atmospheric discoloration calculations, we used values of $X_0$, $Y_0$, $Z_0$ corresponding to the reflected intensity from a perfectly diffuse reflector normal to the direct solar beam. Calculations are normalized such that $Y_0 = 100$.

To determine the liminal or threshold (just perceptible) value of ΔE, we computed ΔE for two color fields with identical chromaticities ($\Delta U^* = \Delta V^* = \Delta a^* = \Delta b^* = 0$) and with a contrast of 0.02 (i.e., $Y_2 = 0.98Y_1$) as:

$$\Delta E = 116\left(\frac{Y_1}{Y_0}\right)^{1/3}\left(1 - 0.98^{1/3}\right) = 0.78\left(\frac{Y_1}{Y_0}\right)^{1/3} \quad .$$

Thus, for a bright horizon (say, $Y_1 = 100$), we obtain a threshold or liminal $\Delta E$ equal to 0.78. This value can be compared with a $\Delta E = 10$, which is the difference between two colors having identical Munsell hue and chroma but with values differing by 1. Thus, $\Delta E$ can be used as indicator of atmospheric discoloration: $\Delta E$'s less than 1 would be imperceptible, those between 1 and 10 would be detected as a discoloration by most people, and the severity of discoloration would increase with increasing $\Delta E$. More work is clearly necessary to determine what the standards of atmospheric discoloration should be.

# IV THE OUTPUT OF VISIBILITY MODELS

This chapter discusses the outputs from several sample calculations using our regional and plume visibility models. The models are described from the viewpoint of a person who will be faced with regulatory, siting, and design decisions based on the output of such models. We provide samples of graphic display alternatives that can be used to translate quantitative descriptions of visibility impairment into color samples, perspective views, artist's renderings, and color television video displays. These display techniques enable the user to understand the meaning of visibility impairment models. Further details of the models and sample outputs are given in Appendices D, E, F, and G.

The following models are illustrated by examples:

- Plume visibility model.
  - Emissions from a hypothetical 2250 Mwe coal-fired power plant meeting New Source Performance Standards.
  - Emissions from a large copper smelter in Arizona.
  - Emissions from a large coal-fired power plant in Arizona.
- Plume/terrain perspective and color graphic displays--emissions from a large coal-fired power plant in Arizona.
- Regional visibility model.
  - 1976 and 1986 $SO_x$ and $NO_x$ emissions from sources in the Northern Great Plains.
  - 1973 $SO_x$ emissions from copper smelters in Arizona and New Mexico.

## A. THE PLUME VISIBILITY MODEL

The plume visibility model predicts the visibility impairment resulting from emissions from a single source, such as a power plant or smelter . The model calculates the reduction in visual range caused by the plume for several observer locations, and it also calculates plume color, plume contrast, and color changes to determine whether the plume can be distinguished by an observer. In this latter regard, the plume model differs from the regional model, which calculates the visual effects of a relatively homogeneous atmosphere. The plume model quantifies the coloration and appearance of a plume in comparison with the homogeneous background atmosphere and thereby characterizes the perceptibility of the plume. The logic flow, program structure, and data requirements of the plume visibility code (PLUVUE) are presented in detail in Appendix D. In this section, we illustrate and discuss sample outputs of the model.

The user of the model must provide the source emission parameters, ambient meteorological conditions, ambient air quality, and background aerosol size distribution parameters. Exhibit 1 lists the parameters of the sample calculation done for the hypothetical 2250 Mwe coal-fired power plant, which was assumed to emit particulates, $SO_2$, and $NO_x$ at the maximum rates permitted by the EPA's New Source Performance Standards. The user must also select the dispersion coefficients ($\sigma_y$, $\sigma_z$) to be used to compute plume dilution as a function of downwind distance. The code has subroutines for Pasquill-Gifford and for TVA dispersion coefficients, and it will also accept values entered by the user.

After computing the initial plume dilution and $NO_2$ formation during plume rise from the stack to the location of final plume rise (1.2 km downwind), the code calculates pollutant concentrations within the plume and parameters characterizing plume visual impact at distances from 1.2 out to 350 km downwind of the source. Exhibit 2 presents an example of the pollutant concentration parameters that are printed out at each downwind distance. In that exhibit, both the plume increments and the total

```
VISUAL IMPACT ASSESSMENT FOR 2250 MW COAL POWER PLANT

   POWER PLANT DATA

      ELEVATION OF SITE =          0.  FEET MSL
                                   0.  METERS MSL

      NO. OF UNITS =    3.

      STACK HEIGHT =  700.  FEET
                      213.  METERS

      FLUE GAS FLOW RATE =   1724000.  CU FT/MIN
                               813.32  CU M/SEC

      FLUE GAS TEMPERATURE =        230.  F
                                    394.  K

      FLUE GAS OXYGEN CONTENT =        1.7  MOL PERCENT

      SO2 EMISSION RATE (TOTAL) =     276.43  TONS/DAY
                                    2.903E+03  G/SEC

      NOX EMISSION RATE (TOTAL,AS NO2) =     161.23  TONS/DAY
                                           1.693E+03  G/SEC

      PARTICULATE EMISSION RATE (TOTAL) =      3.43  TONS/DAY
                                           3.623E+01  G/SEC

   METEOROLOGICAL AND AMBIENT AIR QUALITY DATA

      WINDSPEED =  11.2  MILES/HR
                    3.0  M/SEC

      PASQUILL-GIFFORD-TURNER STABILITY CATEGORY E

      LAPSE RATE =  0.00  F/1000 FT
                    0.          K/M
```

EXHIBIT 1. SAMPLE PLUME MODEL OUTPUT: INPUT EMISSION AND AMBIENT CONDITIONS

```
POTENTIAL TEMPERATURE LAPSE RATE =    9.800E-03  K/M

SOLAR ZENITH ANGLE =  43.0  DEGREES

AMBIENT TEMPERATURE =  77.0  F
                      298.2  K

RELATIVE HUMIDITY =  40.0  %

MIXING DEPTH = 2000.  M

AMBIENT PRESSURE =  1.00  ATM

SO2 TO SO4 CONVERSION RATE =        .300 PERCENT/HR

NOX TO NO3 CONVERSION RATE =       0.000 PERCENT/HR

BACKGROUND NOX CONCENTRATION =      0.000  PPM

BACKGROUND NO2 CONCENTRATION =      0.000  PPM

BACKGROUND OZONE CONCENTRATION =       .040  PPM

BACKGROUND SO2 CONCENTRATION =      0.000  PPM

BACKGROUND COARSE MODE CONCENTRATION =       30.0  UG/M3

BACKGROUND SULFATE CONCENTRATION =        1.7  UG/M3

BACKGROUND NITRATE CONCENTRATION =        0.0  UG/M3

BACKGROUND VISUAL RANGE =      130.0  KILOMETERS

SO2 DEPOSITION VELOCITY =       1.00  CM/SEC

NOX DEPOSITION VELOCITY =       1.00  CM/SEC

COARSE PARTICULATE DEPOSITION VELOCITY =        .10  CM/SEC

SUBMICRON PARTICULATE DEPOSITION VELOCITY =        .10  CM/SEC
```

EXHIBIT 1 (Concluded)

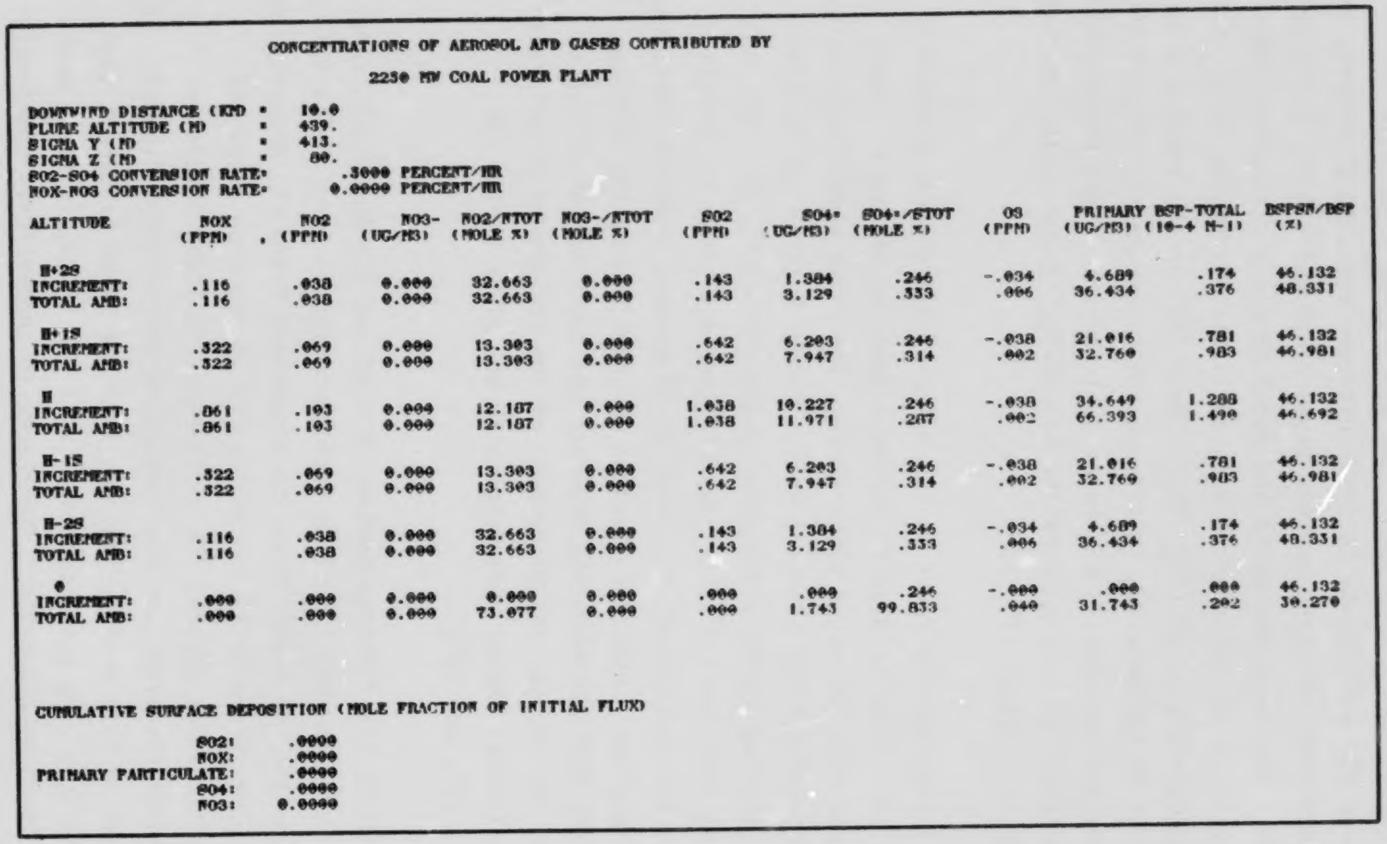

```
                    CONCENTRATIONS OF AEROSOL AND GASES CONTRIBUTED BY

                                  2230 MW COAL POWER PLANT

DOWNWIND DISTANCE (KM) =    10.0
PLUME ALTITUDE (M)     =    439.
SIGMA Y (M)            =    413.
SIGMA Z (M)            =     80.
SO2-SO4 CONVERSION RATE=       .3000 PERCENT/HR
NOX-NO3 CONVERSION RATE=      0.0000 PERCENT/HR

ALTITUDE          NOX        NO2      NO3-   NO2/NTOT  NO3-/NTOT     SO2       SO4=  SO4=/STOT     O3      PRIMARY BSP-TOTAL  BSPSN/BSP
                 (PPM)   , (PPM)   (UG/M3)  (MOLE %)  (MOLE %)     (PPM)    (UG/M3)  (MOLE %)   (PPM)    (UG/M3) (10-4 M-1)  (%)

 H+2S
INCREMENT:       .116       .038     0.000    32.663     0.000      .143      1.384      .246     -.034     4.689       .174     46.132
TOTAL AMB:       .116       .038     0.000    32.663     0.000      .143      3.129      .333      .066    36.434       .376     48.331

 H+1S
INCREMENT:       .322       .069     0.000    13.303     0.000      .642      6.203      .246     -.038    21.016       .781     46.132
TOTAL AMB:       .322       .069     0.000    13.303     0.000      .642      7.947      .314      .002    32.760       .983     46.981

 H
INCREMENT:       .861       .103     0.004    12.187     0.000     1.038     10.227      .246     -.038    34.649      1.288     46.132
TOTAL AMB:       .861       .103     0.000    12.187     0.000     1.038     11.971      .287      .002    66.393      1.490     46.692

 H-1S
INCREMENT:       .322       .069     0.000    13.303     0.000      .642      6.203      .246     -.038    21.016       .781     46.132
TOTAL AMB:       .322       .069     0.000    13.303     0.000      .642      7.947      .314      .002    32.769       .983     46.981

 H-2S
INCREMENT:       .116       .038     0.000    32.663     0.000      .143      1.384      .246     -.034     4.689       .174     46.132
TOTAL AMB:       .116       .038     0.000    32.663     0.000      .143      3.129      .333      .006    36.434       .376     48.331

  0
INCREMENT:       .000       .000     0.000     0.000     0.000      .000       .000      .246     -.000      .000       .000     46.132
TOTAL AMB:       .000       .000     0.000    73.077     0.000      .000      1.743    99.833      .040    31.743       .202     30.270



CUMULATIVE SURFACE DEPOSITION (MOLE FRACTION OF INITIAL FLUX)

                 SO2:    .0000
                 NOX:    .0000
PRIMARY PARTICULATE:    .0000
                 SO4:    .0000
                 NO3:   0.0000
```

EXHIBIT 2.  SAMPLE PLUME MODEL OUTPUT:  POLLUTANT CONCENTRATIONS

ambient concentrations are displayed. The mole ratios of sulfate to total sulfur and $NO_2$ and nitrate to total nitrogen are also displayed, as are the concentrations of ozone and the plume ozone deficit resulting from $NO_2$ production. The plume increment and total particle scattering coefficient ($b_{sp}$ at 0.55 μm) are printed out, as is the percentage of $b_{sp}$ contributed by secondary aerosol ($SO_4^=$, $NO_3^-$). Note that in the example given in Exhibit 1, at 10 km downwind, sulfate--which is assumed to form at the rate of 0.5 percent per hour--contributes 46.1 percent of the plume scattering coefficient, the remainder of the scattering is due to the emitted primary particulate matter (fly ash).

Exhibit 3 provides the first of the three visual effects printouts that the user can choose to display for each downwind distance. These computations are done for sight paths through the plume center and can be done for ground-level sight paths as well. Visual effects can be displayed for scattering angles $\Theta$ selected by the user ($22^\circ$, $45^\circ$, $90^\circ$, $135^\circ$, and $180^\circ$); only $180^\circ$ (back scatter) calculations are shown in Exhibit 3. Visual effects are calculated as a function of assumed observer location relative to the plume. Observer location is specified by the distance (along the sight path) between the observer and the plume at distances that are 2, 5, 10, 20, 50, and 80 percent of the background visual range and at four azimuthal angles with respect to the plume centerline ($\alpha = 30^\circ$, $45^\circ$, $60^\circ$, and $90^\circ$).

In Exhibit 3, the first parameters printed out are the visual range $r_v$ and the percentage reduction from background visual range. The following two columns are the light intensity parameters Y and L*, described in Chapter III. The chromaticity coordinates (x,y) are then displayed, followed by two columns showing the differences in light intensity ($\Delta Y$, $\Delta L^*$) between the plume and the background sky (without clouds). The negative values in this example indicate that the plume is darker than the background sky. The plume contrast (at $\lambda = 0.55$ μm) is shown next, succeeded by the blue-red ratio. The change in chromaticity coordinates between the plume and the background sky is shown next ($\Delta x, \Delta y$). Positive

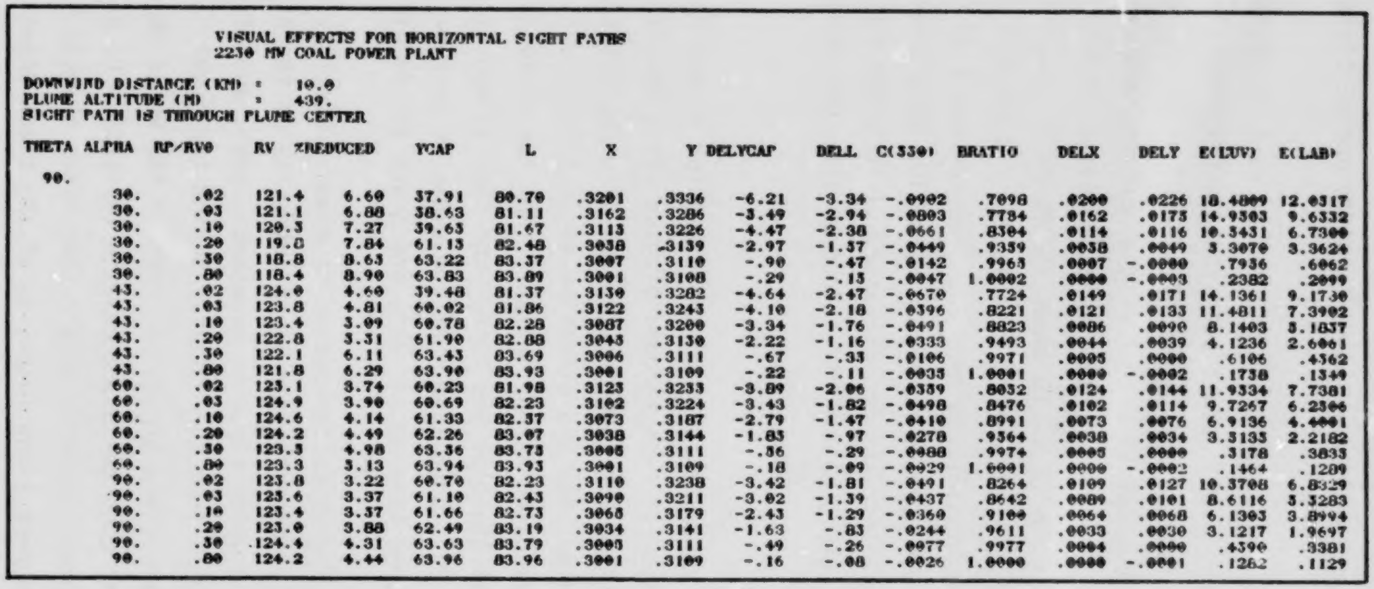

```
                VISUAL EFFECTS FOR HORIZONTAL SIGHT PATHS
                2230 MW COAL POWER PLANT

DOWNWIND DISTANCE (KM) :   10.0
PLUME ALTITUDE (M)     :   439.
SIGHT PATH IS THROUGH PLUME CENTER

THETA ALPHA  RP/RV0     RV  %REDUCED     YCAP        L         X         Y DELYCAP     DELL  C(550)  BRATIO     DELX      DELY  E(LUV)  E(LAB)

  90.
        30.      .02   121.4     6.60    57.91    80.70     .3201     .3336   -6.21    -3.34  -.0902    .7098    .0200     .0226 18.4809 12.0317
        30.      .05   121.1     6.80    58.63    81.11     .3162     .3286   -5.49    -2.94  -.0803    .7784    .0162     .0175 14.9303  9.6332
        30.      .10   120.3     7.27    59.63    81.67     .3115     .3226   -4.47    -2.38  -.0661    .8304    .0114     .0116 10.3431  6.7300
        30.      .20   119.0     7.84    61.15    82.48     .3058     .3139   -2.97    -1.57  -.0449    .9359    .0058     .0049  5.3070  3.3624
        30.      .50   118.8     8.65    63.22    83.37     .3007     .3110    -.90     -.47  -.0142    .9965    .0007    -.0000   .7936   .6062
        30.      .80   118.4     8.90    63.83    83.89     .3001     .3108    -.29     -.15  -.0047   1.0002    .0000    -.0003   .2382   .2099
        45.      .02   124.0     4.60    59.48    81.37     .3130     .3282   -4.64    -2.47  -.0670    .7724    .0149     .0171 14.1361  9.1730
        45.      .05   123.8     4.81    60.02    81.86     .3122     .3245   -4.10    -2.18  -.0396    .8221    .0121     .0133 11.4811  7.3902
        45.      .10   123.4     5.09    60.78    82.28     .3087     .3200   -3.34    -1.76  -.0491    .8823    .0086     .0090  8.1403  5.1837
        45.      .20   122.8     5.31    61.90    82.88     .3045     .3130   -2.22    -1.16  -.0333    .9493    .0044     .0039  4.1236  2.6061
        45.      .50   122.1     6.11    63.45    83.69     .3006     .3111    -.67     -.35  -.0106    .9971    .0005     .0000   .6106   .4362
        45.      .80   121.8     6.29    63.90    83.93     .3001     .3109    -.22     -.11  -.0035   1.0001    .0000    -.0002   .1738   .1349
        60.      .02   125.1     3.74    60.23    81.98     .3125     .3233   -3.89    -2.06  -.0359    .8052    .0124     .0144 11.9334  7.7381
        60.      .05   124.9     3.90    60.69    82.23     .3102     .3224   -3.43    -1.82  -.0498    .8476    .0102     .0114  9.7267  6.2306
        60.      .10   124.6     4.14    61.33    82.57     .3073     .3187   -2.79    -1.47  -.0410    .8991    .0073     .0076  6.9136  4.4001
        60.      .20   124.2     4.49    62.26    83.07     .3038     .3144   -1.85     -.97  -.0278    .9364    .0038     .0034  3.3135  2.2182
        60.      .50   123.5     4.98    63.36    83.75     .3005     .3111    -.56     -.29  -.0088    .9974    .0005     .0000   .3178   .3833
        60.      .80   123.3     5.13    63.94    83.93     .3001     .3109    -.18     -.09  -.0029   1.0001    .0000    -.0002   .1464   .1209
        90.      .02   125.8     3.22    60.70    82.23     .3110     .3238   -3.42    -1.81  -.0491    .8264    .0109     .0127 10.3708  6.8329
        90.      .05   125.6     3.37    61.10    82.45     .3090     .3211   -3.02    -1.39  -.0437    .8642    .0089     .0101  8.6116  5.3283
        90.      .10   125.4     3.57    61.66    82.75     .3065     .3179   -2.45    -1.29  -.0360    .9100    .0064     .0068  6.1303  3.8994
        90.      .20   125.0     3.88    62.49    83.19     .3034     .3141   -1.63     -.85  -.0244    .9611    .0033     .0030  3.1217  1.9697
        90.      .50   124.4     4.31    63.63    83.79     .3005     .3111    -.49     -.26  -.0077    .9977    .0004     .0000   .4390   .3381
        90.      .80   124.2     4.44    63.96    83.96     .3001     .3109    -.16     -.08  -.0026   1.0000    .0000    -.0001   .1262   .1129
```

EXHIBIT 3.   SAMPLE PLUME MODEL OUTPUT:  VISUAL EFFECTS FOR HORIZONTAL SIGHT PATHS

$\Delta x$'s and $\Delta y$'s indicate a shift toward yellow-brown, and negative values indicate a shift toward blue relative to the horizon. The final two columns are the CIE color difference values $\Delta E(L^*U^*V^*)$ and $\Delta E(L^*a^*b^*)$.

To understand how the values in Exhibit 3 can be used to characterize plume color, consider an observer's sight path that is perpendicular to the plume ($\alpha = 90°$) at a distance $r_p/r_{V0} = 0.02$. An L* of 82.23 indicates that the plume is bright, but not as bright as the horizon because $\Delta Y$, $\Delta L^*$, and C are all negative. The chromaticity coordinates (0.3181,0.3253) used in conjunction with L* (which is 10 times the Munsell "value") specify the Munsell color notation, which in this case is 2.5 Y 8.912/0.6, a weakly saturated yellow, essentially grey. The blue-red ratio of 0.9194 also indicates a slight, but perhaps not visible, yellow discoloration. However, the contrast of -0.1611 and the $\Delta E$ values of 10.6 and 6.8 indicate that the plume would be visible because it is darker than the background horizon sky.

Exhibit 4 shows the visual effects of the plume for nonhorizontal sight paths when viewed against a background of blue sky. Note that visual effects are calculated for the permutations of $\alpha$ (azimuthal angle relative to the plume centerline) and elevation angle $\beta$ (15°, 30°, 45°, 60°, 75°, and 90°). These calculations indicate that the plume is more distinctly visible against the blue sky background than it was against the horizon sky (Exhibit 2). Note also that the plume is much brighter than the blue sky background because $\Delta Y$, $\Delta L^*$, and C are all positive.

Exhibit 5 completes the characterization of plume visibility at a given downwind distance by comparing the light intensity of the plume with white (representative of a white cloud or snowbank), grey, and black backgrounds at various distances from the observer behind the plume. The plume appears somewhat darker and bluish in front of the white object (REFLECT = 1) and brighter than the black objects (REFLECT = 0) at close distances. The plume appears slightly darker than black objects at long distances because the apparent light intensity of the black object distant from the observer approaches that of the horizon.

```
            VISUAL EFFECTS FOR NON-HORIZONTAL CLEAR SKY VIEWS THROUGH PLUME CENTER

            2230 MW COAL POWER PLANT

DOWNWIND DISTANCE (KM) :    10.0
PLUME ALTITUDE (M)     :    439.

THETA   ALPHA   BETA     RP    YCAP      L       X        Y DELYCAP    DELL  C(550)  BRATIO    DELX    DELY  E(LUV)  E(LAB)
 90.
         30.     15.   3.31   37.00   67.37   .2842   .3003    2.30    1.91   .0075   .3479   .0278   .0336 23.1732 14.8306
         30.     30.   1.58   27.23   39.22   .2817   .2961    6.34    6.83   .3282   .4340   .0340   .0448 22.7396 16.2136
         30.     45.    .98   23.40   33.32   .2824   .2963    7.86    9.12   .3383   .4094   .0376   .0497 22.0940 17.1202
         30.     60.    .67   21.37   33.60   .2833   .2971    8.39   10.83   .6996   .3846   .0399   .0327 21.8037 17.8216
         30.     75.    .50   20.69   32.65   .2840   .2978    8.93   11.77   .8007   .3715   .0412   .0344 21.7299 18.2687
         30.     90.    .44   20.43   32.35   .2843   .2980    9.03   12.07   .8351   .3673   .0416   .0350 21.7237 18.4234
         45.     15.   2.36   36.27   66.76   .2779   .2928    1.69    1.30   .0615   .6235   .0213   .0281 18.3946 11.7634
         45.     30.   1.16   25.32   37.61   .2740   .2866    4.63    4.74   .2411   .5370   .0263   .0333 17.7689 12.6348
         45.     45.    .76   21.34   33.35   .2742   .2860    5.80    6.93   .3978   .4911   .0294   .0395 17.1462 13.3322
         45.     60.    .37   19.34   31.11.  .2748   .2863    6.36    8.34   .3183   .4646   .0314   .0421 16.8647 13.8824
         45.     75.    .47   18.38   49.99   .2733   .2869    6.62    9.12   .3943   .4303   .0325   .0433 16.7679 14.2343
         45.     90.    .44   18.10   49.63   .2733   .2871    6.70    9.37   .6202   .4461   .0329   .0440 16.7473 14.3346
         60.     15.   1.94   33.93   66.30   .2746   .2888    1.33    1.04   .0300   .6677   .0182   .0241 13.8119 10.1106
         60.     30.    .98   24.73   36.84   .2700   .2813    3.83    3.97   .2003   .3866   .0224   .0302 13.1714 10.8090
         60.     45.    .67   20.36   32.28   .2699   .2806    4.82    5.88   .3314   .5409   .0231   .0340 14.6108 11.3083
         60.     60.    .33   18.28   49.87   .2794   .2808    3.30    7.10   .4324   .5138   .0270   .0364 14.3391 11.8708
         60.     75.    .46   17.29   48.66   .2798   .2811    3.32    7.78   .4960   .4992   .0280   .0377 14.2714 12.1816
         60.     90.    .44   16.99   48.28   .2710   .2813    3.39    8.00   .3177   .4946   .0283   .0382 14.2323 12.2880
         90.     15.   1.70   33.73   66.34   .2725   .2862    1.13     .89   .0432   .6982   .0161   .0215 14.1191  9.0267
         90.     30.    .88   24.24   36.36   .2673   .2783    3.33    3.30   .1732   .6213   .0198   .0270 13.4930  9.6188
         90.     45.    .62   19.76   31.61   .2672   .2770    4.22    5.20   .2903   .3763   .0224   .0304 12.9844 10.1392
         90.     60.    .51   17.63   49.08   .2673   .2771    4.63    6.30   .3793   .3490   .0241   .0327 12.7383 10.3794
         90.     75.    .43   16.61   47.80   .2679   .2773    4.83    6.93   .4332   .3342   .0231   .0339 12.6809 10.8646
         90.     90.    .44   16.30   47.41   .2681   .2774    4.91    7.13   .4343   .3293   .0234   .0344 12.6643 10.9626
```

EXHIBIT 4. SAMPLE PLUME MODEL OUTPUT: VISUAL EFFECTS FOR NONHORIZONTAL SIGHT PATHS

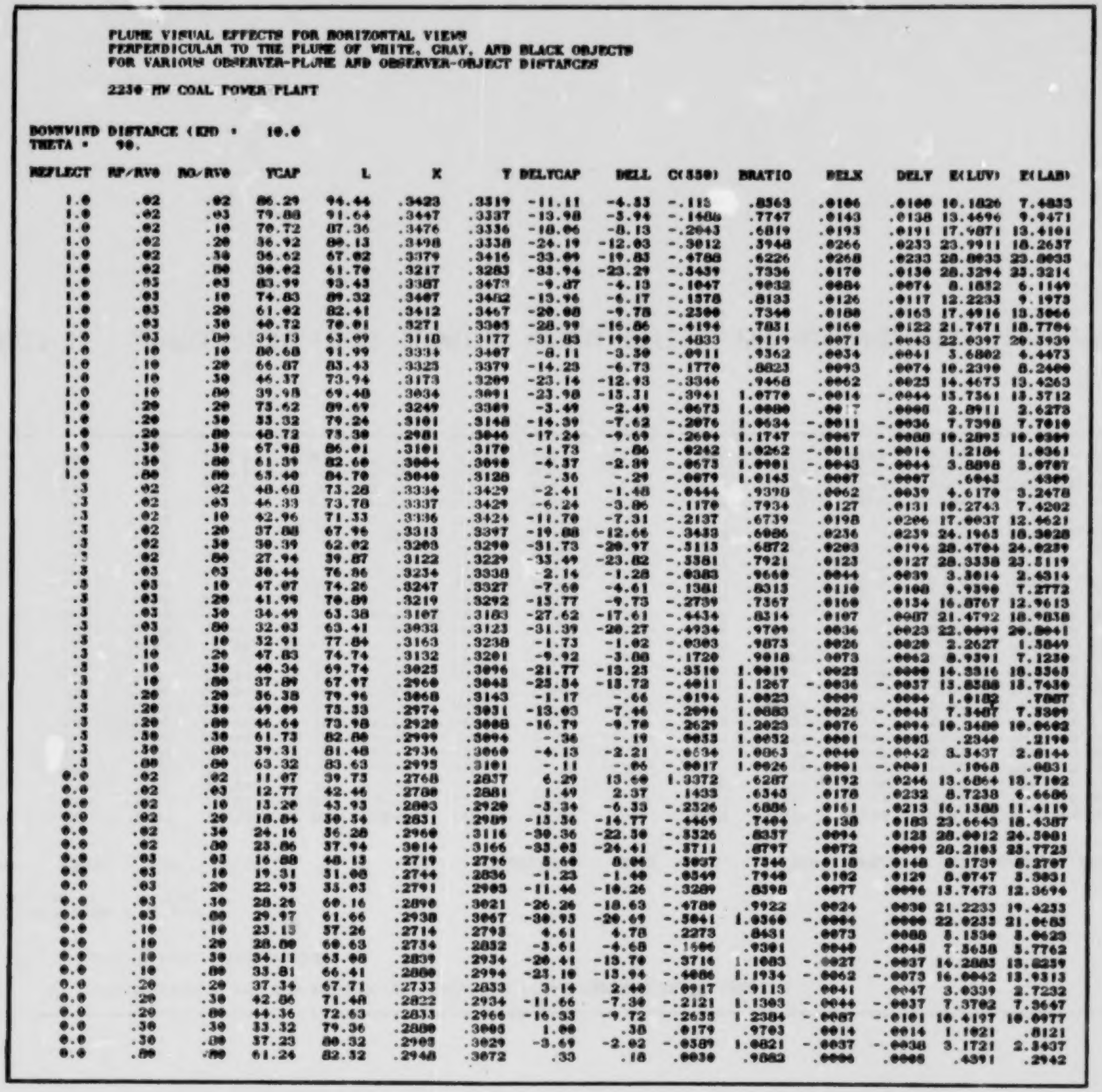

```
        PLUME VISUAL EFFECTS FOR HORIZONTAL VIEWS
        PERPENDICULAR TO THE PLUME OF WHITE, GRAY, AND BLACK OBJECTS
        FOR VARIOUS OBSERVER-PLUME AND OBSERVER-OBJECT DISTANCES

        2230 MW COAL POWER PLANT

DOWNWIND DISTANCE (KM) =    10.0
THETA =    90.

REFLECT  RP/RV0  RO/RV0   YCAP      L       X        Y DELYCAP    DELL  C(550)  BRATIO    DELX     DELY  E(LUV)  E(LAB)

    1.0     .02     .02  86.29  94.44   .3423   .3319  -11.11   -4.33  -.115    .8363   .0106   .0100 10.1826  7.4833
    1.0     .02     .03  79.88  91.64   .3447   .3337  -13.98   -3.94  -.1486   .7747   .0143   .0138 13.4696  9.9471
    1.0     .02     .10  70.72  87.36   .3476   .3336  -18.06   -8.13  -.2043   .6819   .0193   .0191 17.9871 13.4101
    1.0     .02     .20  56.92  80.13   .3498   .3338  -24.19  -12.03  -.3012   .5948   .0266   .0233 23.9911 18.2637
    1.0     .02     .30  36.62  67.02   .3379   .3416  -33.09  -19.83  -.4788   .6226   .0268   .0233 28.8033 23.8033
    1.0     .02     .80  30.02  61.70   .3217   .3283  -33.94  -23.29  -.3439   .7336   .0170   .0130 28.3294 23.3214
    1.0     .03     .03  83.99  93.43   .3387   .3473   -9.87   -4.13  -.1047   .9032   .0084   .0074  8.1852  6.1149
    1.0     .03     .10  74.83  89.32   .3407   .3482  -13.96   -6.17  -.1378   .8133   .0126   .0117 12.2233  9.1973
    1.0     .03     .20  61.02  82.41   .3412   .3467  -20.08   -9.78  -.2300   .7340   .0188   .0163 17.4916 13.5066
    1.0     .03     .30  40.72  70.01   .3271   .3305  -28.99  -16.86  -.4194   .7831   .0160   .0122 21.7471 18.7704
    1.0     .03     .80  34.13  63.09   .3110   .3177  -31.83  -19.90  -.4833   .9119   .0071   .0043 22.0397 20.3939
    1.0     .10     .10  80.68  91.99   .3334   .3407   -8.11   -3.30  -.0911   .9362   .0034   .0041  3.6802  4.4473
    1.0     .10     .20  66.87  83.43   .3325   .3379  -14.23   -6.73  -.1770   .8823   .0093   .0074 10.2390  8.2400
    1.0     .10     .30  46.37  73.94   .3173   .3209  -23.14  -12.93  -.3346   .9468   .0062   .0023 14.4673 13.4263
    1.0     .10     .80  39.98  69.48   .3034   .3091  -23.98  -15.31  -.3941  1.0770  -.0014  -.0044 13.7361 13.3712
    1.0     .20     .20  73.62  89.69   .3249   .3309   -3.49   -2.49  -.0673  1.0080   .0017   .0008  2.8911  2.6273
    1.0     .20     .30  55.32  79.24   .3101   .3148  -14.39   -7.62  -.2076  1.0634  -.0011  -.0036  7.7398  7.7010
    1.0     .20     .80  48.72  75.30   .2981   .3046  -17.24   -9.69  -.2604  1.1747  -.0067  -.0088 10.2893 10.0309
    1.0     .30     .30  67.98  86.01   .3101   .3170   -1.73    -.86  -.0242  1.0262  -.0011  -.0014  1.2184  1.0361
    1.0     .30     .80  61.39  82.60   .3004   .3090   -4.37   -2.39  -.0673  1.0901  -.0043  -.0044  3.8898  3.0787
    1.0     .80     .80  65.40  84.70   .3040   .3128    -.36    -.29  -.0079  1.0145  -.0007  -.0007   .6043   .4309
     .3     .02     .02  45.60  73.28   .3334   .3429   -2.41   -1.48  -.0444   .9398   .0062   .0039  4.6170  3.2478
     .3     .02     .03  46.33  73.78   .3337   .3429   -6.24   -3.86  -.1170   .7934   .0127   .0131 10.2743  7.4202
     .3     .02     .10  42.96  71.33   .3336   .3424  -11.70   -7.31  -.2137   .6739   .0198   .0206 17.0037 12.4621
     .3     .02     .20  37.88  67.96   .3313   .3397  -19.88  -12.66  -.3433   .6086   .0236   .0239 24.1965 18.3028
     .3     .02     .30  30.39  62.02   .3203   .3290  -31.73  -20.97  -.5113   .6872   .0203   .0194 28.4704 24.0239
     .3     .02     .80  27.94  59.87   .3122   .3229  -33.49  -23.82  -.5581   .7921   .0123   .0127 28.3338 23.5119
     .3     .03     .03  50.44  76.86   .3234   .3338   -2.14   -1.28  -.0383   .9660   .0044   .0039  3.3014  2.4314
     .3     .03     .10  47.07  74.26   .3247   .3327   -7.60   -4.61  -.1381   .8313   .0110   .0108  9.9390  7.2772
     .3     .03     .20  41.99  70.89   .3219   .3292  -13.77   -9.73  -.2739   .7367   .0160   .0134 16.8767 12.9613
     .3     .03     .30  34.49  63.38   .3107   .3183  -27.62  -17.61  -.4434   .8314   .0107   .0087 21.4792 18.9838
     .3     .03     .80  32.03  63.41   .3033   .3123  -31.39  -20.27  -.4934   .9709   .0036   .0023 22.0099 20.8041
     .3     .10     .10  52.91  77.84   .3163   .3238   -1.73   -1.02  -.0303   .9873   .0026   .0020  2.2627  1.3849
     .3     .10     .20  47.83  74.74   .3132   .3201   -9.92   -3.88  -.1720   .9018   .0073   .0062  8.9391  7.1239
     .3     .10     .30  40.34  69.74   .3025   .3096  -21.77  -13.23  -.3510  1.0019   .0023   .0008 14.3316 10.5365
     .3     .10     .80  37.89  67.97   .2960   .3048  -25.54  -15.72  -.4011  1.1267  -.0036  -.0037 13.8588 15.7439
     .3     .20     .20  56.38  79.96   .3068   .3143   -1.17    -.66  -.0194  1.0023   .0009   .0004  1.0182   .7087
     .3     .20     .30  49.09  75.33   .2974   .3031  -13.03   -7.46  -.2096  1.0883  -.0026  -.0045  7.3407  7.5309
     .3     .20     .80  46.64  73.98   .2920   .3008  -16.79   -9.70  -.2629  1.2023  -.0076  -.0094 10.3400 10.0602
     .3     .30     .30  61.73  82.80   .2999   .3094    -.36    -.19  -.0055  1.0052  -.0001  -.0003   .2340   .2190
     .3     .30     .80  59.31  81.48   .2936   .3060   -4.13   -2.21  -.0634  1.0863  -.0040  -.0042  3.3437  2.8144
     .3     .80     .80  63.32  83.63   .2995   .3101    -.11    -.06  -.0017  1.0026  -.0001  -.0001   .1068   .0831
    0.0     .02     .02  11.07  39.73   .2768   .2837    6.29   13.60  1.3372   .6287   .0192   .0246 13.6864 15.7102
    0.0     .02     .03  12.77  42.46   .2788   .2881    1.49    2.37   .1433   .6343   .0178   .0232  8.7238  6.6686
    0.0     .02     .10  13.20  43.93   .2803   .2920   -3.34   -6.33  -.2326   .6886   .0161   .0213 16.1388 11.4119
    0.0     .02     .20  18.84  50.54   .2831   .2989  -13.36  -14.77  -.4469   .7404   .0138   .0183 23.6643 18.4387
    0.0     .02     .30  24.16  56.28   .2960   .3116  -30.36  -22.50  -.5326   .8337   .0094   .0123 28.0012 24.5001
    0.0     .02     .80  23.86  55.94   .3014   .3166  -33.03  -24.41  -.5711   .8797   .0072   .0099 28.2103 23.7723
    0.0     .03     .03  16.88  48.13   .2719   .2796    5.60    8.06   .3037   .7546   .0118   .0148  8.1739  8.2707
    0.0     .03     .10  19.31  51.08   .2744   .2836   -1.23   -1.40  -.0549   .7940   .0102   .0129  8.0747  5.3031
    0.0     .03     .20  22.93  55.03   .2791   .2903  -11.46  -10.26  -.3289   .8398   .0077   .0096 13.7473 12.3694
    0.0     .03     .30  28.26  60.16   .2890   .3021  -26.26  -18.63  -.4780   .9922   .0024   .0030 21.2233 19.4233
    0.0     .03     .80  29.97  61.66   .2938   .3067  -30.93  -20.69  -.5041  1.0360  -.0004   .0000 22.0233 21.0683
    0.0     .10     .10  23.13  55.26   .2714   .2793    4.61    4.78   .2273   .8431   .0073   .0088  5.1530  5.0623
    0.0     .10     .20  28.80  60.63   .2734   .2852   -3.61   -4.68  -.1506   .9301   .0040   .0048  7.3658  5.7762
    0.0     .10     .30  34.11  65.08   .2839   .2934  -20.41  -13.70  -.3716  1.1083  -.0027  -.0037 14.2883 13.8239
    0.0     .10     .80  35.81  66.41   .2880   .2994  -23.10  -13.94  -.4086  1.1934  -.0062  -.0073 16.0042 13.9313
    0.0     .20     .20  37.34  67.71   .2733   .2833    3.14    2.40   .0917   .9113   .0041   .0047  3.0339  2.7232
    0.0     .20     .30  42.86  71.48   .2822   .2934  -11.66   -7.30  -.2121  1.1303  -.0044  -.0037  7.3702  7.3647
    0.0     .20     .80  44.36  72.63   .2833   .2966  -16.33   -9.72  -.2635  1.2384  -.0087  -.0101 10.4197 10.0977
    0.0     .30     .30  55.52  79.36   .2880   .3005    1.00     .38   .0179   .9703   .0014   .0014  1.1021   .8121
    0.0     .30     .80  57.23  80.32   .2905   .3029   -3.69   -2.02  -.0389  1.0821  -.0037  -.0038  3.1721  2.3437
    0.0     .80     .80  61.24  82.32   .2948   .3072     .33     .18   .0030   .9882   .0006   .0005   .4391   .2942
```

EXHIBIT 5. SAMPLE PLUME MODEL OUTPUT: VISUAL EFFECTS FOR WHITE, GREY, AND BLACK BACKGROUNDS

The large amount of output required to characterize the visual impact of a plume at a given downwind distance is necessary because of the large number of possible observer locations, sight path orientations, and background objects. We have an optional printout table for plume visual effects for only one given observer location for user-contributed values of $r_p$ and $\alpha$. This output option is useful for describing a plume for an artist's rendering, as discussed in Section B.

We have designed a computer plot package to display plume visual effects for horizontal sight paths as a function of distance. Examples of these computer plots are shown in Figures 27 through 35. Four parameters were selected that most easily characterize (with numbers) the visual impact of a plume:

- > Percentage reduction in visual range.
- > Blue-red ratio (plume color relative to background).
- > Plume contrast (plume light intensity).
- > $\Delta E$ ($L^*a^*b^*$) (plume perceptibility).

We have selected these plots to show the visual effects seen by an observer situated at distance $r_p = 0.02 \times r_{v0}$ and with a horizontal sight path perpendicular to the plume centerline.

Figures 27 through 32 show the results of a sensitivity analysis to determine the effect on plume visibility impairment of:

- > Plume diffusion.
  - Distance downwind (1.2 km $< x <$ 350 km).
  - Atmospheric stability (Pasquill C, D, and E).
- > Scattering angle ($\theta = 45°, 90°, 180°$).
- > Sulfate formation (0 and 0.5 percent per hour).
- > $NO_2$ (0 and 0.7 lb/$10^6$ Btu $NO_x$ emission rate).

The effect on visual range of the 3.4 ton/day primary particulate emission rate assumed here (less than the 0.1 lb/$10^6$ Btu standard in order

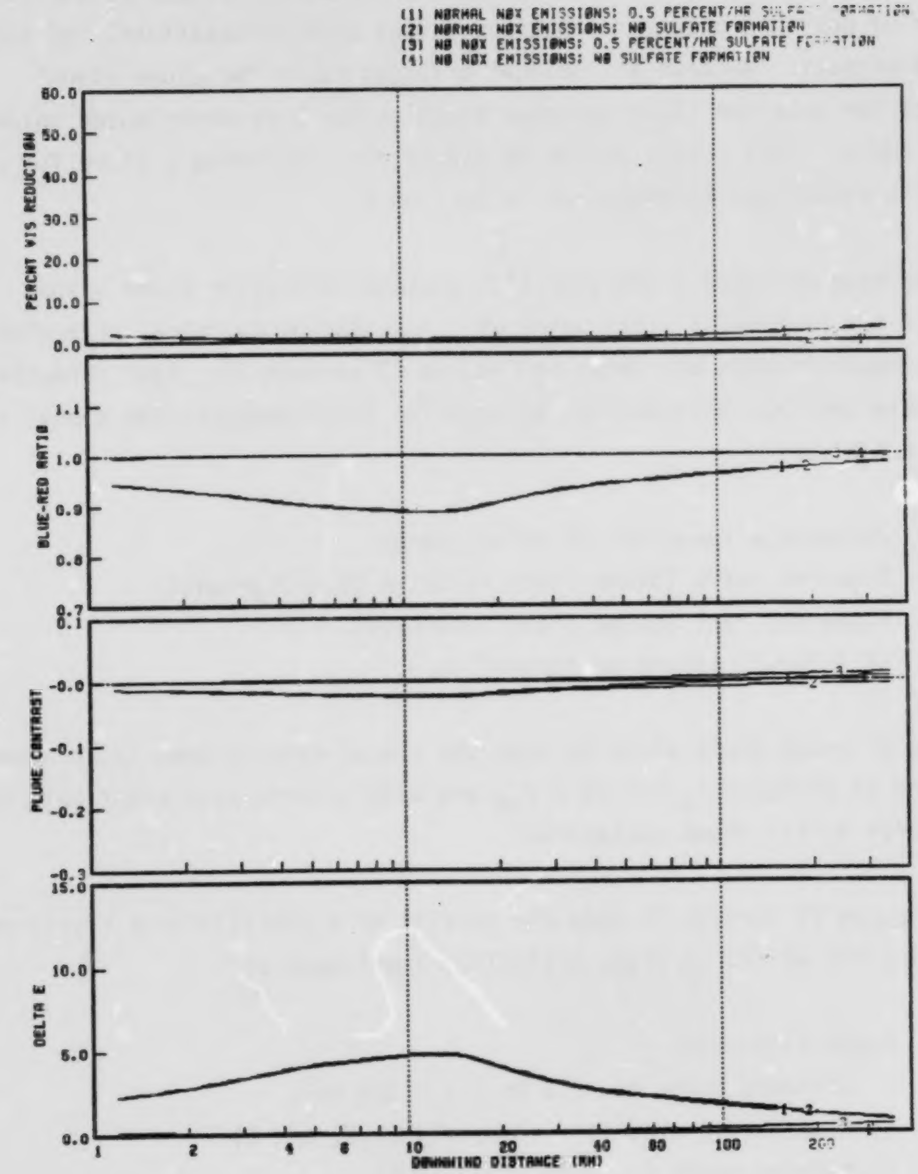

FIGURE 27. CALCULATED PLUME VISIBILITY IMPAIRMENT FOR A HYPOTHETICAL 2250 Mwe COAL-FIRED POWER PLANT WITH A LIGHT SCATTERING ANGLE OF 45° AND STABILITY CLASS C

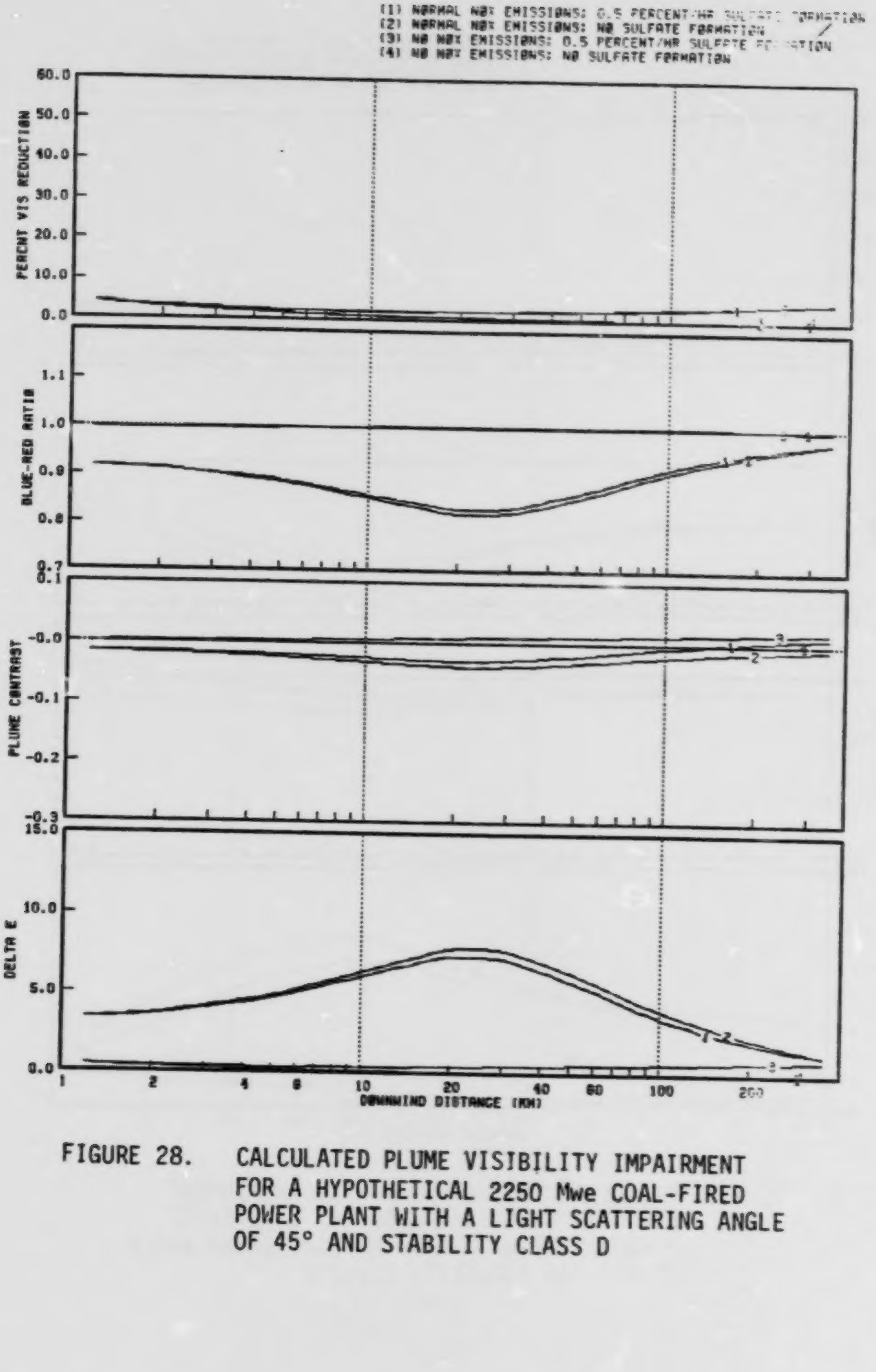

FIGURE 28. CALCULATED PLUME VISIBILITY IMPAIRMENT FOR A HYPOTHETICAL 2250 Mwe COAL-FIRED POWER PLANT WITH A LIGHT SCATTERING ANGLE OF 45° AND STABILITY CLASS D

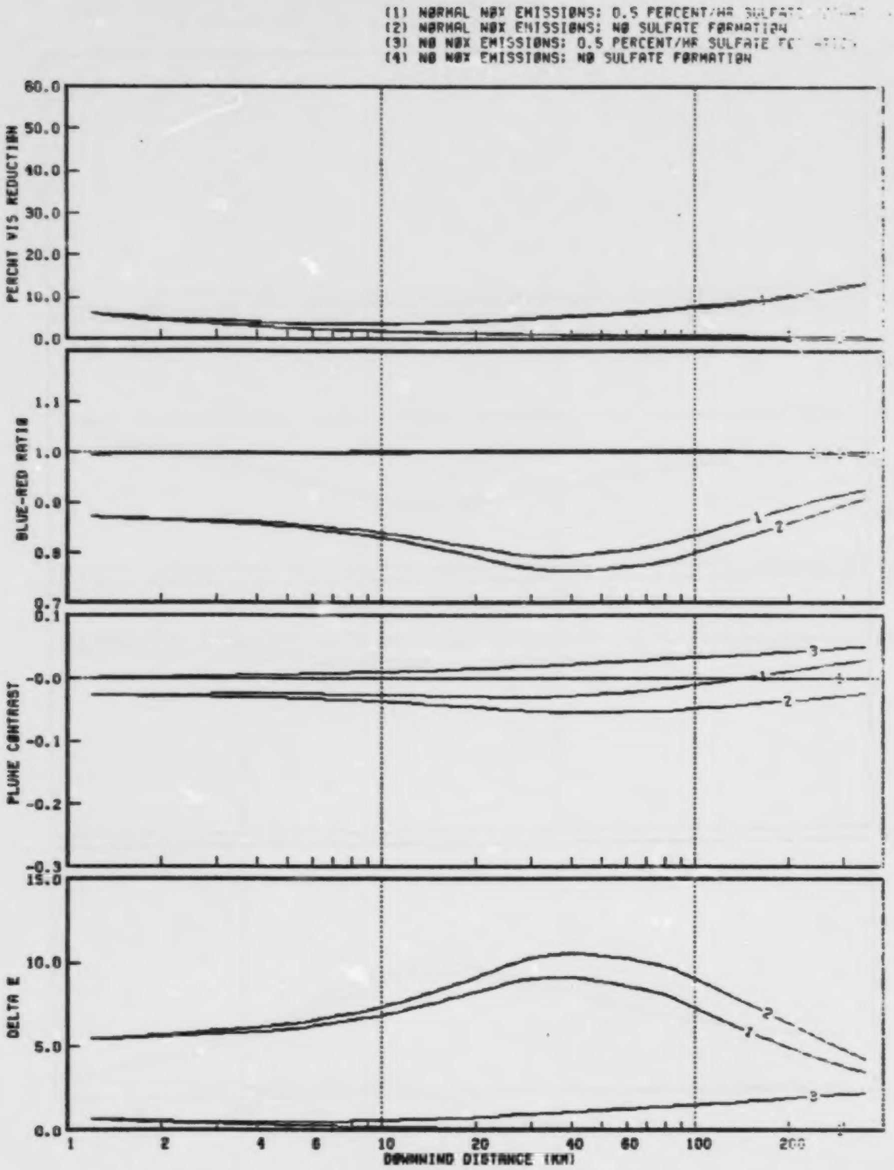

FIGURE 29. CALCULATED PLUME VISIBILITY IMPAIRMENT FOR A HYPOTHETICAL 2250 Mwe COAL-FIRED POWER PLANT WITH A LIGHT SCATTERING ANGLE OF 45° AND STABILITY CLASS E

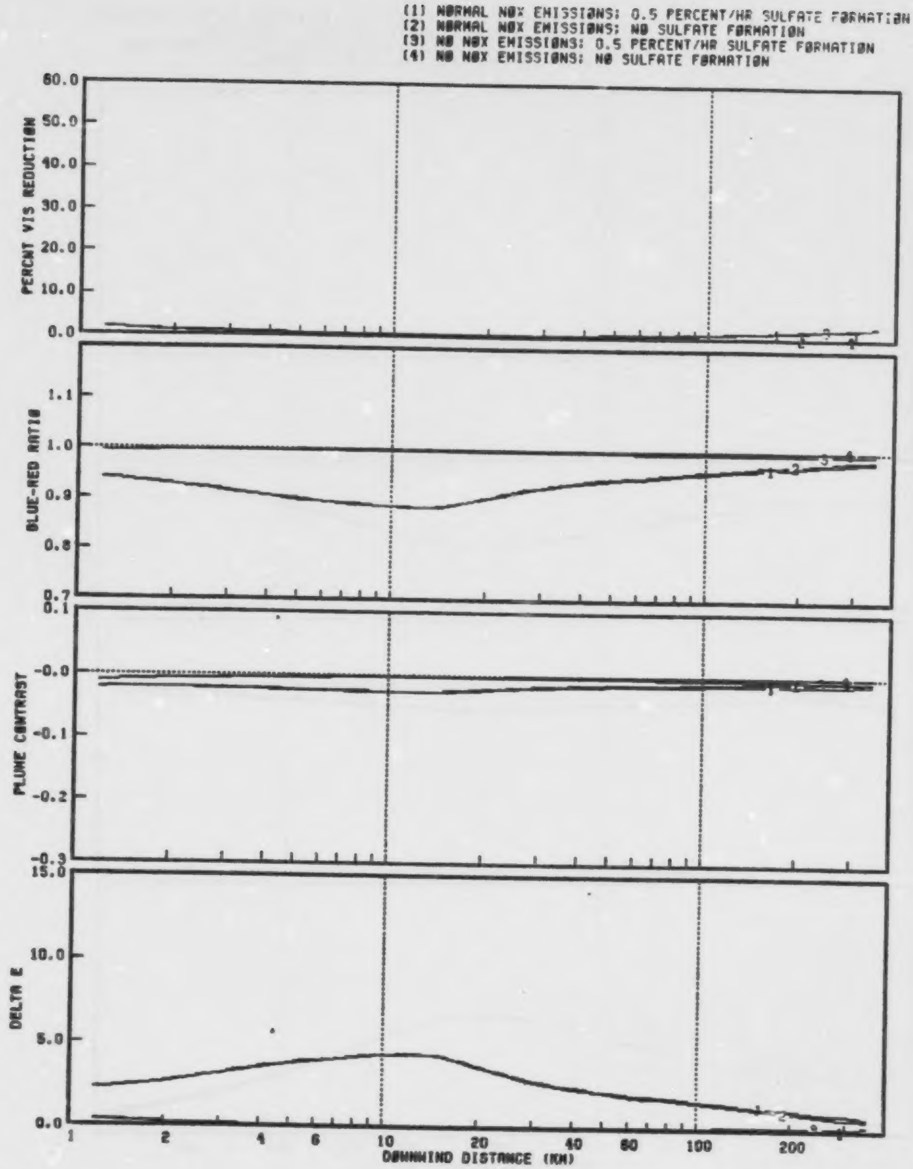

FIGURE 30. CALCULATED PLUME VISIBILITY IMPAIRMENT FOR A HYPOTHETICAL 2250 Mwe COAL-FIRED POWER PLANT WITH A LIGHT SCATTERING ANGLE OF 90° AND STABILITY CLASS C

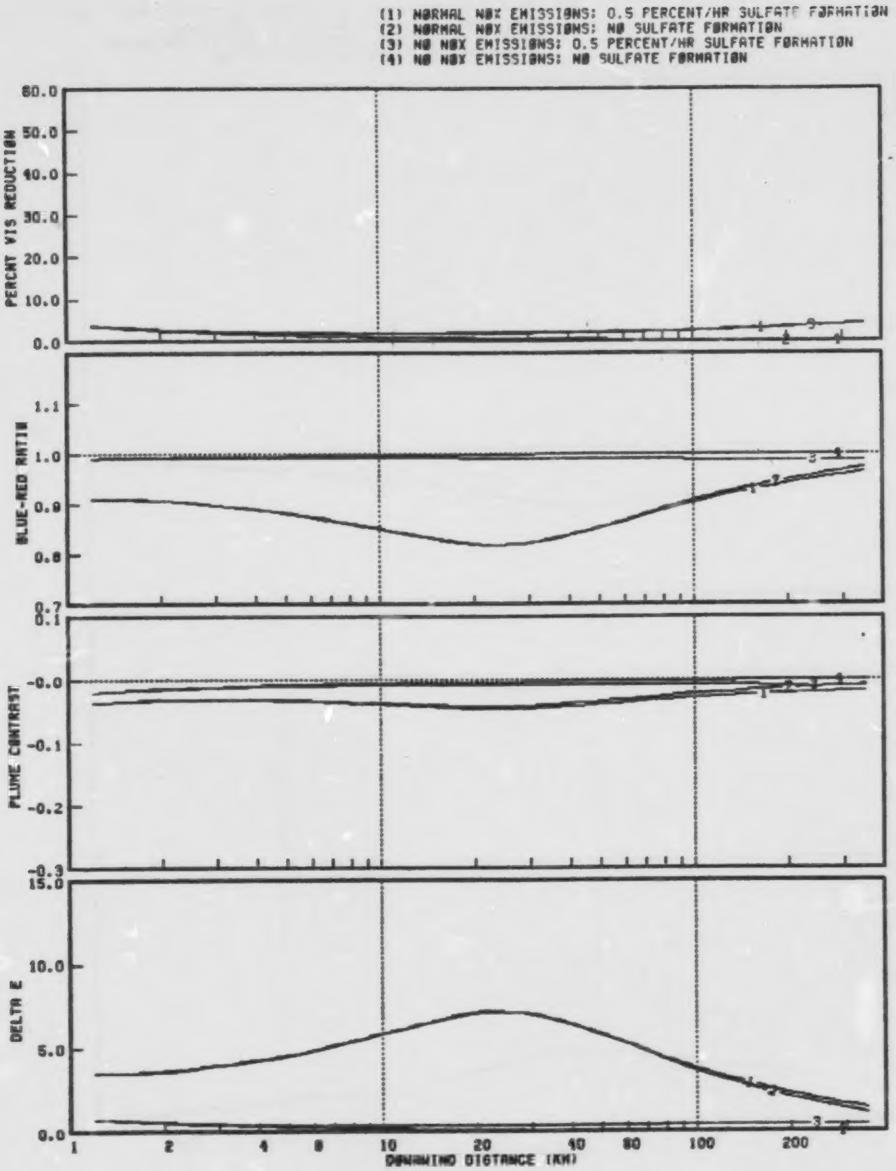

FIGURE 31. CALCULATED PLUME VISIBILITY IMPAIRMENT FOR A HYPOTHETICAL 2250 Mwe COAL-FIRED POWER PLANT WITH A LIGHT SCATTERING ANGLE OF 90° AND STABILITY CLASS D

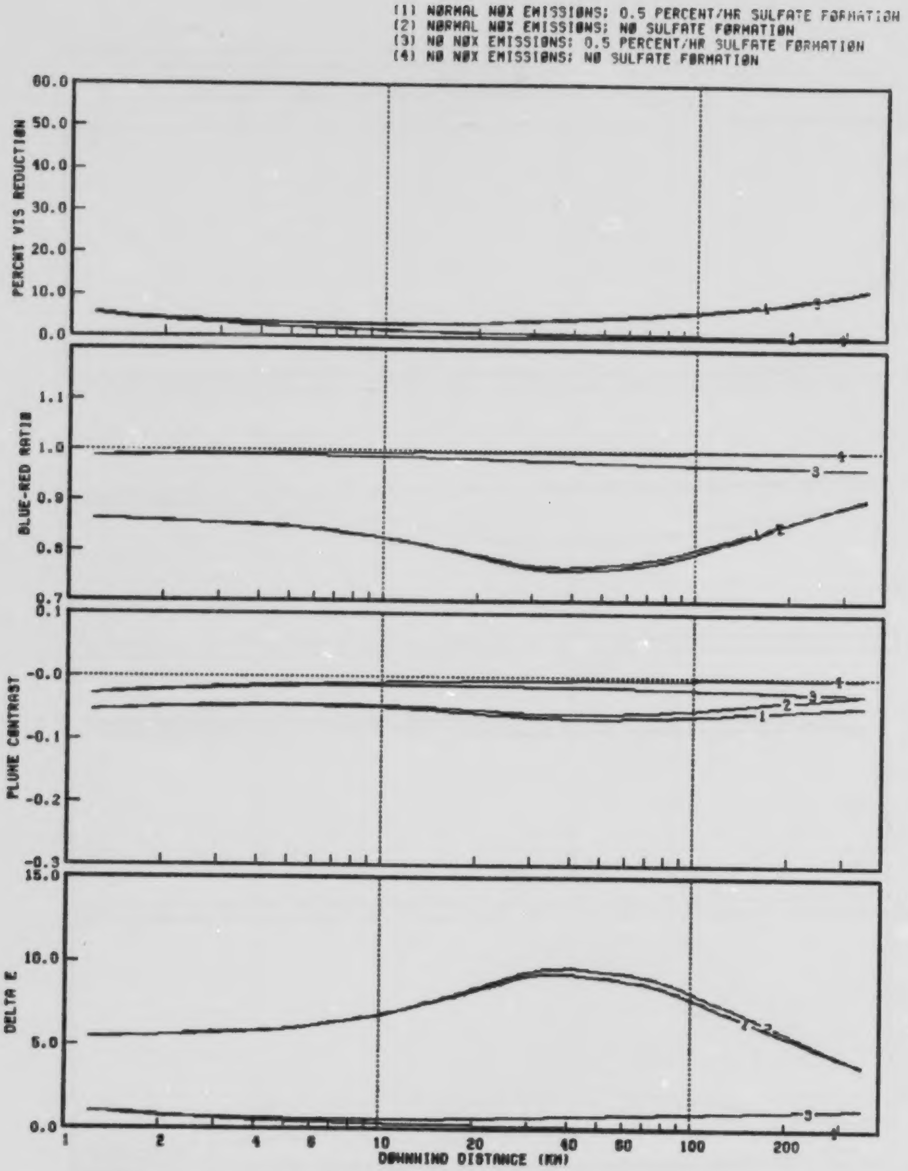

FIGURE 32. CALCULATED PLUME VISIBILITY IMPAIRMENT FOR A HYPOTHETICAL 2250 Mwe COAL-FIRED POWER PLANT WITH A LIGHT SCATTERING ANGLE OF 90° AND STABILITY CLASS E

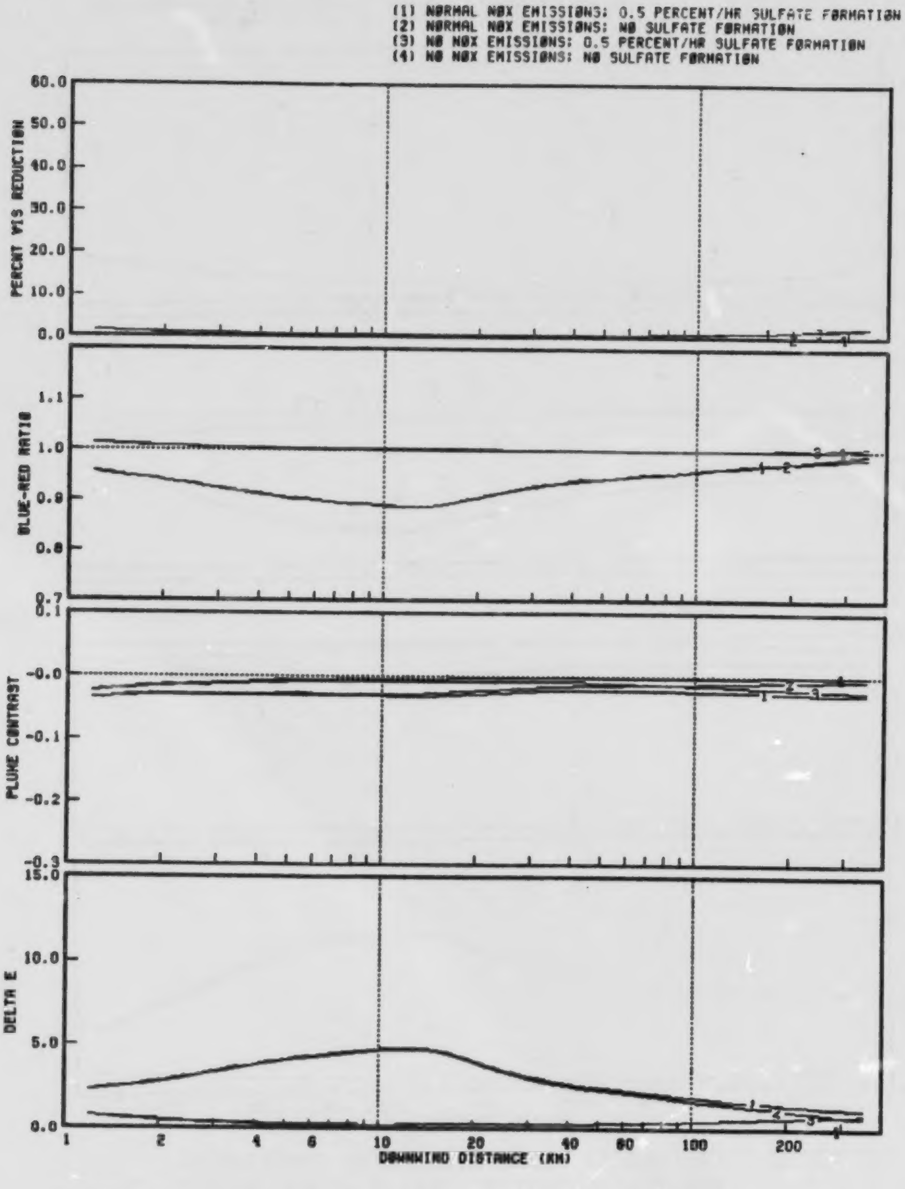

FIGURE 33. CALCULATED PLUME VISIBILITY IMPAIRMENT FOR A HYPOTHETICAL 2250 Mwe COAL-FIRED POWER PLANT WITH A LIGHT SCATTERING ANGLE OF 180° AND STABILITY CLASS C

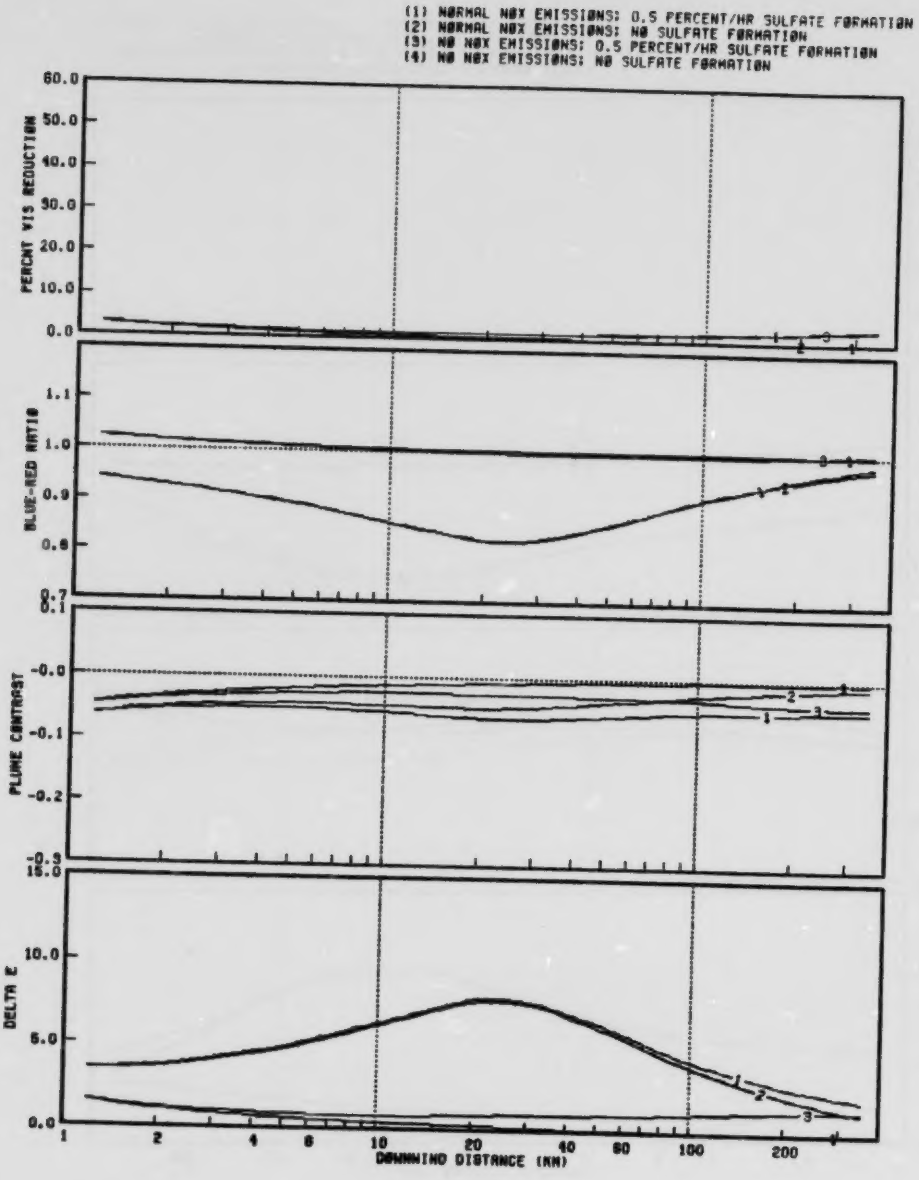

FIGURE 34. CALCULATED PLUME VISIBILITY IMPAIRMENT FOR A HYPOTHETICAL 2250 Mwe COAL-FIRED POWER PLANT WITH A LIGHT SCATTERING ANGLE OF 180° AND STABILITY CLASS D

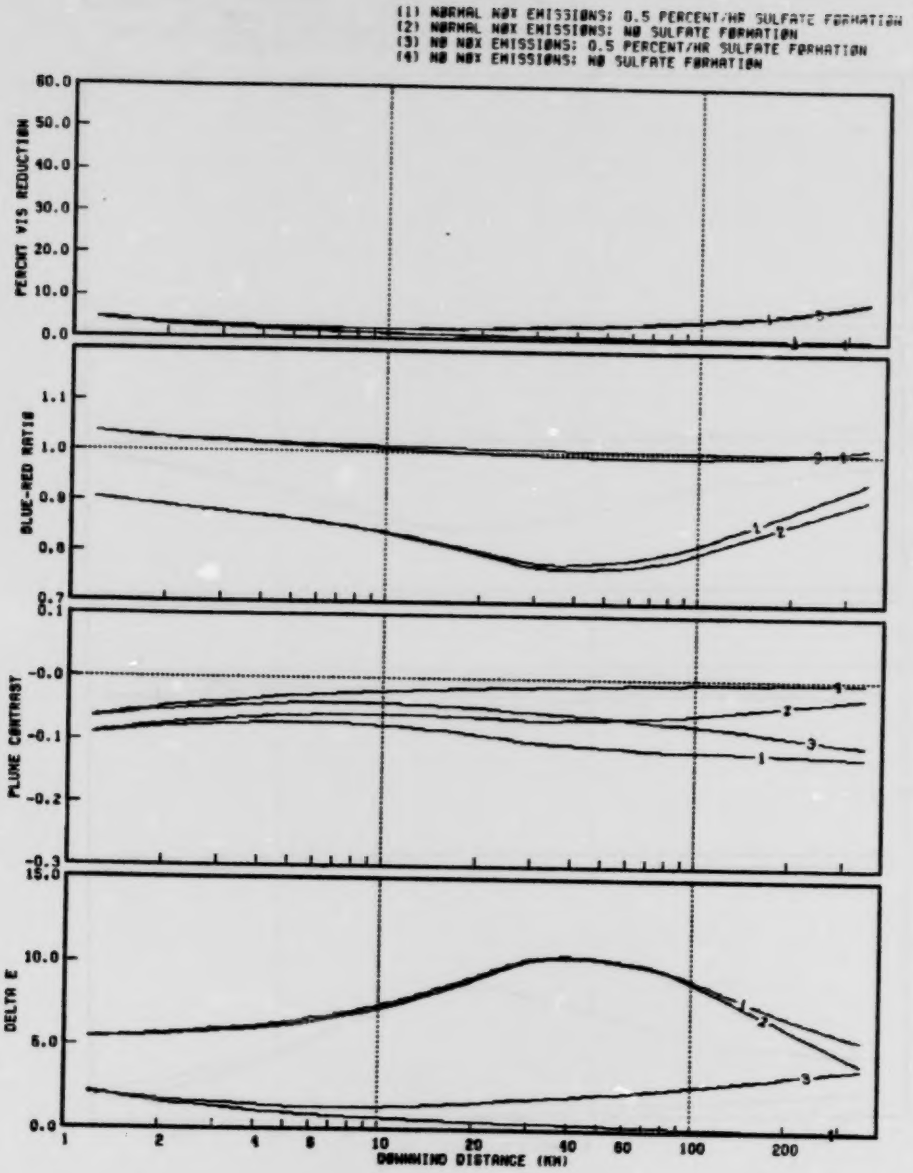

FIGURE 35. CALCULATED PLUME VISIBILITY IMPAIRMENT FOR A HYPOTHETICAL 2250 Mwe COAL-FIRED POWER PLANT WITH A LIGHT SCATTERING ANGLE OF 180° AND STABILITY CLASS E

order to meet the 20 percent opacity standard) is apparent in these figures, particularly for stable atmospheric conditions (Pasquill E). However, the significant reduction in visual range caused by primary particulate is noticed only at short downwind distances. All these effects are for sight paths through the plume centerline. At large downwind distances, the effect of sulfate on visual range becomes very significant, particularly for stable conditions. Indeed, the reduction in visual range increases with increasing downwind distance between 60 and 350 km downwind.* The scattering angle has a small but not negligible effect on visual range: Visual range increases with increasing scattering angle. In other words, the reduction in visual range is greatest for forward scattering.

Plume coloration and contrast are indicated by the values of the blue-red ratio, plume contrast (at $\lambda = 0.55$ μm), and the CIE color difference parameter $\Delta E(L^*a^*b^*)$. The effect of $NO_2$ on plume coloration becomes clear when the curves (Nos. 1 and 2) that assume normal $NO_x$ emissions are compared with those curves (Nos. 3 and 4) that assume no $NO_x$ emissions. Yellow-brown coloration, as indicated by blue-red ratios less than 1.0, is stronger with $NO_2$ than without. Note that the effect of sulfate (Curve 3) on color is very small for all scattering angles; however, sulfate has a significant effect on plume contrast, increasing plume brightness at small scattering angles and decreasing plume brightness at large angles. Comparing Curves 1 and 2, we can see that the pronounced coloration caused by $NO_2$ during stable conditions (E stability) is reduced by light scattered by sulfate. If we use $\Delta E(L^*a^*b^*)$ as an overall indicator of the perceptibility of the plume (because of both plume contrast and color changes), we find that $NO_2$ has the most pronounced effect on plume visibility at significant downwind distances. Sulfate has a significant but smaller effect, and primary particulate has the least effect. Perhaps the most significant result of these calculations is that plume visibility impairment (both a reduction in visual range and an atmospheric discoloration) increases with downwind distance, suggesting that a significant impact could occur hundreds of kilometers from the source.

---

* A cautionary comment is in order here. For this evaluation, the wind speed was assumed to be 5.0 m/s; thus, almost 20 hours would be required for emissions to be carried 350 km. It is unlikely that stable atmospheric conditions will persist that long.

## B. PLUME/TERRAIN PERSPECTIVE MODEL

To supplement the quantitative description of plume visual impact described in Section A, we developed a Perspective Terrain Viewing Program (PTVP). Using computer graphics, this program is capable of displaying views of plumes and background terrain with the perspective of the human observer or camera situated at user-specified positions. These plume and terrain perspective scenes can be used in conjunction with the quantification of plume visibility impairment discussed in the previous section to provide an understanding of the subjective impact of the computer predictions. In addition, these scenes, along with computed Munsell color notation, can be used by a commercial artist to produce color renderings of the visual impression of the background atmosphere and the plume for various assumed emission conditions.

To use the PTVP, the user must provide the following information:

- Boundaries of the region in which the facility is situated or is to be constructed must be identified, and terrain within it must be digitized. (The U.S. Geological Survey supplies digitized terrain elevations.)
- Design parameters of the facility that affect the effluent plume characteristics must be determined. Among these are stack height, flue gas temperature, and flow rate.
- Representative meteorological conditions must be specified; important parameters include wind speed and direction, ambient temperature, lapse rate, atmospheric stability category, and the height of the inversion layer, if one is expected to exist.

> Observation parameters must be decided upon. Among these are the location of the observer with respect to the facility, the direction in which he is viewing, and the field of view of the "conceptual camera" he is using to record the scene. The last of these parameters is required because the PTVP uses the lens characteristics to reproduce the optics of a camera, "recording" by means of computer graphics the appropriate camera film image. Lens "size" as measured by the cone-angle of the field of view may range from a few degrees (telescopic lens), to from 40° to 50° (standard lens), to 90° ("wide-angle" lens), to 180° ("fish-eye" lens).

The use of the PTVP can best be illustrated by means of an example. Digitized terrain elevation data were obtained from the U.S. Geological Survey for an extensive portion of the Southwest. From this data base, a 50 x 50 km portion of terrain immediately west of Page, Arizona, was isolated. A computer-generated plot of the terrain is presented in Figure 36. Among the prominent geographical features contained within that region are the Vermilion Cliffs, the Marble Canyon through which the Colorado River flows, and the Paria Canyon.

In this sample terrain grid, a plume from a hypothetical power plant was displayed and viewed from several different observer vantage points. In the example, the power plant stack is 775 feet high, plume rise was determined using values typical of a large coal-fired power plant, winds were light and headed slightly south of due west (compass heading of 255° and meteorological conditions prevailed that are typical of Pasquill-Gifford Stability Category E (stable). The plume was assumed to be Gaussian, with its "envelope" defined by the locus of 1$\sigma$ dispersion coefficient values.

The hypothetical observer in this example flew around the power plant observing the power plant plume. Using a "camera" having a wide-angle lens (with a 90° field of view), the observer took a series of pictures. The

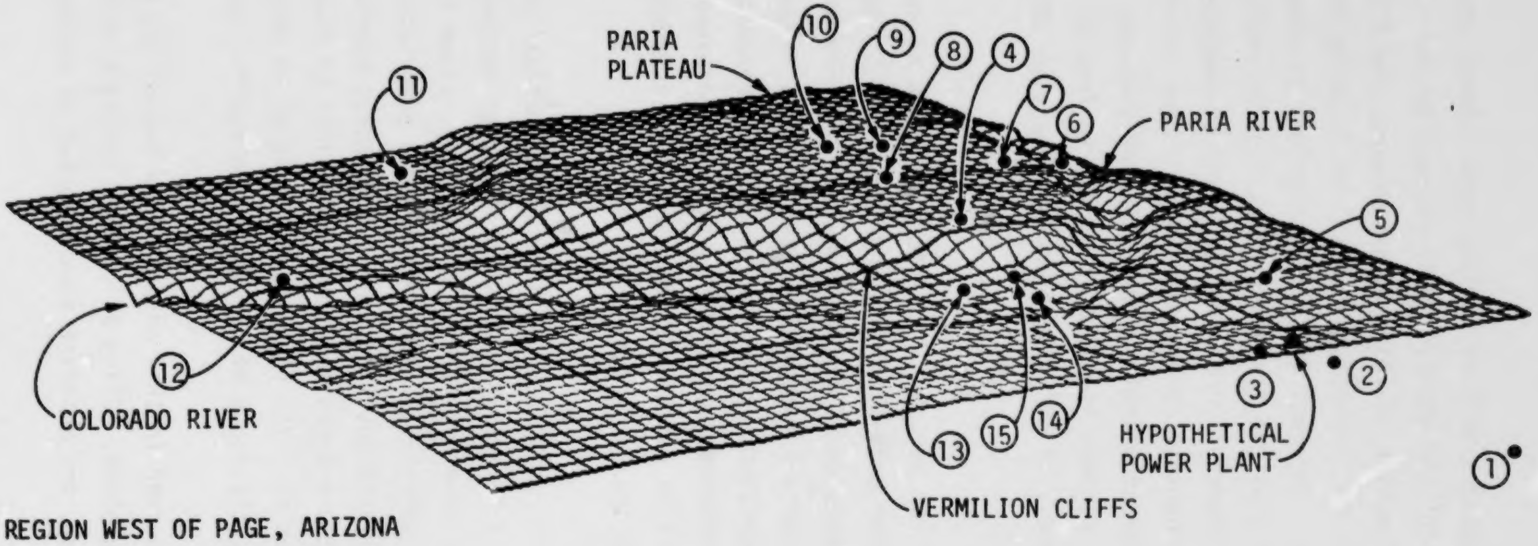
PARIA PLATEAU
⑪
⑩
⑨
⑧
④
⑦
⑥
PARIA RIVER
⑤
⑫
COLORADO RIVER
⑬
⑮
⑭
③
②
HYPOTHETICAL POWER PLANT
①
VERMILION CLIFFS
REGION WEST OF PAGE, ARIZONA

FIGURE 36. OBSERVER LOCATIONS FOR PLUME-TERRAIN PERSPECTIVE VIEWS

location of each picture is shown in Figure 36. The sequence of pictures is presented in Figures 37 through 51. All views are directed at the power plant, except for Figure 39, which is aimed west toward the Vermilion Cliffs.

## C. COLOR DISPLAY TECHNIQUES

The most complete and realistic display of predicted visibility impairment, particularly atmospheric discoloration, is a plume-terrain perspective view in color, with accurately specified and rendered colors calculated from the plume and regional models. We investigated two methods of displaying atmospheric discoloration and plume visual impact:

- A color illustration, drawn or painted by a commercial artist, using Munsell specifications for plume and background color and plume and terrain perspective views.
- A color video display, based on a photograph of a view from a vista, computer-enhanced to display a plume or homogeneous atmospheric discoloration on a color television.

Both of these methods, presented schematically in Figure 52, use the spectral intensity $I(\lambda)$ calculated by the visibility models for specific lines of sight as a base.

These two display methods are the most technically difficult, time-consuming, and expensive output options available for visibility models, but they may be the only ways of giving the user of models an understanding of the calculated visibility impairment. Without the aid of these color display techniques, it is very difficult to translate numbers describing visual impact into an observer's actual visual impression.

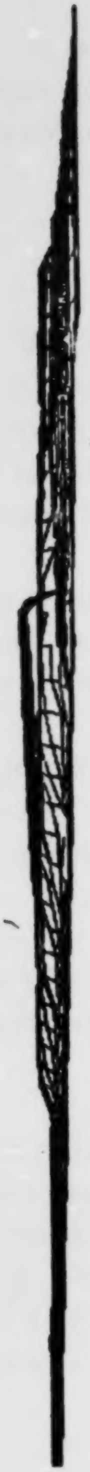

FIGURE 37. VIEW FROM LOCATION 1

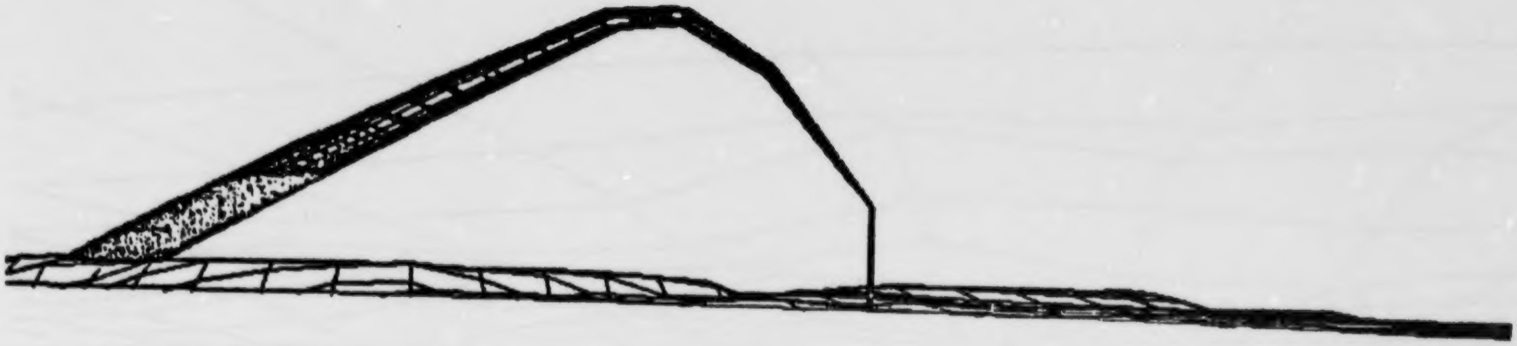

FIRURE 38. VIEW FROM LOCATION 2

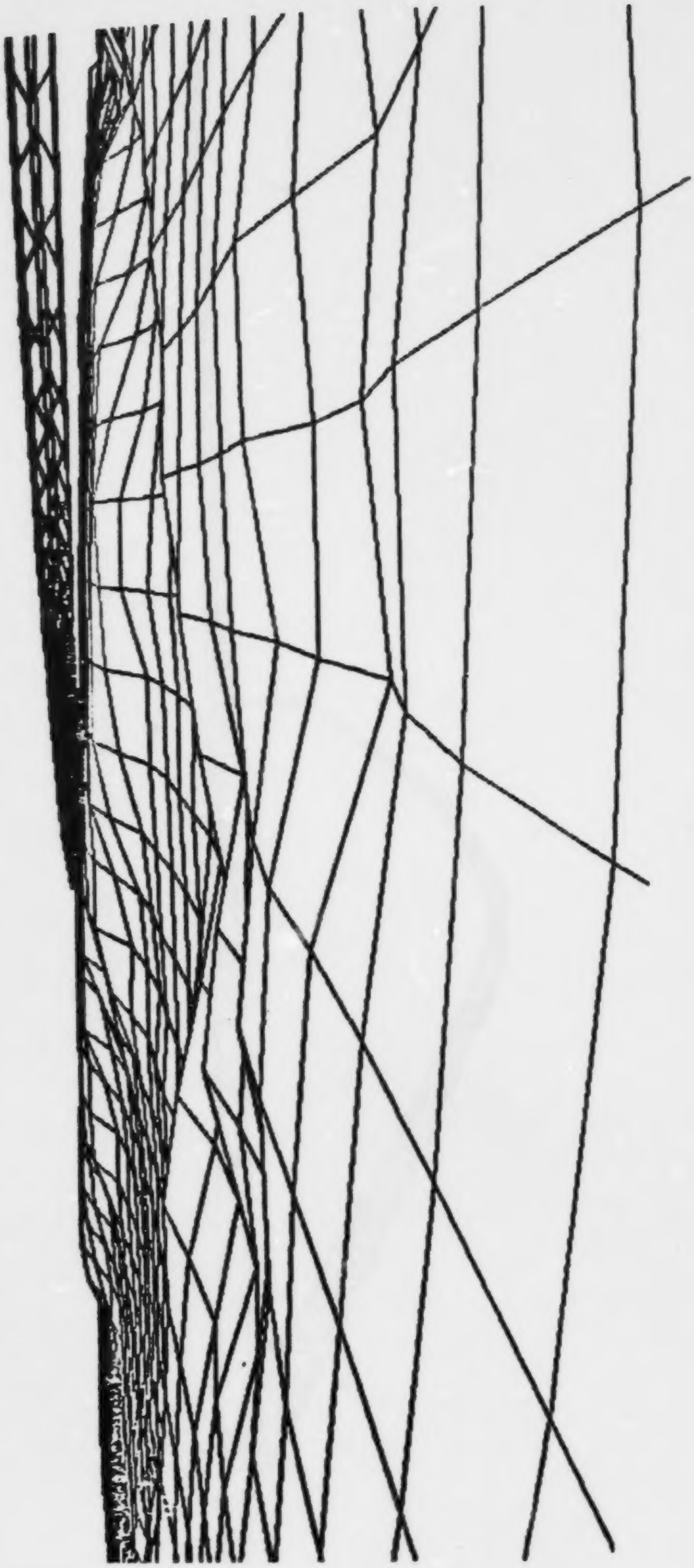

FIGURE 39. VIEW FROM LOCATION 3

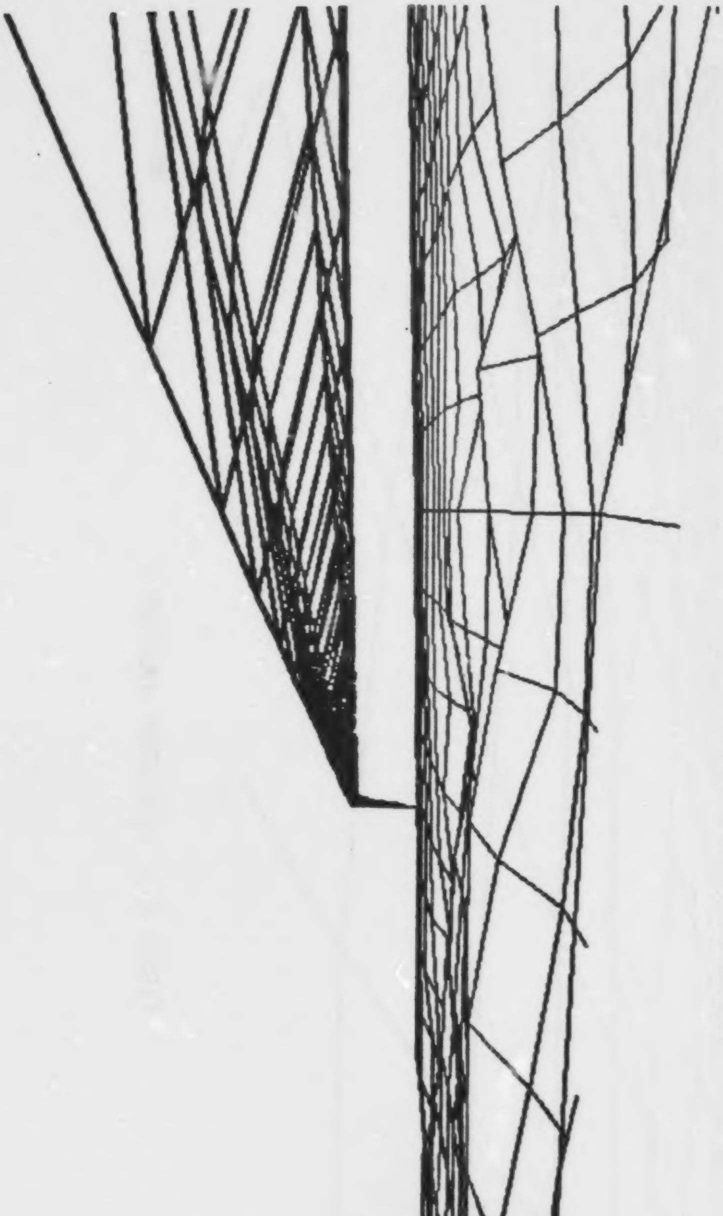

FIGURE 40. VIEW FROM LOCATION 4

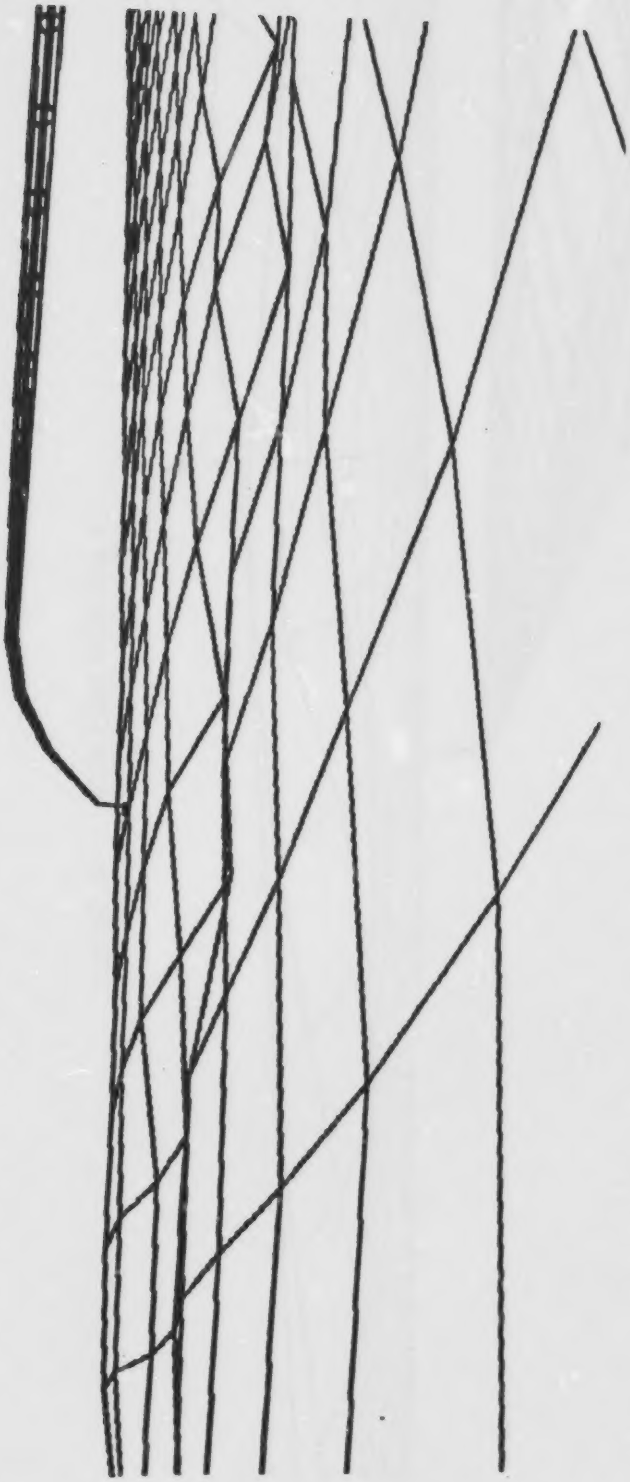

FIGURE 41. VIEW FROM LOCATION 5

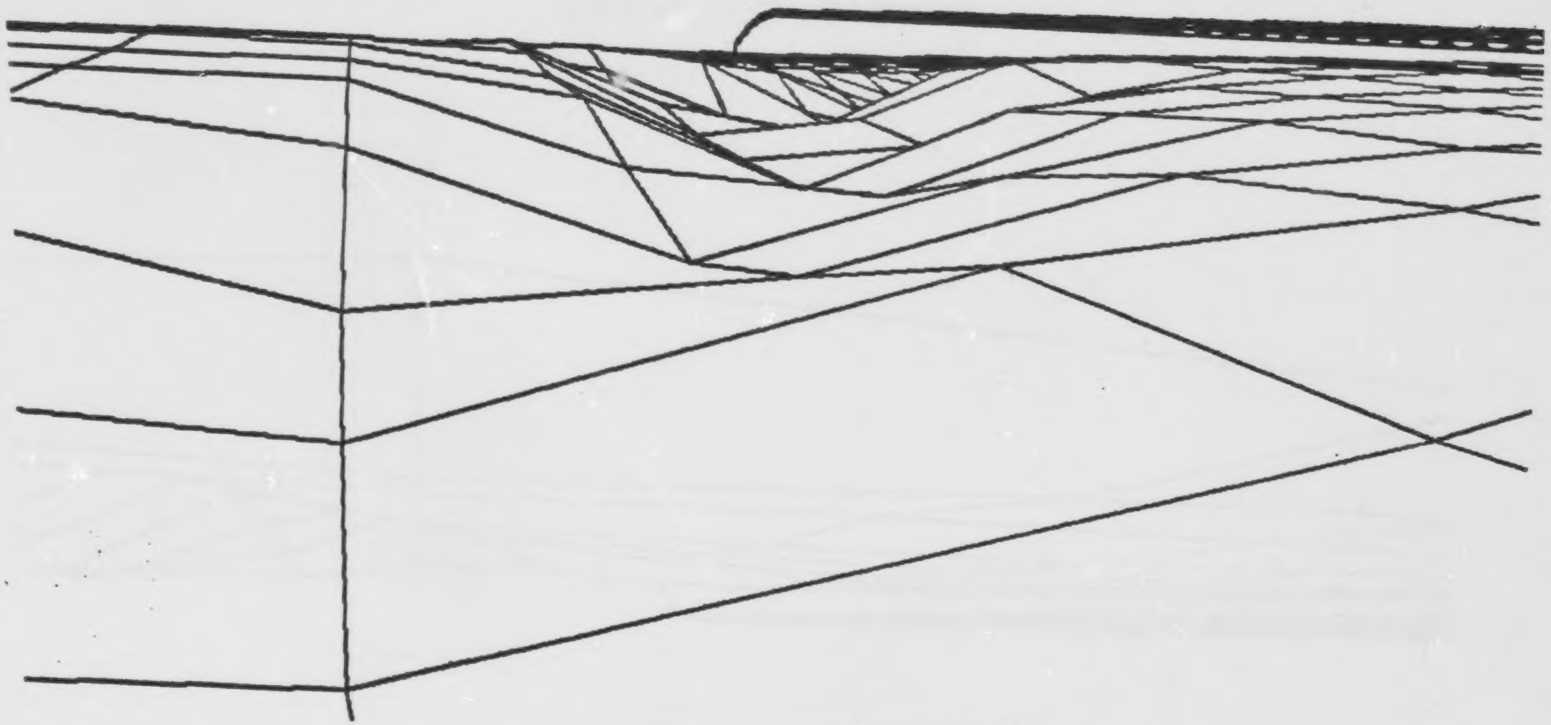

FIGURE 42. VIEW FROM LOCATION 6

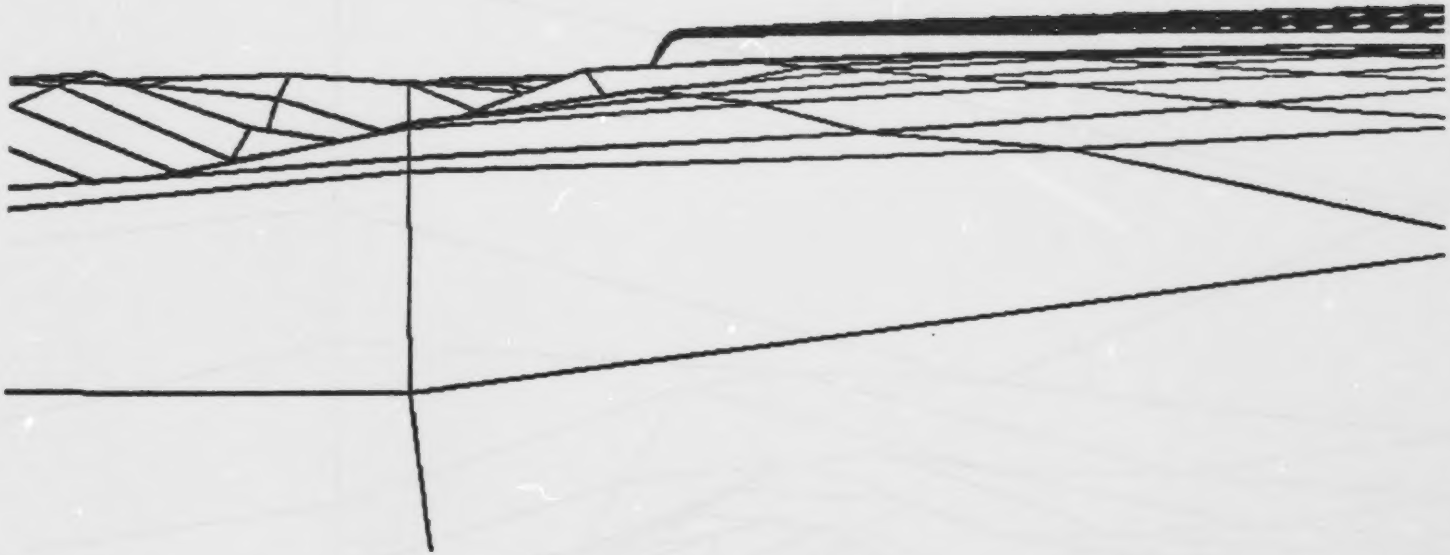

FIGURE 43. VIEW FROM LOCATION 7

FIGURE 44. VIEW FROM LOCATION 8

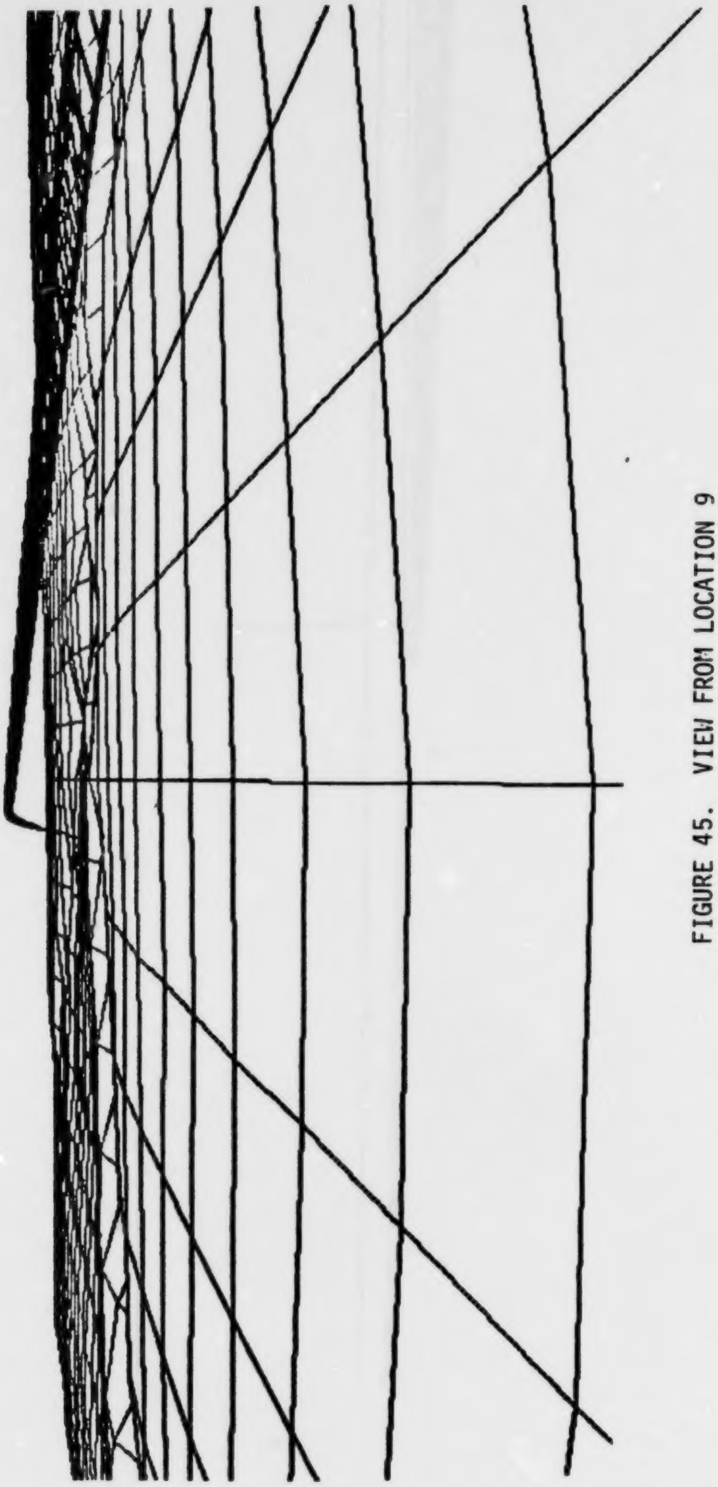

FIGURE 45. VIEW FROM LOCATION 9

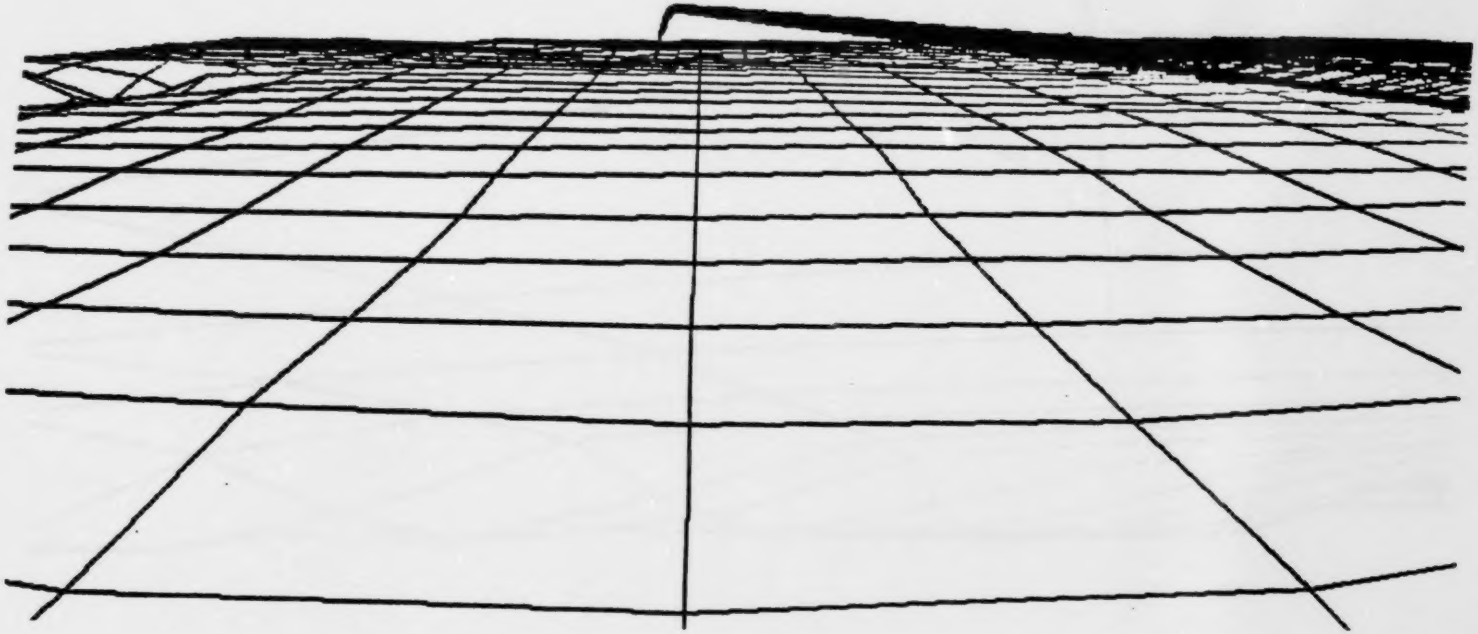

FIGURE 46. VIEW FROM LOCATION 10

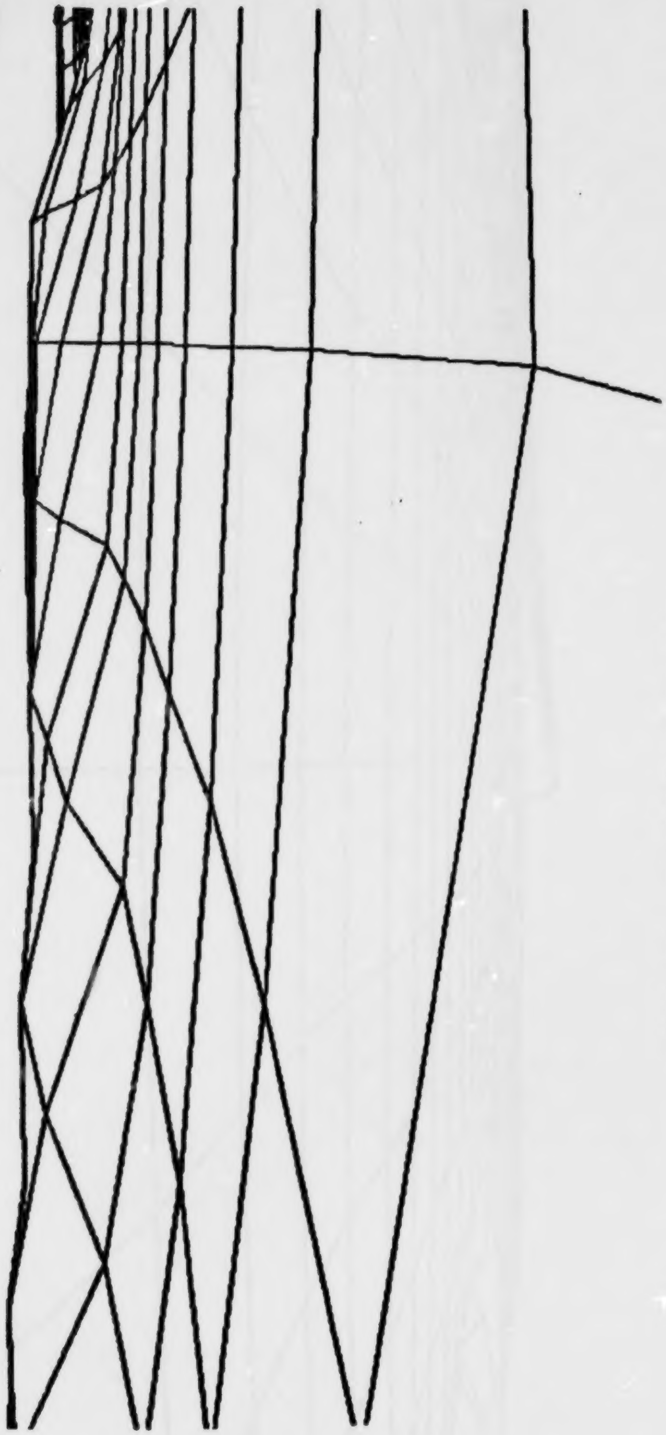

FIGURE 47. VIEW FROM LOCATION 11

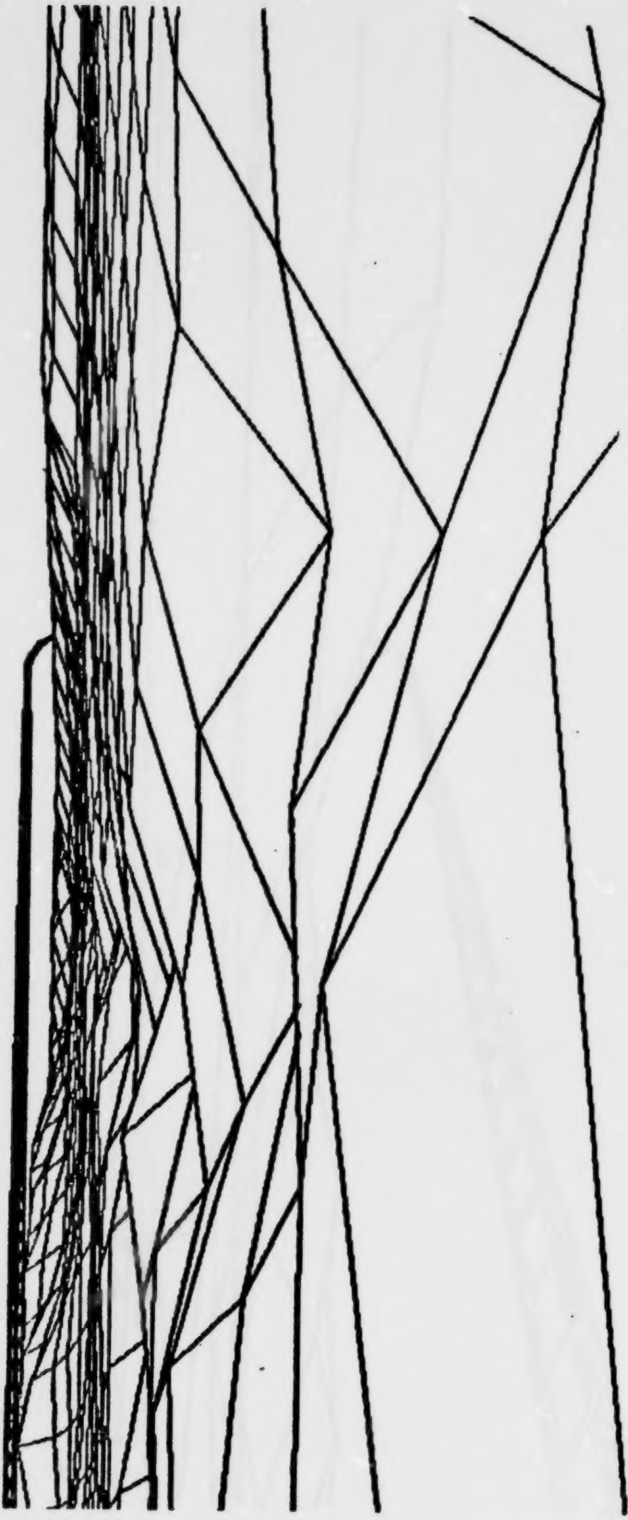

FIGURE 43. VIEW FROM LOCATION 12

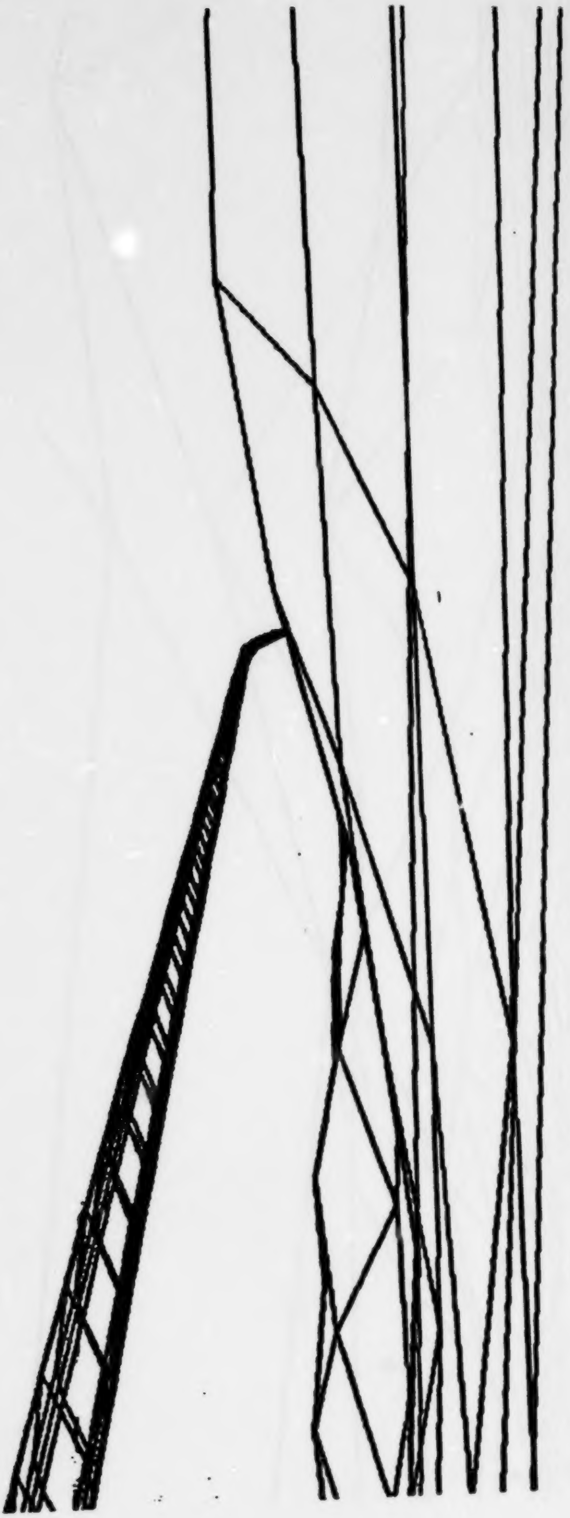

FIGURE 49. VIEW FROM LOCATION 13

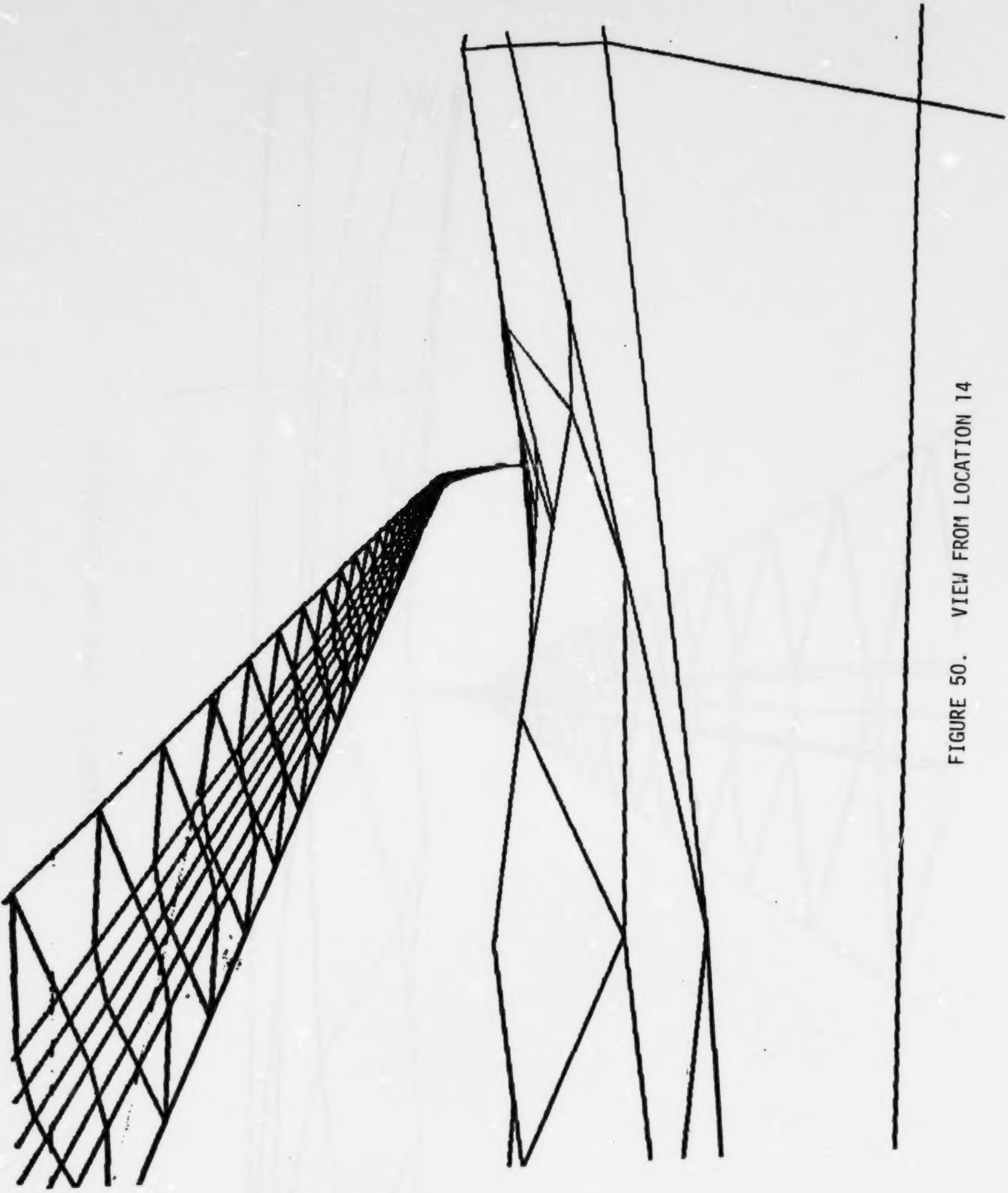

FIGURE 50. VIEW FROM LOCATION 14

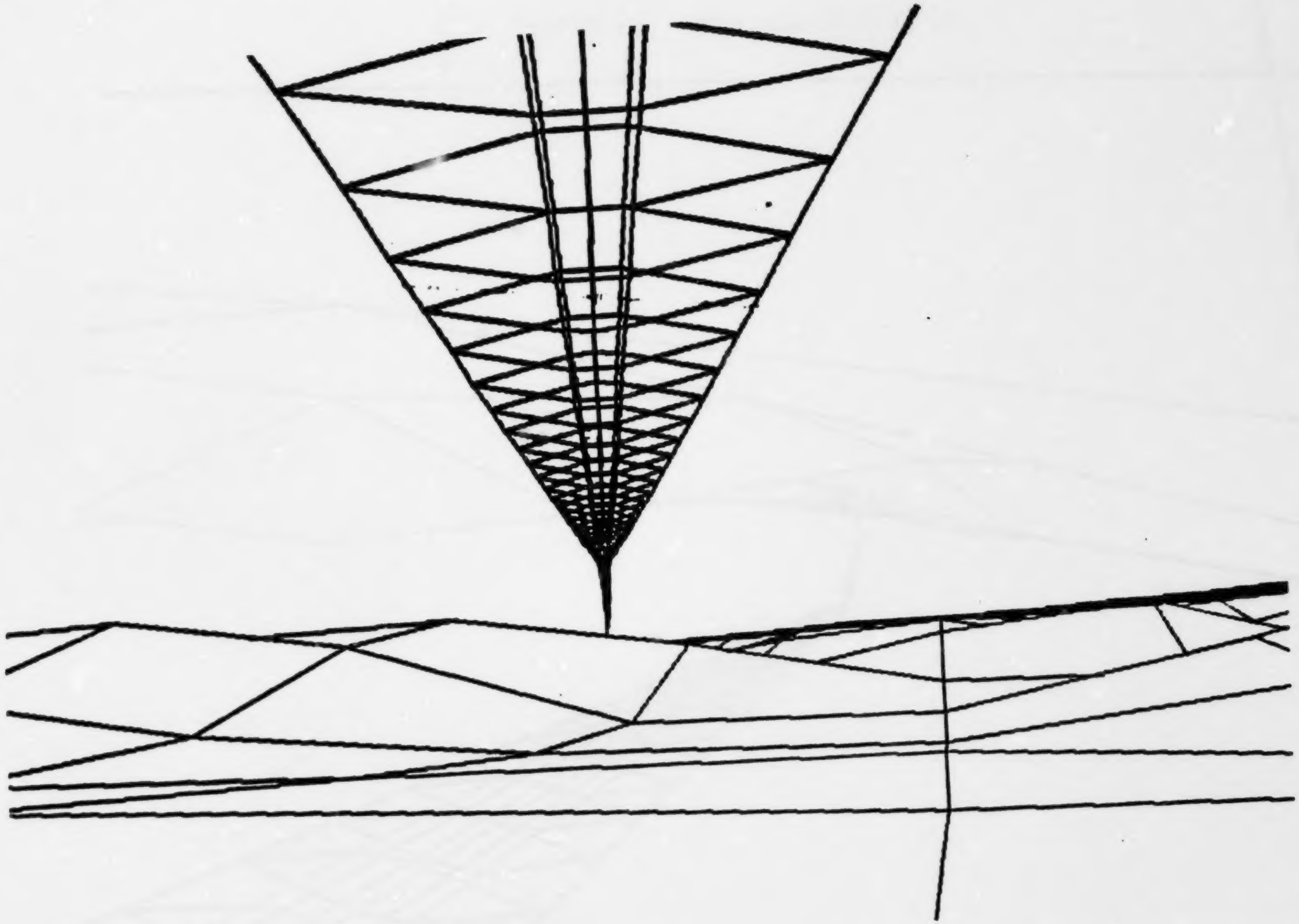

FIGURE 51. VIEW FROM LOCATION 15

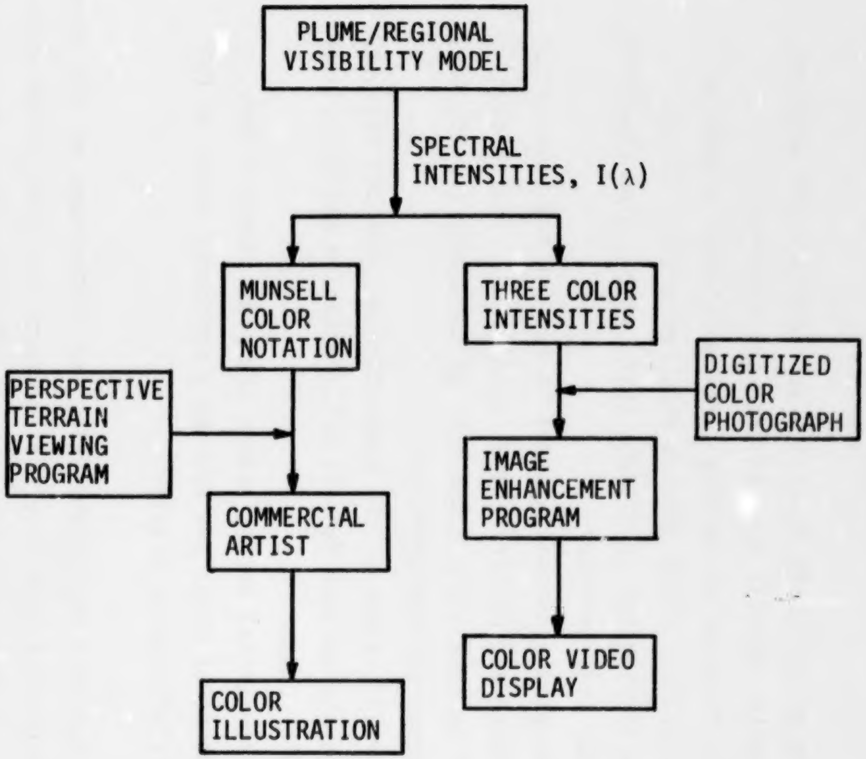
PLUME/REGIONAL VISIBILITY MODEL
SPECTRAL INTENSITIES, I(λ)
MUNSELL COLOR NOTATION
THREE COLOR INTENSITIES
PERSPECTIVE TERRAIN VIEWING PROGRAM
DIGITIZED COLOR PHOTOGRAPH
COMMERCIAL ARTIST
IMAGE ENHANCEMENT PROGRAM
COLOR ILLUSTRATION
COLOR VIDEO DISPLAY

FIGURE 52. SCHEMATIC SHOWING COLOR DISPLAY TECHNIQUES

### 1. Color Illustration

This technique is a synthesis of the regional and plume visibility model outputs and the Perspective Terrain Viewing Program (PTVP) illustrated in Section B. The process requires the following steps:

> The source characteristics and location are selected, and the digital terrain data are obtained.

> The Perspective Terrain Viewing Program is used to generate a plume terrain view for a given set of meteorological conditions (wind speed, wind direction, stability category).

> The plume visibility model is run for the same set of source and meteorological conditions. The coloration of various sight paths through the plume and the background sky are predicted.

> Specific areas of the plume terrain view are assigned the appropriate Munsell color notation and associated color chips.

> A commercial artist colors the plume terrain view. The color chips are used as a reference check on the artist's color display.

To illustrate the capabilities and limitations of this technique, we have constructed a test case that compares our predictions with the actual visual impact of a power plant plume. The comparison demonstrates the need for carefully documented studies of the accuracy of the model.

A test case should have the following attributes:

> A large point source with a visible effluent impact.

> Documentation of the source emissions ($NO_x$, $SO_2$, primary particulates).

> Location near a nonurban area of great aesthetic value.

For our test case, we selected a power plant in northern Arizona for which we had color photographs documenting the visual impact of the plume. The source emissions and dispersion conditions have been studied, but these data were not available to us. However, we were able to estimate the source emission conditions from other similar power plant sources.

The photograph we selected is reproduced in Figure 53, which clearly shows the brown coloration caused by the power plant plume. We chose this example because of the clearly apparent brown coloration. However, upon closer inspection, one notices that the lighting conditions are somewhat unusual because the photograph was taken very early in the morning. The sky is less blue than normal and is slightly yellowish at the horizon. The long shadows of the river canyons are visible, indicating a very low sun angle. As noted in Chapter III and Appendix B, the diffuse component (multiple scattered light) of the solar intensity becomes significant near sunrise and sunset. Since the diffuse component is hard to model correctly, particularly in extreme situations like this, this photograph represents a difficult test case.

For our estimation of the source characteristics and meteorological conditions, the Perspective Terrain Viewing Program was used to generate a plume terrain view, which is shown in Figure 39. A comparison of Figures 39 and 53 shows that the terrain and plume locations are rather faithfully reproduced. Although the resolution of the photograph is much greater than that of the computer graphics algorithm, the resemblance is clear. The distant mountains on the horizon (dark blue on the right-hand side of the photograph) are not plotted because they were outside the terrain boundaries of the program for this particular case. The plume boundaries are plotted at $1\sigma$ $(\sigma_y,\sigma_z)$ concentration values. The vertical extent of the plume in the photograph is less than it is in the computer plot, suggesting that the actual plume $\sigma_z$ was less than a Pasquill E stability. Plume concentration measurements would be required to substantiate this assumption, but the usefulness of the PTVP is clear.

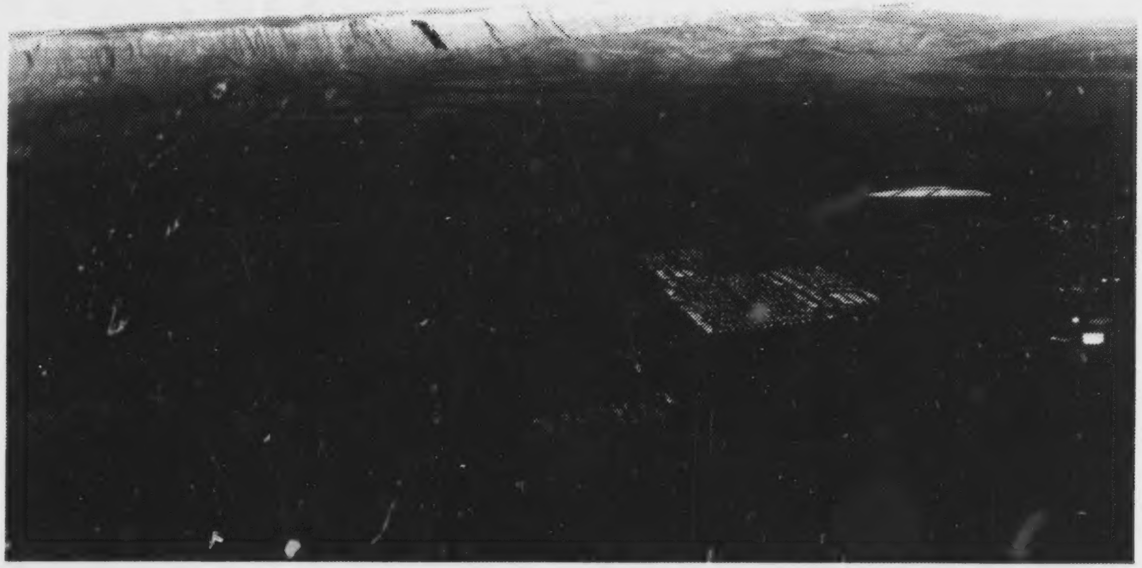

FIGURE 53. PHOTOCOPY OF THE POWER PLANT PLUME IN NORTHERN ARIZONA SELECTED FOR SIMULATION

The plume visibility model was then run for our estimated source and meteorological conditions. The Munsell color notation and associated color chips for various parts of the plume terrain scene are shown in Figure 54. After comparing the color chips and the original photograph, we concluded that the colors are reasonably close. The yellowish color of the horizon and the brownish color of the plume are reproduced, demonstrating that the plume model is capable of predicting the brownish coloration and displaying it correctly to a user of the model. The sky color is approximately the correct saturation and brightness.

The results of the final step of having a commercial artist paint in the correct colors are shown in Figure 55. The artist was never shown the original photograph; he had to rely on the color predictions from the plume visibility model. Unfortunately, we are less satisfied with the results of this step than with the previous two. The problems in this step appear to be that:

- It is difficult to paint and blend the correct colors to maintain fidelity to the predictions.
- The spatial resolution necessary to produce a realistic scene is also difficult and requires a large amount of time.
- The artist has a natural tendency to paint what he thinks the plume should look like.

Despite these difficulties, we believe the technique has promise and should be pursued, though more work on this step is needed.

Overall, we are encouraged with the results of the comparison. The significant findings were that:

- The Perspective Terrain Viewing Program can generate a realistic plume terrain scene.

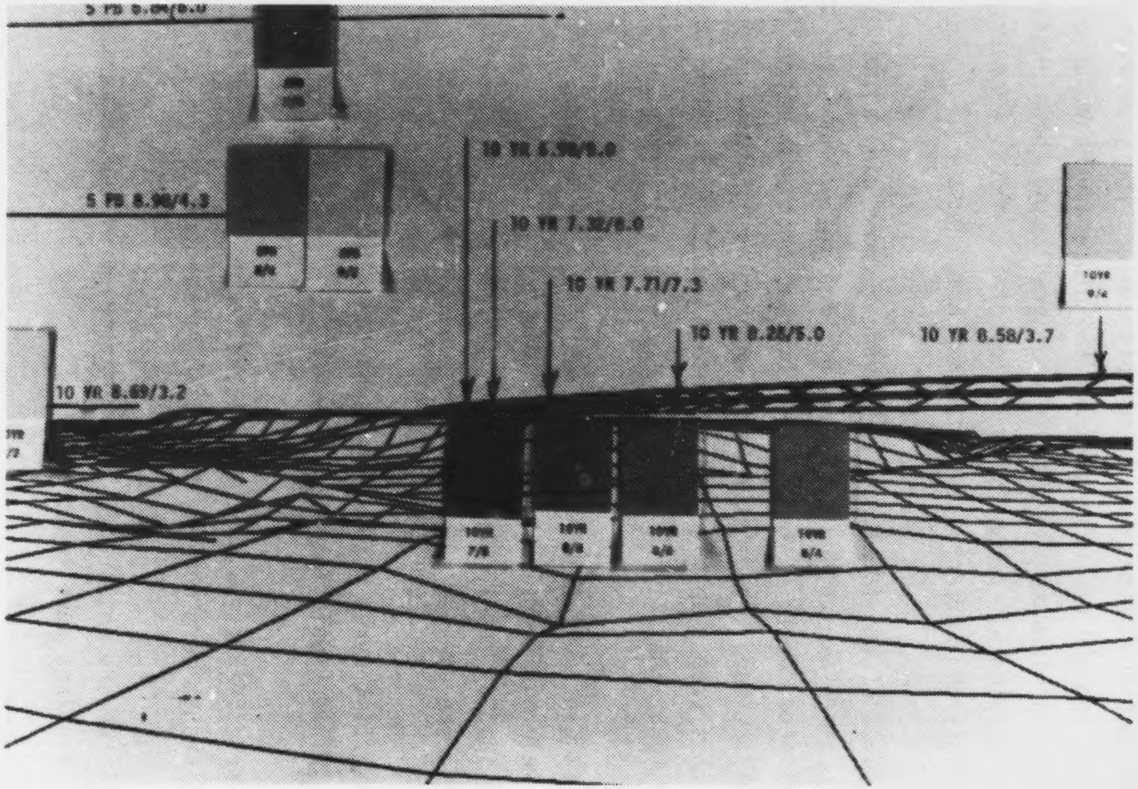
10 YR 6.58/6.0
5 PB 8.90/4.3
10 YR 7.32/6.0
10 YR 7.71/7.3
10 YR 8.28/5.0
10 YR 8.58/3.7
10 YR 8.69/3.2

FIGURE 54. PHOTOCOPY OF THE PERSPECTIVE TERRAIN VIEW AND CALCULATED MUNSELL COLOR NOTATION AND CORRESPONDING COLOR CHIPS

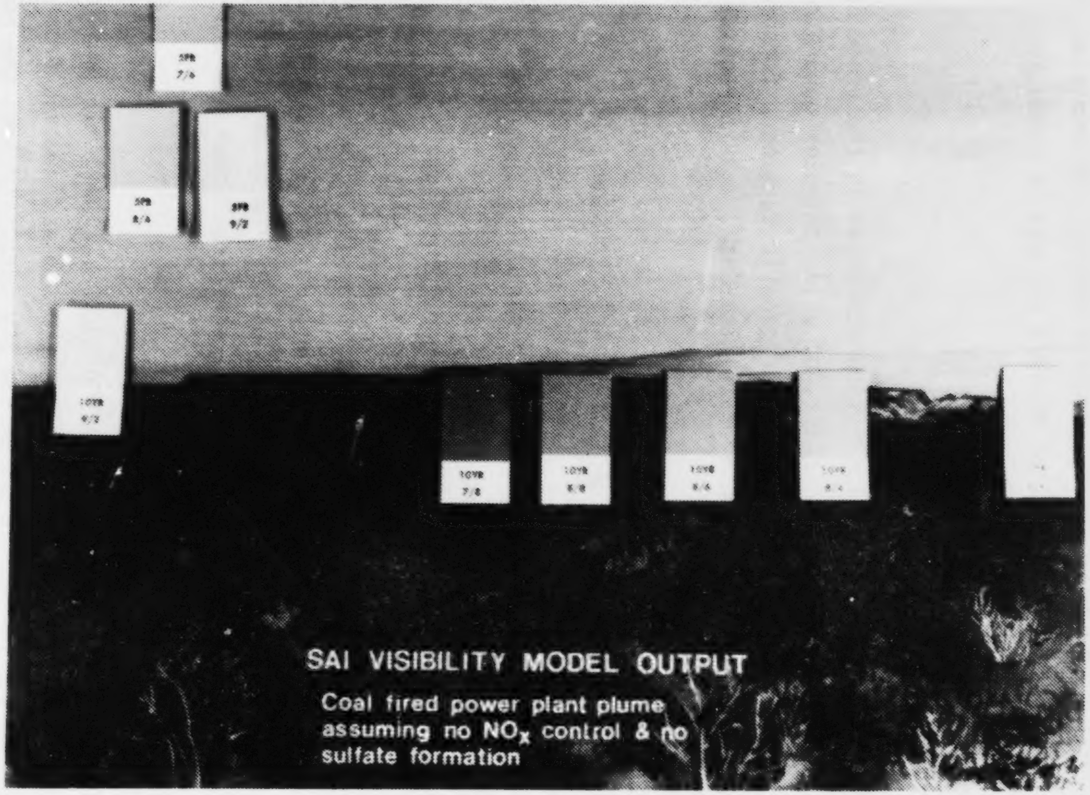
5PB
7/4
5PB
8/4
5PB
9/2
10YR
9/2
10YR
7/8
10YR
8/8
10YR
8/6
10YR
8/4
SAI VISIBILITY MODEL OUTPUT
Coal fired power plant plume assuming no $NO_x$ control & no sulfate formation

FIGURE 55. PHOTOCOPY OF COLOR ILLUSTRATION CREATED BY AN ARTIST FROM INDICATED MUNSELL COLOR CHIPS

> The plume visibility model can predict the plume coloration correctly.

It is important to emphasize that these findings are somewhat preliminary, and testing must continue to verify computer models. In addition, more information must be gathered so that other tests can be conducted.

## 2. Color Video Display

In addition to the color illustration described in the preceding section, we investigated the possibility of using computer-generated color display facilities. This technique was originally developed for processing photographic data, particularly satellite data, and it requires special equipment, including:

> A color densitometer to digitize a color photograph in three colors.
> Image enhancement software to allow manipulation of the digitized information.
> A color video display unit and supporting software.

Although these facilities were not directly accessible, we were fortunately able to acquire the assistance of researchers at Los Alamos Scientific Laboratory who have used this technique. The Los Alamos personnel utilized this technique to predict visibility impairment from power plant plumes (Williams, Wecksung, and Leonard, 1978).

We sent Los Alamos the test case photograph (Figure 53), which was then digitized into three colors. Then the plume was removed from the digitized photograph by interpolating the sky intensity from the horizon below the plume to the sky above it. Next we gave the Los Alamos personnel the results from our plume model for specific locations in the plume. These intensities were displayed on the color video screen, and a photograph was taken. The results are shown in Figure 56. This

FIGURE 56. PHOTOCOPY OF A COLOR VIDEO DISPLAY OF PLUME VISUAL IMPACT

figure is then an illustration of the color video display technique. The photograph can be compared to the test case photograph (Figure 53). Because of compatibility difficulties between our computer output and the Los Alamos facility, the results in Figure 56 should be considered as a qualitative indication of the technique.

The color video display is a very powerful technique that gives the user a rendition of a photograph with the plume effects superimposed. The technique is somewhat cumbersome, however. Specifically, the difficulties are the following:

- > The hardware is expensive, available only at specific locations, and not available on a dedicated basis.
- > It is difficult to transfer information from the original film to the final produced photograph without introducing errors. In other words, a quantitative measure of the color fidelity of the process is not possible at present. This difficulty is due mostly to the problems involved in film processing.

This description of the difficulties of the color video technique is not meant to be a criticism of the Los Alamos personnel and their work. It is simply a listing of problems that must be faced in using the technique on a routine basis.

## D. THE REGIONAL VISIBILITY MODEL

We have modified the Northern Great Plains regional grid model (Liu and Durran, 1976) so that it has the capability to compute regional concentrations of $NO_2$ and sulfate. We show in this section how these pollutant concentrations can be used both to display visual range isopleths for the region and to characterize atmospheric discoloration at specific locations (Class I areas) within the region. We summarize the results of sample calculations using 1975 and 1986 $SO_x$ and $NO_x$ emissions from point sources in the Northern Great Plains. Also, using 1972 $SO_2$ emissions from the copper smelters in Arizona and New Mexico, we constructed a hypothetical situation by assuming that these sources were located in the Northern Great Plains. The objective of that task was to study the effect of the large $SO_x$ emission rates from the copper smelters (6000 tons per day) on regional visibility using the existing Northern Great Plains regional model. The significant impact of copper smelter $SO_x$ emissions on visibility in the Southwest is indicated by the results of the data analysis described in Appendix A and the regional model calculations reported in this section. This impact suggests the need for a regional visibility model for the Southwest capable of handling the transport and diffusion of copper smelter emissions as well as power plant emissions in complex terrain.

Figures 57 through 60 show the isopleths of $SO_2$, $NO_2$, and sulfate concentrations and visual range calculated using the regional grid model. $NO_2$ concentrations were calculated using the technique described in Chapter III from total $NO_x$ emissions assuming a background ozone concentration of 0.020 ppm. Sulfate concentrations were calculated from $SO_x$ emissions using a pseudo-first-order rate constant of 0.5 percent per hour and assuming negligible primary sulfate emissions. Visual range was calculated from the Koschmieder relationship using the following value for the extinction coefficient:

$$b_{ext} = \left(0.24 + 0.04\left[SO_4^{=}, \text{ in } \mu g/m^3\right]\right)\left(10^{-4}\ m^{-1}\right) \quad .$$

With the assumed background $SO_4^{=}$ concentration of 1.5 $\mu g/m^3$, this expression gives $b_{ext} = 0.30 \times 10^{-4}\ m^{-1}$, which corresponds to a visual range of 130 km. The $b_{scat}$-to-mass ratio used here ($0.04 \times 10^{-4}\ m^{-1}/\mu g/m^3$) is appropriate for sulfate aerosol in the accumulation mode at average relative humidity, and it is the average reported by Trijonis and Yuan (1977) for the Southwest.

The calculations of visual range (Figure 60) indicate that anthropogenic emissions from point sources within the Northern Great Plains

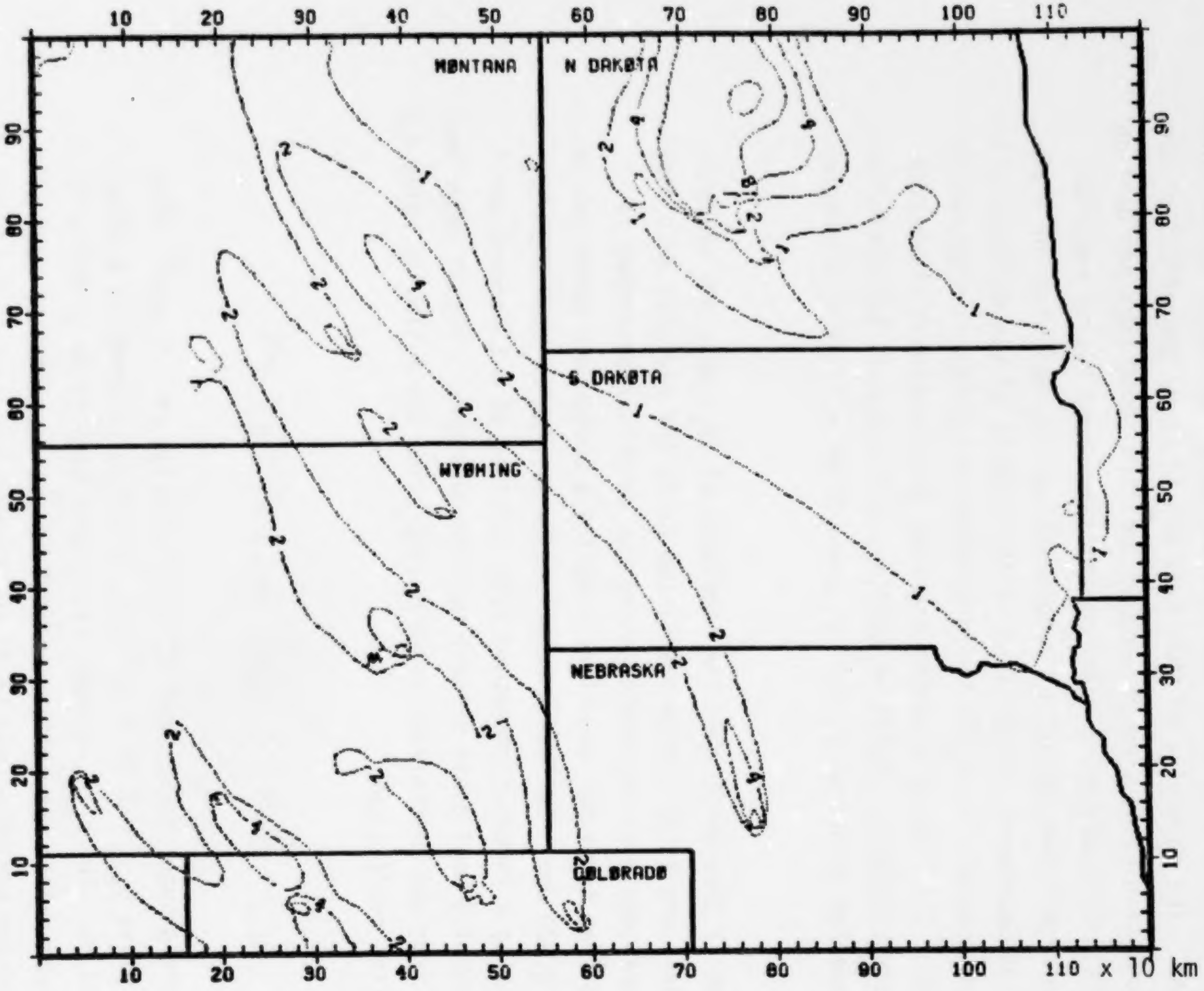
MØNTANA
N DAKØTA
S DAKØTA
WYØMING
NEBRASKA
CØLØRADØ
10
20
30
40
50
60
70
80
90
100
110
x 10 km
1
2
4
8

FIGURE 57. PREDICTED REGIONAL THREE-HOUR-AVERAGE $SO_2$ CONCENTRATIONS ($\mu g/m^3$) BASED ON 1986 EMISSIONS IN THE NORTHERN GREAT PLAINS FOR THE METEOROLOGICAL CONDITIONS OF 1400-1700 MST ON 6 APRIL 1976

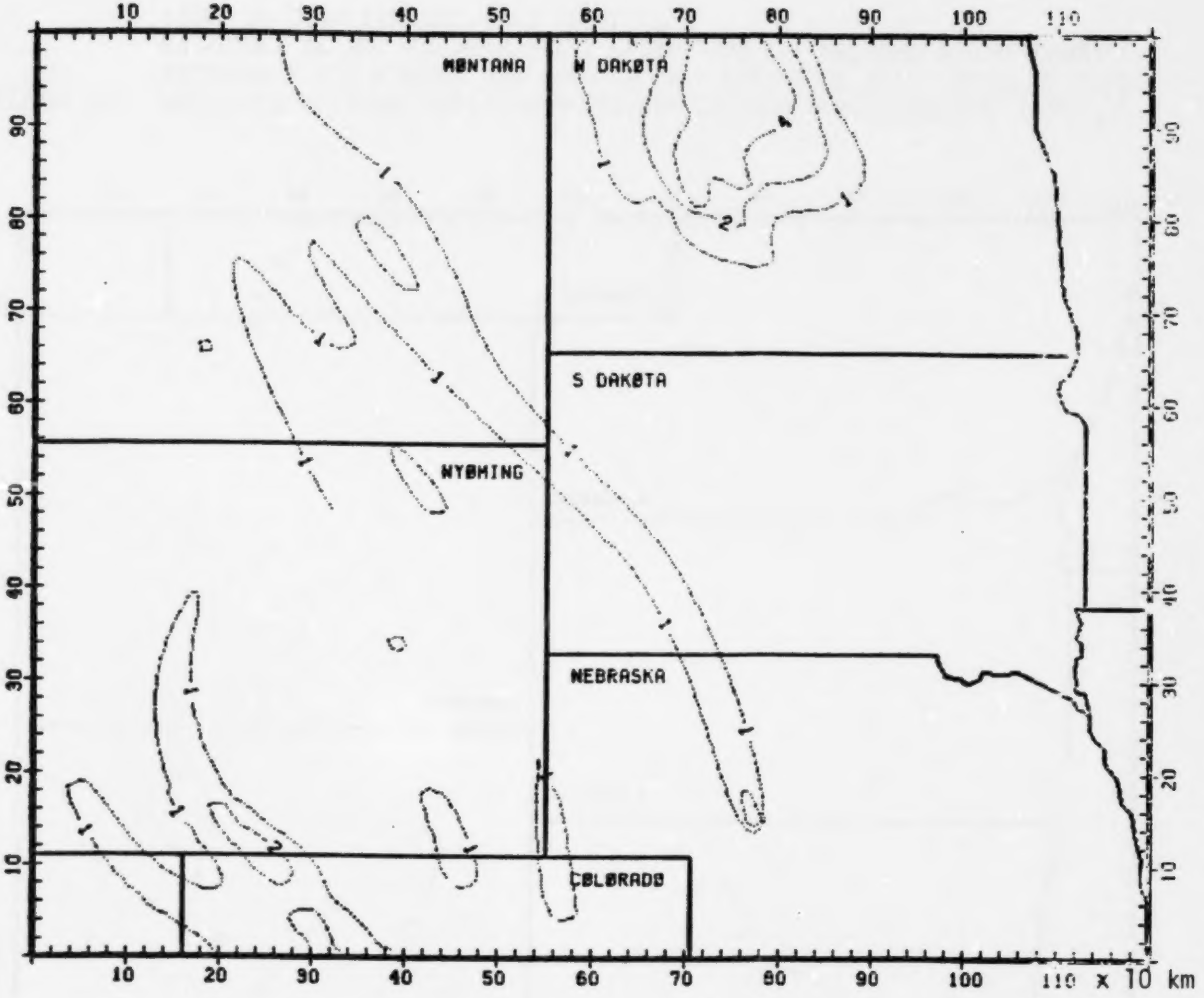
MONTANA
N DAKOTA
S DAKOTA
WYOMING
NEBRASKA
COLORADO
1
2
4
10
20
30
40
50
60
70
80
90
100
110
x 10 km

FIGURE 58. PREDICTED REGIONAL THREE-HOUR-AVERAGE $NO_2$ CONCENTRATIONS (ppb) BASED ON 1986 EMISSIONS IN THE NORTHERN GREAT PLAINS FOR THE METEOROLOGICAL CONDITIONS OF 1400-1700 MST ON 6 APRIL 1976

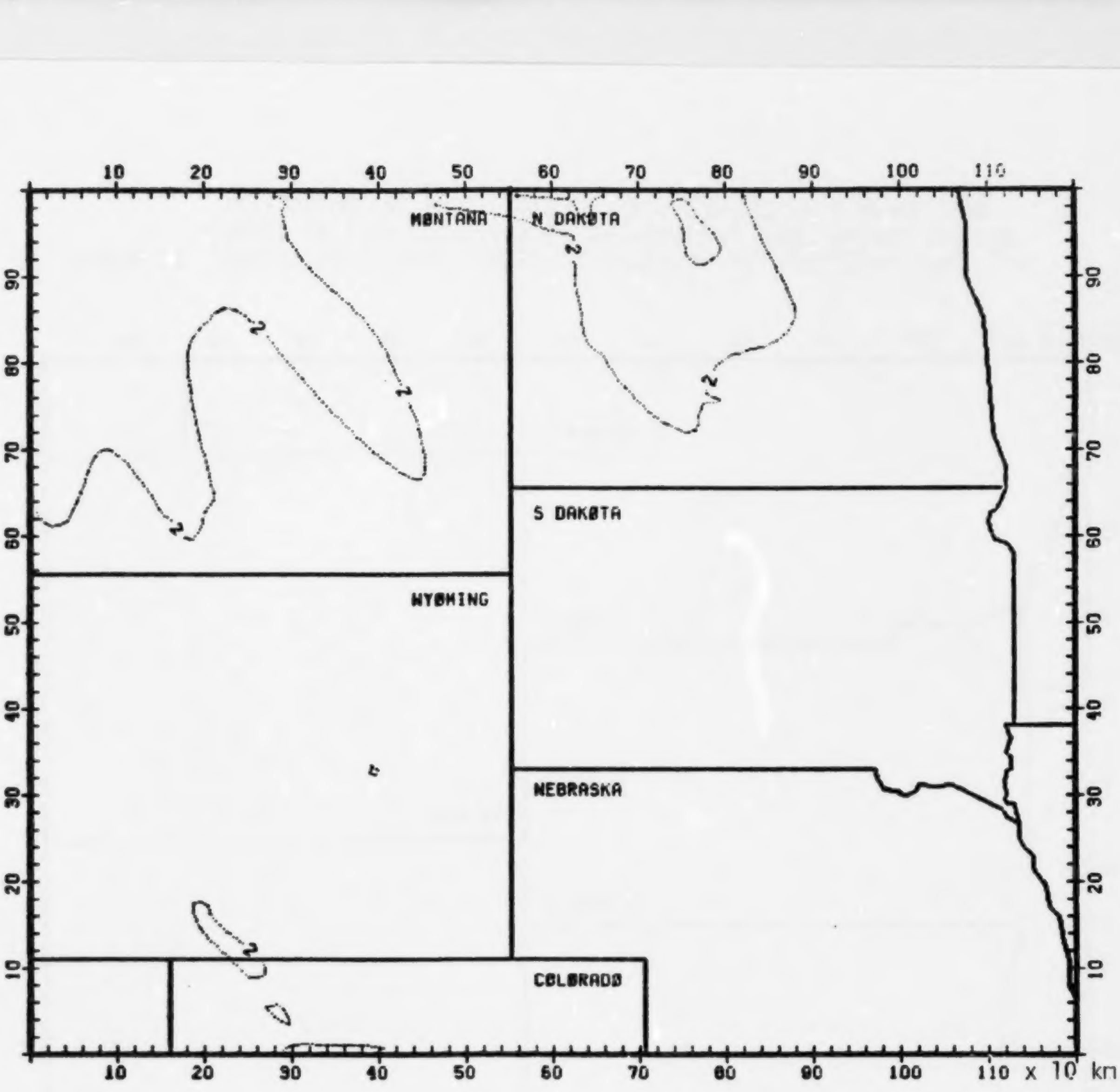
MØNTANA
N DAKØTA
S DAKØTA
WYØMING
NEBRASKA
CØLØRADØ
2
10
20
30
40
50
60
70
80
90
100
110
110 x 10 km

FIGURE 59. PREDICTED REGIONAL THREE-HOUR-AVERAGE SULFATE CONCENTRATIONS ($\mu g/m^3$), ASSUMING A 0.5 PERCENT PER HOUR SULFATE FORMATION RATE, BASED ON 1986 EMISSIONS IN THE NORTHERN GREAT PLAINS FOR THE METEOROLOGICAL CONDITIONS OF 1400-1700 MST ON 6 APRIL 1976

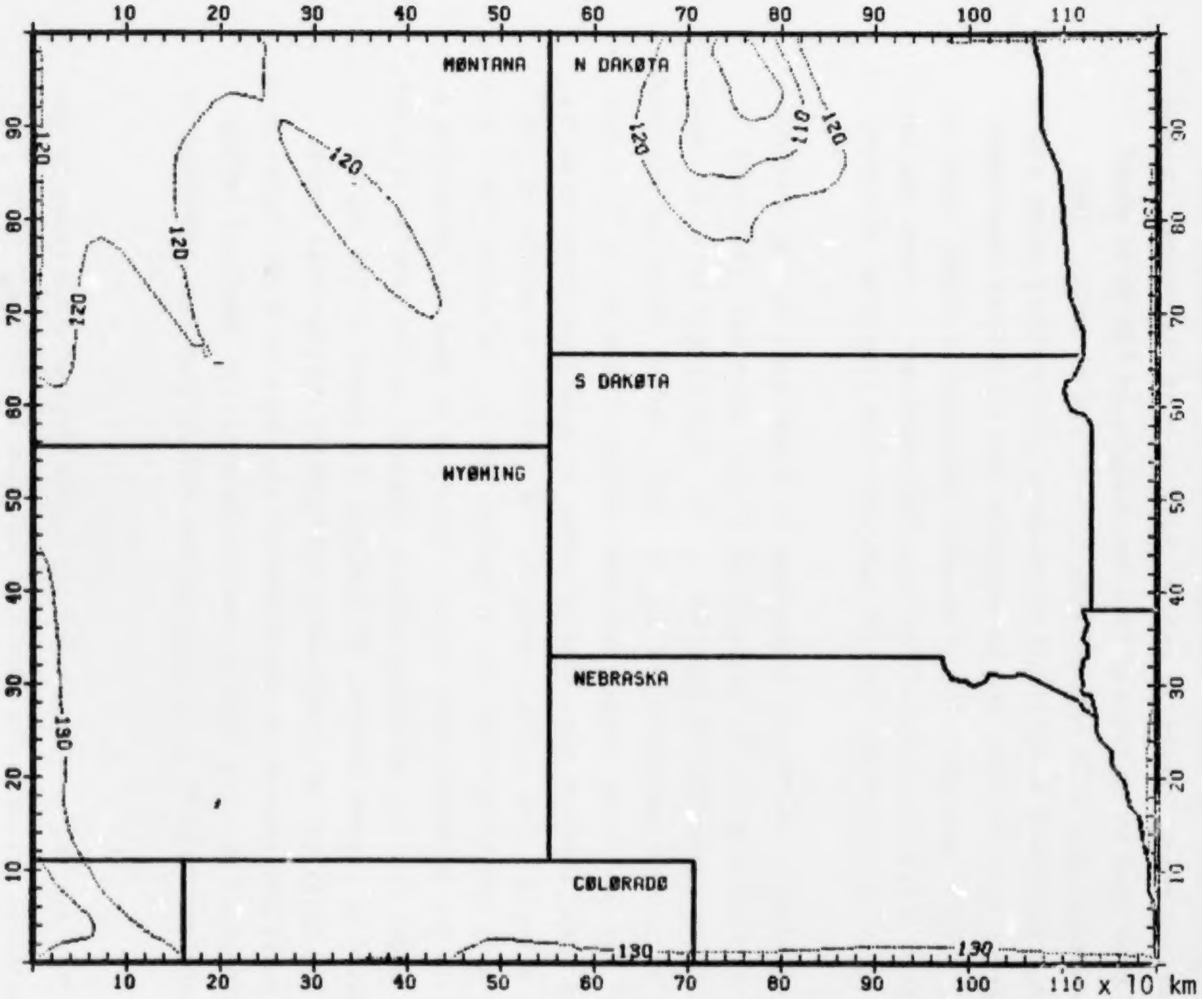
MONTANA
N DAKOTA
S DAKOTA
WYOMING
NEBRASKA
COLORADO
120
110
130
10
20
30
40
50
60
70
80
90
100
110 x 10 km

FIGURE 60. PREDICTED REGIONAL VISUAL RANGE (km), ASSUMING A BACKGROUND VISUAL RANGE OF 130 km AND A 0.5 PERCENT PER HOUR SULFATE FORMATION RATE. BASED ON 1986 EMISSIONS IN THE NORTHERN GREAT PLAINS FOR THE METEOROLOGICAL CONDITIONS OF 1400-1700 MST ON 6 APRIL 1976

cause only a small reduction in visual range, even with the increased emissions projected for 1986. Maximum visibility impairment (i.e., minimum visual range) occurs in only a small part of the region. Visual range is predicted to be reduced from the background 130 km to about 100 km, approximately a 25 percent reduction in visual range. This small reduction would be difficult to measure, particularly using visibility target observations, and to separate from visibility impairment caused by natural sources. The calculated reduction in visual range in the Northern Great Plains resulting from 1975 emissions is even smaller. The results of calculations for 1975 emissions are presented in Appendix G.

Anthropogenic visibility impairment is significant in the Southwest, however, as indicated by the analysis of visual range data presented in Appendix A and summarized in Appendix B. In southeastern Arizona, copper smelters emit large quantities of $SO_x$; in 1972, before pollution abatement equipment was installed, copper smelters emitted an average of 6000 tons of $SO_x$ per day, which is more than an order of magnitude larger than the 1975 $SO_2$ emissions from point sources in the Northern Great Plains (430 tons per day) and three times the projected 1986 $SO_x$ emissions (1990 tons per day) in the Northern Great Plains. Although we have not developed a regional model for the Southwest capable of handling the complex flow patterns caused by rugged terrain, we examined the impact of the copper smelter $SO_x$ emissions on visual range by locating hypothetical copper smelter emissions sources in the middle of the Northern Great Plains grid. The hypothetical emission sources had characteristics identical to the copper smelters located in Arizona and New Mexico that were operating in 1972.

We then ran the grid model for the meteorological conditions of the Great Plains to evaluate the impact of the high $SO_x$ emission rates from the copper smelters. We summarize the results of this calculation for a given time period in one of the test simulations in Figures 61 through 63. The state boundaries have been removed from these plots to emphasize that

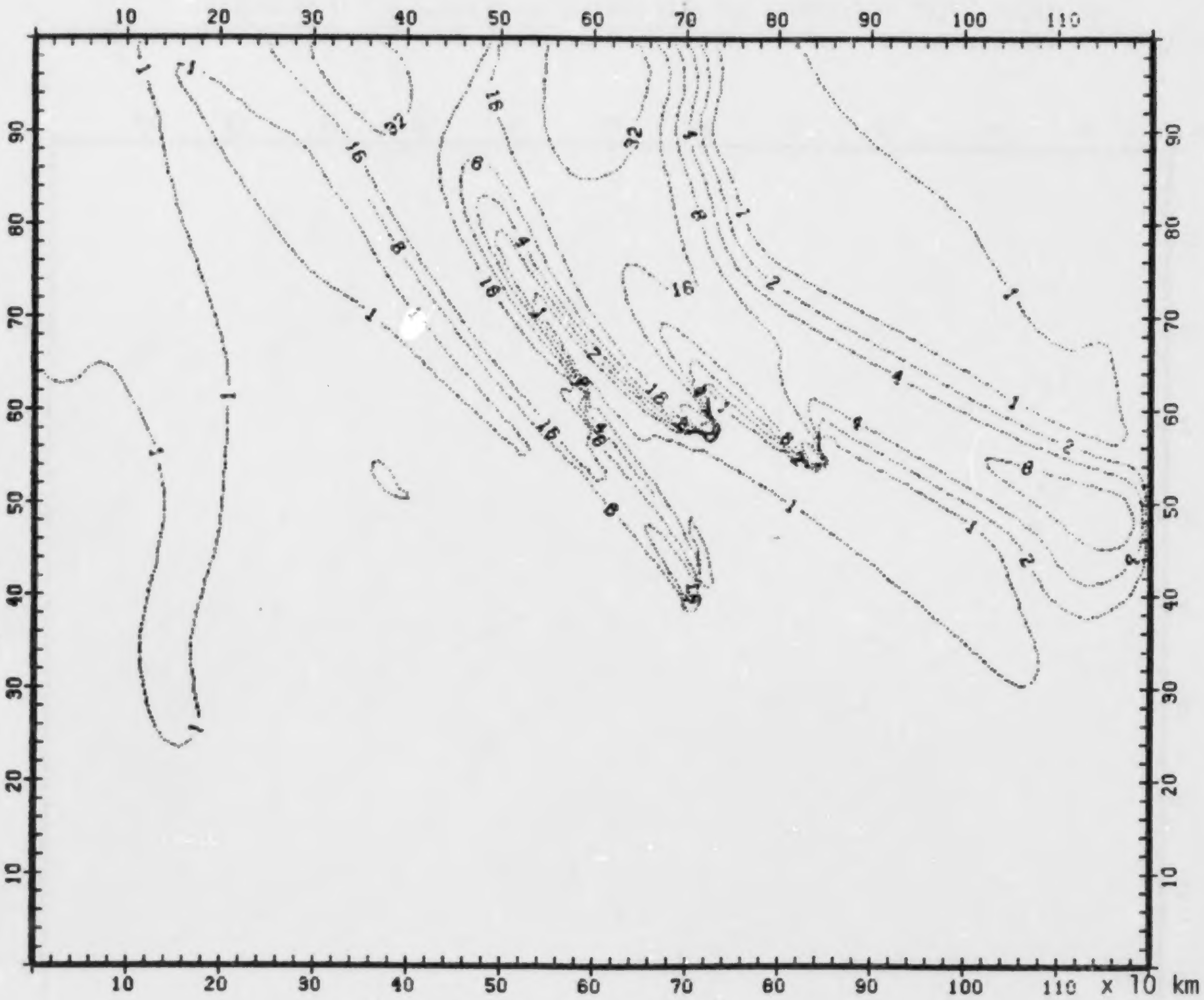
10
20
30
40
50
60
70
80
90
100
110
x 10 km
1
2
4
8
16
32

FIGURE 61. PREDICTED REGIONAL THREE-HOUR-AVERAGE $SO_2$ CONCENTRATIONS ($\mu g/m^3$) BASED ON HYPOTHETICAL COPPER SMELTER EMISSIONS FOR THE METEOROLOGICAL CONDITIONS OF 1400-1700 MST ON 6 APRIL 1976 IN THE NORTHERN GREAT PLAINS

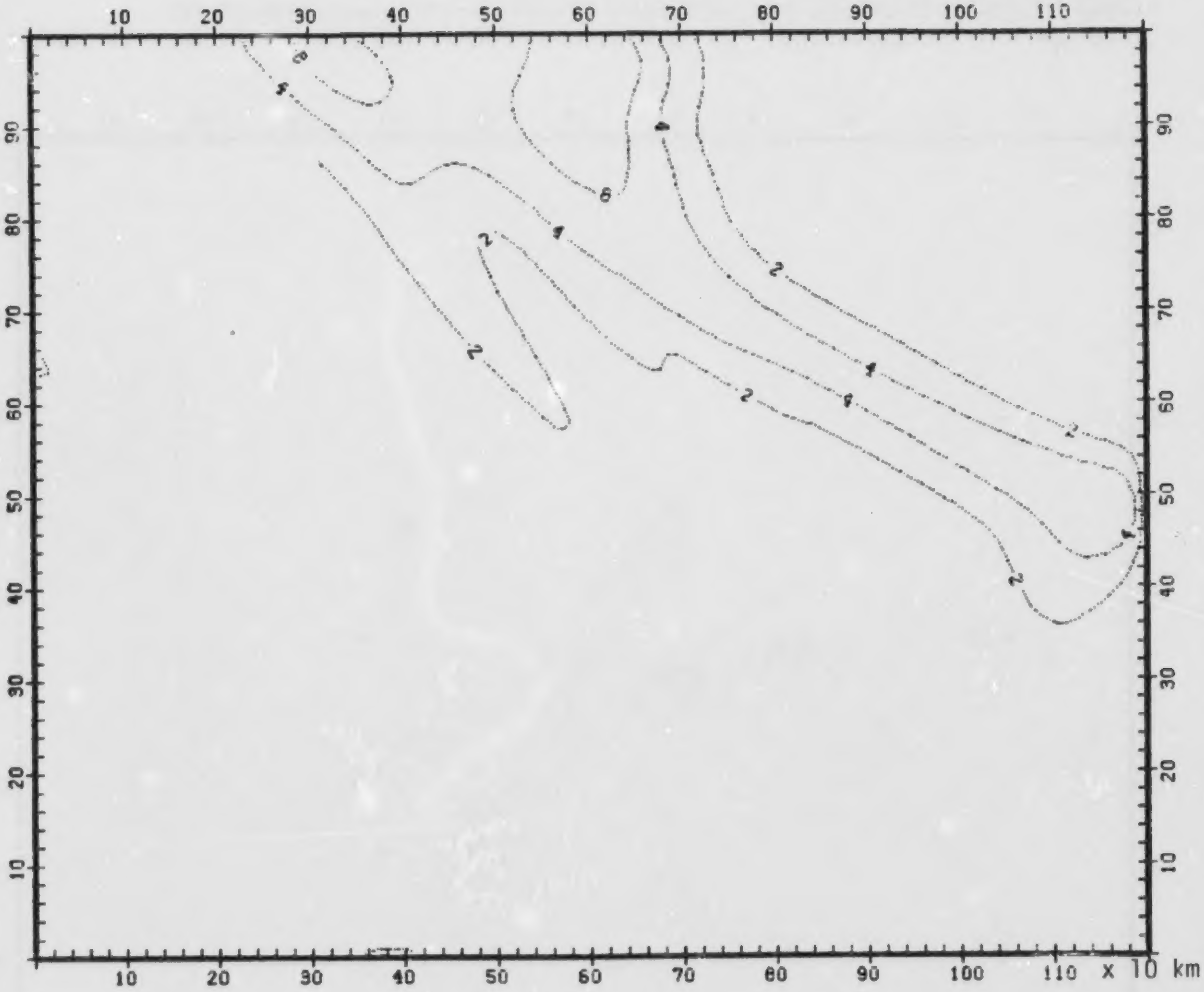
10
20
30
40
50
60
70
80
90
100
110
x 10 km
2
4
6
8

FIGURE 62. PREDICTION REGIONAL THREE-HOUR-AVERAGE SULFATE CONCENTRATIONS (μg/m$^3$), ASSUMING A 0.5 PERCENT PER HOUR SULFATE FORMATION RATE, BASED ON HYPOTHETICAL COPPER SMELTER EMISSIONS FOR METEOROLOGICAL CONDITIONS OF 1400-1700 MST ON 6 APRIL 1976 IN THE NORTHERN GREAT PLAINS

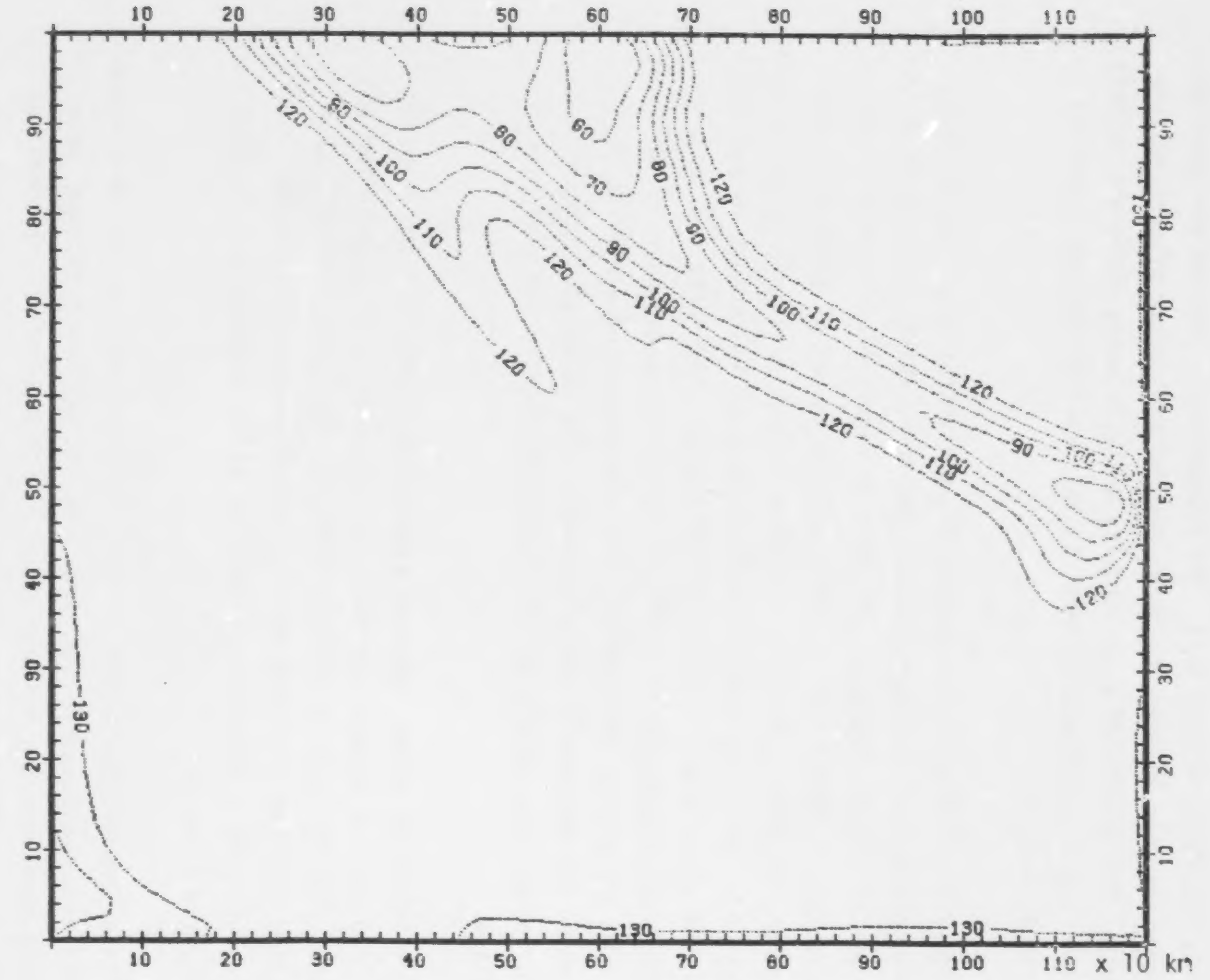
10
20
30
40
50
60
70
80
90
100
110
x 10 km
60
70
80
90
100
110
120
130

FIGURE 63. PREDICTED REGIONAL VISUAL RANGE (km), ASSUMING A BACKGROUND VISUAL RANGE OF 130 km AND A 0.5 PERCENT PER HOUR SULFATE FORMATION RATE, BASED ON HYPOTHETICAL COPPER SMELTER EMISSIONS FOR METEOROLOGICAL CONDITIONS OF 1400-1700 MST ON 6 APRIL 1976 IN THE NORTHERN GREAT PLAINS

this is a hypothetical test case. We assumed a 0.5 percent per hour sulfate formation rate in these calculations and negligible primary sulfate emissions. The results of a sensitivity analysis using different sulfate formation rates are summarized later in this section and are presented in detail in Appendix G.

Figure 61 shows that the maximum $SO_2$ concentrations occur at short distances downwind of the hypothetical smelters, which are located in the center of the region. However, as shown in Figure 62, the maximum $SO_4^=$ concentrations (greater than 8 $\mu g/m^3$) occur hundreds of kilometers downwind of the smelters. The impact of this sulfate on visual range is shown in Figure 63. The worst visibility (less than 60 km) occurs in one small area in the upper middle portion of the region. The increased sulfate concentrations and resultant decreases in visual range occur in two directions from the sources as a result of a change in wind direction that occurred on the day before the simulation. The calculated concentration maps for other time periods of this simulation period are presented in Appendix G.

The impact on visual range of assuming different sulfate formation rates (0.3 and 1.0 percent per hour) is indicated in Figures 64 and 65. Note that with the reduced sulfate formation the minimum visual range is 70 km, and with the increased sulfate formation rate it is 40 km, which compares with the minimum visual range of 60 km computed for the base case of 0.5 percent per hour.

These sample calculations of reduced visual range cannot be compared directly with the observational data from the Southwest because these calculations were based on Northern Great Plains meteorological conditions. However, the results agree qualitatively with some of the conclusions of the data analysis summarized in Chapter II: namely, $SO_x$ emissions from copper smelters in the Southwest can cause a significant reduction in visual range even at locations several hundreds of kilometers downwind. The predicted maximum $SO_4^=$ concentrations in these simulations, ranging from 8 to 16 $\mu g/m^3$, agree qualitatively with measured maxima in Arizona. The

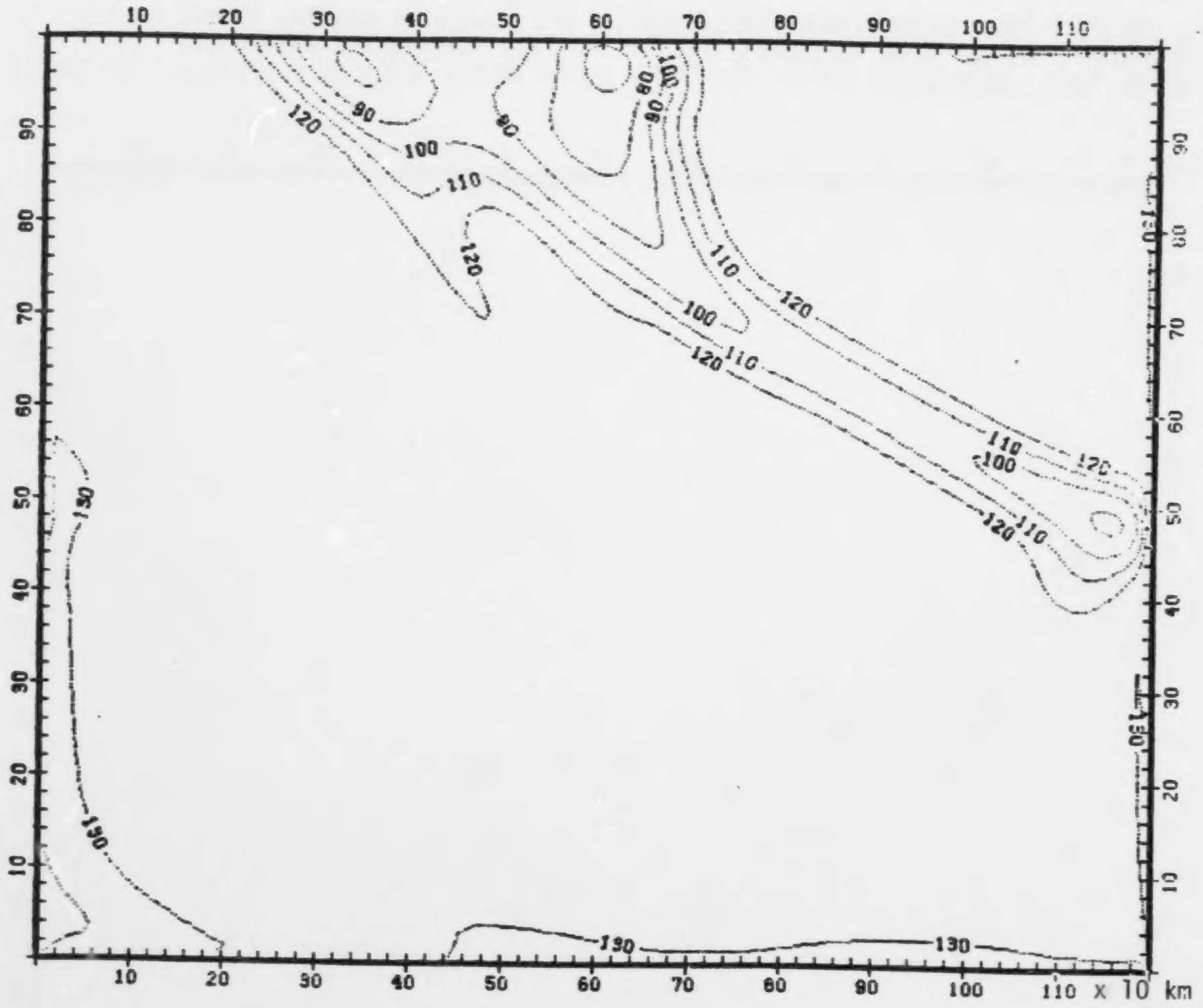

FIGURE 64. PREDICTED REGIONAL VISUAL RANGE (km), ASSUMING A BACKGROUND VISUAL RANGE OF 130 km AND A 0.3 PERCENT PER HOUR SULFATE FORMATION RATE, BASED ON HYPOTHETICAL COPPER SMELTER EMISSIONS FOR METEOROLOGICAL CONDITIONS OF 1400-1700 MST ON 6 APRIL 1976 IN THE NORTHERN GREAT PLAINS

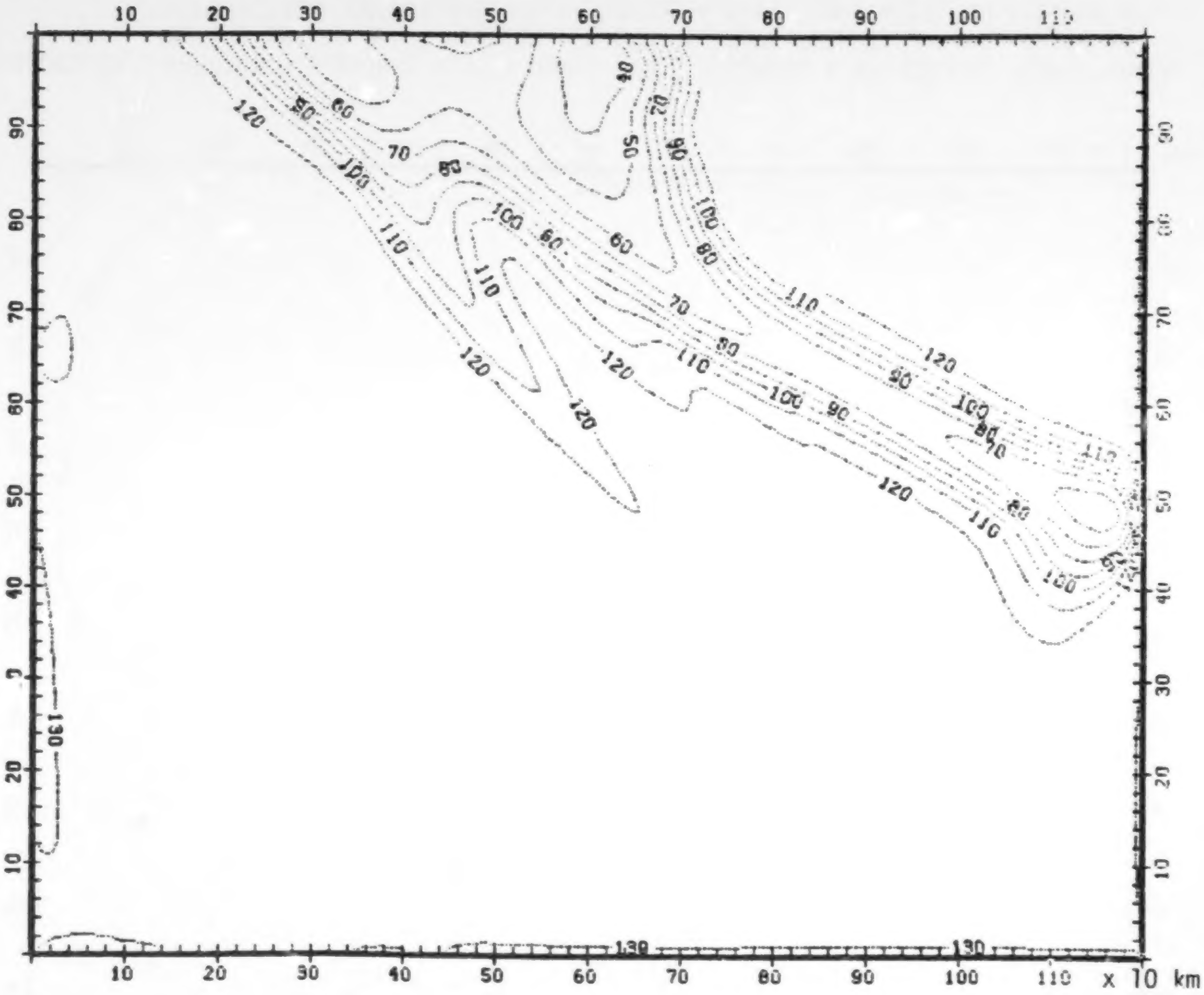
10
20
30
40
50
60
70
80
90
100
110
x 10 km
120
110
100
90
80
70
60
50
40
130

FIGURE 65. PREDICTED REGIONAL VISUAL RANGE (km), ASSUMING A BACKGROUND VISUAL RANGE OF 130 km AND A 1 PERCENT PER HOUR SULFATE FORMATION RATE, BASED ON HYPOTHETICAL COPPER SMELTER EMISSIONS FOR METEROLOGICAL CONDITIONS OF 1400-1700 MST ON 6 APRIL 1976 IN THE NORTHERN GREAT PLAINS

measured mean and maximum $SO_4^=$ concentrations in 1972 and 1973 in several locations in Arizona are summarized in Table 5. Note that mean sulfate concentrations ranged from 2.2 to 12.5 $\mu g/m^3$, and maxima ranged from 5.8 to 41.0 $\mu g/m^3$.

TABLE 5. MEAN AND MAXIMUM 24-HOUR-AVERAGE SULFATE CONCENTRATIONS MEASURED IN ARIZONA IN 1972-1973

($\mu g/m^3$)

| | $[SO_4^=]$ | |
|---|---|---|
| Location | Mean | Maximum |
| Ajo | 12.5 | 41.0 |
| Douglas | 9.1 | 25.9 |
| Flagstaff | 2.6 | 5.8 |
| Grand Canyon | 2.2 | 6.0 |
| Phoenix | 6.5 | 34.5 |
| Superior | 5.2 | 22.1 |
| Tuba City | 2.6 | 9.7 |
| Tucson | 6.4 | 22.0 |

The highest concentrations occurred in the immediate vicinity of smelters (e.g., Ajo, Douglas, and Superior) and in cities (e.g., Phoenix and Tucson), where, presumably, the rate of sulfate formation would increase because of the elevated concentrations of reactive species in polluted urban air. The high sulfate concentrations measured near the smelters may be the result of primary $SO_4^=$ emissions or the rapid conversion to sulfate of emitted $SO_2$ in the initial stages of plume dilution. The measured maximum sulfate concentrations in nonurban areas of Arizona distant from smelters (e.g., Flagstaff, Grand Canyon, and Tuba City) ranged from 6 to 10 $\mu g/m^3$, in qualitative agreement with the regional model calculations.

Our approach to the calculation of atmospheric discoloration on the regional scale has been to compute color parameters for particular locations (e.g., Class I areas) using the $NO_2$ and $SO_4^=$ concentrations obtained using the regional model. In these calculations, we assumed homogeneous pollutant concentrations within the mixed layer, and we computed optical effects for several different sight paths. Exhibit 6 shows the output from an example of these calculations for a location with background concentrations of 3.4 $\mu g/m^3$ of sulfate, 30 $\mu g/m^3$ of coarse mode particulate, and no $NO_2$. For different scattering angles $\Theta$ and sight path elevation angles $\beta$, the following specifications of color and color change (similar to the parameters characterizing plume impact) are printed:

- Optical thickness ($\tau$).
- Light intensity (Y and L*).
- Chromaticity coordinates (x,y).
- Change in light intensity between the given background atmosphere and a Rayleigh (no particles) reference atmosphere for the given $\Theta$ and $\beta$ ($\Delta Y, \Delta L^*$)
- Contrast between the given background atmosphere and the reference at three wavelengths [$C(\lambda)$, $\lambda = 0.40$, 0.55, and 0.70 $\mu m$].
- Blue-red ratio between given background and reference.
- Changes in chromaticity coordinates ($\Delta x, \Delta y$).
- Color difference parameters [$\Delta E(L^*U^*V^*)$ and $\Delta E(L^*a^*b^*)$].

With these parameters, the color of the background sky at a given location in a region can be specified and Munsell color notation can be determined from the values of L*, x, and y. The change in light intensity and color between the given location's sky and the reference atmosphere is specified by contrast values $\Delta Y$, $\Delta L^*$, $\Delta x$, $\Delta y$, and $\Delta E$. These differences do not have the same meaning as the corresponding parameters for plume impact because the observer compares the light intensity and coloration of the

```
    VISUAL EFFECTS CAUSED BY BACKGROUND ATMOSPHERE (WITHOUT PLUME)
    *** CLEAR SKY VIEWS ***

THETA BETA     TAU    YCAP       L       X       Y DELYCAP    DELL  C(400)  C(550)  C(700)  BRATIO    DELX    DELY  E(LUV)  E(LAB)

 22.    0.    6.87  208.61  132.18   .3409   .3462  103.06   30.08   .3906   .8897  1.8769   .4834   .0337   .0221 44.6680 33.3720
       13.     .63   86.43   94.30   .2930   .3041   32.59   29.64   .2697  1.3363  3.6873   .2709   .0337   .0377 42.7131 33.4369
       30.     .34   31.34   77.02   .2830   .2914   31.29   24.87   .2698  1.3446  3.6901   .2707   .0313   .0384 33.4713 29.3383
       43.     .24   30.17   68.18   .2796   .2868   22.87   22.09   .2396  1.4988  3.3837   .2747   .0300   .0377 28.9426 26.0430
       60.     .19   31.83   63.23   .2781   .2847   18.83   20.43   .2483  1.4346  3.4898   .2786   .0492   .0371 26.4661 24.1320
       73.     .17   28.81   60.63   .2774   .2837   16.90   19.33   .2403  1.4233  3.4274   .2801   .0488   .0367 25.1872 23.1479
       90.     .17   27.91   59.84   .2771   .2834   16.32   19.24   .2374  1.4132  3.4059   .2809   .0487   .0366 24.7891 22.8313

 43.    0.    6.87  110.33  103.93   .3184   .3313   18.44    7.07   .0384   .1844   .6363   .6390   .0132   .0097 13.9237  9.9126
       13.     .63   49.33   73.81   .2731   .2893   19.92   14.43  -.0146   .6939  1.8232   .3488   .0369   .0430 26.7399 20.7632
       30.     .34   29.77   61.49   .2633   .2760   12.11   12.36   .0011   .7177  1.8439   .3320   .0347   .0447 20.6836 17.3462
       43.     .24   22.10   54.17   .2623   .2712    8.79   10.90  -.0011   .6942  1.7900   .3380   .0336   .0437 17.6649 13.3729
       60.     .19   18.43   50.07   .2608   .2690    7.16    9.97  -.0071   .6686  1.7376   .3627   .0329   .0430 16.0248 14.2198
       73.     .17   16.71   47.93   .2601   .2680    6.38    9.46  -.0118   .6310  1.7029   .3636   .0325   .0426 13.1837 13.6030
       90.     .17   16.19   47.26   .2399   .2677    6.14    9.29  -.0136   .6449  1.6909   .3666   .0324   .0423 14.9229 13.4110

 90.    0.    6.87   64.12   84.04   .3000   .3111   -9.26   -4.60  -.0336  -.1380   .0762   .8794   .0008  -.0039  6.4643  3.7798
       13.     .63   29.82   61.33   .2633   .2744    6.04    3.63  -.1374   .2684   .8930   .4446   .0272   .0334 18.1834 12.6828
       30.     .34   18.02   49.36   .2341   .2608    3.93    3.19  -.1323   .3008   .9263   .4303   .0232   .0327 13.7199 10.6172
       43.     .24   13.40   43.40   .2311   .2369    2.86    4.36  -.1292   .2917   .9017   .4379   .0242   .0318 11.3752  9.4079
       60.     .19   11.20   39.93   .2497   .2338    2.29    4.10  -.1311   .2778   .8737   .4637   .0236   .0311 10.4403  8.7073
       73.     .17   10.14   38.14   .2490   .2328    2.01    3.83  -.1333   .2676   .8543   .4673   .0232   .0307  9.8713  8.3374
       90.     .17    9.83   37.38   .2488   .2323    1.92    3.73  -.1344   .2639   .8478   .4684   .0231   .0305  9.6968  8.2212

135.    0.    6.87   67.25   83.64   .2962   .3078  -24.84  -11.22  -.1169  -.2824  -.1689  1.0626  -.0070  -.0139 13.7082 12.6947
       13.     .63   34.22   63.17   .2394   .2704    4.60    3.81  -.1306   .1614   .3979   .3316   .0212   .0239 13.7603 10.4331
       30.     .34   20.76   32.72   .2303   .2366    3.10    3.60  -.1293   .1860   .6168   .3384   .0193   .0232 11.9361  8.7032
       43.     .24   13.46   46.30   .2472   .2317    2.13    3.03  -.1291   .1726   .3887   .3482   .0183   .0242 10.1441  7.6643
       60.     .19   12.92   42.69   .2439   .2495    1.63    2.38  -.1334   .1362   .3600   .3333   .0179   .0235  9.2144  7.0697
       73.     .17   11.71   40.79   .2432   .2484    1.38    2.32  -.1371   .1446   .3497   .3601   .0176   .0231  8.7399  6.7606
       90.     .17   11.33   40.20   .2431   .2481    1.30    2.23  -.1383   .1403   .3340   .3616   .0173   .0229  8.6228  6.6647

138.    0.    6.87   78.98   91.23   .3021   .3120  -26.37  -10.87  -.1267  -.2733  -.1061   .9770  -.0031  -.0121 13.4426 12.4763
       13.     .63   40.73   70.01   .2623   .2728    6.89    3.13  -.1272   .2008   .7229   .3066   .0230   .0264 16.9212 11.2614
       30.     .34   24.69   36.81   .2329   .2389    4.44    4.63  -.1090   .2213   .7363   .3131   .0212   .0239 12.0980  9.3774
       43.     .24   18.38   30.00   .2498   .2340    3.08    3.91  -.1108   .2043   .7014   .3226   .0202   .0249 10.9639  8.2293
       60.     .19   13.36   46.17   .2484   .2317    2.36    3.36  -.1163   .1832   .6673   .3299   .0193   .0241  9.9673  7.3663
       73.     .17   13.92   44.16   .2477   .2307    2.01    3.04  -.1211   .1720   .6430   .3343   .0192   .0237  9.4779  7.2204
       90.     .17   13.49   43.33   .2476   .2304    1.90    2.94  -.1228   .1674   .6373   .3358   .0191   .0236  9.3301  7.1127

180.    0.    6.87   91.22   96.30   .3122   .3200  -19.38   -7.33  -.1083  -.1897   .0879   .8196   .0063  -.0049 11.7339  9.6383
       13.     .63   43.89   73.30   .2688   .2781   10.41    7.33  -.1027   .3064  1.0237   .4434   .0291   .0312 20.7931 13.9390
       30.     .34   27.73   39.70   .2390   .2640    6.49    6.43  -.0864   .3243  1.0339   .4492   .0270   .0305 13.8738 11.3107
       43.     .24   20.63   32.60   .2338   .2391    4.37    3.48  -.0892   .3042   .9904   .4376   .0239   .0293 13.3176 10.0998
       60.     .19   17.23   48.61   .2344   .2369    3.38    4.82  -.0936   .2824   .9492   .4640   .0232   .0287 12.2872  9.2880
       73.     .17   13.63   46.33   .2337   .2338    3.10    4.44  -.1007   .2676   .9221   .4679   .0248   .0283 11.6738  8.8623
       90.     .17   13.13   43.87   .2333   .2333    2.96    4.32  -.1026   .2624   .9127   .4692   .0247   .0281 11.4896  8.7294
```

EXHIBIT 6. EXAMPLE OF VISUAL EFFECTS AT A GIVEN LOCATION IN A REGION WITH 2 µg/m$^3$ $SO_4^=$ AND 30 µg/m$^3$ OF COARSE MODE PARTICULATE

plume and the background simultaneously; a relatively sharp line of demarcation separates the plume and the background. For the homogeneous regional, background atmosphere, the observer compares the given atmosphere with a recollection of a clean atmosphere. An exception would be an observer on a mountain looking down on a homogeneous mixed layer from a position where he can compare the color of the mixed layer with the clean air above it. These characteristics of the color differences for the homogeneous, regional background atmosphere must be kept in mind when interpreting the values of color difference parameters for determining the perceptibility and the significance of atmospheric discoloration. Further work is necessary to identify the threshold values of the color difference parameters for the homogeneous atmosphere.

# V RECOMMENDATIONS FOR FUTURE WORK

As stated in Chapter I, we have followed a pragmatic approach to the development of models to predict anthropogenic visibility impairment. Our goal has been to develop predictive tools helpful in:

> Writing the report to Congress on visibility for setting policy and promulgating regulations.
> Evaluating the impact of proposed sources and making siting and pollution control decisions.
> Determining the requirements for retrofitting pollution abatement equipment on existing sources.

This chapter recommends additional work that we believe is necessary in the near term to refine and test the models, to assess the impact of proposed visibility regulations, to improve color display techniques, to develop a regional visibility model for the Southwest and other regions, and to verify the predictions of the models by comparing them with field measurements.

Figure 3 in Chapter I illustrates the potential uses for visibility models in environmental policy and regulatory decisions, emission source siting, and pollution control. Assessment of the extent of existing or past visibility impairment can be accomplished through measurements using such methods as (1) visual range and coloration observation by trained personnel, (2) photographic documentation of visual range and atmospheric discoloration, (3) telephotometry, (4) integrating nephelometry, and (5) transmissometry. However, estimation of the extent of future impairment (e.g., impairment caused by new sources or by the abatement of existing sources) requires a scientifically based prediction capability that can provide estimates of visual range and atmospheric discoloration.

Visibility modeling will clearly play an important role in determining a rational definition of "significant visibility impairment," in setting environmental policy (regulation promulgation, new source and existing source retrofit reviews, and long-term goals), and in determining pollution abatement and siting requirements on a case-by-case basis. It is expected that visibility impairment rather than ground-level air quality will become the dominant air quality issue and will have a significant influence on siting and pollution abatement decisions, particularly in the West.

The following sections outline the work that we believe is necessary to support the EPA's efforts in visibility regulation promulgation. These recommendations are presented in the order of their urgency. In our view, further testing of models and analysis of the impacts of visibility regulations should be done as soon as possible.

## A. IMPACT ANALYSIS IN SUPPORT OF REGULATION DEVELOPMENT

The most urgent requirement for the application of visibility models is the development of regulations. Modeling work will be necessary to determine siting constraints on new sources and requirements for pollution abatement, both for new and existing sources, that will be imposed by proposed visibility regulations.

We have drawn two conclusions of major regulatory importance in our initial applications of visibility models:

> The sulfate formed from $SO_2$ emitted from such sources as smelters and power plants may cause significantly reduced visual range at locations hundreds of kilometers away from the sources. Indeed, the magnitude of the visibility impairment may increase with increasing distance downwind from the source, thereby making identification of cause and effect more difficult.

> $NO_x$ emissions from large coal-fired power plants may cause perceptible yellow-brown plumes and atmospheric discoloration more than 100 km downwind, particularly during stable atmospheric conditions. Control of particulate and $SO_2$ emissions will make the discoloration more prominent by reducing the masking effect due to light scatter.

The implications of these conclusions for siting and control are obvious. Impacts at large distances from emissions sources must be considered in siting studies. Although the impact of power plant emissions on visual range will be reduced by controlling $SO_x$ emissions, $NO_x$ control is needed to reduce the yellow-brown discoloration that is caused by $NO_2$.

In the analysis of the impact of visibility on industry, consideration must be given to:

> The magnitude and the spatial and temporal extent of impairment for various sources, ambient conditions, and geographical locations.

> The siting constraints imposed on new sources.

> The pollutants that must be controlled.

> The degree of control required to reduce visibility impairment to acceptable levels compared with the capability for, feasibility of, and cost of implementation of various pollutant control technologies.

> The appropriate regulatory policy to deal with visibility impairment (i.e., emission standards, ambient air quality standards, or some standard of visual range and atmospheric coloration).

## B. MODEL REFINEMENT AND TESTING

Further work is recommended to test and refine the visibility models in the near term, including:

- Further testing of the models through sensitivity analyses.
- Incorporation of more sophisticated gas-to-particle and aerosol growth algorithms in the code.
- Further assessment of the subjective visual impact of and human threshold response to light intensity and color changes.
- Refinement of color display.

We limit our discussion here to work that should be done in the near term to support the development of visibility regulations. In the future, when a complete set of measurements are available (e.g., from EPA's VISTTA program), visibility models should be verified. Measurements needed to validate models include source emission rates, primary particulate size distribution, meteorological conditions, plume dimensions, plume and ambient chemistry, aerosol size distribution and chemical composition, scattering and absorption coefficients, solar direct and diffuse intensity, and spectral light intensities and color photographs for several lines of sight. Model validation is discussed in Section C.

### 1. Model Testing

As we noted in Chapter IV and demonstrated in Appendices E and G, we have started to test the models by applying them to different emission and ambient conditions to test their sensitivity to various input parameters, including:

- Atmospheric stability (rate of dilution)
- Background ozone concentration
- Solar zenith angle
- Scattering angle
- Observer location and sight path orientation
- Background object light intensity and color
- Pollutant emission rate.

We recommend that more sensitivity analyses be performed with the plume model for a variety of emission sources, meteorology, ambient conditions, and viewing conditions to evaluate the model qualitatively. The results of this sensitivity analysis could be displayed in graphical and tabular form so that they could be used by environmental engineers in regulatory actions, impact analyses, siting studies, and design.

Further parametric analyses should be performed to evaluate the sensitivity of model results to:

> Primary, secondary, and background aerosol size distribution.
> Ratio of diffuse to direct solar flux.
> Ratio of $[NO_2]$ to $b_{scat}$.
> Locations of the background object and the plume relative to the observer.

In a manner analogous to the ozone isopleth diagram, it may be possible to characterize on an isopleth diagram the impact on visibility of a range of combinations of the precursor pollutants. By plotting contours of constant value for some visibility-related objective function, these precursor mixtures which lead to the same visibility conditions may be identified. Among the candidate objective functions are the contrast, visual range, blue-red ratio, and $\Delta E$.

Another sort of visibility isopleth diagram might be constructed to characterize general regional visibility. Instead of HC and $NO_x$ as "precursors," sulfate and nitrogen dioxide could be viewed as "indices" of visibility degradation. By plotting concentrations of $SO_4^=$ and $NO_2$ along the axes, one could determine isopleth lines that correspond to constant objective function values.

One of the chief values of the ozone isopleth diagram is that it provides an easily computed estimate of the reduction in precursor emissions from current ambient levels required to reach the NAAQS. If the objective function chosen for use in the visibility isopleth diagrams were the same as that employed in setting the federal standard, these diagrams might have a similar use. Required reductions in either $SO_2/NO_x$ or $SO_4^=/NO_2$ might be directly estimable. If the development and use of visibility plots were shown to be both feasible and reliable, they might prove to be important tools as promulgation and implementation of a federal visibility standard occurs. This could be of particular significance for state and local agencies, having limited resources and expertise, since they are required to incorporate visibility considerations in State Implementation Plans.

## 2. Gas-to-Particle Conversion and Aerosol Growth

Currently in the visibility models gas-to-particle conversion ($SO_2$ to $SO_4^=$ and $NO_x$ to $NO_3^-$) is treated in a simple manner through the use of pseudo-first-order rate constants. Secondary aerosol is assumed to form in the accumulation mode with properties observed by Whitby and Sverdrup (1978), in the Labadie plume. Although this is a first approximation, it is a reasonable assumption for modeling purposes.

We recommend that further work be done to identify the reaction mechanisms effecting the conversion of $SO_2$ and $NO_x$ to sulfates and nitrates and typical concentrations of reactive species in various nonurban areas (Class I) in the United States. Reactions with the following species should be considered:

> $OH\cdot$
> $HO_2^{\cdot}$
> $O_2$ and $O_3$ (in clouds)
> $NH_3$
> $RO\cdot$
> $RO_2^{\cdot}$.

Through evaluation of the concentrations of reactive species in nonurban areas and resultant formation rates, appropriate formation rates can be selected by the user or computed in the code.

We recommend that an aerosol growth model be studied for possible incorporation in the plume model. Such a model would compute the equilibrium particle size distribution as sulfate and nitrate form and water condenses onto the particle surfaces. We would determine if such a growth model would improve the existing model sufficiently to justify its use.

### 3. Assessment of Color Impact Thresholds

We have incorporated into the visibility models the most recent methods for quantifying color differences developed by the CIE in 1976 [$\Delta E(L^*U^*V^*)$ and $\Delta E(L^*a^*b^*)$]. More work is necessary to determine what standards for atmospheric coloration should be used (if any) in the visibility regulations. The $\Delta E$'s appear to be reasonable parameters to characterize color changes associated with pollution; however, more work is needed to determine what $\Delta E$ values mean subjectively in various cases and what perceptibility-threshold and acceptability-threshold values should be adopted in the analysis of atmospheric discoloration.

### 4. Refinement of Color Display

In few instances is the display of model results so important as it is in the prediction of visibility impact. A considerable number of separate lists of information are required in order to characterize a single scene. However, the human eye and brain together are able to assemble and integrate all this input, synthesizing it to a final impression of visual impairment. It is the subjective judgments based on these impressions that constitute "visual impact" of the most fundamental sort.

Consequently, the practical utility of a model depends on its ability to collapse its predictions into a similarly simple and usable format. It is for this reason that model predictions in this study have been expressed not only by means of specific visibility-related parameters, but also through artist renderings of entire scenes with colors and intensities of sky and pollutant determined by model predictions.

Several advantages have been achieved as a result. Predictions can be assimilated more easily. Judgments about visual impairment are facilitated. The visibility impact projected to result from construction or alteration of a facility can be more readily presented to and evaluated by policy-makers and the general public.

While considerable progress has been made in this study to develop suitable means for displaying model predictions, the following continued efforts seem to hold the promise of substantial payoff:

- Additional studies could be conducted of the feasibility of using artist-produced color illustrations to represent visibility model predictions.
- A study could be performed of the feasibility of using artist renderings of plume and atmospheric coloration predictions "overlayed" onto actual photographs of terrain. This "photo-montage" technique has been used successfully by the U.S. Forest Service's MOSAIC land use assessment program.
- A study could be undertaken of the comparative accuracy and acceptability of each of the above two display techniques, as well as with the color video approach used by workers at Los Alamos.
- The Perspective Terrain Viewing Program (PTVP) could be linked to the plume visibility prediction model (PLUVUE). By doing so, one could first display the terrain as seen from a specified location, select a point whose coloration was desired (as expressed in chromaticity coordinates, perhaps), and calculate directly the visibility predicted at that point. In this way, use of the visibility model would be much more tightly integrated conceptually with terrain views.

## C. MODEL VALIDATION

In this section we discuss our preliminary thoughts on a model validation effort, including:

- The type of measurement program that is needed.
- The specific measurements that should be made.
- The type of analysis of measurements and model predictions needed to assess model performance and to provide direction for model refinement.

### 1. The Type of Measurement Program

No attempt should be made to validate SAI's regional visibility model at this time. Rather, efforts should be aimed at providing a comprehensive set of measurements downwind of a point source so that the plume visibility model can be validated. Information obtained from the point source measurement program will be useful later in regional model validation and refinement.

A large, coal-fired power plant should be selected for the measurement program. The visibility regulations required by the Clean Air Act Amendments of 1977 are likely to affect power plants, particularly in the western United States, more than any other single class of emissions source. Although copper smelters emit large quantities of $SO_x$, which has been shown to significantly affect visual range in the Southwest, most of those sources are exempted from the requirements of Section 169A on visibility protection because they are more than 15 years old.

The power plant that is selected for measurement should have the following attributes:

- Pollutant emissions should be easily measurable and should be relatively constant during the measurement program.

- Particulate emissions should be well controlled using state-of-the-art abatement equipment, such as efficient electrostatic precipitators or wet scrubbers, so the plant is representative of modern coal-fired power plants. A major objective of the measurement program is not to measure the visibility impairment caused by large emission rates of primary particulates from older plants, but to assess the visibility impairment caused by secondary aerosols (i.e., sulfates and nitrates) and $NO_2$. Large emission rates of primary particulate might interfere with the measurement of secondary aerosol generation and light scattering.
- Sulfur dioxide ($SO_2$) emissions should not be controlled by scrubbers so that a significant amount of $SO_2$ is available for conversion to sulfate.
- The power plant should be located in the western United States and should be isolated so that the plume can easily be identified, tracked, and measured without interference from plumes from other sources.

The emphasis of the measurement program should be on the visibility impairment caused at far downwind distances. This contrasts with the objectives of most air quality monitoring programs, which are designed to determine the maximum ground-level pollutant concentrations, which generally occur within 20 to 30 km of the source. Visibility impairment appears to be a long-range air pollution problem because it is caused by secondary pollutants ($NO_2$, sulfates, and nitrates) that are formed relatively slowly in the atmosphere. Preliminary calculations show that the maximum reductions in visual range occur hundreds of kilometers from power plants and maximum plume discoloration due to $NO_2$ occurs during stable conditions 40 to 100 km downwind. Visibility impairment at distances 100 km or more downwind of proposed or existing emissions sources will be the controlling factor in determining the amount of pollution control equipment that must be retrofitted on existing sources and in evaluating what the siting and emission constraints on new sources will be. Therefore, long-range impacts must be measured so that the visibility model can be validated.

A crucial part of the long-range tracking and measurement of plume visibility impairment will be the measurement of upper air transport winds at frequent intervals and several locations so that accurate, real-time plume trajectories can be calculated. These trajectories will be needed to help track the plume and to identify the plume location relative to fixed observation locations. Also, the upper air wind data can be used later in conjunction with National Weather Service measurements to calculate back trajectories and air parcel histories, so that potential sources of background aerosol and trace gases can be identified. For example, during a measurement program at a point source in a nonurban area of the Southwest, there might be several days when air originating from an urban area or from a copper smelter complex would get transported to the measurement area. One could thus, with little additional expenditure, supplement the information regarding point-source plume impact with information regarding the regional impact of distant sources.

An attempt should be made to measure plume visibility impairment during stable meteorological conditions. Greatest visibility impairment, according to model calculations, occurs during stable conditions (e.g., Pasquill E or F). However, even greater impacts might occur during stagnant conditions or in locations where there are flow reversals (e.g., drainage flows) that could cause a build-up of pollutants in a confined area. A study of climatological records could be carried out prior to the measurement program so that periods of the year most likely to have stable or stagnant conditions could be selected. For example, in the Southwest stable conditions occur most frequently in the winter.

### 2. Specific Measurements

A large number of measurements will be required to validate the plume visibility model. The necessity of each measurement can be appreciated by examining Figure 13 (Chapter III), which shows the schematic logic flow diagram of the visibility models. Most air quality measurement programs and models are concerned only with the first two elements of the visibility model--the emissions and the atmospheric transport, diffusion, and removal processes. The desired measurements and output are time-averaged pollutant concentrations at given ground-level locations. However, in the visibility model and in measurements to validate visibility models, the desired result is a light intensity, perceived by an observer at a given ground-level location, which is affected by air pollutants some distance away from the observer.

Thus, the most important single measurement necessary for the validation of visibility models is of the spectral light intensity $I(\lambda)$ for specific observer locations and lines of sight. The spectral light intensity, a strictly physical parameter, can be translated to visibility-related psychophysical parameters, such as luminance (Y), chromaticity (x, y), contrast (C), and the color difference parameter ($\Delta E$), by weighting the light intensity by the spectral response characteristics of the three different light sensors of the human eye. These psychophysical parameters are directly related to what an observer sees and are necessary and sufficient for quantitying visual range and atmospheric discoloration. The multiwavelength telephotometer is the only instrument with which we are familiar that can directly measure these psychophysical parameters. By equipping the instrument with color filters corresponding to the spectral response of the three light receptors of the human eye, one can measure tristimulus values (X, Y, and Z) for a given line of sight and calculate Y, x, y, C, and $\Delta E$. The telephotometer can also be used to determine visual range by measuring the contrast between a distant mountain and the horizon sky. Since the light intensity of several lines of sight can be measured with a single telephotometer at one location, three or four ground-based telephotometer measurement stations might be sufficient for a measurement program at a single point source. Station locations might be in a preferred transport direction (in stable conditions) at distances from the source of 20, 50, 100, and 150 km. If possible, some of these stations might be at vista points in Class I areas. Telephotometer stations can be moved fairly easily, depending on the transport of the plume, to the most strategic locations and could be located on high terrain where views in many directions are possible. It would be valuable to have stations on opposite sides of a plume so that the same sight path could be sampled from different angles to study the effect of the scattering angle $\theta$. One telephotometer could be constantly moved to obtain views of the plume from several angles and distances to characterize fully the effects of plume-observer geometry. For example, measurements of the plume could be made at several locations along a road or highway to evaluate the effect of the plume-observer distance and the angles between the line of sight and the plume centerline and between the line of sight and the horizon.

Each telephotometer operator should take color photographs of the scenes that he is measuring with the telephotometer for later documentation of contrast, atmospheric coloration, and the positions of the plume and the sampling aircraft. At the edge of the camera's field of view in each photograph, a color test strip should be placed (in direct sunlight, if possible) so that the quality of the development of the color film can be controlled and checked. In cases of forward scatter ($\theta < 90°$) where the sun is in front of the camera, the color test strip cannot be placed both in the field of view and in direct sunlight. In such cases, the test strip can be photographed separately at some interval. It may be possible to maintain and check color film development quality by calibration using the color test strip only once per role of film. The feasibility of cross-checking the color photographs with the multiwavelength telephotometer measurements should be evaluated. Color time-lapse movies from strategic vista points could also be taken.

To link the measured spectral intensity to air pollution, one must know the aerosol and $NO_2$ concentrations along the specific sight paths. Thus, airborne measurements of $NO_2$ concentration, scattering coefficient ($b_{scat}$), and aerosol size distribution will be necessary. Attempts should be made to make aircraft traverses of the plume as close to the lines of sight used in the telephotometer measurements as possible. It is essential to measure the location of the plume relative to telephotometer stations since coloration will depend on the proximity of the plume to the telephotometer. Airborne measurements could be supplemented and checked with correlation spectrometer measurements of $NO_2$ burden. Since the plume optical depth due to $NO_2$ is directly proportional to the $NO_2$ burden, this measurement would be valuable. The correlation spectrometer should be considered as an optional supplement to airborne monitoring.

Direct and diffuse solar flux should be measured using a pyrheliometer/pyranometer combination. The occurrence of cloud cover should be documented. The location of the sun should either be measured or calculated so that the solar zenith angle and the scattering angle for all telephotometer and photographic lines of sight can be calculated later. Alternatively, scattering angles could be measured at the time of measurement. It is imperative that the line of sight of each light intensity measurement be specified and recorded; measurements of the scattering angle, solar zenith angle, sight path azimuth, sight path elevation angle, observer location, plume location, and plume dimensions fully describe each line of sight.

An important part of the measurement program should be the determination of the production site, chemical composition, size distribution, and causes of secondary aerosol production, particularly at large downwind distances. The secondary aerosol production rate could be determined by calculating $[SO_4^=]/[SO_2]$, $[NO_3^-]/[NO_x]$, $[b_{scat}]/[SO_2]$, and $[b_{scat}]/[NO_x]$. Each of these ratios will increase with secondary aerosol formation. The measured aerosol size distribution, chemical composition, mass concentration, and scattering coefficient should be cross-checked using Mie theory and accounting for the cations and liquid water associated with sulfates and nitrates. Hypotheses regarding the mechanisms of secondary aerosol formation should be tested by looking at the time-dependent rate of aerosol formation. If possible, measurements of background and plume ammonia and radical concentrations should be made to identify possible fundamental reactions effecting gas-to-particle conversion. Some attempt should be made to measure the refractive indices, including the imaginary (absorption) components, of the background, fly ash, and secondary aerosols.

The conversion of NO to $NO_2$ in the plume should be measured. Ozone concentrations in the background air and in the plume and ultraviolet radiation should be measured to test the validity of the steady-state assumption used in calculating plume $NO_2$ production.

Plume dispersion parameters ($\sigma_y$, $\sigma_z$) should be calculated from the measurements of peak plume concentrations. The wind field at the plume centerline should be measured by pibal releases from several locations at hourly or three-hourly intervals. The plume position and transit times based on measured wind speed and direction at plume height should be computed on a real-time basis and should be compared with actual plume position. Real-time calculations of plume position in the field would be used by the pilot and ground-level observers to determine the location of the plume, and to direct the airborne plume measurements at night and at far downwind distances. These calculations could also be used in conjunction with weather forecasts to relocate ground-based stations to optimize plume impact measurement. Vertical temperature gradients should be measured during the aircraft flights.

Finally, the emissions from the power plant must be measured accurately. If possible, the following measurements should be made throughout the measurement program: mass emission rates or flue gas concentrations of $SO_2$, NO, $NO_2$, and fly ash, in-stack opacity, flue gas volumetric flow rate, flue gas temperature, and flue gas oxygen concentration. It would be desirable in simplifying the measurement program if the power plant operated at constant capacity throughout the measurement program.

## 3. Data Analysis, Assessment of Model Performance, and Model Refinement

Data collected during the measurement program must be reduced and compiled in a format useful for providing input data for the visibility computer simulation models. After the plume visibility model is run, the calculated $SO_2$, NO, $NO_2$, $O_3$, $SO_4^=$, and $NO_3^-$ concentrations, scattering coefficients, spectral light intensities, and visual effects (reduction in visual range, plume perceptibility, and atmospheric discoloration) should be compared with measurements.

Model calculations should be made based on the measured values of:

- > Emission rates
- > Upper air wind speed and direction
- > Plume dilution ($\sigma_y$, $\sigma_z$)
- > Secondary aerosol formation rates
- > Aerosol size distributions
- > Ambient conditions
- > Geometry of sun, plume, and observer.

Calculations and measurements of the following parameters could be compared:

- > Pollutant concentrations
- > $[NO_2]/[NO_x]$
- > $b_{scat}$
- > $b_{scat}$/mass ratios
- > Visual range
- > Luminance (Y)
- > Chromaticity (x, y)
- > Perceptibility ($\Delta E$)
- > Contrast.

In addition, SAI's plume perspective and color display techniques could be used to create color renderings of certain vistas for comparison with color photographs.

In comparing model calculations and measurements necessary for model validation it is important to consider the errors that can occur in:

> Measurement of input parameters
> Measurement of output parameters
> Model formulation.

Since we want to test and validate the model formulation, it is essential that errors in measurement of input and output data be minimized, error bounds established, and that all parameters necessary for defining model input and output be measured.

Model performance can be evaluated using:

> Correlation coefficients.
> Differences between measured and calculated values: Either mean or root-mean-square, and either absolute or relative differences.
> Ratio of measured to calculated values.
> Regression statistics.
> Qualitative comparisons.

A thorough model evaluation may identify directions for model refinement. Limits on model applicability and accuracy may also be established. After further model refinement and development based on the information gained from the comparison with measurements, it could be advantageous to test the model again using another set of measurements, possibly from another emissions source, and allowing no intermediate fine tuning of the model input parameters.

## D. FURTHER DATA ANALYSIS

We have obtained an extensive data base with which further analyses of anthropogenic visibility impairment can be made, including:

- Nearly 500 station-years of National Weather Service (NWS) visibility and meteorological data.
- About 10 station-years of National Park Service visibility data.
- Holzworth mixing depth and mixed layer wind speed for all NWS upper air stations in the United States for 1960 through 1964.

We recommend that further data analysis be coupled with the development of a regional visibility model for the Southwest. The objectives of this analysis would be to determine through an analysis of upper air flow trajectories typical transport wind fields which could be used for regional calculations. Temporal and spatial variations in visual range could be studied in conjunction with calculated trajectories to determine the transport of emissions from source areas to clean nonurban areas (for example, southern Utah). Also, inferences could be made as to the rate of sulfate formation and removal by studying trajectories, ground-level sulfate measurments, and visual range observations.

In this report, visual range has been shown to be correlated with many variables. Correlations with meteorological variables as well as diurnal and seasonal variations have been explored. However, these relationships have been studied one variable at a time, and no attempts have been made to elucidate the simultaneous effects of many variables. In statistical terms, only univariate analyses have been made thus far, though multivariate analyses are needed.

A question of great interest is what combinations of meteorological conditions are associated with poor visibility? This question could be investigated using a multivariate classification technique, such as linear discriminant analysis [e.g., Gnanadesikan (1977), Morrison (1976)], which is a method that assigns multivariate observations to one of several classes. This is done by finding planes in the multidimensional space of the independent variables (in this case, the meteorological variables) that optimally divide the observations (visual ranges) into different classes (e.g., visual range between 80 and 100 km). Discriminant functions for subsets of the data can be determined, for example, for different years or for the period of the copper strike. Differences between discriminant functions would indicate that the conditions associated with various visual ranges were changing. Misclassification rates should be evaluated for each discriminant function to indicate its utility as a predictor.

Another technique that could be applied to the data set to elucidate the dependence of visual range on other variables is multiple regression. However, since many of the independent variables that would be used in the regression (e.g., the meteorological variables) are likely to be highly correlated, some dimensionality-reducing method, such as factor analysis, should be applied to these variables first. In this way, some smaller number of uncorrelated surrogates could be generated, and the multiple regression could be made more meaningful and useful. Alternatively, a variable selection method such as $C_p$ analysis (Daniel and Wood, 1971) could be used in conjunction with the regression.

Intervention analysis can be applied to determine whether a sudden shift in conditions was associated with a corresponding change in visual range (Box and Tiao, 1965, 1975). This technique would be applicable to quantifying the changes in visual range that may have occurred during the copper strikes. This time series method allows for the nonindependence of successive observations in evaluating a change in level of a series of observations. (A t-test of the difference in levels before and after the event would be invalid because of the dependence between successive observations.) The analysis proceeds by calculating a function of the observations, with a known statistical distribution, which estimates the shift in level. Straightforward statistical inference then gives the level of significance of the observed shift. Application of time series techniques should enable both an analysis of trends in visual range and sudden shifts due to events such as the copper strike.

## E. DEVELOPMENT OF A SOUTHWEST REGIONAL VISIBILITY MODEL

For several reasons, the Southwest is likely to be the first region in which visibility regulations, which are to be promulgated by August 1979, are implemented. First, there are a large number of mandatory federal Class I areas in the Southwest, including national parks of such obvious scenic value as the Grand Canyon, Bryce Canyon, Canyonlands, and Arches. Second, the existing visual range in clean areas of the Southwest is probably the best of anywhere in the contiguous United States. According to our analysis of visibility data (see Appendix A), there are several locations in the Southwest, notably in northern Arizona, Utah, Colorado, and New Mexico, where visual range is often greater than 160 km (100 miles). Indeed, based on nephelometer measurements in Bryce Canyon reported by Charlson (private communication, 1978), visual range at times may approach the Rayleigh scattering limit of 390 km (240 miles) in the Southwest. Third, significant energy development is planned for the Southwest, particularly in Utah and Colorado. Several large coal-fired power plants are currently being proposed to be located at sites in the Southwest, including Harry Allen (2000 Mwe), Intermountain Power Project (3000 Mwe), Warner Valley (500 Mwe), and Garfield (2000 Mwe). Fourth, several large coal-fired power plants are currently in operation in the Southwest, some of whose plumes have been observed from scenic vistas in national parks such as Bryce Canyon and Mesa Verde. These plants include Four Corners (2175 Mwe), Mohave (1500 Mwe), Huntington Canyon (800 Mwe), Navajo (2300 Mwe), and San Juan (1500 Mwe). Finally, several very large emissions sources are located in the Southwest or are in the prevailing upwind direction from the Southwest. These sources include the copper smelters, whose current aggregate $SO_x$ emissions are more than 3000 tons per day, and the metropolitan areas of Phoenix, Tucson, Las Vegas, Salt Lake City, and Los Angeles, from which pollution may be transported to Southwest mandatory Class I areas.

Since spectacular scenery in the Southwest is enhanced by generally excellent visibility and since considerable development of coal resources is planned or has already occurred, a regional visibility model that can study and answer the following questions is needed:

- Will a proposed power plant have an impact on visual range in mandatory Class I areas located 100, 200, 500, or even 1000 km away? Will yellow-brown haze be visible? What siting alternatives exist, and how much pollution abatement is required?
- Does an existing power plant's plume have a significant impact on visual range and atmospheric color in national parks? Where? How much? How often? What pollution abatement equipment is required (i.e., particulate, $SO_x$, or $NO_x$ control)?
- Does the existing copper smelter complex have to control $SO_x$ emissions further to reduce visibility impairment? Where does $SO_x$ get transported, how much is removed by natural atmospheric processes, and how much is converted to sulfates?
- Are sulfate, nitrate, and organic aerosols emitted from urban areas, such as Phoenix, Salt Lake City, or even Los Angeles, transported to mandatory Class I areas in the Southwest? Do they have a significant impact on visibility?

These questions have potentially significant technical, socioeconomic, and political implications. For example, if anthropogenic pollution is found to be the cause of significant visibility impairment in the Grand Canyon, the question to be answered is which combinations of sources contribute--urban areas, the copper smelters, or a nearby coal-fired power plant? A Southwest regional visibility model should be developed to point toward the answers to these questions and to provide guidance for critical decisions.

# REFERENCES

Alkezweeny, A. J., and D. C. Powell (1977), "Estimation of Transformation Rate of $SO_2$ to $SO_4$ from Atmospheric Concentration Data," Atmos. Environ., Vol. 11, pp. 179-182.

American Society for Testing and Materials (1974), "Standard Method of Specifying Color by the Munsell System," D1535-68, Philadelphia, Pennsylvania.

Arizona Department of Health Services (1977), "First Annual Report on Arizona Copper Smelter Pollution Control Technology, Phoenix, Arizona.

Atkinson, R., R. A. Perry, and J. N. Pitts, Jr. (1976), "Rate Constants for the Reactions of the OH Radical with $NO_2$ (M = Ar and Ne) and $SO_2$ (M = Ar)," J. Chem. Phys., Vol. 65, pp. 306-310.

Barrie, L., and H. W. Georgii (1976), "An Experimental Investigation of the Absorption of Sulfur Dioxide by Water Drops Containing Heavy Metal Ions," Atmos. Environ., Vol. 10, pp. 743-749.

Bassett, H., and W. G. Parker (1951), "The Oxidation of Sulfurous Acid," J. Chem. Soc., Pt. 2, pp. 1540-1560.

Bauer, E. (1973), "Dispersion of Tracers in the Atmosphere: Survey of Meteorological Data," Paper P-925, Institute of Defense Analysis, Arlington, Virginia.

Baulch, D. L., D. D. Drysdale, and D. G. Horne (1973), Evaluated Kinetic Data for High Temperature Reactions, Volume 2--Homogeneous Gas Phase Reactions of the $H_2$-$N_2$-$O_2$ System (CRC Press, Cleveland, Ohio).

Beilke, S., and G. Gravenhorst (1977), "Heterogeneous $SO_2$ Oxidation in the Droplet Phase," International Symposium on Sulfur in the Atmosphere, Dubrovnik, Yugoslavia.

Beilke, S., D. Lamb, and J. Mueller (1975), "On the Uncatalyzed Oxidation of Atmospheric $SO_2$ by Oxygen in Aqueous Systems," Atmos. Environ., Vol. 9, pp. 1083-1090.

Benarie, M., A. Nonat, and T. Menard (1973), "Etude de la Transformation de L'Anhydride Sulfureaux en Acide Sulfurique en Relation avec les Donnees Climatologiques, dans un Ensembly Urbain in a Caractere Industriel, Rouen," Atmos. Environ., Vol. 7, pp. 403-421.

Benson, S. W. (1968), *Thermochemical Kinetics* (John Wiley & Sons, New York, New York).

Bergstrom, R. W. (1973), "Extinction and Absorption Coefficients of the Atmospheric Aerosol as a Function of Particle Size," *Beiträge Zur Physik der Atmosphäre*, Vol. 46, pp. 223-234.

Bergstrom, R. W., and J. T. Peterson (1977), "Comparison of Predicted and Observed Solar Radiation in an Urban Area," *J. Appl. Meteor.*, Vol. 16, pp. 1107-1116.

Bergstrom, R. W., and R. Viskanta (1974), "Spherical Harmonics Approximation for Radiative Transfer in Polluted Atmospheres," *Progress in Astronautics and Aeronautics*, Vol. 35, pp. 23-40 (MIT Press, Cambridge, Massachusetts).

Boris, J. P., and D. L. Book (1973), "Flux-Corrected Transport--I: SHASTA A fluid Transport Algorithm That Works," *J. Computational Phys.*, Vol. 11, pp. 38-69.

Box, G.E.P., and G. C. Tiao (1975), "Intervention Analysis with Applications to Economic and Environmental Problems, *J. Amer. Stat. Assoc.*, Vol. 70, p. 70.

__________ (1965), "A Change in Level of a Non-stationary Time Series," *Biometrika*, Vol. 52, Nos. 1 and 2, p. 181.

Briggs, G. A. (1969), "Plume Rise," Office of Information Services, U.S. Atomic Energy Commission, Washington, D.C. (National Technical Information Service TID-25075).

Brimblecomb, P., and D. J. Spedding (1974), "The Catalytic Oxidation of Micromolar Aqueous $SO_2$--I. Oxidation in Dilute Solutions Containing Iron (III)," *Atmos. Environ.*, Vol. 8, pp. 937-945.

Businger, J. A., et al. (1971), "Flux-Profile Relationships in the Atmospheric Surface Layer," *J. Atmos. Sci.*, Vol. 28, pp. 181-189.

Calvert, J. G., et al. (1978), "Mechanism of the Homogeneous Oxidation of Sulfur Dioxide in the Troposphere," *Atmos. Environ.*, Vol. 12 (in press).

__________ (1977), "Mechanism of the Homogeneous Oxidation of Sulfur Dioxide in the Troposphere," International Symposium on Sulfur in the Atmosphere, 7-14 September 1977, Dubrovnik, Yugoslavia.

Cass, G. R. (1976), "The Relationship Between Sulfate Air Quality and Visibility at Los Angeles," EQL Memorandum No. 18, California Institute of Technology, Pasadena, California.

Chamberlain, A. C. (1966), "Transport of Gases to and from Grass and Grass-like Surfaces," *Proc. Roy. Soc.*, Vol. A290, pp. 236-260.

Charlson, R. J., and N. C. Ahlquist (1969), "Brown Haze: $NO_2$ or Aerosol?," Atmos. Environ., Vol. 3, pp. 653-656.

Charlson, R. J., N. C. Ahlquist, and H. Horvath (1968), Atmos. Environ., Vol. 2, p. 455.

Chen, T., and C. H. Barron (1972), "Some Aspects of the Homogenous Kinetics of Sulfite Oxidation," Ind. Eng. Chem. Fund., Vol. 11, pp. 446-470.

Cheng, R. T., M. Corn, and J. I. Frohliger (1971), "Contribution to the Reaction Kinetics of Water Soluble Aerosols and $SO_2$ in Air at ppm Concentrations," Atmos. Environ., Vol. 5, pp. 987-1008.

Committee on Colorimetry, Optical Society of America (1963), "The Science of Color," Washington, D.C.

Conner, W. D., and J. R. Hodkinson (1972), "Optical Properties and Visual Effects of Smoke-stack Plumes," AP-30, Office of Air Programs, Environmental Protection Agency, Research Triangle Park, North Carolina.

Covert, D. S., R. J. Charlson, and N. C. Ahlquist (1972), "A Study of the Relationship of Chemical Composition and Humidity to Light Scattering by Aerosols," J. Appl. Meteor., Vol. 11, pp. 968-976.

Cox, R. A., and S. A. Penkett (1972), "Aersol Formation from Sulphur Dioxide in the Presence of Ozone and Olefinic Hydrocarbons," J. Chem. Soc., Vol. 68, p. 1735.

__________ (1971a), "Photo-Oxidation of Atmospheric $SO_2$," Nature, Vol. 229, pp. 486-487.

__________ (1971b), "Oxidation of Atmospheric $SO_2$ by Products of the Ozone-Olefin Reaction," Nature, Vol. 230, pp. 321-322.

__________ (1970), "The Photo-Oxidation of Sulphur Dioxide in Sunlight," Atmos. Environ., Vol. 4, p. 425.

Crutzen, P. J., and J. Fishman (1977), "Average Concentration of OH in the Northern Hemisphere Troposphere, and the Budgets of $CH_4$, CO, and HC," Geophys. Res. Letters, in press.

Daniel, C., and F. S. Wood (1971), Fitting Equations to Data (John Wiley & Sons, New York, New York).

Dave, J. V. (1970), "Subroutines for Computing the Parameters of the Electromagnetic Radiation Scattered by a Sphere," IBM System 360 Program 3600-17.4.002

Davis, D. D., W. Heaps, and T. McGee (1976), "Direct Measurements of National Tropospheric Levels of OH Via an Aircraft Borne Tunable Dye Laser," Geophys. Res. Letters, Vol. 3, pp. 331-333.

Davis, D. D., G. Smith, and J. Klauber (1974), "Trace Gas Analysis of Power Plant Plumes Via Aircraft Measurements: $O_3$, $NO_x$ and $SO_2$ Chemistry," Science, Vol. 186, pp. 733-736.

Durran, D. D., et al. (1978), "A Study of Long Range Air Pollution Problems Related to Coal Development in the Northern Great Plains," Systems Applications, Incorporated, San Rafael, California.

Egan, B. A., and J. R. Mahoney (1972), "Numerical Modeling of Advection and Diffusion of Urban Area Source Pollutants," J. Appl. Meteor., Vol. 11, pp. 312-322.

Ensor, D. S., L. E. Sparks, and M. J. Pilat (1973), "Light Transmittance Across Smoke Plumes Downwind from Point Sources of Aerosol Emissions," Atmos. Environ., Vol. 7, pp. 1267-1277.

EPA (1976a), "1973 National Emissions Report," EPA-450/2-76-007, National Air Data Branch, Office of Air Quality Planning and Standards, Environmental Protection Agency, Research Triangle Park, North Carolina.

__________ (1976b), "Monitoring and Air Quality Trends Report, 1974," EPA-450/1-76-001, Environmental Protection Agency, Washington, D.C.

__________ (1976c), "Existing and Proposed Fuel Conversion Facilities Summary," TS-5, EPA Region VIII, Denver, Colorado.

ER&T (1977), "Development of an Atmospheric Model for Sulfate Formation," Document No. P-1534, Environmental Research & Technology, Incorporated, Santa Barbara, California.

Ettinger, H. J., and G. W. Royer (1972), "Visibility and Mass Concentration in a Nonurban Environment," J. Air Poll. Contr. Assoc., Vol. 22, pp. 108-111.

Federal Power Commission (1976), "FPC Form 67: Steam Electric Plant Air and Water Quality Control Data for the Year Ending December 31, 1975," Washington, D.C.

Forrest, J., and L. Newman (1977a), "Further Studies on the Oxidation of Sulfur Dioxide in Coal-Fired Power Plant Plumes," Atmos. Environ., Vol. 11, pp. 465-474.

__________ (1977b), "Oxidation of Sulfur Dioxide in the Sudbury Smelter Plume," Atmos. Environ., Vol. 11, pp. 517-520.

Forsythe, G. E., and W. R. Wasow (1960), Finite-Difference Methods for Partial Differential Equations (John Wiley & Sons, New York, New York).

Foster, P. M. (1969), "The Oxidation of $SO_2$ in Power Station Plumes," Atmos. Environ., Vol. 3, pp. 157-175.

Freiberg, J. (1975), "The Mechanism of Iron Catalyzed Oxidation of $SO_2$ in Oxygenated Solutions," Atmos. Environ., Vol. 9, pp. 661-672.

__________ (1974), "Effects of Relative Humidity and Temperature on Iron-Catalyzed Oxidation of $SO_2$ in Atmospheric Aerosols," Environ. Sci. Technol., Vol. 8, pp. 731-734.

Friedlander, S. K. (1977), Smoke, Dust and Haze: Fundamentals of Aerosol Behavior (John Wiley & Sons, New York, New York).

Fuller, E. C., and R. H. Crist (1941), "The Rate of Oxidation of Sulfite Ions by Oxygen," J. Am. Chem. Soc., Vol. 63, pp. 1644-1650.

Galbally, I. F., (1974), "Gas Transfer Near the Earth's Surface," Advances in Geophysics, Vol. 18B, pp. 329-340.

Gartrell, F. E., F. W. Thomas, and S. B. Carpenter (1963), "Atmospheric Oxidation of $SO_2$ in Coal-Burning Power Plant Plumes," Am. Ind. Hyg. J., Vol. 24, pp. 113-120.

Gerhard, E. R., and H. F. Johnstone (1955), "Photochemical Oxidation of Sulfur Dioxide in Air," Ind. Eng. Chem., Vol. 47, p. 972.

Gnanadesikan, R. (1977), Methods for Statistical Data Analysis of Multivariate Observations (John Wiley & Sons, New York, New York).

Grosjean, P., and S. K. Friedlander (1975), "Gas-Particle Distribution Factors for Organic and Other Pollutants in the Los Angeles Atmosphere," J. Air Poll. Contr. Assoc., Vol. 10, pp. 1038-1044.

Hagen, L. J., and N. P. Woodruff (1973), "Air Pollution from Duststorms in the Great Plains," Atmos. Environ., Vol. 7, pp. 323-332.

Halow, J. S., and S. J. Zeek (1973), "Predicting Ringelmann Number and Optical Characteristics of Plumes," J. Air Poll. Contr. Assoc., Vol. 23, pp. 676-684.

Hanson, J. E., and L. D. Travis (1974), "Light Scattering in Planetary Atmospherics," Space Science Reviews, Vol. 16, pp. 527-610.

Heisenberg, W. (1948), "Zur Statistischen Theorie der Turbulenz," Z. Phys., Vol. 124, p. 614.

Hidy, G. M., et al. (1975), "Characterization of Aerosols in California (ACHEX)," Science Center, Rockwell International, Thousands Oaks, California.

Hodkinson, J. R. (1966), "Calculations of Colour and Visibility in Urban Atmospheres Polluted by Gaseous $NO_2$," Air Water Poll. Int. J., Vol. 10, pp. 137-144.

Holzworth, G. C. (1972), "Mixing Heights, Wind Speeds, and Potential for Urban Air Pollution Throughout the Contiguous United States," AP-101, Office of Air Programs, Environmental Protection Agency, Research Triangle Park, North Carolina.

Horvath, H. (1972), "Author's Reply: On the Brown Colour of Atmospheric Haze," Atmos. Environ., Vol. 6, pp. 143-148.

__________ (1971), "On the Brown Colour of Atmospheric Haze," Atmos. Environ., Vol. 5, pp. 333-344.

Husar, R. B., and W. H. White (1976), "On the Color of the Los Angeles Smog," Atmos. Environ., Vol. 10, pp. 199-204.

Irvine, W. M. (1975), "Multiple Scattering in Planetary Atmospheres," Icarus, Vol. 25, pp. 175-204.

Jarman, R. T., and C. M. DeTurville (1969), "The Visibility and Length of Chimney Plumes," Atmos. Environ., Vol. 3, pp. 257-280.

Jerskey, T. N., and C. S. Burton (1977), "The Prediction of Visibility on a Regional Scale: The Status of Visibility Models and Measurements," EI77-23, Systems Applications, Incorporated, San Rafael, California.

Johnstone, H. F., and D. R. Coughanowr (1958), "Absorption of Sulfur Dioxide from Air: Oxidation in Drops Containing Dissolved Catalysts," Ind. Eng. Chem., Vol. 50, p. 1169.

Johnstone, H. F., and A. J. Moll (1960), "Formation of Sulfuric Acid in Fogs," Ind. Eng. Chem., Vol. 52, p. 861.

Judd, D. B., and G. Wyszecki (1975), Color in Business Science and Industry (John Wiley & Sons, New York, New York).

Junge, C. E. (1963), Air Chemistry and Radioactivity (Academic Press, New York, New York).

Junge, C. E., and T. G. Ryan (1958), "Study of the $SO_2$ Oxidation in Solution and Its Role in Atmospheric Chemistry," Quart. J. Roy. Meteor. Soc., Vol. 84, pp. 46-55.

Katz, M. (1950), "Photoelectric Determination of Atmospheric $SO_2$ Employing Dilute Starch-Iodine Solutions," Anal. Chem., Vol. 22, p. 1040.

LACAPCD (1971), "Profile of Air Pollution Control," Air Pollution Control District, County of Los Angeles, Los Angeles, California.

Larson, T. V., N. R. Horike, and H. Harrison (1977), "Oxidation of Sulfur Dioxide by Oxygen and Ozone in Aqueous Solution: A Kinetic Study with Significance to Atmospheric Rate Processes," Atmos. Environ., in press.

Latimer, D. A., and G. S. Samuelsen (1978), "Visual Impact of Plumes from Power Plants," Atmos. Environ., Vol. 12, pp. 1455-1465.

__________ (1975), "Visual Impact of Plumes from Power Plants," UCI-ARTR-75-3, UCI Air Quality Laboratory, School of Engineering, University of California, Irvine, California.

Leighton, P. A. (1961), Photochemistry of Air Pollution (Academic Press, New York, New York).

Levy, A. H., D. R. Drewes, and J. M. Hales (1976), "$SO_2$ Oxidation in Plumes: A Review and Assessment of Relevant Mechanistic and Rate Studies," EPA-450/3-76-022, Environmental Protection Agency, Research Triangle Park, North Carolina.

Liu, M. K., and D. Durran (1977), "The Development of a Regional Air Pollution Model and Its Application to the Northern Great Plains," EPA-908/1-77-001, Systems Applications, Incorporated, San Rafael, California.

__________ (1976), "On the Modeling of Transport and Diffusion of Air Pollutants over Long Distances," ER76-55, Systems Applications, Incorporated, San Rafael, California.

Liu, M. K., M. A. Wojcik, and D. Henderson (1978), "Numerical Experiments of the Effect of Lateral Diffusion on Mesoscale Pollutant Dispersion," Summer Computing Conference, 24-26 July 1978, Newport Beach, California.

Matteson, M. J. (1978), "Capture of Atmospheric Gases by Water Vapor Condensation on Carbonaceous Particles," Conference on Carbonaceous Particles in the Atmosphere, 20-22 March 1978, Lawrence Berkeley Laboratory, Berkeley, California.

Matteson, J. J., W. Stober, and H. Luther (1969), "Kinetics of the Oxidation of $SO_2$ by Aerosols of Manganese Sulfate," Ind. Eng. Chem. Fund., Vol. 8, pp. 677-687.

McKay, H.A.C. (1971), "The Atmospheric Oxidation of Sulphur Dioxide in Water Droplets in Presence of Ammonia," Atmos. Environ., Vol. 5, pp. 7-14.

Megaw, W. J. (1977), "Thin Layer Brown Haze," J. Aerosol Sci., Vol. 8, pp. 21-29.

Middleton, W.E.K. (1952), Vision Through the Atmosphere (University of Toronto Press, Toronto, Canada).

Miller, J. M., and R. G. DePena, (1972), "Contribution of Scavenged $SO_2$ to the Sulfate Content of Rain Water," J. Geophys. Res., Vol. 77, pp. 5905-5916.

Morrison, D. F. (1976), Multivariate Statistical Methods (McGraw-Hill, New York, New York).

Munsell Color Company (1976), "Munsell Book of Color," Baltimore, Maryland.

Newman, L., J. Forrest, and B. Manowitz (1975), "The Application of an Isotopic Ratio Technique to a Study of the Atmospheric Oxidation of Sulfur Dioxide in the Plume from an Oil-Fired Power Plant," Atmos. Environ., Vol. 9, pp. 959-968.

NGPRP (1974), "Atmospheric Aspects Work Group Report," Northern Great Plains Resource Program, Denver, Colorado.

Niki, H. (1974), "Reaction Kinetics Involving O and N Compounds," Can. J. Chem., Vol. 52, pp. 1397-1404.

Nixon, J. K. (1940), "Absorption Coefficient of Nitrogen Dioxide in the Visible Spectrum," J. Chem. Phys., Vol. 8, pp. 157-160.

Noll, K. E., P. K. Mueller, and M. Imada (1968), "Visibility and Aerosol Concentration in Urban Atmospheres," Atmos. Environ., Vol. 2, pp. 465-475.

Nordlund, G. G. (1975), "A Quasi-Lagrangian Cell Method for Calculating Long-Distance Transport of Airborne Pollutants," J. Appl. Meteor., Vol. 14, pp. 1095-1104.

Nordö, J. (1973), "Meso-Scale and Large-Scale Transport of Air Pollutants," Proc. Third International Clean Air Congress, B105-B108, Dusseldorf, Federal Republic of Germany, VDI-Verlag.

Nordö, J., A. Eliassen, and J. Saltbones (1974), "Large-Scale Transport of Air Pollutants," Advances in Geophysics, Vol. 18B, pp. 137-150.

Novakov, T., S. G. Chang, and A. B. Harker (1974), "Sulfates in Pollution Particulates: Catalytic Oxidation of $SO_2$ on Carbon Particles," Science, Vol. 186, pp. 259-261.

Orel, A. E., and J. H. Seinfeld (1977), "Nitrate Formation in Atmospheric Aerosols," Environ. Sci. Technol., Vol. 11, pp. 1000-1007.

Payne, W. A., L. J. Stief, and D. D. Davis (1973), "A Kinetics Study of the Reaction of $HO_2$ with $SO_2$ and NO," J. Am. Chem. Soc., Vol. 95, pp. 7614-7619.

Penkett, S. A. (1972), "Oxidation of $SO_2$ and Other Atmospheric Gases by Ozone in Aqueous Solution," Nature, Phys. Sci., Vol. 240, pp. 105-106.

Penkett, S. A., and J. A. Garland (1974), "Oxidation of $SO_2$ in Artificial Fogs by Ozone," Tellus, Vol. 26, pp. 284-290.

Pilat, M. J., and D. S. Ensor (1971), "Comparison Between the Light Extinction Aerosol Mass Concentration Relationship of Amtospheric and Air Pollutant Emission Aerosol," Atmos. Environ., Vol. 5, pp. 209-215.

Roberts, E. M., et al. (1975), "Visibility Measurements in the Painted Desert Through Photographic Photometry," Engineering Bulletin 47, Dames & Moore, Santa Barbara, California.

Roberts, P. T., and S. K. Friedlander (1975), "Conversion of $SO_2$ to Sulfur Particulate in the Los Angeles Atmosphere," Environ. Health Perspectives, Vol. 10, pp. 103-108.

Rodhe, H. (1972), "A Study of the Sulphur Budget for the Atmosphere over Northern Europe," Tellus, Vol. 24, pp. 128-138.

Samuels, H. J., S. Twiss, and E. W. Wong (1973), "Visibility, Light Scattering and Mass Concentration of Particulate Matter," California Air Resources Board, Sacramento, California.

Sander, S. P., and J. H. Seinfeld (1976), "Chemical Kinetics of Homogeneous Atmospheric Oxidation of Sulfur Dioxide," Environ. Sci. Technol., Vol. 10, pp. 1114-1123.

Schroeter, L. C. (1963), "Kinetics of Air Oxidation of Sulfurous Acid Salts," J. Pharm. Sci., Vol. 52, pp. 559-563.

Schwartz, S. E., and L. Newman (1978), "Processes Limiting Oxidation of Sulfur Dioxide in Stack Plumes," Environ. Sci. Technol., Vol. 12, No. 1, pp. 67-73.

Scott, W. D., and P. V. Hobbs (1967), "The Formation of Sulfate in Water Droplets," J. Atmos. Sci., Vol. 24, pp. 54-57.

Scriven, R. A., and B.E.A. Fisher (1975a), "The Long-Range Transport of Airborne Material and Its Removal by Deposition and Washout--I. General Considerations," Atmos. Environ., Vol. 9, pp. 49-58.

__________ (1975b), "The Long-Range Transport of Airborne Material and Its Removal by Deposition and Washout--II. The Effect of Turbulent Diffusion," Atmos. Environ., Vol. 9, pp. 59-68.

Sellers, W. D. (1965), Physical Climatology (University of Chicago Press, Chicago, Illinois).

Smagorinsky, J. (1963), "General Circulation Experiments with the Primitive Equations: I. The Basic Experiment," Mon. Wea. Rev., Vol. 91, pp. 99-164.

Spicer, C. W., and P. M. Schumacher (1977), "Interferences in Sampling Atmospheric Particulate Nitrate," Atmos. Environ., Vol. 11, pp. 873-876.

Thom, A. S. (1972), "Momentum, Mass and Heat Exchange of Vegetation," Quart. J. Roy. Met. Soc., Vol. 98, pp. 124-134.

Trijonis, J., and K. Yuan (1978), "Visibility in the Northeast: Visibility Trends and Visibility/Pollutant Relationships," Technology Service Corporation, Santa Monica, California.

_________ (1977), "Visibility in the Southwest: An Exploration of the Historical Data Base," Technology Service Corporation, Santa Monica, California.

Urone, P., and W. H. Schroeder (1969), "$SO_2$ in the Atmosphere: A Wealth of Monitoring Data but Few Reaction Rate Studies," Environ. Sci. Technol., Vol. 3, pp. 436-445.

Urone, P., et al. (1968), "Static Studies of Sulfur Dioxide Reactions in Air," Environ. Sci. Technol., Vol. 2, pp. 611-618.

van der Heuvel, A. P., and B. J. Mason (1963), "The Formation of Ammonium Sulfate in Water Droplets Exposed to Gaseous $SO_2$ and $NH_3$," Quart. J. Roy. Meteor. Soc., Vol. 89, pp. 271-275.

Van de Hulst, H. C. (1957), Light Scattering by Small Particles (John Wiley & Sons, New York, New York).

Waggoner, A. P., and R. J. Charlson (1971), "Simulating the Color of Polluted Air," Applied Optics, Vol. 10, pp. 957-958.

Waggoner, A. P., R. J. Charlson, and N. C. Ahlquist (1972), "Discussion: On the Brown Color of Atmospheric Haze," Atmos. Environ., Vol. 6, pp. 143-148.

Waggoner, A. P., et al. (1976), "Sulfate-Light Scattering Ratio as an Index of the Role of Sulfur in Tropospheric Optics," Nature, Vol. 261, pp. 120-122.

Weir, A., et al. (1976), "Factors Influencing Plume Opacity," Environ. Sci. Technol., Vol. 10, pp. 539-544.

_________ (1975), "Measurement of Particle Size and Other Factors Influencing Plume Opacity," International Conference on Environmental Sensing and Assessment, 14-19 September 1975, Las Vegas, Nevada.

Whitby, K. T., and G. M. Sverdrup (1978), "California Aerosols: Their Physical and Chemical Characteristics," to be published in the ACHEX Hutchinson Memorial Volume, Particle Technology Laboratory Publication Number 347, University of Minnesota, Minneapolis, Minnesota.

White, W. H. (1977), "$NO_x$-$O_3$ Photochemistry in Power Plant Plumes: Comparison of Theory with Observation," Environ. Sci. Technol., Vol. 11, No. 10, pp. 995-1000.

White, W. H., and P. T. Roberts (1975), "The Nature and Origins of Visibility Reducing Aerosols in Los Angeles," 68th Annual Meeting, Air Pollution Control Association, 15-20 June 1975, Boston, Massachusetts.

Whitten, G. Z., and H. Hogo (1977), "Mathematical Modeling of Simulated Photochemical Smog," EPA-600/3-77-001, Systems Applications, Incorporated, San Rafael, California.

Williams, M. D., and R. Cudney (1976), "Predictions and Measurements of Power Plant Plume Visibility Reductions and Terrain Interactions," Proc. of the Third Symposium on Atmospheric Turbulence Diffusion and Air Quality, American Meteorological Society, pp. 415-420.

Williams, M. D., M. J. Wecksung, and E. M. Leonard (1978), "Computer Simulation of the Visual Effects of Smoke Plumes," Society of Photo-Optical Instrumentation Engineers Technical Symposium, 30 March 1978, Washington, D.C.

Winkelmann, D. (1955), "Die Electrochemische Messung du Oxidationsgeschwindigkeit von $Na_2SO_3$ Durch Gelösten Sauerstoff," Z. Elektrochemie, Vol. 59, pp. 891-895.

Winkler, P. (1973), "The Growth of Atmospheric Aerosol Particles as a Function of the Relative Humidity--II. An Improved Concept of Mixed Nuclei," Aerosol Sci., Vol. 4, pp. 373-387.

Yanenko, N. N. (1971), The Method of Fractional Steps (Springer-Verlag, Berlin, Germany).

# GLOSSARY

accumulation mode--Submicron particles in the range 0.1 to 1.0 μm, which are formed from smaller nuclei by coagulation or by direct condensation of gases. This particle mode is most effective per unit mass in light scattering. Secondary particles such as sulfates, nitrates, and organics are found predominantly in this size range. Since coagulation is relatively slow for particles larger than 1 μm, particles in the accumulation mode are generally removed from the atmosphere by precipitation and surface deposition before they grow larger.

aerosol--A suspension of fine solid or liquid particles in air or a gas. In the context of visibility impairment, aerosol means a suspension of nuclei, accumulation mode, and coarse particles (and gaseous pollutants) in ambient air. Aerosol is also sometimes used to signify the liquid or solid particles themselves.

anthropogenic--Caused directly by man or indirectly by man's technology (e.g., anthropogenic pollutant emissions from combustion sources such as automobiles and boilers).

appearance--The subjective visual impression or aspect of a thing observed by a human (e.g., the appearance of distant mountains or a plume).

atmospheric discoloration--An imprecise term describing the change in color of the sky or distant mountains or clouds observed through the atmosphere due to natural or man-made pollution. The term implies that there is an atmospheric color or set of colors that can be defined as natural and not discolored. Examples of atmospheric discoloration are white, grey, yellow, brown, or black haze or plumes.

background--An object being viewed by an observer (e.g., sky, cloud, or mountain). Light reflected (if any) from the object and light scattered and absorbed by the atmosphere along the sight path or line of sight between the object and the observer determines the color perceived by the observer. The nature of the background affects the apparent coloration of a plume or haze layer.

back scatter--Situation where the sun is behind the observer ($\theta > 90°$).

chroma--The numerical index in the Munsell color notation system that describes the degree of saturation or the departure from grey. A chroma of 0 is grey; a chroma of 2 is slightly colored; a chroma of 6 is highly colored.

chromaticity diagram and coordinates--A mathematical description of the relative spectral distribution (hue and saturation) of a given color. Chromaticity coordinates uniquely describe the position of a given color on a two-dimensional plot called a chromaticity plot. Chromaticity coordinates provide information only on the relative mix of light of different wavelengths, not the overall light intensity or luminance. For example, chromaticity coordinates are not sufficient to describe the difference between yellow and brown (a dark yellow).

C.I.E.--Commission Internationale de l'Eclairage, or International Commission on Illumination, a scientific organization responsible for setting standards for light and color measurement and specification.

Class I areas--Areas such as national parks, wilderness areas, and national forests that are afforded the most stringent air quality protection both in terms of the significant deterioration air quality increments and the visibility protection and restoration mandates of the Clean Air Act (Section 169). Mandatory Class I areas are those areas designated as such by the legislature; however, Class II areas may be redesignated as Class I.

coagulation--The process of particle growth resulting from particle collision.

coarse particles--Particles larger than 1 μm, caused principally by grinding and mechanical process (e.g., soil dust).

color difference parameter ($\Delta E$)--An index quantifying the difference between two colors, in terms of light intensity differences as well as chromaticity differences, transformed such that equal values of $\Delta E$ correspond to equally perceived differences. The parameter is useful to characterize the overall perceptibility of haze layers resulting from color differences.

color solid or volume--A three-dimensional representation of color. A color can be located in a color volume by specifying Munsell hue, value, and chroma or by specifying overall light intensity or luminance ($Y$) and chromaticity coordinates ($x$, $y$). The color difference parameter ($\Delta E$) may be visualized as a distance between two points in a color volume which has been transformed such that equal distances correspond to equally perceived color differences.

contrast--The fractional difference in light intensities of two colors. The contrast defined at specific wavelengths of light is useful in characterizing color changes. The contrast between a black object and the clear, horizon sky is used in defining visual range.

diffuse radiation--See "multiple scattering."

elevation angle ($\beta$)--Angle between the horizontal and the line of sight (sight path).

extinction coefficient ($b_{ext}$)--The derivative of transmitted light intensity with respect to distance along a sight path of light attenuation due to light scatter and absorption. The extinction coefficient is a function of wavelength and depends on concentrations and characteristics of aerosol particles and absorbing gases such as $NO_2$. The extinction coefficient is the sum of the scattering coefficient ($b_{scat}$) and the absorption coefficient ($b_{abs}$).

fly ash--Primary particulate matter emitted from furnaces and boilers, usually consisting chiefly of silica with traces of oxides of metals such as aluminum and iron. Plume opacity at the top of a stack is usually caused by fly ash.

forward scatter--Situation where the sun is in front of the observer so that direct solar radiation is scattered less than 90° into the observer's line of sight ($\theta<90°$).

hue--Index in the Munsell color notation system characterizing the dominant coloration (e.g., red, green, or blue).

integrating nephelometry--A technique that measures the scattering coefficient of a small volume of air within a chamber.

Koschmieder relationship--The mathematical expression for calculating the visual range in a homogeneous atmosphere:

$$r_v = \frac{3.912}{b_{ext}} \quad .$$

liminal contrast--The contrast that is barely perceptible. This contrast threshold will depend on the observer and lighting conditions, but a liminal contrast of 0.02 is common and is used in the definition of visual range.

line of sight (or sight path)--The line connecting the observer and the observed object. Particles and gases in the atmosphere along this line will affect the perceived color of the object by absorbing light and by scattering light into and out of the line of sight.

luminance (Y)--The overall light intensity within the visible spectrum, weighted by the photopic response of the human eye.

Mie scattering--The theory describing scattering of electromagnetic radiation by spherical particles of diameters of the same order as the wavelength ($\lambda$) of the radiation. Rayleigh scattering theory covers scattering by particles with diameters much shorter than $\lambda$.

multiple scattering--Radiation that has been scattered more than once. Single scattering results when direct solar radiation is scattered into the line of sight. Multiple scattering occurs when direct solar radiation is scattered at least once by gases and particles not in the line of sight or is reflected from the surface of the earth or clouds before being scattered by particles and gases along the line of sight. Diffuse radiation has been scattered or reflected at least once, while direct solar radiation, as its name implies, is radiation directly from the sun.

Munsell color notation--A system of describing a color quantitatively by reference to three indices (hue, value, and chroma). The Munsell Book of Color displays color paint chips at specific intervals of hue, value, and chroma.

nuclei mode--Particles less than 0.1 μm in diameter, which are not effective in light scattering, but grow by coagulation to the accumulation mode.

opacity--A term characterizing the optical thickness of an aerosol layer, usually used to characterize smoke plumes in or near the stack. Opacity is usually expressed in percent and is defined as

$$\text{Opacity} = 1 - \text{Transmittance} \quad ,$$

where transmittance is related to the optical thickness $\tau$ as follows:

$$\text{Transmittance} = e^{-\tau} \quad .$$

optical thickness ($\tau$)--The integral of the extinction coefficient of an aerosol between two points along a given line of sight.

particulate matter--Small solid or liquid particles, consisting of many molecules, that are suspended in air.

perceptibility--As used herein, the characteristic of an object that makes it visible to a human observer. Perceptibility results from differences in light intensity and color between two objects. For example, a distant mountain is perceptible because it is darker than the background sky. Air pollution is perceptible if color differences exist between a plume and a background, a haze layer and a capping layer, or between a haze and a recollection of a clear day. (See also "liminal contrast").

phase function--See "scattering distribution function."

pollutant flux--The total mass of a pollutant species in a plume passing through a plane perpendicular to the plume centerline per unit of time.

primary particulate--Particles emitted directly from an emissions source (e.g., fly ash).

Rayleigh scattering--The theory describing scattering of radiation by molecules or particles much smaller than the wavelength of the radiation, resulting from a dipole interaction with the electric field of the radiation.

saturation--See "chroma."

scattering angle--The angle between the vector describing the unscattered radiation on an object and the vector along the line of sight between the object and the observer.

scattering distribution function (or phase function)--The function describing the direction in which radiation is scattered. For aerosols the scattering distribution function is largest in forward scatter ($\theta<45°$), which explains why haze layers are bright when the sun is in front of the observer.

solar flux--The intensity of solar radiation (watts/$m^2$) incident on a given plane perpendicular to the solar rays.

spectral light intensity--The light intensity along a particular line of sight at wavelength $\lambda$ (watts/$m^2$/steradian). The spectral light intensity can be considered the increment of radiant energy of wavelength $\lambda$ to $\lambda + d\lambda$ passing through an elemental area dA within a solid angle $d\omega$ along the given line of sight:

$$I(\lambda) = \frac{\partial^4 E}{\partial t \partial A \partial \omega \partial \lambda}$$

telephotometry--A technique for measuring the light intensity of a distant object using a photometer coupled to a telescope. By measuring the differences in light intensity between the clear horizon sky and distant mountains, one can estimate the visual range.

transmissometry--A technique of measuring the transmission of light through the atmosphere by which the overall extinction can be determined.

tristimulus values--Indices that describe a given color by indicating the amount of red, green, and blue light needed to match the color. Tristimulus values (X, Y, Z) are keyed to the wavelength responses of the three color sensors in the human eye. They can also be translated into chromaticity coordinates (x, y).

value--The index in Munsell color notation related to brightness (luminance or overall light intensity).

visibility--See "visual range."

visibility impairment--A reduction in visual range, the presence of atmospheric discoloration, or both. The Clean Air Act Amendments of 1977 refer to "any" and "significant" visibility impairment, terms which have yet to be defined in regulations.

visual range (or visibility)--The distance at which a large, black object is barely visible when viewed against the horizon sky. For calculations, it is convenient to use a more strict definition of visual range, i.e., the distance at which the contrast between a black object and the clear (cloudless) horizon sky is reduced to 0.02. When calculating contrast, one should use overall light intensity or luminance (Y) or, as an approximation, the spectral light intensity at $\lambda = 0.55$ μm, which is the midpoint of the visible spectrum and the wavelength to which the human eye is most sensitive.

zenith angle--The angle between the solar beam and the vertical at a given location on Earth.